September, 2015 1-208

PERIODICO di MINERALOGIA

established in 1930

ISSN 0369-8963

An International Journal of
MINERALOGY, CRYSTALLOGRAPHY, GEOCHEMISTRY, ORE DEPOSITS, PETROLOGY, VOLCANOLOGY
and applied topics on Environment, Archaeometry and Cultural Heritage

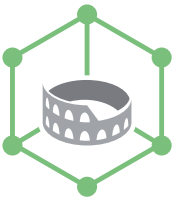

E C M S 2 0 1 5

EUROPEAN CONFERENCE ON MINERALOGY AND SPECTROSCOPY

Proceedings of the
8th European Conference on
Mineralogy and Spectroscopy
Rome, Italy, September 9-11, 2015

Edited by
Giovanni B. Andreozzi and Ferdinando Bosi

SAPIENZA
UNIVERSITÀ DI ROMA

Edizioni Nuova Cultura

PERIODICO di MINERALOGIA
established in 1930

http://www.periodicodimineralogia.it
periodicodimineralogia@uniroma1.it

September, 2015

ECMS 2015

Proceedings of the 8th European Conference on Mineralogy and Spectroscopy

Property of Università degli Studi di Roma "La Sapienza"
Piazzale Aldo Moro 5, I-00185 Roma, Italy

Edizioni Nuova Cultura

ISSN PRINT: 0369-8963
ISSN ON LINE: 2239-1002

Director
ANTONIO GIANFAGNA

Dipartimento di Scienze della Terra, Università degli Studi di Roma "La Sapienza"
Piazzale Aldo Moro 5, I-00185 Roma, Italy
Tel. +39 0649914921; Fax +39 064454729;
e-mail: antonio.gianfagna@uniroma1.it - periodicodimineralogia@uniroma1.it

Authorization by Tribunale di Roma n. 313/2000
This journal is printed with funds by Università degli Studi di Roma "La Sapienza"

ECMS 2015
8th European Conference on Mineralogy and Spectroscopy

Preface

Rome is proud to host the eighth edition of the European Conference on Mineralogy and Spectroscopy (ECMS 2015). This is a welcome back, after the starting point of this conference cycle in Rome (1988) and following editions held in Berlin (1995), Kiev (1996), Paris (2001), Vienna (2004), Stockholm (2007) and Potsdam (2011).

The Rome 2015 conference will hopefully reflect the philosophy of previous conferences and provide a common forum to present new ideas, concepts and results related to mineral spectroscopy. It will also offer an opportunity for students and young scientists to meet and interact with established, well-known scientists. The conference deals with mineralogy, spectroscopy and related fields of science, bringing together both theoretically and experimentally oriented scientists and providing an opportunity to share ideas and learn from one another.

The ECMS 2015 is housed in the headquarters of the National Research Council, and consists of three days of oral presentations and two days of poster sessions. Keynote lectures will be presented by Frank C. Hawthorne, Laurence Galoisy, Robert D. Shannon, Giancarlo Della Ventura, Bjorn Winkler and Catherine McCammon.

This volume is the joint effort of all conference participants largely coming from Europe, but also from America, Asia and Australia. It contains 100 contributions, many of which present experimental results and applications based on new or well-established analytical techniques, while others highlight theoretical and computational approaches to our better understanding of short-range and long-range structures of minerals and materials.

We are very grateful for the constant support of Francesco Di Benedetto (publicity chair), Sabrina Nazzareni (treasurer) and our scientific advisory board: Danilo Bersani, Giuseppe Cruciani, Michele Dondi, Ulf Hålenius, Monika Koch-Müller, Roberta Oberti, Henrik Skogby and Sergio Speziale. Without the generous sponsoring from the Società Italiana di Mineralogia e Petrologia (SIMP), Italian National Research Council (CNR) and Periodico di Mineralogia and the support of Sapienza Università di Roma, it would have been very difficult to organize this meeting and this volume. We also appreciate the sponsorship and scholarship grant from the European Mineralogical Union (EMU) and the International Union of Crystallography (IUCr), and contributions from private companies (Bruker, Geologica, Gemmoraman, Masterstones, PANalytical).

Thanking all participants for coming in the Eternal City, we wish you all a stimulating, informative and enjoyable conference and offer a sincere welcome to the ECMS 2015.

Giovanni B. Andreozzi and Ferdinando Bosi
Co-chairmen
On behalf of the Organizing Committee

Keynote Lectures

Periodico di Mineralogia, ECMS 2015, 1-2

PERIODICO di MINERALOGIA
established in 1930

An International Journal of
MINERALOGY, CRYSTALLOGRAPHY, GEOCHEMISTRY,
ORE DEPOSITS, PETROLOGY, VOLCANOLOGY
and applied topics on *Environment*, *Archaeometry* and *Cultural Heritage*

Short-range order in rock-forming and accessory minerals: a review of the present state of affairs and some suggestions as to what to do next

Frank C. Hawthorne

Department of Geological Sciences, University of Manitoba, Winnipeg, R3T2N2, Canada
Corresponding author: *frank_hawthorne@umanitoba.ca*

Short-range order involves local clusters of atoms that occur either more or less frequently than predicted by a random distribution. Where solid solutions involve coupled replacement of ions by ions of different charge, the valence-sum rule of bond-valence theory constrains the relative positions of the substituent ions. This constraint produces short-range order as the relative arrangements of the ions is not random. The ubiquity of polyvalent substitutions in minerals means that short-range order is the rule rather than the exception in many rock-forming and accessory minerals. I will briefly review those groups of minerals in which short-range order is a common feature: amphiboles (e.g., Hawthorne and Della Ventura, 2007), tourmalines (e.g., Bosi, 2011), micas (e.g., Sanz et al., 2015), spinels (e.g., Bosi et al., 2012) etc., and will discuss the difficulties in deriving short-range arrangements of atoms experimentally. Hydrogen is a key probe of short-range order in hydroxyl minerals, and careful work can determine much of the short-range order present in these minerals. Anhydrous minerals are more difficult to deal with, as the spectroscopic techniques sensitive to short-range order are not as comprehensive in their sensitivity as infrared spectroscopy in the OH-stretching region.

[1] Bond-valence theory has been used in a qualitative way to predict short-range order in a few minerals. A more quantitative approach may be possible using *a priori* bond-valence calculations, and I will examine this possibility here. [2] One of the major problems in rigorously considering short-range order in crystal structures is the propagation of this order throughout the structure: how do we get a handle on what happens as short range becomes medium range? Current ways of looking at these issues always involve mean-field approaches; are the derivation of "real" solid-solution structures possible? If we are to improve our understanding of short-range order and develop more realistic thermodynamic models for solid solutions, we need to address these issues.

References

Bosi, F. (2011) - Stereochemical constraints in tourmaline: from a short-range structure to a long-range structure. *Canadian Mineralogist*, 49, 17-27.

Bosi, F., Halenius, U., D'Ippolito, V. and Andreozzi, G.B. (2012) - Blue spinel crystals in the $MgAl_2O_4$-$CoAl_2O_4$ series: Part II. Cation ordering over short-range and long-range scales. *American Mineralogist*, 97, 1834-1840.

Hawthorne, F.C. and Della Ventura, G. (2007) - Short-range order in amphiboles. In: Amphiboles: Crystal Chemistry, Occurrence and Health Issues (Hawthorne, F.C., Oberti, R., Della Ventura, G., Mottana, A., eds.) Reviews in Mineralogy and Geochemistry 67, Mineralogical Society of America and Geochemical Society, Washington D.C., 173-222.

Sanz, J., Sobrados, I. and Robert, J-.L. (2015) - Influence of hydration on ^{23}Na, ^{27}Al, and ^{29}Si MAS-NMR spectra of sodium saponites and sodium micas. *American Mineralogist*, 100, 1076-1083.

Periodico di Mineralogia, ECMS 2015, 3-4

PERIODICO di MINERALOGIA
established in 1930

An International Journal of
MINERALOGY, CRYSTALLOGRAPHY, GEOCHEMISTRY,
ORE DEPOSITS, PETROLOGY, VOLCANOLOGY
and applied topics on *Environment*, *Archaeometry* and *Cultural Heritage*

Structural control of the color of minerals and glasses using spectroscopic tools

Laurence Galoisy

Institut de Minéralogie, de Physique des Matériaux et de
Cosmochimie (IMPMC) - Sorbonne Universités – UPMC
UMR CNRS 7590 - IRD UMR 206 – MNHN - 4 place Jussieu F-75005 Paris, France
Corresponding author: *laurence.galoisy@upmc.fr*

Color is one of the most important properties in minerals and glasses. Light absorption by transition elements, either as major part of the mineral chemistry or as impurities, is one of the most important coloring mechanisms. To induce coloration, transition elements should be located in specific surroundings in minerals and glasses. This local environment depends on the structure and composition of the materials and on the prevailing thermodynamic conditions during their formations. Different colorations in the same mineral group may arise from ions with the same oxidation state and substituted site: for instance, Cr^{3+} in octahedral sites may give rise to purple, red or green colors depending on the mineral structure and composition.

Naturally multi-faceted garnets form wide solid-solutions with each other and captivate people with their incomparable range of colors (from green to orange and red) which are largely controlled by the crystal chemistry of substituted transition elements (Galoisy, 2013). The variations of colors and hues of garnets are related to the presence of coloring elements such as Fe, Mn, Cr, V, Ti substituted in the structure of garnet minerals between various end-members $A_3B_2(SiO_4)$. Spectroscopic techniques (UV-Visible-Near IR spectroscopy, Electron Paramagnetic Resonance and X-ray Absorption Spectroscopy) demonstrate how the nature and concentration of these cations explain the color variation in the various structures. The recent evidence of a structural relaxation around octahedral Cr^{3+} substituted in garnets and spinels demonstrates the role played by mineral chemistry in defining the actual crystal field responsible for the green or red color in these mineral groups (Juhin et al., 2007, 2008).

The structural studies of glasses have largely beneficiated from such data obtained on a broad range of minerals. The environment of cations in multicomponent silicate, aluminosilicate and borosilicate glasses has been investigated with the same spectroscopic methods as in minerals. These data give either a description of the geometry and symmetry of the cationic site, including the nature of the chemical bond, or a chemically resolved radial distribution function. In glasses, the coordination numbers of transition elements are often lower than in the corresponding crystalline compounds. Cations exhibit several original structural properties in oxide glasses. Transition elements such as Ni or Ti may occur in unusual 5-coordinated sites

that may coexist with other coordination numbers, depending on glass composition (Galoisy et al., 2005). The environment of cations such as Zn, Zr or Mo is discussed using the bond valence theory, which predicts the way to charge compensate the oxygen neighbors and which indicates the linkage of cationic sites with the silicate framework (Calas et al., 2003). The modification of crystal field spectra of octahedral Cr^{3+} in glasses as a function of temperature, has been followed up to 800 K. Using the dependence of crystal field splitting energy on cation-oxygen distances, local thermal expansion coefficients (TEC) can be extracted from in-situ spectroscopic measurements. Site (microscopic) TEC values obtained in glasses are different from the macroscopic thermal expansion of the glass, and similar to those observed in crystals (Calas et al., 2006). Concerning medium range order, unique information has been obtained by EXAFS spectroscopy. These data lend support that cations are located in domains extending up to more than 8 Å radius, in which cationic polyhedra may be linked together either by edges or by corners. In low alkali borate and borosilicate glasses, transition elements such as Co, Ni, Zn are located in these peculiar highly ordered domains, that may arise from the presence of rigid borate super-units (Galoisy et al., 2001). In magmatic silicate systems, the determination of the sites occupied by Fe in its different oxidation states, allows to rationalize the chemical dependence of redox equilibria, which is the way to predict Fe behavior. This provides information on the physico-chemical conditions prevailing at the magmatic stage as well as on the cooling conditions of the magma. In natural glasses such as obsidians, the presence of Fe-oxide nanoclusters, suspected from EPR spectroscopy, is confirmed by variable- temperature UV-visible-Near IR spectroscopy. Intervalence charge transfers (IVCT), are characterized by a spectacular increase of intensity with a lowering of the temperature from ambient to 10K. These clusters, showing a specific local arrangement around Fe, are related to the cooling history of the glass, as they are not found in synthetic glasses (Sakaguchi and Uchino, 2007). They may be precursors of amorphous and crystalline Fe-oxides (Ti-magnetite and magnetite), 5-10 nm large, evidenced using Transmission Electron Microscopy.

References

Calas G., Le Grand M., Galoisy L. and Ghaleb D. (2003) - Structural role of molybdenum in nuclear glasses: an EXAFS Study. *Journal of Nuclear Materials*, 322, 15-20.

Calas G., Majérus O., Galoisy L. and Cormier L. (2006) - Determination of the thermal expansion of Cr^{3+} sites in glasses. *Applied Physics Letters*, 88, 121918.

Galoisy L., Cormier L., Calas G. and Briois V. (2001) - Environment of Ni, Co and Zn in low alkali borate glasses: information from EXAFS and XANES spectra. *Journal of non crystalline solids*, 293-295, 105-111.

Galoisy L., Calas G., Cormier L., Marcq B. and Thibault M.H. (2005) - Overview of the environment of Ni in oxide glasses in relation to glass colouration. *Physics and Chemistry of Glasses*, 46(4), 394-399.

Galoisy L. (2013) - Garnets: from stone to star. *Elements Magazine*, 9, 453-456.

Juhin A., Calas G., Cabaret D., Galoisy L. and Hazemann J.L. (2007) - Structural relaxation around substitutional Cr^{3+} in $MgAl_2O_4$. *Physical Review B*, 76(5), 054105.

Juhin A., Calas G., Cabaret D., Galoisy L. and Hazemann J.L (2008) - Structural relaxation around substitutional Cr^{3+} in pyrope garnet. *American Mineralogist*, 93, 800–80.

Sakaguchi K. and Uchino T. (2007) - Compositional dependence of infrared absorption of iron-doped silicate glasses. *Journal of Non-crystalline Solids*, 353,4753–4761.

Periodico di Mineralogia, ECMS 2015, 5-6

PERIODICO di MINERALOGIA
established in 1930

An International Journal of
MINERALOGY, CRYSTALLOGRAPHY, GEOCHEMISTRY, ORE DEPOSITS, PETROLOGY, VOLCANOLOGY
and applied topics on *Environment*, *Archaeometry* and *Cultural Heritage*

Empirical electronic polarizabilities in oxides, hydroxides, oxyfluorides and oxychlorides

Robert D. Shannon[1,*] and Reinhard X. Fischer[2]

[1]Geological Sciences/ CIRES, University of Colorado, Boulder, Colorado 80309
[2]Universität Bremen, FB 5 Geowissenschaften, Klagenfurter Str., D-28359 Bremen (Germany)
*Corresponding author: *bob@theshannons.net*

An extensive set of refractive indices was determined at λ = 589.3 nm (n_D) from 2385 measurements on approximately 1150 minerals and 675 synthetic compounds. Included in that number were ~200 F-containing compounds, 65 Cl-containing compounds, 500 non-hydrogen-bonded hydroxyl-containing compounds, approximately 175 moderately strong hydrogen-bonded hydroxyl-containing compounds and 35 minerals with very strong H-bonded hydroxides. Also included were 105 carbonates, 18 nitrates, ~230 sulfates and 14 perchlorates. Some of the measurements (560) were on 2 or more samples of minerals or oxides with the same or similar compositions so there were actually only 1825 different minerals and synthetic compounds whose refractive indices had been determined. Compounds and minerals containing the lone-pair ions, Tl^{+}, Sn^{2+}, Pb^{2+}, As^{3+}, Sb^{3+}, Bi^{3+}, S^{4+}, Se^{4+}, Te^{4+}, Cl^{5+}, Br^{5+}, I^{5+}, and uranyl ions U^{6+} , as well as most zeolites, were deleted.

These data, using the Gladstone-Dale-Eggleton relationship (Eggleton, 1991):

$$\alpha_T = \frac{(n_D^2 - 1)V_m}{4\pi + \left(\frac{4\pi}{3} - c\right)(n_D^2 - 1)}$$

where α_T = the total polarizability of a mineral or synthetic compound, n_D= the refractive index at λ = 589.3 nm, V_m = molar volume in Å^3, and c = 2.26 (electron-overlap factor approximating the Gladstone-Dale relationship), in conjunction with the polarizability additivity rule and a least-squares procedure, were used to obtain electronic polarizabilities for 73 cations in various coordinations, H_2O, $5H_xO_y$ species [$(H_3O)^+$, $(H_5O_2)^+$, $(H_3O_2)^-$, $(H_4O_4)^{4-}$, $(H_7O_4)^-$] and 4 anions (F^-, Cl^-, OH^-, O^{2-}). As in a previous publication, we modified the light-scattering (LS) model by Jemmer, Fowler, Wilson, and Madden (1998) to give the expression:

$$\alpha(CN) = \left(a_1' + a_2' \cdot CN_{ca} \cdot e^{-a_3' \cdot CN}\right)^{-1}$$

where CN_{ca}= the number of nearest-neighbor ions (cation-anion interactions), and a_1, a_2, and a_3 are least squares parameters (Shannon and Fischer, 2006). This expression provides for a smooth decrease in polarizability at low CN's to near free-cation values at infinite CN's (infinite distance) and allowed fitting polarizability values for Li , Na, K, Rb, Cs, Mg, Ca, Sr, Ba, Mn, Fe, Y, (Lu → La), Zr and Th. This refinement process excluded zeolites and compounds with (1) structures containing lone-pair and uranyl ions, (2) sterically-strained (SS) structures, (3) corner-shared octahedral (CSO) network and chain structures such as perovskites, tungsten bronzes and titanite-related structures, (4) edge-shared Fe^{3+} and Mn^{3+} structures (ESO) such as piemontite and pumpellyite and (5) compounds exhibiting fast-ion conductivity. The refinement for 2385 polarizability values using 73 cation polarizabilities with values for Li, Na, K, Rb, Cs, Ag, Mg, Ca, Sr, Ba, Mn, Fe^{2+}, Co, Cu, Zn, B, Al, Ga, Fe^{3+}, Sc, Y, Lu→La, Si, Ge, Ti, Th and V^{5+}in varying CN's, yields a standard deviation of the least squares fit of 0.25(corresponding to a correlation coefficient R^2 of 0.9997) and no discrepancies between observed and calculated polarizabilities > 3%.

Systematic discrepancies are associated with compounds (not included in the refinement used to obtain polarizability values) having SS, CSO, ESO and structures that support fast-ion conductivity. Underbonded cations lead to augmented cation polarizabilities that result in increased observed total calculated polarizabilities. Examples are Ca in mayenite [$Ca_{12}Al_{14}O_{33}$] and K in $K_6Si_3O_9$ with deviations, Δ, of observed from total calculated polarizability of ~+7% and +4.7%, respectively. Conversely, overbonded cations in anhydrite [$CaSO_4$], kieserite [$MgSO_4$. H_2O], and langbeinite [$K_2Mg_2(SO_4)_3$] lead to diminished cation polarizabilities and deviations of observed from total calculated polarizabilities of -3.5% , -3.6 and -4.1%, respectively. Octahedral face- , corner-, and edge-sharing and Mn^+-O^{2-}-Mn^+ one-dimensional chains lead to enhanced covalency accompanying the M *nd* – O *2p* hybridization that, in turn, leads to augmented total polarizabilities and refractive indices. Values of Δ, up to 10%, are found in perovskite compounds such as $SrTiO_3$.

References

Eggleton R.A. (1991) - Gladstone-Dale constants for the major elements in silicates: coordination number, polarizability, and the Lorentz-Lorentz relation. *Canadian Mineralogist*, 29, 525-532.

Jemmer P., Fowler P.W. and Wilson, M. and Madden P.A. (1998) -Variation with lattice parameter and coordination number. *Journal of Physical Chemistry*, A102, 8377-8385.

Shannon R.D. and Fischer R.X. (2006) - Empirical electronic polarizabilities in oxides, hydroxides, oxyfluorides, and oxychlorides. *Physical Review*, B73, 235111, 1-28.

Periodico di Mineralogia, ECMS 2015, 7-8

PERIODICO di MINERALOGIA
established in 1930

An International Journal of
MINERALOGY, CRYSTALLOGRAPHY, GEOCHEMISTRY,
ORE DEPOSITS, PETROLOGY, VOLCANOLOGY
and applied topics on *Environment*, *Archaeometry* and *Cultural Heritage*

FTIR spectroscopy at HT: applications and problems

Giancarlo Della Ventura[1,2]

[1]Dipartimento di Scienze, Università Roma Tre, I-00146 Roma.
[2]INFN-LNF, I-00044 Frascati (Rome)
Corresponding author: giancarlo.dellaventura@uniroma3.it

Most natural (geologic/geophysic) and technical/industrial processes do involve HT phenomena such as dehydration/dehydroxylation, chemical transformations and phase-transitions which need to be characterized by using combinations of *in situ* analytical methods, such as TG/DTA, HT-SC-XRD, and HT spectroscopies.

As one of the most sensitive techniques for hydrous species, FTIR spectroscopy has been widely used in high-T materials research; experiments have been typically done by measuring the absorbance as a function of evolving temperatures and relating the intensity changes to evolving amounts of the target molecule(s). However several studies done in the last decade (Zhang et al., 2007, 2010, Tokiwai and Nakashima, 2010) have shown that the temperature dependencies of OH bands obtained from *in situ* IR experiments are significantly different from those obtained from quench experiments. More recently Radica et al. (2015) have shown that this is the case also for CO_2 (Fig. 1).

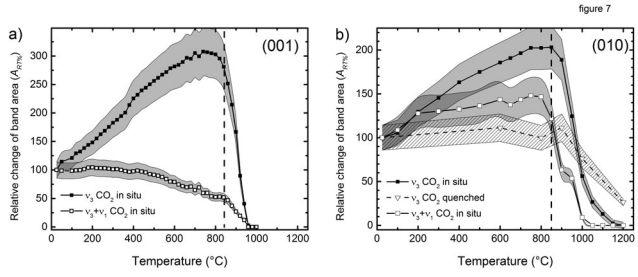

Figure 1. In situ *vs* quenched CO_2 absorbance as a function of increasing T, measured for different modes and crystal sections (from Radica et al., 2015).

The most important drawback of these findings is that the constant of proportionality between measured absorbance and concentration of the target molecule in the Beer-Lambert equation (the molar absorption coefficient, ε) is also dependent on temperature; hence, this dependence must be properly calibrated if the spectroscopic data are to be used for quantitative studies. An additional source of complexity in this issue arises from the observation that the

dependence of the absorbance on T can be extremely different for the different vibrational modes in the same sample (e.g. Zhang et al., 2007).

One of the principal applications of HT-FTIR spectroscopy in Materials Science is the study of diffusion processes and measurement of diffusion coefficients in minerals and glasses. With this respect, recent results have shown that the mechanisms wereby hydrous species migrate across the studied materials are far from being understood; this is true for simple (and deeply studied) structures such as the phyllosilicates, where the escape pathway is relatively well defined (Zhang et al., 2006), but is much more complex in minerals where the proton release is associated with local structural/electronic rearrangements, such as oxidation of multivalence elements (e.g. Susta et al., 2015) or charge-transfer phenomena (Taran and Koch-Müller, 2013).

This presentation will review existing data on HT-FTIR study, and will underline both advantages and problems of this technique. New data collected by our group on several H_2O/OH and CO_2 will be described, and the use of HT spectroscopy in diffusion studies will be presented and discussed. Recent tests done by using *in situ* FTIR-FPA imaging techniques (Della Ventura et al., 2014) in HT experiments will be finally shown.

References

Della Ventura G., Marcelli A., Bellatreccia F. (2014) - SR-FTIR microscopy and FTIR imaging in the Earth Sciences. *Reviews in Mineralogy and Geochemistry*, 78, 447-479.

Radica F., Della Ventura G., Bellatreccia F., Cestelli Guidi M. (2015) - HT-FTIR microspectroscopy of cordierite: the CO_2 absorbance from in situ and quench experiments. *Physics and Chemistry of Minerals*, submitted.

Susta U., Della Ventura G., Bellatreccia F., Hawthorne F.C., Boiocchi M., Oberti R. (2015) - HT-FTIR spectroscopy of riebeckite. *Periodico di Mineralogia*, ECMS 2015, 167-168.

Taran M.N. and Koch-Müller M. (2013) - FTIR spectroscopic study of natural andalusite showing electronic Fe-Ti charge transfer processes: zoning and thermal evolution of OH-vibration bands. *Physics and Chemistry of Minerals*, 40, 63-71.

Tokiwai K., and Nakashima S. (2010) - Integral molar absorptivities of OH in muscovite at 20 to 650°C by in-situ high-temperature IR microspectroscopy. *American Mineralogist,* 95, 1052-1059.

Zhang M., Hui Q., Lou X.J., Redfern S.A.T., Salje E.K.H., Tarantino, S. (2006) - Dehydroxylation, proton migration, and structural changes in heated talc: An infrared spectroscopic study. *American Mineralogist,* 91, 816-825.

Zhang M., Salje E.K.H., Carpenter M.A., Wang J.Y., Groat L.A., Lager G.A., Wang L., Beran A., Bismayer U. (2007) - Temperature dependence of IR absorption of hydrous/hydroxyl species in minerals and synthetic materials. *American Mineralogist,* 92, 1502-1517.

Zhang M., Redfern S.A.T., Salje E.K.H., Carpenter M.A., Hayward C.L. (2010) - Thermal behavior of vibrational phonons and hydroxyls of muscovite in dehydroxylation: in situ high-temperature infrared spectroscopic investigations. *American Mineralogist,* 95, 1444-1457.

Periodico di Mineralogia, ECMS 2015, 9-10

PERIODICO di MINERALOGIA
established in 1930

An International Journal of
MINERALOGY, CRYSTALLOGRAPHY, GEOCHEMISTRY,
ORE DEPOSITS, PETROLOGY, VOLCANOLOGY
and applied topics on *Environment*, *Archaeometry* and *Cultural Heritage*

DFT-based calculations for the interpretation of mineral spectra

Björn Winkler[1,*] and Victor Milman[2]

[1] Goethe University, Institute of Geosciences, Altenhoeferallee 1, D-60438 Frankfurt a.M. Germany
[2] Dassault Systemes, BIOVIA Ltd. 334 Cambridge Science Park, Cambridge CB4 0WN, UK
* Corresponding author: *b.winkler@kristall.uni-frankfurt.de*

The identification of minerals, and the study of their structure-property relations generally requires both a characterisation of the long range ordered arrangement of atoms by diffraction and the investigation of local environments, bond strengths and excited states by spectroscopic methods. While the quantitative interpretation of diffraction pattern has been established more than 100 years ago, the development of generally applicable, predictive and quantitative models for the interpretation of mineral spectra is more recent and closely linked to the development of mature codes to study crystals based on density functional theory.

While the theoretical foundations for lattice dynamics, which are probed by infrared and Raman spectroscopy and inelastic X-ray and neutron scattering studies, have long been established (Born and Huang, 1954) it was only with the advent of DFT-based models that predictive calculations for complex structures became possible. Initially, these studies were restricted to the derivation of the interatomic forces by imposing a known displacement vector, calculating the energy changes and then obtaining the frequencies. Today, "linear response"- (Baroni et al., 2001) or "finite displacement"-based methods allow us to obtain vibrational spectra and phonon dispersion curves of complex silicates and related structures with very good accuracy. These calculations can be expanded to understand the effect of particle shape (Balan et al., 2001) or the influence of anharmonicity. They also form the basis to model thermal diffuse scattering (Bosak et al., 2012). The phonon density of states, which can be obtained from the lattice dynamical calculations can be used to accurately compute the enthalpies and entropies of crystals.

Other applications of DFT-based calculations employed to quantitatively interpret mineral spectra include the prediction of electric field gradients, NMR spectra and core-level electron energy loss spectra (Milman et al., 2010; Winkler et al., 2013), all of which are determined by the local environment around the target atom. Predicted elastic stiffness coefficients are often required for a quantitative interpretation of resonant ultrasound spectra (e.g. Arbeck et al., 2012).

In summary, the availability of mature implementations of DFT, in conjunction with pow-

erful computers, now allows the prediction and interpretation of a large variety of spectra, and thus helps to better understand structure-property relations of complex materials.

References

Arbeck D., Haussuehl E., Vinograd V.L., Winkler B., Paulsen N., Haussuehl S., Milman V. and Gale J.D. (2012) - Elastic stiffness coefficients of thenardite and their pressure and temperature dependence. *Zeitschrift für Kristallographie*, 227, 503-513.

Balan E., Saitta A.M., Mauri F. and Calas G. (2001) - First-principles modeling of the infrared spectrum of kaolinite. *American Mineralogist*, 86, 1321-1330.

Baroni S., de Gironcoli S., Dal Corso A. and Giannozzi P (2001) - Phonons and related crystal properties from density-functional perturbation theory. *Reviews Of Modern Physics*, 73, 515-562.

Born M. and Huang K. (1954) Dynamical Theory of Crystal Lattices. Oxford Claredon Press.

Bosak A., Krisch M., Chernyshov D., Winkler B., Milman V., Refson K. and Schulze-Briese C. (2012) - New insights into the lattice dynamics of alpha-quartz. *Zeitschrift für Kristallographie*, 227, 84-91.

Milman V., Refson K., Clark S., Pickard C., Yates J., Gao S., Hasnip P., Probert M., Perlov A. and Segall M. (2010) - Electron and vibrational spectroscopies using DFT, plane waves and pseudopotentials: CASTEP implementation. *Journal of Molecular Structure: THEOCHEM*, 954, 22-35.

Winkler B., Avalos-Borja M., Milman V., Perlov A., Pickard C.J. and Yates J.R. (2013) - Oxygen K-edge electron energy loss spectra of hydrous and anhydrous compounds. *Journal of Physics-Condensed Matter,* 25, 485401.

Periodico di Mineralogia, ECMS 2015, 11

PERIODICO di MINERALOGIA
established in 1930

An International Journal of
MINERALOGY, CRYSTALLOGRAPHY, GEOCHEMISTRY,
ORE DEPOSITS, PETROLOGY, VOLCANOLOGY
and applied topics on *Environment*, *Archaeometry* and *Cultural Heritage*

Magnetism meets Mössbauer spectroscopy and the stories they tell

Catherine McCammon*

Bayerisches Geoinstitut, Universität Bayreuth, 95440 Bayreuth, Germany
* Corresponding author: *catherine.mccammon@uni-bayreuth.de*

The concept of magnetism has been around for thousands of years, dating back at least to ancient Greece and the lodestones and other ores from the Magnesia region that gave its name to magnets and magnetite as well as the elements magnesium and manganese. Magnetic materials are all around us and nearly every material is influenced in some way by magnetic fields, described by their magnetic properties that provide a metric for their response. While libraries are full of volumes describing methodologies for sensing magnetic fields and measuring magnetic properties, surprisingly few involve any significant focus on spectroscopy.

Mössbauer spectroscopy is a modern concept dating back to the 1950s and the doctoral thesis of Rudolf Mössbauer that described the recoil-free resonant absorption of gamma rays by a nucleus that is sensitive to its nuclear environment (in particular the electrons). The method is so sensitive that movement of a gamma ray source by mere millimetres per second using the Doppler effect is sufficient to sweep through the energies of all interactions of an iron nucleus with its electrons. These include the magnetic dipole interaction of the nuclear magnetic moment with internal magnetic fields arising from magnetically ordered systems or paramagnetic systems with long relaxation times, as well as externally applied magnetic fields. Advantages of Mössbauer spectroscopy over more conventional methods to monitor magnetic properties include its isotope-specificity that provides a discrimination of the magnetic signal from iron-containing phases, even when they are vastly outnumbered by other phases (both magnetic and non-magnetic) in the assemblage, and the possibility to monitor magnetic interactions at extreme conditions, in particular pressure and temperature.

My plenary talk will focus on two stories at the interface of magnetism and Mössbauer spectroscopy, each one highlighting a special advantage. The first involves tiny grains of ilmeno-hematite in metamorphic rocks that provide a new tool for mineral-based magnetic anomaly interpretation on Earth and other planetary bodies, while the second involves measurements to more than 100 GPa in a laser-heated diamond anvil cell with new constraints on the nature of the light element in the Earth's core, the source of the magnetic field that protects us from the harmful effects of the solar wind.

Contributions

Periodico di Mineralogia, ECMS 2015, 15-16

PERIODICO di MINERALOGIA
established in 1930

An International Journal of
MINERALOGY, CRYSTALLOGRAPHY, GEOCHEMISTRY,
ORE DEPOSITS, PETROLOGY, VOLCANOLOGY
and applied topics on *Environment*, *Archaeometry* and *Cultural Heritage*

Innovative micro-Laser Induced Breakdown Spectroscopy of Enstatite Chondrites: preliminary data of Sahara 97072 EH3

Giovanna Agrosì[1], Paola Manzari[2], Giorgio S. Senesi[3] and GioacchinoTempesta[1,*]

[1]Dipartimento di Scienze della Terra e Geoambientali (DiSTeGeo), University of Bari, Via E. Orabona 4, 70125 Bari, Italy
[2]Istituto Nazionale di Astrofisica - Istituto di Astrofisica e Planetologia Spaziali (INAF-IAPS), via Fosso del Cavaliere 100, Roma, Italy
[3]Istituto di Nanotecnologia (NANOTEC) – CNR, Via Amendola 122, 70126 Bari, Italy
* Corresponding author: *gioacchino.tempesta@uniba.it*

The study of enstatite chondrites (ECs) may play an important role in understanding the evolution of Earth, inner Solar System and asteroid belt. ECs are very scarce among chondritic meteorites. The chemical composition of their silicates, sulphides and metals reflect their formation under highly reducing conditions. Most ECs are completely dry and lack any evidence of hydrous alteration, thus ECs were formed likely within the snow line and are good candidates to be considered the building blocks of inner planets, like Mercury. ECs represent the most reduced group among chondrites, featuring enstatite chondrules (FeO < 1 wt%), low olivine content, Fe-Ni alloy, and oxygen isotopic ratios that match the terrestrial fractionation line (TFL) and are subdivided in two groups: EH and EL, i.e. high and low Fe-metal content, respectively (Keil, 1968).

In this work a thin section of the EC labelled Sahara 97072 EH3 previously investigated by multi-analytical approach (Manzari, 2010), was studied by means of Laser Induced Breakdown Spectroscopy (LIBS). LIBS advantages with respect to conventional analytical techniques are: simultaneous multi-element qualitative and quantitative analysis in real time, high sensitivity, stratigraphic analysis of a sample by profiling, especially sensitive to light elements such as C, B, Be, H and Li, no need of an analytical chamber, sampling and surface treatment (Senesi, 2014). Recently, the potentiality of LIBS was exploited even in remote elemental analysis of extraterrestrial rocks. LIBS technique was installed onboard of NASA Mars Science Laboratory rover named Curiosity, as part of ChemCam to provide chemical analyses on Martian rocks (Wiens et al., 2013; Gordon et al., 2014). In this study, an innovative LIBS prototype (Fig. 1a), operating with a Nd:YAG laser in double pulse configuration, was used coupled with a petrographic microscope (micro-LIBS) that allows chemical investigations directly on the thin section (Fig. 1b). This innovative approach enables to perform chemical analyses preserving a

qualitative knowledge of the phases in a thin section taking into account the distribution of the grains, the texture and any preferred orientations at the microscale. In particular, qualitative micro-LIBS data (Fig. 1c) of metal-sulfide-nodules consisting of kamacite Fe, Ni, Cr-troilite, and oldhamite CaS resulted in good agreement with data previously obtained by SEM-EDS.

Future investigations on martian meteorites using micro-LIBS will be carried out to validate the data obtained in remote mode by ChemCam.

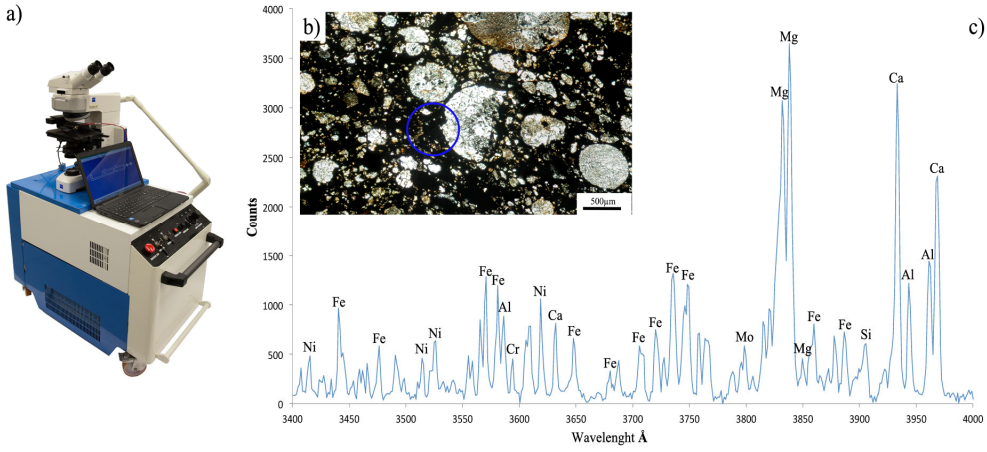

Fig. 1: a) Laser Induced Breakdown Spectroscopy (LIBS) Modì prototype coupled with a microscope; b) thin section of Sahara 97072 EH3. The blue circle show where the spectrum was acquired; c) LIBS emission spectrum of Sahara 97072 EH3 analysed in the spectral range: 340–400 nm.

References

Gordon S.R., Newsom H.E., Agee C.B., Clegg S.M., Lasue J., Wiens R.C., Santos A.R., and the MSL team (2014) - A preliminary study comparing LIBS on martian meteorite NWA 7034 and ChemCam data, Eighth international conference on Mars, Pasadena, California, 1047.

Keil K. (1968) - Mineralogical and chemical relationships among enstatite chondrites, *Journal of Geophysical Research*, 73, 22, 6945–6976.

Manzari P. (2010) - Investigation of Enstatite Chondrites: Mineralogical and Chemical Features of EH3 and EL3 Chondrules, PhD thesis, University of Bari (Italy).

Senesi G.S. (2014) - Laser-Induced Breakdown Spectroscopy (LIBS) applied to terrestrial and extraterrestrial analogue geomaterials with emphasis to minerals and rocks, *Earth-Science Reviews*, 139, 231–267.

Wiens, R.C., Maurice, S., Lasue, J., Forni, O., Anderson, R.B., Clegg, S., Bender, S., Blaney, D., Barraclough, B.L., Cousin, A., Deflores, L., Delapp, D., Dyar, M.D., Fabre, C., Gasnault, O., Lanza, N., Mazoyer, J., Melikechi, N., Meslin, P.-Y., Newsom, H., Ollila, A., Perez, R., Tokar, R.L., Vaniman, D. (2013) - Pre-flight calibration and initial data processing for the ChemCam laser-induced breakdown spectroscopy instrument on the Mars Science Laboratory rover. *Spectrochimica Acta B*, 82, 1–27.

Periodico di Mineralogia, ECMS 2015, 17-18

PERIODICO di MINERALOGIA
established in 1930

An International Journal of
MINERALOGY, CRYSTALLOGRAPHY, GEOCHEMISTRY,
ORE DEPOSITS, PETROLOGY, VOLCANOLOGY
and applied topics on *Environment*, *Archaeometry* and *Cultural Heritage*

Characterization of plagioclase solid solution by Raman spectroscopy: a procedure for the determination of the chemical composition

Irene Aliatis[1*], Erica Lambruschi[1], Luciana Mantovani[1], Artur Benisek[2], Danilo Bersani[1], Michael A. Carpenter[3]; Diego G. Gatta[4], Mario Tribaudino[1] and Pier Paolo Lottici[1]

[1] Università di Parma, Dipartimento di Fisica e Scienze della Terra, Parco Area delle Scienze 7/A, 43124 Parma, Italy
[2] Universitaet Salzburg, Materialforschung und Physik, Hellbrunnerstr. 34, 5020 Salzburg, Austria
[3] University of Cambridge, Department of Earth Sciences, Downing Street, Cambridge CB2 3EQ, UK
[4] Università degli Studi di Milano, Dipart. di Scienze della Terra, Via Botticelli 23, 20133 Milano, IT
* Corresponding author: *irene.aliatis@difest.unipr.it*

Plagioclases are framework silicates occurring in planetary crusts: on Earth they are the most common rock-forming minerals of igneous, metamorphic and sedimentary rocks, the most abundant minerals on the Moon and widespread in basaltic rocks on Mars and in asteroids like Vesta. Plagioclases are involved in several key reactions of petrologic interest, as igneous and metamorphic reactions. Plagioclases can be described as a solid solution ranging from the Na-endmember, albite ($NaAlSi_3O_8$), to the Ca-endmember, anorthite ($CaAl_2Si_2O_8$), in which the Si:Al ratio varies.

The investigation of their chemical composition is a key-point to understand the petrologic evolution of the parent rocks. EDS or WDS chemical analyses or laser ablation are common techniques used to get information about plagioclase composition. They require the preparation of the sample and are time-consuming and expensive.

In this work, we propose Raman spectroscopy as a procedure to gain chemical information from plagioclases. A similar approach has already been applied to different classes of minerals as garnets, amphiboles and serpentine group. Unlike the aforementioned minerals, the major problem in plagioclases is their mixing behaviour which is complicated by the various compositional-driven phase transitions and by the Al,Si ordering. Over most of the compositional range, plagioclases have the collapsed $C\bar{1}$ structure with no Al,Si order (*i.e.* the high albite structure), whereas on the anorthite-rich side the solid solution has the $I\bar{1}$ structure due to the increasing tendency to Al,Si ordering. The complete order with strictly alternating Al,Si is achieved only in pure anorthite.

The most comprehensive Raman investigation on feldspars (Freeman et al., 2008) led to a classification of the major structural types without a detailed study of the changes of the Raman features within the plagioclase composition. We performed Raman investigation on a series of well characterized plagioclases, previously analysed by powder-XRD, TEM, IR spectroscopy and calorimetry (Carpenter et al., 1985; Tribaudino et al., 2010; Atkinson et al., 1999;

Benisek et al., 2013). The samples consist of 20 homogeneous purified natural, low structural state plagioclases, showing the highest degree of Al,Si order possible for each composition. The chemical composition ranges from An_0 to An_{100}.

The difference in Raman wavenumber between the two major peaks (I_a and I_b) of the plagioclases is here proposed to be indicative of their composition in terms of An composition. From Fig. 1 (*left side*), where I_a and I_b differences are plotted *vs*. the An content, it is possible to directly read the composition for the An-rich terms (An > 60%). In order to obtain compositional information for Ab-rich plagioclases too, we need to plot I_a and I_b differences *vs*. the linewidth of the most intense Raman mode w(I_a), as shown in Fig. 1 (*right side*). We point out that the dependence of the composition from the linewidth can be obtained only for ordered plagioclases. For that reason, the composition of disordered Ab-rich plagioclases cannot be correctly obtained with this method. Both methods have been tested on three different mineralogical case studies: plagioclase crystals found in Juvinas eucrite meteorite, anorthite crystals into a CAI inclusion within the Renazzo carbonaceous chondrite meteorite, and plagioclase crystals with heterogeneous chemical composition from the Marsili volcano. The "Raman chemical compositions" suggested by our methods are in good agreement with the chemical analyses for plagioclase samples with An content > 60 mol%. The methods fail for disordered albite-rich samples where the contribution to the linewidth by the disorder is unknown.

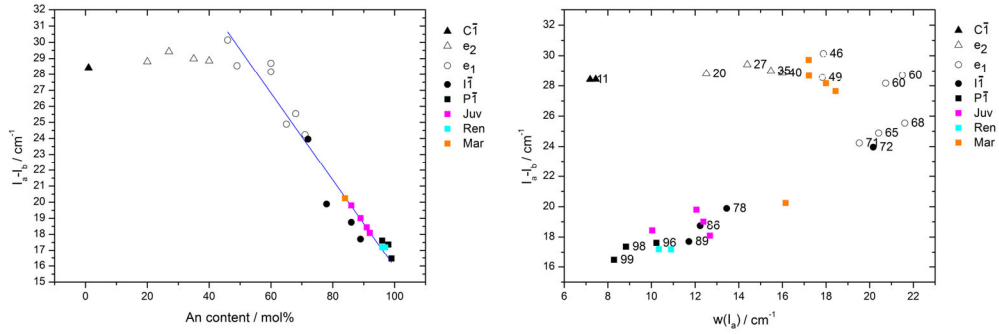

Fig. 1: Wavenumber differences I_a-I_b versus the An content (*left side*) and versus the linewidth of the most intense Raman mode w(I_a) (*right side*). Coloured squares refer to the case studies.

References

Atkinson A.J., Carpenter M.A. and Salje E.K.H. (1999) - Hard mode infrared spectroscopy of plagioclase feldspars. *European Journal of Mineralogy*, 11, 7-21.

Benisek A., Dachs E. and Carpenter M.A. (2013) - Heat capacity and entropy of low structural state plagioclases. *Physics and Chemistry of Minerals* 40, 167-173.

Carpenter M.A., McConnell J.D.C and Navrotsky A. (1985) - Enthalpies of ordering in the plagioclase feldspar solid solution. *Geochimica et Cosmochimica Acta*, 49, 947-966.

Freeman J.J., Wang A., Kuebler K.E., Jollif B.L. and Haskin L.A. (2008) - Characterization of natural feldspars by Raman spectroscopy for future planetary exploration. *Canadian Mineralogist*, 46, 1477-1500.

Tribaudino M., Angel R. J., Camara F., Nestola F., Pasqual D. and Margiolaki I. (2010) - Thermal expansion of plagioclase feldspars. *Contributions to Mineralogy Petrology,* 160, 899-908.

Periodico di Mineralogia, ECMS 2015, 19-20

PERIODICO di MINERALOGIA
established in 1930

An International Journal of
MINERALOGY, CRYSTALLOGRAPHY, GEOCHEMISTRY,
ORE DEPOSITS, PETROLOGY, VOLCANOLOGY
and applied topics on *Environment*, *Archaeometry* and *Cultural Heritage*

Crystal chemistry of "$Li_7La_3Zr_2O_{12}$" garnet doped with Al, Ga, and Fe: a review of NMR- and Mössbauer spectroscopy studies

Georg Amthauer[1,*], Julia Langer[2], Maria Elisabeth Meyer[1], Daniel Rettenwander[1], Reinhard Wagner[1] and Martin Wilkening[2]

[1]Department of Materials Research and Physics, University of Salzburg, Austria
[2]Institute for Chemistry and Technology of Materials, Graz University of Technology, Austria
*Corresponding author: *georg.amthauer@sbg.ac.at*

Recent research has shown that certain Li-oxide garnets with more than 3 Li atoms per formula unit, such as $Li_7La_3Zr_2O_{12}$, have high ionic conductivities, as well as good chemical and physical properties for use in solid-state batteries (Murugan et al., 2007).

"Garnet" is the common name for a large number of natural and synthetic metal-oxide phases. Conventional oxide garnets have the general formula $A_3B_2C_3O_{12}$ and crystallize in the cubic space group $Ia\bar{3}d$. The O^{2-} ions, in the general crystallographic positions 96*h*, form an oxygen-atom framework with interstices occupied by the A cations, such as Ca^{2+}, Fe^{2+}, Y^{3+}, La^{3+} in the 8-fold coordinated position 24*c* (point symmetry 222), the B cations, such as Al^{3+}, Fe^{3+}, Zr^{4+}, Sn^{4+}, Sb^{5+}, etc. in the 6-fold coordinated position 16*a* (point symmetry -3), and the C cations, such as Li^{+}, Al^{3+}, Fe^{3+}, Ga^{3+}, Ti^{4+}, Si^{4+}, etc. in the 4-fold coordinated 24*d* position (point symmetry $\bar{4}$). In addition to these cation sites, there are other interstices within the oxygen framework, which are empty in the conventional garnet structure, e.g. (i) the 6-fold coordinated 16*b* positions with point symmetry 32, (ii) the 6-fold coordinated 48*g* positions with point symmetry 2, and (iii) an additional 4-fold coordinated 96*h* position with point symmetry 1 (Hellner et al., 1979). In "$Li_7La_3Zr_2O_{12}$" garnet (LLZO)**,** these interstices are filled by "excess" Li^{+} ions giving rise to the excellent ionic conductivity.

There is a low temperature tetragonal modification of pure LLZO (SG: $I4_1/acd$) and a high temperature non quenchable cubic phase of LLZO (SG: $Ia\bar{3}d$). The tetragonal phase has a distinctly lower ion conductivity than the cubic phase. Fortunately, the cubic phase can be stabilized at low temperatures by doping with low amounts of Al, Ga, and Fe (Buschmann et al., 2011; Geiger et al., 2011; Rettenwander et al., 2014a, 2014b, 2015). In our contribution the results of Mössbauer studies on ^{57}Fe as well as of NMR studies on ^{27}Al and ^{71}Ga in LLZO will be presented, compared and discussed with special regard to their crystal chemical role for the ionic conductivity.

References

Buschmann H., Dölle J., Berendts S., Kuhn A., Bottke P., Wilkening M., Heitjans P., Senyshyn A., Ehrenberg H. and Lotnyk, A. (2011) – Structure and dynamics of the fast lithium ion conductor „$Li_7La_3Zr_2O_{12}$". *Physical Chemistry and Chemical Physics,* 13, 19378-19392.

Geiger C.A., Alekseev E., Lazic B., Fisch M., Armbruster T., Langner R., Fechtelkord M., Kim N., Pettke T. and Weppner, W. (2011) – Crystal chemistry and stability of „$Li_7La_3Zr_2O_{12}$" garnet: A fast lithium-ion conductor. *Inorganic Chemistry*, 50, 1089-1097.

Hellner E., Gerlich R., Koch E. and Fischer W. (1979) - The oxygen framework in garnet and its occurence in $Na_3Al_2Li_3F_{12}$, $Ca_3Al_2(OH)_{12}$, $RhBi_4$ and Hg_3TeO_6. *Physics Data Fachinformationszentrum Energie, Physik, Mathematik, Karlsruhe*, Germany, 16-1, 1-31.

Murugan R., Thangadurai V. and Weppner W. (2007) - Fast Lithium ion conduction in garnet-type $Li_7La_3Zr_2O_{12}$. *Angewandte Chemie International Edition*, 46, 7778-7781.

Rettenwander D., Blaha P., Laskowski R., Schwarz K., Bottke P., Wilkening M., Geiger C.A. and Amthauer G. (2014a) - DFT study of the role of Al^{3+} in the fast ion-conductor $Li_{7-3x}Al^{3+}_x La_3Zr_2O_{12}$ garnet. *Chemistry of Materials*, 26, 2617-2623.

Rettenwander D., Geiger C.A., Tribus M., Tropper P. and Amthauer, G. (2014b) - A synthesis and crystal chemical study of the fast ion conductor $Li_{7-3x}Ga_xLa_3Zr_2O_{12}$ with x = 0.08 to 0.84. *Inorganic Chemistry*, 53, 6264-6269.

Rettenwander D., Geiger C.A., Tribus M., Tropper P., Wagner R., Tippelt G., Lottermoser W. and Amthauer G. (2015) - The solubility and site preference of Fe in $Li_{7-3x}Fe_xLa_3Zr_2O_{12}$ garnets. *Journal of Solid State Chemistry*. In press DOI: 10.1016/j.jssc.2015.01.016.

Periodico di Mineralogia, ECMS 2015, 21-22

PERIODICO di MINERALOGIA
established in 1930

An International Journal of
MINERALOGY, CRYSTALLOGRAPHY, GEOCHEMISTRY, ORE DEPOSITS, PETROLOGY, VOLCANOLOGY
and applied topics on *Environment*, *Archaeometry* and *Cultural Heritage*

Diffraction and spectroscopic characterization of jeffbenite: a high-pressure marker in diamonds

Chiara Anzolini[1], Fabrizio Nestola[1], Antony D. Burnham[2,6], Luca Peruzzo[3], Leonardo Tauro[1], Matteo Alvaro[4], Michael J. Walter[2], Mickey Gunther[5] and Simon C. Kohn[2]

[1] Università degli Studi di Padova, Dipartimento di Geoscienze, Via G. Gradenigo 6, 35131, Padova, Italy
[2] University of Bristol, Department of Earth Sciences, Queen's Road, Bristol BS8 1RJ, UK
[3] CNR-IGG, Padova, Via G. Gradenigo 6, 35131 Padova, Italy
[4] Università di Pavia, Dipartimento di Scienze della Terra e dell'Ambiente, Via Ferrata 1, 27100, Pavia, Italy
[5] University of Idaho, Geological Sciences, 875 Perimeter MS 3022, Moscow, 83844-3022, USA
[6] Now at Australian National University, Research School of Earth Sciences, Canberra, Australia
* Corresponding author: f*abrizio.nestola@unipd.it*

Jeffbenite is a new mineral, recently approved by IMA (IMA 2014-097), which could cover a key role in determining the depth of formation of the so-called super-deep diamonds. This category of diamonds is thought to crystallize in sub-lithospheric conditions, i.e. below about 250 km (corresponding to ~7-8 GPa; see the *Nature* paper published by Pearson et al. in 2014 on a Brazilian diamond bearing an inclusion of ringwoodite) and represents only 6% of diamonds investigated so far. On the contrary, the so-called lithospheric diamonds represent the remaining 94% and are those typically formed inside the cratons at depths between 120-130 and 250 km. Jeffbenite is a tetragonal high-pressure phase, emerald green in colour (Figure 1), which can be found only in super-deep diamonds and shows a chemical composition very similar to that of Mg-Fe garnets. More in detail, the recently approved jeffbenite has composition $(Mg_{2.62}Fe^{2+}_{0.27})(Al_{1.86}Cr_{0.16})(Si_{2.91}Al_{0.09})O_{12}$ with very minor amounts of Mn, Na and Ca, as it is highlighted by the EDS spectrum (Figure 2). Jeffbenite has unit-cell parameters a = 6.5231(1) Å and c = 18.1756(3) Å; its space group is I-42d and its X-ray calculated density is 3.576 g/cm^3 (Nestola et al., 2015).

The first crystal structure of jeffbenite was published in 1997 (*Nature*, Harris et al.). Nevertheless, at that time the mineral was simply reported with the acronym "TAPP", due to its similar composition to garnet (Tetragonal Almandine-Pyrope Phase), and never submitted to IMA to get an official approval. Thanks to our new re-investigation of TAPP, we were able not only to give a name to such important marker, but also to provide new mineralogical features besides crystal structure and chemistry. Indeed, in addition to the microprobe WDS and the single-crystal X-ray diffraction analyses, we measured the jeffbenite Raman spectrum, its trace elements composition by Laser ablation ICP-MS, its optical properties and its micro-hardness. Finally, we verified the chemical homogeneity by mapping all its main elements. In terms of vibrational spectroscopy, although jeffbenite has a Raman spectrum close to that of peridotitic garnets, this technique should be able to distinguish the two phases. In detail, the main peaks of

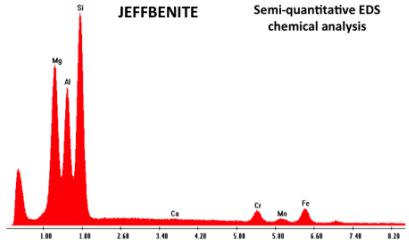

Figure 1. Single crystal of jeffbenite.
Figure 2. EDS spectrum of jeffbenite.

jeffbenite (in order of decreasing intensity and in cm^{-1}) are: 865, 935, 318, 995, 499, 204, 635. An analysis on a kimberlitic peridotitic garnet performed both by the same instrument and at the same working conditions adopted to measure jeffbenite (ThermoScientific DXR Raman microscope) shows the following main peaks: 919, 362, 860, 560, 600, 643, 1052. This is essential to identify jeffbenite even without breaking the host diamond, basic condition if you want to determine its depth of formation. In this light, we must remark that at present there are not definitive data on the depth of formation of jeffbenite; the unique available experimental work was published by Armstrong and Walter (2012), but their data were obtained on a jeffbenite rich in Ti (totally absent in the IMA-approved jeffbenite) and poor in Fe. However, these authors report for their Ti-rich jeffbenite conditions of formation of ~13 GPa and ~1700 K, which would locate the mineral at about 390 km depth, close to the upper mantle-transition zone boundary.

We are performing new synthesis experiments in order to determine which is the effect of Ti on the jeffbenite stability field and, as a consequence, to figure out if it can be really formed in the transition zone as some authors stated (e.g. Brenker et al., 2002).

References

Armstrong, L. S. and Walter, M. J. (2012) – Tetragonal almandine pyrope phase (TAPP): retrograde Mg-perovskite from subducted oceanic crust? *European Journal of Mineralogy*, 24(4), 587-597.

Brenker, F. E., Stachel, T. and Harris, J. W. (2002) – Exhumation of lower mantle inclusions in diamond: A TEM investigation of retrograde phase transitions, reactions and exsolution. *Earth and Planetary Science Letters*, 198(1), 1-9.

Harris, J., Hutchison, M., Hursthouse, M., Light, M. and Harte, B. (1997) – A new tetragonal silicate mineral occurring as inclusions in lower-mantle diamonds. *Nature*, 387(6632), 486-488.

Nestola, F., Burnham, A. D., Peruzzo, L., Tauro, L., Alvaro, M., Walter, M. J., Gunther, M. and Kohn, S. C. (2015) – Tetragonal Almandine-Pyrope Phase, TAPP: finally a name for it, the new mineral jeffbenite. *Mineralogical Magazine,* under review.

Pearson, D. G., Brenker, F. E., Nestola, F., McNeill, J., Nasdala, L., Hutchison, M. T. and Vincze, L. (2014) – Hydrous mantle transition zone indicated by ringwoodite included within diamond. *Nature*, 507(7491), 221-224.

Periodico di Mineralogia, ECMS 2015, 23-24

PERIODICO di MINERALOGIA
established in 1930

An International Journal of
MINERALOGY, CRYSTALLOGRAPHY, GEOCHEMISTRY,
ORE DEPOSITS, PETROLOGY, VOLCANOLOGY
and applied topics on *Environment*, *Archaeometry* and *Cultural Heritage*

Ni-Ti co-doped hibonite ceramic pigments by combustion synthesis: crystal structure and optical properties

Matteo Ardit[1,*], Silvana Borcănescu[2], Giuseppe Cruciani[1], Michele Dondi[3], Ioan Lazău[2], Cornelia Păcurariu[2] and Chiara Zanelli[3]

[1] University of Ferrara, Department of Physics and Earth Sciences, via Saragat 1, Ferrara, Italy
[2] University of Timişoara, Faculty of Industrial Chemistry and Environmental Engineering, Timişoara, Romania
[3] CNR-ISTEC, Institute of Science and Technology for Ceramics, via Granarolo 64, Faenza, Italy
* Corresponding author: *rdtmtt@unife.it*

Hibonite ($CaAl_{12}O_{19}$, space group P_{63}/mmc) has the structural formula $A^{[XII]}M1^{[VI]}M2^{[V]}M3_2^{[IV]}M4_2^{[VI]}M5_6^{[VI]}O_{19}$ where Ca is 12-fold coordinated at site A and Al^{3+} ions are distributed over five different sites: 3 distinct octahedra [M1 (D_{3d}), M4 (C_{3v}) and M5 (C_s)], the M3 tetrahedron (C_{3v}), and the unusual 5-fold coordinated trigonal bipyramid M2 (D_{3h}); (Bermanec et al., 1996; Nagashima et al., 2010).

Hibonite is able to accommodate a wide range of ions with different valence states and coordination numbers, making its structure a promising ceramic pigment. One of the main challenges is to understand and control incorporation mechanisms and the threshold of chromophores solubility. It is known that M^{2+} ions tend to be hosted at the M3 site, while M^{4+} ions are preferentially accommodated at the M4 site: the introduction of divalent ions might be promoted by the associated incorporation of tetravalent cations, which ensure the lattice electroneutrality and are ordered over the M4 face-sharing octahedral dimers (Fig. 1).

In this work, the mechanism of the coupled substitution $2Al^{3+} \rightarrow (Ni^{2+} + Ti^{4+})$ was investigated by combining X-ray powder diffraction and diffuse reflectance spectroscopy techniques. Hibonite turquoise pigments with increasing Ni + Ti doping ($CaAl_{12-2x}Ni_xTi_xO_{19}$, where x = 0.1 - 2.0 apfu) were prepared by combustion synthesis, utilizing fuel mixtures (urea, glycine, β-alanine) set up according to their compatibility with metal nitrates used as raw materials. The ignition temperature of combustion reaction was 400 ºC, but samples underwent an additional annealing at 1200 ºC. Samples up to x = 0.4 are monophasic; for higher doping, hibonite is the main component accompanied by growing percentages of spinel and perovskite as associated phases. The addition of Ni and Ti induced a regular increase of the hibonite unit-cell parameters till x = 1.0, that is proportional to the amount and difference in ionic radii of the dopants. In particular, an elongation of the ⟨M–O⟩ bond distances of both M3 and M4 sites was observed. In terms of opti-

cal parameters, Ni^{2+} is preferentially incorporated in tetrahedral coordination, up to 0.3 apfu at the M3 site, and at the M4 octahedron as well (up to 0.19 apfu). The crystal field strength of fourfold coordinated Ni^{2+} is regularly decreasing, implying an elongation of the local Ni–O bond that is consistent with the volume increasing from AlO_4 to NiO_4 tetrahedra registered by XRD. Ti^{4+} ions are accommodated at both the M2 and M4 octahedra which expand proportionally to the amount of dopants. Pigment purity and colour strength vary with doping depending on the multistep mechanism of Ni and Ti incorporation in the hibonite lattice.

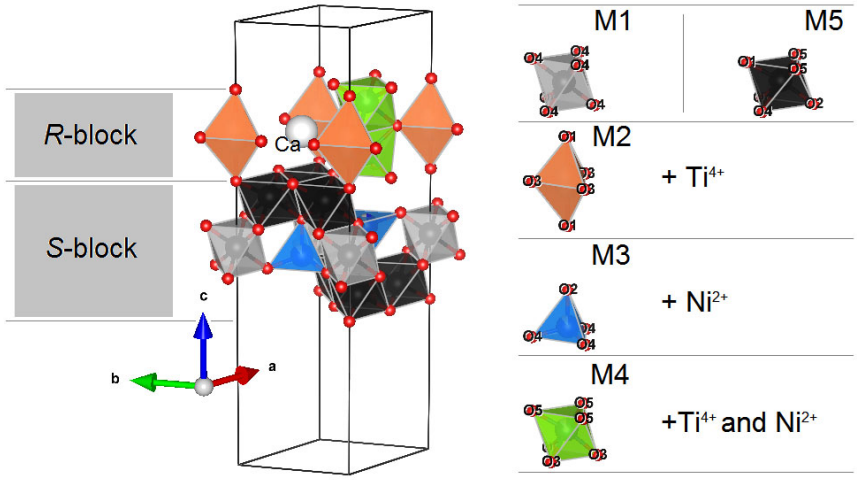

Figure 1. Polyhedral representation of the two structural layers, the hexagonal close-packed *R*-block (i.e. the Ca site, the trigonal bipyramidal M2 site, and the octahedral face-sharing M4 site) and the so-called spinel layer *S*-block (i.e. layers of M5 octahedra interspaced by the M3 tetrahedra and the M1 octahedra), of Ni and Ti co-doped hibonite (s.g. P_{63}/mmc) in a perspective as view along [110]. The atom of Ca (a white sphere) is twelve-fold coordinated by 6 × O3 and 6 × O5. On the right side, a representation of each polyhedron with their respective ligands and the occupancy of the dopants.

References

Bermanec V., Holtstam D., Sturman D., Criddle A. J., Back M. E. and Šćavničar S. (1996) - Nežilovite, a new member of the magnetoplumbite group, and the crystal chemistry of magnetoplumbite and hibonite. *Canadian Mineralogist*, 34, 1287-1297.

Nagashima M., Armbruster T. and Hainschwang T. (2010) - A temperature-dependent structure study of gem-quality hibonite from Myanmar. *Mineralogical Magazine*, 74, 871-885.

Periodico di Mineralogia, ECMS 2015, 25-26

PERIODICO di MINERALOGIA
established in 1930

An International Journal of
MINERALOGY, CRYSTALLOGRAPHY, GEOCHEMISTRY,
ORE DEPOSITS, PETROLOGY, VOLCANOLOGY
and applied topics on *Environment*, *Archaeometry* and *Cultural Heritage*

Order-disorder phase transitions in the minerals with antiperovskite structures

Margarita S. Avdontceva[1,*], Maria G. Krzhizhanovskaya[1], Andrey A. Zolotarev[1], Sergey V. Krivovichev[1] and Victor N. Yakovenchuk[2]

[1]Department of crystallography, Institute of Earth Sciences, St. Petersburg State University, University Emb. 7/9, St.Petersburg, 199034, Russia
[2]Geological Institute, Kola Science Center, Russian Academy of Sciences, Apatity 184209, Russia
* Corresponding author: *margarita.avdontceva@spbu.ru*

Experimental studies of phase transitions in minerals with perovskite-type structures continue to attract considerable attention due to their importance for the understanding of behavior of mineral matter subjected to the effects of high temperature and pressure in the deep Earth geospheres (Xiao et al., 2013; Knight et al., 2014).

Kogarkoite, Na_3SO_4F, and nacaphite, Na_2CaPO_4F, are typical minerals with antiperovskite-type structures which are based upon corner- and face-sharing fluorine-centered octahedra (Krivovichev et al., 2008).

Synthetic crystals of kogarkoite were prepared by evaporation from aqueous solutions of sodium sulfate and sodium fluoride at 25°C. The sample of nacaphite used for this study was taken from hydrothermal microcline – pectolite – sadolite – aegirine vein within ijolite – urtite at Mt. Koashva. Thermal behavior of minerals was studied by high-temperature X-ray powder diffraction method using a Rigaku Ultima IV ($CuK\alpha_{1+2}$ radiation, 40 kV/30 mA, Bragg-Brentano geometry, PSD D-Tex Ultra) diffractometer. The unit cell parameters were calculated using the program package Topas 4.2 (Bruker). The crystal structure of synthetic kogarkoite was also studied by single crystal X-Ray diffraction analysis by means of the Bruker Kappa Apex Duo diffractometer equipped with the CCD detector at room temperature and at 423 K using low-temperature Oxford Cobra Plus system.

The temperature of the phase transition in kogarkoite can be estimated as 112.5±12.5 °C. The low-temperature phase, α-Na_3SO_4F, at 293 K, is monoclinic, $P2_1/m$, a = 18.065(3), b = 6.958(1), c = 11.446(1) Å, β = 107.711(1)°, Z = 12. The structure contains thirteen symmetrically independent Na sites with coordination numbers varying from 6 to 8, and six independent S sites. The high-temperature β-phase at 423 K is rhombohedral, $R\bar{3}m$, a = 6.981(1), c =

24.691(3) Å, $Z = 9$. The crystal structure of both polymorphs of Na_3SO_4F can be described as a 9*R* antiperovskite polytype based upon triplets of face-sharing [FNa_6] octahedra linked into a three-dimensional framework by sharing corners (Fanfani et al.,1980). In the α-modification, the SO_4 tetrahedra are completely ordered and located in the framework cavities. In the β-modification, there are only two symmetrically independent Na atoms in the structure. The main difference between the structures of the α- and β-phases is the degree of ordering of the SO_4 tetrahedra: in the α-modification they are completely ordered, whereas in the β-modification the complete disorder is observed, which is manifested in a number of low-occupied O sites around fully occupied S sites.

The monoclinic-to-orthorhombic phase transition in nacaphite has been observed at 330 °C associated with the appearance of the Ca/Na disorder at one of the two crystallographically inequivalent Na sites. At room temperature, nacaphite is monoclinic, $P2_1/c$, $a = 13.3185(14)$, $b = 7.0964(8)$, $c = 10.6490(11)$ Å, $\beta = 113.526(1)°$, $V = 922.81(17)$ Å^3. The structure is based upon one-dimensional antiperovskite units consisting of face-sharing $[FNa_4Ca_2]^{7+}$ anion–centered octahedra running parallel to the **c** axis. The structure is fully ordered and contains two Ca and four Na sites. The crystal structure of the high–temperature modification (R_B 0.025 at 400 °C from the powder X-ray diffraction data) is orthorhombic, *Pnma*, $a = 5.4123(1)$, $b = 7.1196(1)$, $c = 12.3171(1)$ Å, $V = 474.62(1)$ Å^3. The structure has one fully occupied *Na*1 site and one mixed-occupied *Na*2 site, the latter being equally occupied by Na and Ca. The *Na*1 and *Na*2 sites are coordinated by two F^- and four O^{2-} anions each. Thermal expansion of both modifications has an anisotropic character with the degree of anisotropy increasing from the low- to the high-temperature phase. The direction of the strongest thermal expansion is parallel to the direction of chains of face-sharing anion-centered octahedra that can be explained by the temperature-induced expansion of the F-Na/Ca bonds.

Thus the phase transition in both minerals has an order-disorder character and is associated with the decrease of structural complexity (Krivovichev, 2014) measured as an information content per unit cell [577.528 bits for the low- (α) and 154.830 bits for the high- (β) temperature modifications in kogarkoite and 300.235 bits for the low- and 98.117 bits for the high-temperature modifications in nacaphite].

This research was supported by St. Petersburg State University (internal grants 3.38.136.2014, 3.38.243.2015). All X-Ray studies were carried out in the Research Centre for X-Ray diffraction studies.

References

Fanfani, L., Giuseppetti G., Tadini C. and Zanazzi P.F. (1980) - The crystal structure of kogarkoite, Na_3SO_4F. *Mineralogical Magazine*, 43,753-759.

Knight K.S., Marshall W.G. and Hawkins P.M. (2014) - A high-pressure neutron diffraction study of the ferroelastic phase transition in $RbCaF_3$. *Physics and Chemistry of Minerals*, 41, 461-472.

Krivovichev S.V. (2008) - Minerals with antiperovskite structure: A review. *Zeitschrift für Kristallographie*, 223, 109-113.

Krivovichev S.V. (2014) - Which inorganic structures are the most complex? *Angewandte Chemie - International Edition*, 53, 654-661.

Xiao W., Tan D., Zhou W., Liu J. and Xu J. (2013) - Cubic perovskite polymorph of strontium metasilicate at high pressures. *American Mineralogist*, 98, 2096-2104.

Periodico di Mineralogia, ECMS 2015, 27-28

PERIODICO di MINERALOGIA
established in 1930

An International Journal of
MINERALOGY, CRYSTALLOGRAPHY, GEOCHEMISTRY,
ORE DEPOSITS, PETROLOGY, VOLCANOLOGY
and applied topics on *Environment*, *Archaeometry* and *Cultural Heritage*

Fast on-site identification of minerals by using portable Raman equipment in gemological trade contexts and in collectors exhibitions

Germana Barone[1]*, Danilo Bersani[2], Jan Jehlička[3], Paolo Mazzoleni[1], Simona Raneri[1] and Peter Vandenabeele[4]

[1]Department of Biological, Geological and Environmental Sciences, University of Catania, Corso Italia, 57, 95129 Catania, Italy
[2] Department of Physics and Earth Sciences, University of Parma, Parco Area delle Scienze, 7/A 43124 Parma, Italy
[3]Institute of Geochemistry, Mineralogy and Mineral Resources, Charles University in Prague, Faculty of Science, Albertov 6, 128 43 Prague, Czech Republic
[4]Department of Archaeology, Ghent University, Sint-Pietersnieuwstraat 35, 9000 Gent, Belgium
*Corresponding author: *gbarone@unict.it*

In the gemological trade the availability of well-manufactured imitations and synthetic gems and the use of treatments has become a common trend, causing new problems in gems certification. Minerals having a gemological interest can be investigated by performing standard tests, but the identification and certification of gemological materials is not always easy and immediate, especially in the case of gems mounted in jewels. In addition, at exhibitions, collectors often request a fast identification of minerals in very difficult environmental conditions. In these cases, fast, non-invasive and non-destructive methods that give reliable information on composition of minerals are extremely valuable for gemologist and collectors. Raman spectroscopy represents the most powerful of these methods, especially considering the availability of high-resolution portable systems (Barone et al., 2014; Jehlička et al., 2011; Vítek et al., 2012; Víteket al., 2013). However, some problems related to in-situ measurements such as noise due to environmental conditions have to be considered.

The main aim of this work is to highlight the potential of portable Raman spectrometry in the fast characterization of minerals at events as exhibitions, during which collectors and gemologists may purchase gems, often without compliance certifications. Measurements have been carried out on two set of samples, namely loose/mounted gems and minerals supplied by gemologists and collectors, respectively. In detail, data have been collected by means a handheld Rock Hound (Delta Nu) Raman spectrometer equipped by a 785 nm diode laser and a portable Enwave Optronics EZRAMAN-I-DUAL (Lauwers et al., 2014) equipped with a diode laser (785 nm) and a Nd:YAG laser (532 nm). A large number of samples, representing some of the most diffused and valuable examples of gems and minerals available in the gemological market and the collecting field have been analyzed and characterized in really easy way and short time

(Figure 1). The instruments can be connected via a USB cable to a laptop and Raman spectra have been simultaneously visualized, allowing a live identification of materials. Among gems supplied by gemologists, several varieties of quartz, as well as garnets, beryl, corundum and feldspars have been identified. The most useful results have been obtained for mounted gems, for which traditional gemological tests cannot be performed without removing the stones from their sets. During the Monza 2013 Mineral Exhibition about 64 tests were performed on anatase, apatite, demantoid garnets, topaz, benitoite, vesuvianite and other minerals, allowing the absolute identification of the 80% of the studied materials.

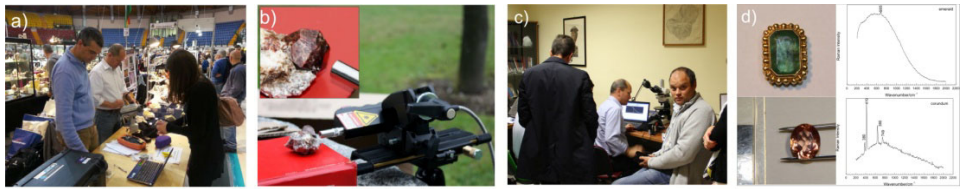

Figure 1. (a) Raman in-situ measurements at the Monza 2013 Mineral exhibition; (b) measurement on almandine with Enwave instrument; (c) Raman in-situ measurements with gemologist; (d) Examples of measurements performed on mounted and loose gems with Delta Nu instrument.

We have demonstrated the potential of portable Raman equipment in the fast in situ certification of minerals, even in very difficult environmental conditions. Additional strategies such as focusing optimization, the use of enclosures to reduce stray light, adjustable laser power and multiple laser energies can further improve the performance of portable Raman systems. In conclusions, by using this method, it is possible to supply fundamental information for gemologist and collectors, especially in the framework of sales agreements.

Special thanks go to gemologist Longobardo, Saguto, Rapisarda, Avolio, Salini and anonymous collectors who provided all the studied materials.

References

Barone G., Bersani D., Crupi V., Longo F., Longobardo U., Lottici P.P, Aliatis I., Majolino D., Mazzoleni P., Raneri S. and Venuti V. (2014) - A portable versus micro-Raman equipment comparison for gemmological purposes: the case of sapphires and their imitations. *Journal of Raman Spectroscopy*, 45, 1309–1317.

Lauwers D., Cattersel V., Vandamme L., Van Eester A., De Langhe K., Moens L. and Vandenabeele P. (2014) - Pigment identification of an illuminated mediaeval manuscript De Civitate Dei by means of a portable Raman equipment. *Journal of Raman Spectroscopy*, 45, 1266–1271.

Jehlička J., Culka A., Vandenabeele P. and Edwards H.G.M. (2011) - Critical evaluation of a handheld Raman spectrometer with near infrared (785 nm) excitation for field identification of minerals. *Spectrochimica Acta A*, 80, 36-40.

Vítek P., Ali E.M.A., Edwards H.G.M., Jehlička J., Cox R. and Page K. (2012) - Evaluation of portable Raman spectrometer with 1064 nm excitation for geological and forensic applications. *Spectrochimica Acta A*, 86, 320–327.

Vítek P., Jehlička J. and Edwards H.G.M. (2013) - Practical Considerations for the Field Application of Miniaturized Portable Raman Instrumentation for the Identification of Minerals. *Applied Spectroscopy*, 67, 767–778.

Periodico di Mineralogia, ECMS 2015, 29-30

PERIODICO di MINERALOGIA
established in 1930

An International Journal of
MINERALOGY, CRYSTALLOGRAPHY, GEOCHEMISTRY, ORE DEPOSITS, PETROLOGY, VOLCANOLOGY
and applied topics on *Environment*, *Archaeometry* and *Cultural Heritage*

FTIR spectroscopy of minerals with complex H-bonds network

Fabio Bellatreccia[1,2,*], Giancarlo Della Ventura[1,2], Susanna Grita[1], Simone Bernardini[1], Gennaro Ventruti[3] and Francesco Capitelli[4]

[1] Università Roma Tre Dipartimento di Scienze, Largo San Leonardo Murialdo 1, 00146 Rome, Italy
[2] Istituto Nazionale di Fisica Nucleare – Laboratori Nazionali di Frascati (INFN-LNF), Via E. Fermi 40, 00044 Frascati, Rome, Italy
[3] Università di Bari Aldo Moro Dipartimento di Scienze della Terra e Geoambientali, Via Orabona 4, 70125 Bari, Italy
[4] Istituto di Cristallografia – CNR, Via Salaria Km 29.300, 00016 Monterotondo, Rome, Italy
* Corresponding author: *Fabio.bellatreccia@uniroma3.it*

Hydrogen bond has a central role in stabilizing the crystal structures of many H-bearing minerals as in the case of oxysalts, for example hydroxy-hydrated phosphates (HHPh) and hydroxy-hydrated (iron) sulfates (HHSf). Indeed, in these structures the hydrogen bond supplies the additional bond-valence (0.1-0.3 vu) contribution to the anions. Hence, the (PO_4) and (SO_4) groups can link easily to all other interstitial cations (Hawthorne et al., 2000; Huminicki and Hawthorne, 2002). For this reason, most HHPhs and HHSfs are characterized by the presence of complex tridimensional networks of O-H…O hydrogen bonds, which connect the polyhedral units making up a three dimensional framework. Consequently, the dimensionality of the structural unit is controlled primarily by the amount and role of hydrogen in the structure (Hawthorne, 1998).

FTIR spectroscopy is a powerful tool for the study of hydrogen in minerals, but HHPhs and HHSfs are rather challenging to study because of their complex structures. Moreover, due the high OH/H_2O contents, these minerals show extremely intense IR absorptions in the OH region.

In this work, we describe the results obtained by IR spectroscopy in different spectral regions of selected HHPhs and HHSfs. O-H and hydrogen bonds orientation were studied by single crystal polarized light μ-IR-spectroscopy, and experiments at HT- and LT were performed to study phase transitions and dehydration mechanisms with the aim of defining the thermal stability of these minerals. Finally, some applications done by using the novel FPA-FTIR imaging method are presented.

References

Hawthorne F.C. (1998) - Structure and chemistry of phosphate minerals. *Mineralogical Magazine*, 62, 141-164.

Hawthorne F.C., Krivovichev S.V. and Burns P.C. (2000) - The crystal chemistry of sulfate minerals. In Alpers C.N., Jambor J.L., Nordstrom B.K., Eds., Sulfate Minerals - Crystallography, Geochemistry, and Environmental Significance. *Reviews in Mineralogy and Geochemistry*, 40, 1-112.

Huminicki D.M.C. and Hawthorne F.C. (2002) - The crystal chemistry of the phosphate minerals. In: Kohn M.L., Rakovan J., & Hughes J.M., Eds., Phosphates Geochemical, Geobiological, and Materials Importance. *Reviews in Mineralogy and Geochemistry*, 48, 123-254.

Periodico di Mineralogia, ECMS 2015, 31

PERIODICO di MINERALOGIA
established in 1930

An International Journal of
MINERALOGY, CRYSTALLOGRAPHY, GEOCHEMISTRY,
ORE DEPOSITS, PETROLOGY, VOLCANOLOGY
and applied topics on *Environment*, *Archaeometry* and *Cultural Heritage*

V *K*-edge XANES in V-bearing model compounds: a Full Multiple Scattering study

Federico Benzi[1], Gabriele Giuli[1*], Stefano Della Longa[2] and Eleonora Paris[1]

[1] University of Camerino, School of Science and Technology, Geology Division, 62032 Camerino, Italy
[2] University of Aquila, Department Medicina Clinica, Sanita Pubblica,
Scienze della Vita e dell'Ambiente, Piazzale S. Tommasi 1, 67100, Coppito (AQ), Italy,
*Corresponding author: *gabriele.giuli@unicam.it*

We present a systematic study on a set of V-bearing model compounds, representative of the most common V coordination geometries and oxidation states, analysed by means of vanadium *K*-edge X-ray Absorption Near Edge Spectroscopy (XANES) calculations in the Full Multiple Scattering (FMS) framework. The analysis and the calibration of the free parameters of the theory under the Muffin-Tin approximation (Muffin Tin overlap and interstitial potential) has been carried out by fitting the experimental spectra with the MXAN program. The analysis shows a correlation of the fit parameters with the V coordination geometry and oxidation state. By making use of this correlation it is possible to approach the study of unknown V-bearing compounds with rigorous preliminary information.

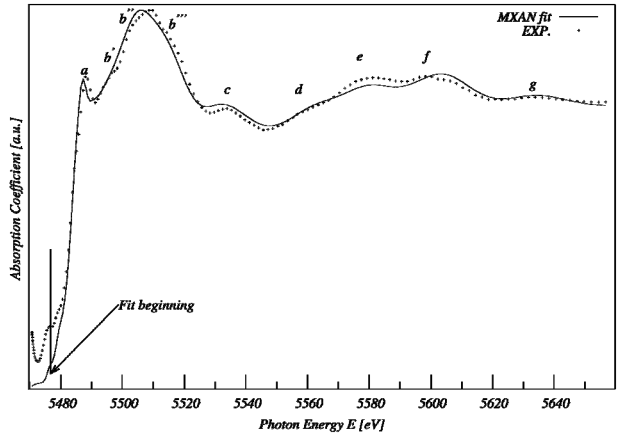

Comparison between experimental and theoretical XANES spectra of a $^{[4]}V^{5+}$ compound.

Periodico di Mineralogia, ECMS 2015, 33-34

PERIODICO di MINERALOGIA
established in 1930

An International Journal of
MINERALOGY, CRYSTALLOGRAPHY, GEOCHEMISTRY,
ORE DEPOSITS, PETROLOGY, VOLCANOLOGY
and applied topics on *Environment*, *Archaeometry* and *Cultural Heritage*

As^{5+} incorporation into rhomboclase and its dehydration product $(H_3O)Fe(SO_4)_2$ – An EXAFS study

Ralph Michael Bolanz[1,*], Jörg Göttlicher[2] and Ralph Steininger[2]

[1] Friedrich-Schiller-University Jena, Institute of Geosciences, Carl-Zeiss-Promenade 10, 07745 Jena, Germany
[2] Karlsruhe Institute of Technology, ANKA Synchrotron Radiation Facility, Hermann-von-Helmholtz Platz 1, D-76344 Eggenstein-Leopoldshafen, Germany
* Corresponding author: *ralph.bolanz@uni-jena.de*

In arid and semi-arid mining regions, iron sulfates represent an essential short-term sink for the toxic element arsenic (As). Acidic mine waters, rich in As, evaporate due to the high temperatures and low relative humidity and form efflorescence of Fe-sulfoarsenates from which copiapite $[Fe^{2+}Fe_4^{3+}(SO_4)_6(OH)_2 \cdot 2H_2O]$ and rhomboclase $[(H_5O_2)Fe^{3+}(SO_4)_2 \cdot 2H_2O]$ incorporate a predominant fraction of the toxic element (Gieré et al., 2003). However, information about the exact modes of structural incorporation of As into iron sulfates has not been investigated by short-range order techniques so far.

The most likely scenario is the heterogeneous substitution of S^{6+} by As^{5+}. Both cations are tetrahedrally coordinated by oxygen, while the AsO_4 tetrahedron is significantly larger than SO_4. A second incorporation mechanism, at least for the layered structure of rhomboclase, is the presence of uncharged molecules of H_3AsO_4 between the iron sulfate layers, since the fully protonated arsenic acid (H_3AsO_4) is the predominant arsenate species in aqueous solutions with a pH below 2 (Guan et al., 2009). Further information about the structural position of As^{5+} in rhomboclase can be obtained by its dehydration product $(H_3O)Fe(SO_4)_2$. During the dehydration of rhomboclase the interlayer space between the iron sulfate layers shrinks, leaving not enough space for the uncharged H_3AsO_4. It could therefore be assumed that As^{5+} substituting S^{6+} in rhomboclase would remain in the $(H_3O)Fe(SO_4)_2$ structure, whereas molecules of H_3AsO_4 in the interlayer space would be expelled.

In this study, the structural incorporation of As into rhomboclase and its dehydration product $(H_3O)Fe(SO_4)_2$ was investigated by inductively-coupled plasma optical emission spectrometry (ICP-OES), powder X-ray diffraction (XRD), field emission scanning electron microscopy (FE-SEM), and X-ray absorption spectroscopy (XAS) with a focus on extended X-ray absorption fine structure spectroscopy (EXAFS). The results show that synthetic crystals of rhomboclase can incorporate up to 1.8 wt.% As, whereas the unit cell parameters *a*, *b*, and *c* gradually increase with increasing As-content. At the same time, the crystal size decreases from 304 to

176 nm, but the starting and end temperatures for the dehydration of rhomboclase to $(H_3O)Fe(SO_4)_2$ remain unaffected by the presence of As^{5+}.

The local structure of As^{5+} in rhomboclase and $(H_3O)Fe^{3+}(SO_4)_2$ indicates that As resides on the S^{6+} position for both phases, while the additional polymerization of AsO_4 and FeO_6 in $(H_3O)Fe(SO_4)_2$ results in a significant distortion of the AsO_4 tetrahedron.

References

Gieré R., Sidenko N.V. and Lazareva E.V. (2003) - The role of secondary minerals in controlling the migration of arsenic and metals from high-sulfide wastes (Berikul gold mine, Siberia). *Applied Geochemistry*, 18, 1347-1359.

Guan X., Dong H., Ma J. and Jiang L. (2009). Removal of arsenic water: Effect of competing anions on As(III) removal in $KMnO_4$-Fe(II) process. *Water Research*, 43, 3891-3899.

Periodico di Mineralogia, ECMS 2015, 35-36

PERIODICO di MINERALOGIA
established in 1930

An International Journal of
MINERALOGY, CRYSTALLOGRAPHY, GEOCHEMISTRY,
ORE DEPOSITS, PETROLOGY, VOLCANOLOGY
and applied topics on *Environment*, *Archaeometry* and *Cultural Heritage*

Raman Spectroscopy as a tool for magnesium estimation in Mg-calcite

Laura Borromeo[1,2,*], Udo Zimmermann[1,2], Sergio Andò[3], Giovanni Coletti[3], Danilo Bersani[4], Daniela Basso[3], Paolo Gentile[3] and Eduardo Garzanti[3]

[1]Department of Petroleum Engineering, University of Stavanger, Norway
[2] National IOR Center of Norway, 4036, Stavanger
[3] Department of Earth and Environmental Sciences, University of Milano-Bicocca, Milano, Italy
[4] Department of Physics and Earth Sciences, University of Parma - Italy
* Corresponding author: *laura.borromeo@uis.no*

Despite their importance in several applications in geological and biological sciences and their strong Raman scattering, Mg-calcites have not been thoroughly investigated by Raman spectroscopy to quantify their chemical signature so far. The relationship between their magnesium content and the Raman peaks position has been investigated by Bischoff et al. (1985), Urmos et al. (1991) and Vagenas et al. (2003), but a clear link or standard calibration have not been proposed yet. A pioneer paper by Chave et al. (1952) reported a linear relationship between the position of the main X-ray diffraction peak of skeletal calcites and their Mg concentration. Following a different and user-friendly approach, we investigated whether Raman spectra of carbonates are sufficiently sensitive to the structural and chemical changes occurring when Mg^{2+} substitutes Ca^{2+} in the calcite lattice and whether a function linking the Mg content and the position of the Raman peaks can be determined. Different carbonate samples with variable Mg content and with both biological and inorganic origin (most of them certified M.A.C. standards) have been first beamed under a Raman spectrometer and then analyzed by EDS and WDS electron microprobes to determine their chemistry and obtain insights on crystal structure. The biological samples (foraminifers, algae, barnacles, echinoderms) were collected in areas situated at different latitudes and in different depositional environments encompassing different water temperatures and saturations, all factors affecting Mg content in the shells of marine organisms.

We have observed that all peaks of Mg-calcite spectra show a consistent increase in Raman shifts according to their Mg content, which is a consequence of decreased inter-atomic distances following the substitution of Ca^{2+} with the smaller Mg^{2+} ion (Krishnamurti, 1956; Bischoff et al., 1985).

This study demonstrates that Raman spectroscopy provides an interesting innovative work perspective in marine biology, geology and oil exploration in $MgCl_2$ flooded chalk representing important unconventional reservoirs for Enhanced Oil Recovery.

References

Bischoff W.D., Sharma S.K. and Mackenzie F.T. (1985) - Carbonate ion disorder in synthetic and biogenic magnesian calcites: a Raman spectral study. *American Mineralogist* 70, 581–589.

Chave K.E. (1952) - A solid solution between calcite and dolomite. *Journal of Geology*, 60, l90-192.

Krishnamurti D. (1956) - Raman spectrum of magnesite: *Proceedings of the Indian Academy of Sciences* - Section A, 43, 210-212.

Urmos J., Sharma S. K. and Mackenzie F.T. (1991) - Characterization of some biogenic carbonates with Raman spectroscopy. *American Mineralogist*,76, 641-646.

Vagenasa N.V. and Kontoyannis C.G. (2003) - A methodology for quantitative determination of minor components in minerals based on FT-Raman spectroscopy. The case of calcite in dolomitic marble. *Vibrational Spectroscopy*, 32, 261–264.

Periodico di Mineralogia, ECMS 2015, 37-38

PERIODICO di MINERALOGIA
established in 1930

An International Journal of
MINERALOGY, CRYSTALLOGRAPHY, GEOCHEMISTRY,
ORE DEPOSITS, PETROLOGY, VOLCANOLOGY
and applied topics on *Environment*, *Archaeometry* and *Cultural Heritage*

Tourmaline from the eclogite hosting gneisses in the Tso Morari UHP metamorphic terrane (Ladakh, India): characteristics and evolution

Igor Broska[1,*], Marian Janák[1] , Peter Bačík[2] and Santosh Kumar[3]

[1] Geological Institute, Slovak Academy of Sciences, Dúbravská cesta 9, 840 05 Bratislava
[2] Faculty of Natural Sciences, Comenius University, Mlynská dolina G, 842 15 Bratislava
[3] Dept. of Geology, Kauman University, Nainital 263 002, India
* Corresponding author: *igor.broska@savba.sk*

Tourmaline is stable at wide P-T conditions including high- to ultrahigh-pressure metamorphism and events connected with subduction of slabs to a depth greater than 100 km (Ertl et al., 2010). Tourmaline-bearing gneiss, named as Puga gneiss, belongs to the Tso Morari complex exposed in the northern part of the Indian plate. Puga gneisses (both ortho- and para-gneisses) host many eclogite lenses and boudins. Coesite, found in these eclogites, indicates UHP metamorphism of the Tso Morari complex resulting from deep subduction of the Indian plate below Asia (Sachan et al., 2004). The studied locality (a ca. 100 m high cliff), exposes several metre-scale eclogite boudins in a compositionally heterogeneous sequence of tourmaline-bearing gneisses. Four tourmaline types have been recognised in these gneisses and some of them formed probably during the UHPM.

The composition of tourmaline I in felsic orthogneiss is slightly Al-deficient, schorlitic tourmaline (Al = 5.8 in average), with low vacancy content on X site (= 0.1). Some segments of tourmaline crystals contain unusual quartz inclusions of vermicular shape. Their size is ca 50-100 μm long and 10-30 μm thick. The tiny, vermicular quartz is enriched in Fe (up to 0.5 wt. %) with elevated Al (0.04 wt. %) and Ti content. Temperature of the quartz origin estimated from TitaniQ thermometer is in range of 650-700 °C. Other large quartz inclusions in tourmaline are compositionally similar to those observed in the matrix – they are low in Fe, Al and Ti contents. In this sense two quartz types recognised in tourmaline point to the presence of exsolved quartz from tourmaline which grew by Ostwald ripening process.

The strongly disintegrated tourmaline I dissolved and reprecipitated to schorlitic tourmaline II preserving the Al-deficiency. Also Al-deficient zonal and dravitic tourmaline III is present in the intercalated paragneiss. The schorlitic-dravitic tourmaline IV occurring in secondary veins form fluidal texture. This tourmaline is only partly Al deficient; many grains are significantly saturated in Al with more than 0.5 Al is in the Z site. Unusual fluidal structure of tourmalines

IV indicates their precipitation during intensive hydrothermal activity within late decompression stage.

Presence of disintegrated tourmaline with quartz exsolutions evokes the survival of the tourmaline in HP/UHP conditions within the Tso Morari complex. In spite of missing typical UHP inclusions in tourmaline, such as coesite, the unusual microtexture of quartz exsolutions is only indicator of primary excess of silica in former tourmaline. Generally at HP/UHP conditions silica may enter the octahedral Z-site of the tourmaline crystal structure as was already shown by experimental work of Wunder et al. (2014), doping the system by $(NH_4)_2$. During decompression in Tso Morari complex, the exsolution of silica from the tourmaline octahedral site could have formed new quartz, stabilizing the whole system. Silica released from the Z site may have been replaced by excess of Fe^{3+}, as indicated by the X-ray diffraction data of the investigated tourmaline. Average bond lengths in the octahedral sites can be calculated from unit-cell parameters of tourmaline with use of empirical equations. The *c* parameter and the ZO_6 octahedron size of tourmaline are in positive correlation to Mg amount in Fe-Mg tourmalines from large set of world localities indicating the presence of Mg in the Z site. In tourmaline from the Tso Morari, the content of Mg is not sufficient to produce such a large expansion of ZO_6 octahedra but it can be explained by the incorporation of Fe^{3+} into the Z site.

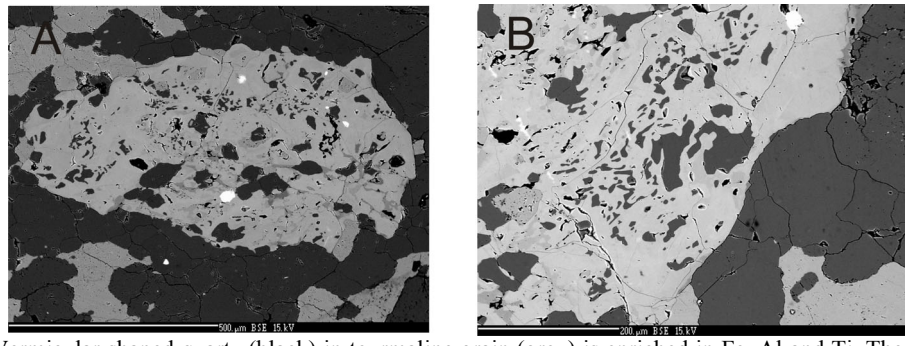

Fig. 1 Vermicular shaped quartz (black) in tourmaline grain (grey) is enriched in Fe, Al and Ti. The tiny quartz contains up to 0.4 wt.% of FeO_{tot}. A) The whole grain with parts of tiny vermicular shaped quartz; B) a detail of quartz texture in tourmaline.

Acknowledgement: This work was supported by the Slovak Research and Development Agency project no. 0080-11.

References

Ertl A. Marschall H.R., Giester G., Henry D.J., Schertl H.P., Ntaflos T., Luvizotto G.L., Nasdala L. and Tillmans E. (2010) - Metamorphic ultrahigh-pressure tourmaline: Structure, chemistry, and correlations to P-T conditions. *American Mineralogist*, 95, 1-10.

Sachan H., Mukherjee B., Ogasawara Y., Maruyama S., Ishida H., Muko A. and Yoshioka N. (2004) - Discovery of coesite from Indus Suture Zone (ISZ), Ladakh, India: Evidence for deep subduction. *European Journal of Mineralogy*, 16, 235-240.

Wunder B., Berryman E., Rhoede D., Koch-Müller M., Plessen, B., and Heinrich W. (2014) - NH_4-bearing tourmaline: experiments and natural occurrences. *IMA 2014 abstracts*, 277 p.

Periodico di Mineralogia, ECMS 2015, 39-40

PERIODICO di MINERALOGIA
established in 1930

An International Journal of
MINERALOGY, CRYSTALLOGRAPHY, GEOCHEMISTRY,
ORE DEPOSITS, PETROLOGY, VOLCANOLOGY
and applied topics on *Environment*, *Archaeometry* and *Cultural Heritage*

Mechanical anisotropy of a quartz crystal investigated by depth-sensing indentation

Enrico Bruschini* and Giovanni B. Andreozzi

Department of Earth Sciences, Sapienza University of Rome, I-00185 Rome, Italy
* Corresponding author: *enrico.bruschini@uniroma1.it*

We performed an extensive and detailed investigation of the mechanical properties of quartz by using a Shimadzu DUH-211S depth-sensing indentation system equipped with a Berkovitch indenter (Fig. 1).

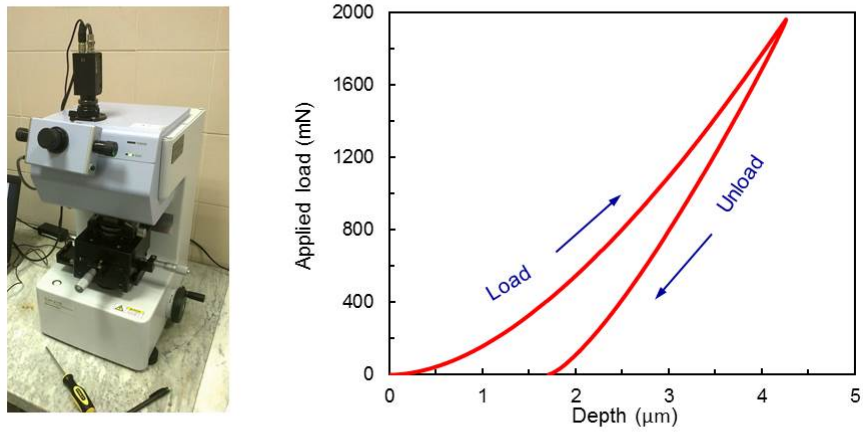

Figure 1. Shimadzu DUH-211S depth-sensing indentation system, with an example of load-unload cycle.

An euhedral quartz single crystal was sliced up into ten sections cut along different crystallographic directions. Each section was reduced to a thickness of 300 μm and glued on a standard thin section glass. At the polarizing optical microscope all the samples were confirmed to be inclusion free and untwinned. According to Oliver and Pharr (1992), both dynamic hardness (H) and indentation modulus (Eit) were measured on each sample for each applied load (F) in the range between 10 and 2000 mN, with a constant velocity of penetration. Measurements were repeated on five sections with a different velocity of penetration to evaluate the dependence of the measured hardness and indentation modulus on the penetration speed. Our results show a measurable difference in the mechanical anisotropy (H and Eit) of quartz as a function of crystallographic direction (Fig. 2). We also assessed how the mechanical properties are affected by the velocity of indentation. Moreover, each sample displayed a systematic and well pronounced decrease of the hardness with the maximum applied load (i.e., the so called "*Indentation Size Effect*").

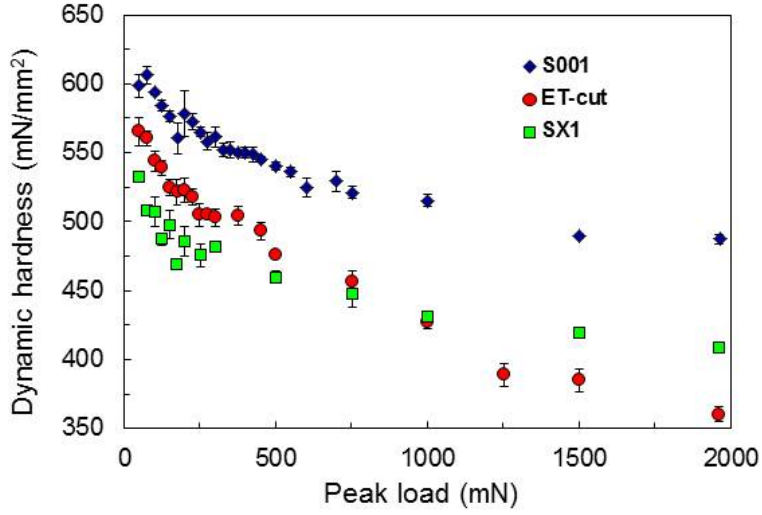

Figure 2. Experimental results for quartz dynamic hardness measured along different crystallographic directions

References

Oliver W.C. and Pharr G.M (1992) - An improved technique for determining hardness and elastic modulus using load and displacement sensing indentation experiments. *Journal of Materials Research*, 7, 1564-1583.

Periodico di Mineralogia, ECMS 2015, 41-42

PERIODICO di MINERALOGIA
established in 1930

An International Journal of
MINERALOGY, CRYSTALLOGRAPHY, GEOCHEMISTRY,
ORE DEPOSITS, PETROLOGY, VOLCANOLOGY
and applied topics on *Environment*, *Archaeometry* and *Cultural Heritage*

Study of the asbestos bodies and chemical-physical modification of mineral fibres in rat histological tissues using electron microscopy and micro-Raman spectroscopy

Nicola Bursi Gandolfi[1*], Simone Pollastri[1], Alessandro F. Gualtieri[1] and Alberto Viani[2]

[1] Department of Chemical and Geological Sciences, University of Modena and Reggio Emilia, Via G. Campi 103, 41125, Modena, Italy
[2] Centre of Excellence Telč , Batelovská 485-6, 588 56, Telč, Czech Republic
* Corresponding author: *nicola.bursigandolfi@unimore.it*

Asbestos minerals chrysotile and fibrous amphiboles have been widely used since a long time for the manufacture of many industrial products, thanks to their outstanding technological properties such as durability, insulation, flame resistance and many others. Unfortunately, asbestos minerals were discovered to induce lung diseases such as mesothelioma if inhaled (Lemen, 1980; Mossman et al., 1996; Kamp, 2009). Erionite is a fibrous zeolite, morphologically similar to asbestos minerals and assumed to be even more carcinogenic than chrysotile and crocidolite (Baumann et al., 2013).

If asbestos minerals are found in the histological tissues of human and animal lungs, they usually appear as coated by irregularly shaped bodies called "asbestos bodies" (Roggli, 1989). To better understand the mechanism of formation of asbestos bodies and subsequent modification of the mineral fibres surrounded by the coating, three mineral fibres were analysed *in situ* in histological tissues of rats by high resolution FEG-SEM microscopy. The three mineral fibres are: (1) UICC standard crocidolite amphibole asbestos; (2) UICC standard chrysotile asbestos; (3) fibrous erionite from Jersey, Nevada (USA). The fibres are embedded in unique histological slides of rats which were part of a past long term project for the determination of the cancerogenicity of mineral fibres conducted by the Ramazzini Cancer Research Institute (Bentivoglio, Bologna, Italy). In that project, Sprague Dawley rats were inoculated with mineral fibres and subjected to a 3 years long animal testing aimed to the assessment *in vivo* of the fibres cancerogenicity (mesothelioma formation). The project started in 1981 at the Bologna Institute of Oncology with a systematic and integrated study involving long-term experimental bioassays of this three types of mineral fibres, in a highly standardized manner. These animal histological slides represent a complete set useful to study the interaction between cellular environment and natural mineral fibres. The microscopic observation of the fibres within the or-

ganic tissues were performed using a FEG-SEM. Each mineral fibre observed in the section could be clearly distinguished due to Energy Dispersive X-ray Spectrometry (X-EDS) analysis, also the different elemental composition of the asbestos bodies was studied, in this regard parts of histological tissue was dissolved and the asbestos bodies and fibres recovered were subsequently analysed with micro-Raman technique at CET (Centre of Excellence Telč, Czech Republic) for collecting structural information. The combination of the two experimental methods allowed to study in detail the nature of the asbestos bodies and the morpho-chemical changes that occurred in the three mineral fibres in contact with the organic medium. The results permit to shed some more light on the mechanism of formation of asbestos bodies with respect to other biochemical and physical parameters of the fibres.

References

Baumann F., Ambrosi J.P. and Carbone M. (2013) - Asbestos is not just asbestos: an unrecognized health hazard. *The Lancet Oncology*, 14, 576 – 578.

Kamp D. W. (2009) - Asbestos-induced lung diseases: an update. *Translational Research : The Journal of Laboratory and Clinical Medicine*, 153, 143–152.

Lemen, R.A., Dement J.M. and Wagoner J.K. (1980) - Epidemiology of Asbestos-Related Diseases. *Environmental Health Perspectives*, 34, 1–11.

Mossman B.T., Kamp D.W. and Weizman S.A. (1996) - Mechanisms of carcinogenesis and clinical features of asbestos associated cancers. *Cancer Investigation*, 14, 466–80.

Roggli V.L. (1989) - Pathology of human asbestosis: a critical review. In: Advances in Pathology. Vol. 2. (eds): C.M. Fenoglio Preiser, Yearbook Publishers, Chicago (U.S.A.), 31–60.

Periodico di Mineralogia, ECMS 2015, 43

PERIODICO di MINERALOGIA
established in 1930

An International Journal of
MINERALOGY, CRYSTALLOGRAPHY, GEOCHEMISTRY,
ORE DEPOSITS, PETROLOGY, VOLCANOLOGY
and applied topics on *Environment*, *Archaeometry* and *Cultural Heritage*

ECMS 1988-2015:

An overview of mineral spectroscopy in the last 30 years

Georges Calas

Institute of Mineralogy, Condensed Matter Physics and Cosmochemistry, Paris, France
and
2014-2015 Sustainable Development Chair, College de France, Paris, France
Corresponding author: *georges.calas@college-de-france.fr*

Mineral spectroscopy was already well established when the first European Meeting on "*Absorption Spectroscopy in Mineralogy*" was organized in Rome on October 1988 by A. Mottana and F. Burragato of the University of Rome “La Sapienza” and held at the Accademia Nazionale dei Lincei (Palazzo Corsini). After earlier studies by pioneers such as Roger Burns, Bill Fyfe or Colin Farmer, mineral spectroscopy appeared soon to be a major link between Earth and environmental sciences and physical and chemical sciences, bringing at the same time a wealth of original information on mineral properties and formation conditions as well as on geochemical and geophysical properties of crustal and mantle rocks. Since then, mineral spectroscopy has much expanded and diversified, being a major facet of the "Mineral physics" field. It brings an original understanding of the structure of (multicomponent) minerals, glasses, melts and solutions. For instance, the current discussion about the validity of the accepted definition of minerals relies largely on spectroscopic information of nanominerals, mineral nanoparticles, nuclei and clusters.

Since 30 years, mineral spectroscopy is currently used in most Earth and environmental science departments. The classical fingerprint approach is being progressively supported by modeling and simulation methods, with the success of first-principle calculations that provide a way to predict spectroscopic properties of minerals. A brief overview of some progresses accomplished in a large variety of domains will be presented, including large user facilities, extreme conditions, microscale measurements or field measurements and remote sensing and molecular environmental science.

Periodico di Mineralogia, ECMS 2015, 45-46

PERIODICO di MINERALOGIA
established in 1930

An International Journal of
MINERALOGY, CRYSTALLOGRAPHY, GEOCHEMISTRY,
ORE DEPOSITS, PETROLOGY, VOLCANOLOGY
and applied topics on *Environment*, *Archaeometry* and *Cultural Heritage*

Health effects of crystalline silica: a methodological approach to the study of industrially processed materials

Fabio Capacci[1], Francesco Di Benedetto[2,*], Luca Pardi[3] and Maurizio Romanelli[2]

[1] Health Agency of Florence, Firenze, Italy
[2] Department of Earth Sciences, Università di Firenze, Firenze (Italy)
[3] Istituto per i Processi Chimico-Fisici (CNR-IPCF), Pisa (Italy)
* Corresponding author: *francesco.dibenedetto@unifi.it*

The growing attention paid to the health and environmental effects of the exposure to minerals in the airborne dusts includes among the most relevant topics the crystalline silica (CS). The interest in the health effects correlated to the respiration of dusts rich in quartz and cristobalite is not only related to the well studied pneumoconiosis (the silicosis), but also to the ascertained carcinogenic effects of CS towards the lung tissues.

The identification of a molecular scale aetiologic correlation between the physical and chemical properties of CS and its health effects is still under consideration by the recent literature. Apparently, not only experimental studies carried out under laboratory conditions, but also characterisation of the industrial CS-bearing materials in their own physico-chemical conditions will contribute to shed some light on this correlation.

In this study, we review the most recent literature studies carried out on materials coming from numerous industrial production processes, in which CS occurs as raw, support or processed material. Some common features of these studies can be evidenced. Firstly, the sampling within the process is performed before and after a specific manipulation of the CS (indeed, some chemical, thermal or mechanical modification can be inferred), and in relation with the generated amount of suspended dusts. Secondly, the analytical approach: not only the obvious determination of the chemical composition, but also the mineralogical speciation, the presence of radical species, the presence of heteroelements at the silica surface, the presence of homo- and heterospecies with unsaturated coordination shells. Most of these analytes require the use of specific element selective spectroscopic techniques, among which mainly X-ray Absorption Spectroscopy and Electron Paramagnetic Resonance (also in the so-called spin trapping approach) can be outlined.

The main obtained results suggest that while CS is more or less unchanged (if its bulk chemistry and crystal structure are considered), the presence of radical species and heteroele-

ments at the surface can be drastically modified by any of the considered industrial manipulation, thus marking as different the workers' exposure to CS before and after the manipulation. We also suggest that the variability of the health effects ascribed to CS, long debated, is in some way correlated to this variability of the radical speciation and of the crystal surface properties.

Finally, we want to show, as a case study the preliminary results of a recent investigation involving the so-called “artificial stone”, industrial products made up by a mixture of epoxy resins and quartz: objects are realised through fluid forming, hardening the resins and finally polishing (as natural stones). The preliminary EPR confirms the appearance of a new radical species, unprecedented for all considered CS-bearing materials, which is formed during the final polishing of the artificial stone. This species is also formed with pathways empirically correlated to the type of performed polishing. We want to stress that there is a worldwide alert on workers belonging to this industrial branch, because of the particularly heavy health consequences.

Periodico di Mineralogia, ECMS 2015, 47-48

PERIODICO di MINERALOGIA
established in 1930

An International Journal of
MINERALOGY, CRYSTALLOGRAPHY, GEOCHEMISTRY,
ORE DEPOSITS, PETROLOGY, VOLCANOLOGY
and applied topics on *Environment*, *Archaeometry* and *Cultural Heritage*

The crystal structure of girvasite, $NaCa_2Mg_3(PO_4)_3(CO_3)(H_2O)_6$, a complex phosphate carbonate hydrate based upon electroneutral heteropolyhedral layers

Anastasia P. Chernyatieva[1], Sergey V. Krivovichev[1,2,*], Sergey N. Britvin[1,2] and Victor N. Yakovenchuk[2]

[1] St. Petersburg State University, Department of Crystallography, University Emb. 7/9, St. Petersburg 199034, Russia
[2] Nanomaterials Research Centre, Kola Science Centre, Russian Academy of Sciences, 14 Fersman Str., Apatity 184200, Murmansk Region, Russia
*Corresponding author: *s.krivovichev@spbu.ru*

The crystal structure of girvasite, $NaCa_2Mg_3(PO_4)_3(CO_3)(H_2O)_6$, has been refined using X-ray diffraction data collected at 173 K, which allowed to revise its crystal chemical formula. The mineral is monoclinic, $P2_1/c$, a = 6.4784(2), b = 12.2313(3), c = 21.3494(6) Å, β = 89.624(2)°, V = 1691.67(8) Å^3 (at 173 K), Z = 4, R_1 = 0.037 for 6471 unique observed reflections (Krivovichev et al., 2015). The crystal structure of girvasite contains three Mg, two Ca and one Na sites. The Mg atoms are octahedrally coordinated by O atoms and H_2O molecules. The Ca sites are coordinated by eight anions each, whereas the Na site has a coordination number equal to seven. The crystal structure is based upon heteropolyhedral sheets formed by polymerization of Mg octahedra, PO_4 tetrahedra and CO_3 groups. The sheets consist of fundamental building units (FBBs) formed by two Mg octahedra that share edges to form dimers decorated by three PO_4 tetrahedra and linked to a unit consisting of a MgO_6 octahedron sharing an edge with a carbonate triangle. The FBBs polymerize to form chains running parallel to the *a* axis. The chains are further polymerized to compose heteropolyhedral sheets stuffed by the Ca^{2+} and Na^+ cations, and H_2O groups to form electroneutral layers parallel to (001).

The adjacent layers connect to each other via a complex system of hydrogen bonds. The interesting feature of the structure is a bidentate coordination of Mg2 atom by a CO_3 group.

Girvasite is the most structurally complex mineral among natural phosphate carbonates known to date. Its high structural complexity reflects its chemical complexity and high hydration state, which are the result of the specific geochemical and thermodynamic conditions of its formation (low-temperature and low-pressure interactions of phosphate-bearing solutions with primary dolomite carbonatites).

Girvasite, a rare hydrous Na-Ca-Mg phosphate carbonate, has been first described by Britvin et al. (1990) from hydrothermal veins in dolomite carbonatites of the Zhelezny (Iron)

Mine, Kovdor massif, Kola Peninsula, Russia. The mineral was probably the result of reaction of primary dolomite with phosphate-bearing hydrothermal solutions. The Zhelezny mine is known as a type locality for several phosphate minerals, including rimkorolgite, $BaMg_5(PO_4)_4(H_2O)_8$ (Britvin et al., 1995; Krivovichev et al., 2002), strontiowhitlockite, $Sr_9Mg(PO_3OH)(PO_4)_6$ (Britvin et al., 1991), bakhchisaraitsevite, $Na_2Mg_5(PO_4)_4(H_2O)_7$ (Liferovich et al., 2000; Yakubovich et al. 2000), cattiite, $Mg_3(PO_4)_2(H_2O)_{22}$ (Britvin et al. 2002; Chernyatieva et al., 2013), etc.

This observation allows us to revise the crystal chemical formula of girvasite as $NaCa_2Mg_3(PO_4)_3(CO_3)(H_2O)_6$. This formula excludes simultaneous occurrence of the basic $(OH)^-$ and acid $(PO_3OH)^{2-}$ anions originally postulated for girvasite by Sokolova and Yegorov-Tismenko (1990).

Acknowledgements

This work was supported for by the Russian Foundation for Basic Research (grant # 14-05-00910) and internal grant of St. Petersburg State University (# 3.38.136.2014). X-ray diffraction measurements have been performed at the SPbSU X-ray Diffraction Resource Centre.

References

Britvin S.N., Ferraris G., Ivaldi G., Bogdanova A.N. and Chukanov N.V. (2002) - Cattiite $Mg_3(PO_4)_2 \cdot 22H_2O$, a new mineral from Zhelezny mine (Kovdor Massif, Kola Peninsula, Russia). *Neues Jahrbuch für Mineralogie Monatshefte*, 4, 160-168.

Britvin S.N., Pakhomovskii Y.A., Bogdanova A.N. and Skiba V.I. (1991) - Strontiowhitlockite, $Sr_9Mg(PO_3OH)(PO_4)_6$, a new mineral species from the Kovdor deposit, Kola-Peninsula, USSR. *Canadian Mineralogist*, 29, 87- 93.

Britvin S.N., Pakhomovskii Y.A., Bogdanova A.N., Khomyakov A.P. and Krasnova N.I. (1995) - Rimkorolgite, $(Mg,Mn)_5(Ba,Sr,Ca)(PO_4)_4 \cdot 8H_2O$, a new mineral. *Zapiski Vsesoyuznyi Mineralogicheskoe Obshchestva*, 124, 90-95 (in Russian).

Chernyatieva A.P., Krivovichev S.V. and Britvin S.N. (2013) - The crystal structure of cattiite, $Mg_3(PO_4)_2(H_2O)_{22}$. *Zapiski Rossiiskogo Mineralogicheskogo Obshchestva*. 142(2), 120-128 (in Russian).

Krivovichev S.V., Britvin S.N., Burns P.C. and Yakovenchuk V.N. (2002) - Crystal structure of rimkorolgite, $Ba[Mg_5(H_2O)_7(PO_4)_4](H_2O)$, and its comparison with bakhchisaraitsevite. *European Journal of Mineralogy*, 14, 397-402.

Krivovichev S.V., Chernyatieva A.P. and Britvin S.N., Yakovenchuk V.N. (2015) - The crystal structure of girvasite, $NaCa_2Mg_3(PO_4)_3(CO_3)(H_2O)_6$, a complex phosphate carbonate hydrate based upon electroneutral heteropolyhedral layers. *Russian Geology and Geophysics*, 56, 155-163.

Kampf A.R., Mills S.J., Housley R.M., Rossman G.R., Nash B.P., Dini M. and Jenkins R.A. (2013) - Joteite, $Ca_2CuAl[AsO_4][AsO_3(OH)]_2(OH)_2 \cdot 5H_2O$, a new arsenate with a sheet structure and unconnected acid arsenate groups. *Mineralogical Magazine*, 77, 2811-2823.

Liferovich R.P., Pakhomovsky Ya.A., Yakubovich O.V., Massa W., Laajoki K., Gehör S., Bogdanova A.N. and Sorokhtina N.V. (2000) - Bakhchisaraitsevite, $Na_2Mg_5[PO_4]_4 \cdot 7H_2O$, a new mineral from hydrothermal assemblages related to phoscorite – carbonatite complex of the Kovdor massif, Russia. *Neues Jahrbuch für Mineralogie Monatshefte*, 402-418.

Sokolova E.V. and Yegorov-Tismenko Y.K. (1990) - Crystal structure of girvasite. *Doklady Akademii Nauk SSSR*, 331, 1372-1376 (in Russian).

Yakubovich O.V., Massa W., Liferovich R.P. and Pakhomovsky Y.A. (2000) - The crystal structure of bakhchisaraitsevite, $[Na_2(H_2O)_2]\{(Mg_{4.5}Fe_{0.5})(PO_4)_4(H_2O)_5\}$, a new mineral species of hydrothermal origin from the Kovdor phoscorite - carbonatite complex, Russia. *Canadian Mineralogist*, 38, 831-838.

Periodico di Mineralogia, ECMS 2015, 49-50

PERIODICO di MINERALOGIA
established in 1930

An International Journal of
MINERALOGY, CRYSTALLOGRAPHY, GEOCHEMISTRY,
ORE DEPOSITS, PETROLOGY, VOLCANOLOGY
and applied topics on *Environment*, *Archaeometry* and *Cultural Heritage*

Geology and occurrence of Ti deposits in Hadong, Korea

Jinbeom Choi* and Jiyoung Kwak

Department of Geology, Gyeongsang National University, Jinju 660-701, Korea
* Corresponding author: *jbchoi586@gmail.com*

Massif-type anorthosites is located in Sancheong-Hadong area, southcentral part of Korea. The anorthosites in the Jirisan gneiss complex of Yeongnam massif comprise the diamond-like shaped Sancheong body (about 10km×12km) in the north and the N-S elongated Hadong body (about 2-3km×25km) in the south. Ti ore deposits are developed along and within the Hadong anorthosites (Fig.1). Based on mafic minerals and their textures, the Hadong anorthosites are divided into 3 types of massive and foliated, and intercumulated, where the intercumulated type narrowly occurs in the foliated one. All types of anorthosites mainly consist of plagioclase, showing labradorite in composition.

The vein types of Ti orebodies run north-south in direction with exposure of outcrops in several spots. Ti ores mainly show disseminated and partly layered in texture. Bukcheon area, the south end of the Hadong anorthosite, is of the biggest Ti ore deposit with large tonnage and high grade, of which ore veins vary 1.9~23 m in width and 50~110 m in length. Ilmenite as a main ore mineral occurs in the interstistics among minerals of the cumulated anorthosite commonly associated with hornblende, plagioclase, apatite, etc.

Ilmenite orebodies as well as anorthosite is mainly composed of mafic mineral of amphiboles. Amphiboles show subhedral to anhedral in shape and mostly blueish green and/or green in color in plane polarized light. The amphiboles exhibit two types in terms of chemical composition, that is, ferrohornblende found in matrices and ferropargasite in crystals with over 1mm in size. Ferropargasite sometimes show zonal texture with brownish to blueish green in color from core to rim. It is altered by clinopyroxene.

The intruded diorite is in contact with anorthosite in south end. Ilmenite orebodies in anorthosite extend to this diorite. Ilmenite found in diorite shows exsolution texture of hematite lamellae with rutile, leading to experience of thermal alteration by intrusive diorite after ilmenite mineralization.

Assessment of Ti ores is tried for future exploration and mining. Geostatistical method is applied to 17 drill holes of total 1,620 m in depth using GOCAD. Ilmenite ore bodies intend to be located in eastern part of anorthosite showing NW strike and W and/or NE dipping. Ore bodies display vein type with tabular or lenticular in shape. Main orebodies seem to extend to

about 100 m below the ground. The measured resources in study area are estimated about 7.5 million tons of ores with average grade of 4.98 wt.% TiO_2.

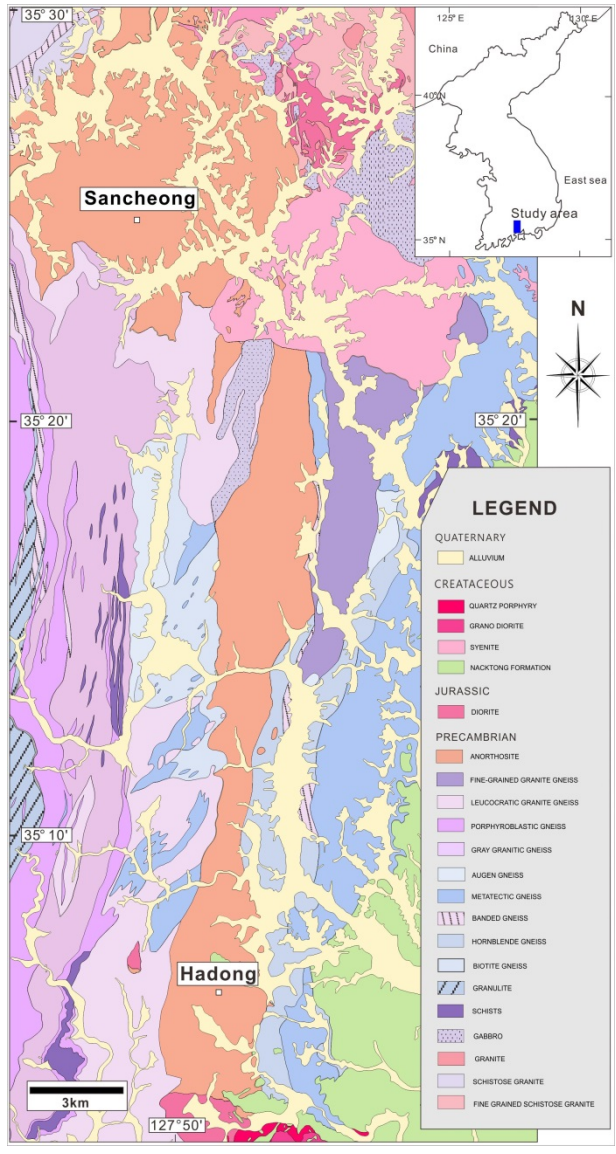

Figure 1. Geological map of the study area
(modified from Sancheong, Danseong and Jingyo 1:50,000 geological sheets).

Periodico di Mineralogia, ECMS 2015, 51-52

PERIODICO di MINERALOGIA
established in 1930

An International Journal of
MINERALOGY, CRYSTALLOGRAPHY, GEOCHEMISTRY,
ORE DEPOSITS, PETROLOGY, VOLCANOLOGY
and applied topics on *Environment*, *Archaeometry* and *Cultural Heritage*

Multicomponent solid solutions in secondary oxyminerals from a polymetallic deposit in the Sudetes, Poland

Justyna Ciesielczuk[1,*] and Janusz Janeczek[2]

[1] University of Silesia Department of Geology, Będzińska 60 41-200 Sosnowiec Poland
[2] University of Silesia Department of Geochemistry, Mineralogy and Petrography, Będzińska 60 41-200 Sosnowiec Poland
* Corresponding author: *justyna.ciesielczuk@us.edu.pl*

Experimental data (e.g., Artl and Ambruster, 1999; Jambor and Dutrizac, 1995; Magalhães et al., 1988) suggest the continuous solid solution among secondary arsenates, phosphates, sulfates, vanadates and carbonates. However, mineralogical observations in numerous oxide zones of weathered ore deposits (e.g., Ciesielczuk and Bzowski, 2003; Ciesielczuk et al., 2004; Holeczek and Janeczek, 1991; Plášil et al., 2009; Siuda and Gołębiowska, 2011; Siuda and Kruszewski, 2006) suggest the contrary. Whether this discrepancy results from the limited number of observations or it reflects the limited solid solutions in natural samples is disputable. Results of EPMA supported by SEM, FTIR and X-ray powder diffraction of a suite of secondary minerals formed from the weathering of primary sulfide minerals in a polymetallic ore deposit in the Sudety Mts, SW Poland, reveal a complex scheme of both cationic (Cu, Co, Fe, Zn) and anionic (AsO_4, PO_4, VO_4) substitutions leading to multicomponent solid solutions. For instance, the simple scheme of cationic substitutions ($Co^{2+} \leftrightarrow Zn^{2+}$) in zoned crystals of the erythrite-köttigite solid solution is complicated by the additional substitution of Zn^{2+} by Cu^{2+} in minerals with compositions close to the köttigite end-member. While there are no crystal chemical constraints on continuous solid solutions among structurally keen minerals, the metal and anions concentrations, pH and redox conditions are major factors determining the extent of solid solutions.

References

Artl T. and Ambruster T. (1999) - Single-crystal X-ray structure refinement of cornwallite, $Cu_5(AsO_4)_2(OH)_4$: A comparson with its polymorph cornubite and the PO_4-analogue pseudomalachite. *Neues Jahrbuch für Mineralogie Monatshefte*, 10: 468–480.

Ciesielczuk J. and Bzowski Z. (2003) - Secondary (Cu,Zn)-oxyminerals from the Miedzianka copper deposit in Rudawy Janowickie, Sudetes Mts. Preliminary report. *Mineralogical Society of Poland – Special Papers*, 17, 150–152.

Ciesielczuk J., Szełęg E., Kuźniarski M. and Bylina P. (2004) - Preliminary data of erythrite

from Ciechanowice (Miedzianka Deposit, Sudetes Mts.). *Mineralogical Society of Poland – Special Papers*, 24, 123-126.

Holeczek J. and Janeczek J. (1991) - Pseudomalachite from Radzimowice and some comments on its occurrence in Miedzianka (Sudetes Mts.). *Mineralogia Polonica*, 22, 17-26.

Jambor J.L., Dutrizac J.E. (1995) - Solid solutions in the annabergite-erythrite-hornesite synthetic system. *Canadian Mineralogist*, 33, 1063-1071.

Magalhães M.C.F., Pedrosa de Jesus J.D. and Williams P.A. (1988) - The chemistry of formation of some secondary arsenate minerals of Cu(II), Zn(II) and Pb(II). *Mineralogical Magazine,* 52, 679-690.

Plášil J., Sejkora J., Čejka J., Škoda R., Goliáš V. (2009) - Supergene mineralization of the Medvědín uranium deposit, Krkonoše Mountains, Czech Republic. *Journal of Geosciences,* 54, 15-56.

Siuda R., Gołębiowska B. (2011) - New data on supergene minerals from Miedzianka-Ciechanowice deposit in the Rudawy Janowickie Mountains (Lower Silesia, Poland). *Polish Geological Review*, 59, 226-234.

Siuda R. and Kruszewski Ł. (2006) - New data on bayldonite, cornwallite, olivenite and philipsburgite from Miedzianka (Rudawy Janowickie Mts., Sudetes, Poland). *Mineralogical Society of Poland – Special Papers*, 28, 202-204.

Periodico di Mineralogia, ECMS 2015, 53-54

PERIODICO di MINERALOGIA
established in 1930

An International Journal of
MINERALOGY, CRYSTALLOGRAPHY, GEOCHEMISTRY,
ORE DEPOSITS, PETROLOGY, VOLCANOLOGY
and applied topics on *Environment*, *Archaeometry* and *Cultural Heritage*

Identification by micro-Raman spectroscopy of iron-rich mineral particles lying on the surface of erionite fibers from Rome (Oregon - USA) and from Karlik (Cappadocia - Turkey)

Alessandro Croce[1], Mario Allegrina[1], Giovanni Gaudino[2], Haining Yang[2], Michele Carbone[2] and Caterina Rinaudo[1,*]

[1] Department of Science and Technological Innovation, Università del Piemonte Orientale 'Amedeo Avogadro', Viale Teresa Michel, 11 - 15121 Alessandria, Italy
[2] University of Hawai'i Cancer Center, University of Hawai'i, Honolulu, Hawaii, USA
* Corresponding author: *caterina.rinaudo@uniupo.it*

Erionite, a mineral belonging to the family of zeolite, is well known for its impact on human health. In fact, the high incidence of mesothelioma observed in some villages of Cappadocia (Turkey) has been ascribed to the presence of this mineral present in the rocks of that region (Dogan et al., 2006; Dogan et al., 2008; Carbone et al., 2011). Erionite crystallizes with fibrous morphology as the "asbestos", minerals responsible for important respiratory diseases, such as mesothelioma, asbestosis and malignant pulmonary carcinoma. Although high incidence of mesothelioma detected in villages of Cappadocia as well as the levels of erionite found in urban areas of North Dakota similar to those of Cappadocia, indicating a high risk of erionite/induced mesothelioma in US (Carbone et al., 2011) erionite has never been introduced in the list of the "asbestos" minerals (Baumann et al., 2013), although its carcinogenic potential has been shown higher than that of the asbestos fibers, both *in vitro* and in animal models (Guthrie, 1992).

Samples of erionite from Rome, Oregon, and from Karlik, Cappadocia, were at first characterized by micro-Raman spectroscopy, which allowed to identify the fibrous phase as erionite and to exclude the presence of other zeolite phases like, for example, offretite (Croce et al., 2013). After, a detailed study of the fiber surfaces under an Environmental Scanning Electron Microscope, E-SEM Quanta 200 model of the FEI group, equipped with an EDS detector, EDAX system was carried out. The used equipment allowed the morphological and chemical characterization of unpolished samples without previous coating, which means that changes consequent to sample preparation (for example loss in particles or small fibers) were minimized, but only qualitative chemical data can be recorded. By means of the BSE images, at high magnifications particles/grains micrometric -on samples from Rome- or sub-micrometric- on the fibers from Karlik- have been observed as light contrasts on the fiber surface. Addressing the electron beam selectively on the areas of the fiber free from the light particles or on the light grains we acquired EDS spectra of pure erionite- without iron- or of erionite and iron. The micro-Raman spectroscopy has therefore been applied to define the mineral phases associated with the observed particles/grains. Focusing the laser beam onto the

light particles on the erionite from Rome Raman spectra could be recorded. Based on the Raman results, three minerals were identified as constituent of the micrometric particles lying on the fiber surface: goethite-FeO(OH), hematite-Fe_2O_3 and jarosite-$KFe_3^{3+}(SO_4)_2(OH)_6$. The obtained Raman data allowed to demonstrate: a) that iron is not a chemical ion constituent of the erionite phase, b) that not all the K detected by chemical analyses, performed using ICP or EDS techniques (Dogan et al., 2006; Dogan et al., 2008), is a constituent of Oregon erionite phase but may be due to the presence of jarosite on the fiber surface.

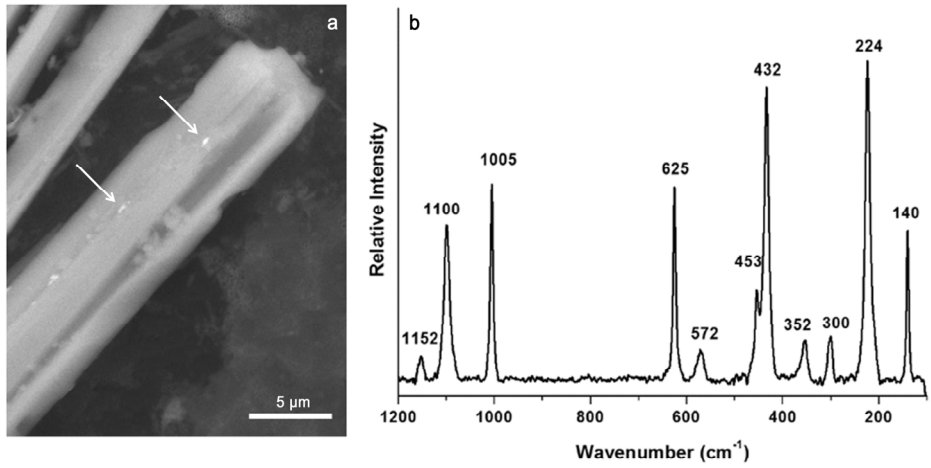

Figure 1. (a) BSE image of a bundle of fibers from Rome, showing lighter particles on its surface (some of them are indicated by arrows). (b) Raman spectrum obtained addressing the laser beam onto one of these particles. In this case, the Raman bands indicate jarosite.

References

Baumann F., Ambrosi J. P. and Carbone M. (2013) - Asbestos is not just asbestos: an unrecognised health hazard. *Lancet Oncology*, 14, 576-578.

Carbone M., Baris Y.I., Bertino P., Brass B., Comertpay S., Dogan A.U., Gaudino G., Jube S., Kanodia S., Partridge C.R., Pass H.I., Rivera Z.S., Steele I., Tuncer M., Way S., Yang H. and Miller A. (2011) - Erionite exposure in North Dakota and Turkish villages with mesothelioma. *Proceedings of the National Academy of Science of U S A*, 108, 13618-13623.

Croce A., Musa M., Allegrina M., Rinaudo C., Baris Y.I., Dogan A.U., Powers A., Rivera Z., Bertino P., Yang H., Gaudino G. and Carbone M. (2013) - Micro-Raman spectroscopy identifies crocidolite and erionite fibers in tissue sections. *Journal of Raman Spectroscopy*, 44, 1440-1445.

Dogan A.U., Baris Y.I., Dogan M., Emri S., Steele I., Elmishad A.G. and M. Carbone (2006) - Genetic predisposition to fiber carcinogenesis causes a mesothelioma epidemic in Turkey. *Cancer Research*, 66, 5063-5068.

Dogan A.U., Dogan M. and Hoskins J.A. (2008) - Erionite series minerals: mineralogical and carcinogenic properties. *Environmental Geochemistry and Health*, 30, 367-381.

Guthrie G.D. (1992) - Biological effects of inhaled minerals. *American Mineralogist*, 77, 225-243.

Periodico di Mineralogia, ECMS 2015, 55-56

PERIODICO di MINERALOGIA
established in 1930

An International Journal of
MINERALOGY, CRYSTALLOGRAPHY, GEOCHEMISTRY,
ORE DEPOSITS, PETROLOGY, VOLCANOLOGY
and applied topics on *Environment*, *Archaeometry* and *Cultural Heritage*

Perettiite-(Y), $Y^{3+}{}_2Mn^{2+}{}_4Fe^{2+}[Si_2B_8O_{24}]$, a new mineral from Momeik, Myanmar

Rosa Micaela Danisi[1, 2*], Thomas Armbruster[1], Hao A.O. Wang[3], Detlef Günther[3], Mariko Nagashima[4], Eric Reusser[5] and Willy Bieri[2]

[1]Mineralogical Crystallography, Institute of Geological Sciences, University of Bern, Freiestrasse 3, 3012 Bern, Switzerland
[2]GRS Gemresearch Swisslab AG, Baldismoostrasse 14, 6043 Adligenswil, Switzerland
[3]ETH Zurich, Laboratory of Inorganic Chemistry, Vladimir-Prelog-Weg 1, 8093 Zürich, Switzerland
[4]Graduate School of Science and Engineering, Yamaguchi University, Yamaguchi 753-8512, Japan
[5]Institut für Geochemie und Petrologie, ETHZ, Clausiusstrasse 25, 8082 Zürich, Switzerland
*Corresponding author: *rosamicaela.danisi@libero.it*

The new mineral, perettiite-(Y), endmember formula $Y^{3+}{}_2Mn^{2+}{}_4Fe^{2+}[Si_2B_8O_{24}]$, from pegmatites in the region of Momeik, north of Mogok, Myanmar, occurs as yellow needles enclosed in phenakite crystals. The mineral was named after the mineralogist and Head of GRS Gemresearch Swisslab AG, Dr. Adolf Peretti.

The empirical formula using the LA-ICP-MS data (based on 24 O atoms *pfu*) is $Y_{2.06}Ln_{0.53}Zr_{0.02}Th_{0.01}Mn_{3.24}Ca_{0.38}Fe_{0.71}Mg_{0.07}Al_{0.11}Li_{0.22}Si_{1.95}B_{7.44}Be_{0.31}O_{24}$. The perettiite-(Y) crystals show a tetragonal X-ray diffraction pattern but the structure could only be solved as a 50/50 pseudo-merohedral orthorhombic twin with the *a* and *c* axes having the same length. The structure (space group *Pmna* with $a = 12.8252(5)$, $b = 4.6187(2)$, $c = 12.8252(5)$ Å, $V = 759.71(5)$ Å^3, $Z = 2$) is characterized by 2 eight-coordinated sites: one dominated by Y and lanthanoids (Ln) and the other by Mn^{2+} (with additional Ca^{2+} and Y^{3+}). An octahedrally coordinated site is occupied by (Fe^{2+}, Mg) with additional Li^+. These cation sites form an interlayer between two tetrahedral sheets of $Si_2B_8O_{24}$ composition (Fig. 1). Boron is to a low degree substituted by beryllium. The borosilicate tetrahedral layers form 4-, 5- and 8-membered rings within (010).

Perettiite-(Y) is brittle, with irregular fracture and (010) cleavage; the estimated Mohs hardness is ~7. Using the empirical formula the density was estimated to be 4.533 g cm^{-3}. Perettiite-(Y) is biaxial, $\alpha = 1.82(1)$, $\gamma = 1.84(1)$ (589 nm).

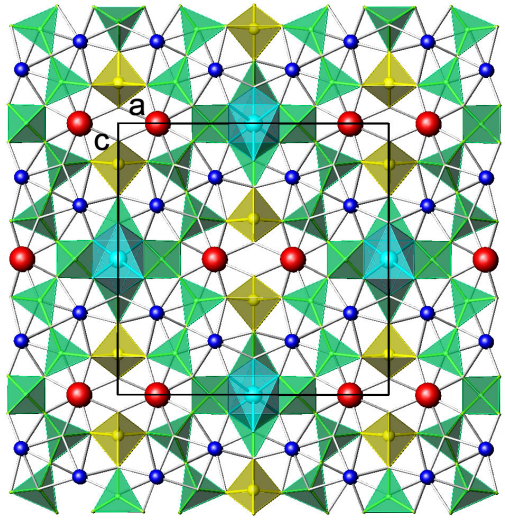

Figure 1. The tetrahedral sheet in perettiite-(Y) (Si tetrahedra yellow, B tetrahedra green). The interlayer octahedron (Fe, Mg, Li) between the 4-rings of BO_4 tetrahedra is shown in light blue. Mn^{2+} rich interlayer sites are blue; Y and lanthanoids interlayer sites are red. Unit-cell outlines are shown.

Periodico di Mineralogia, ECMS 2015, 57-58

PERIODICO di MINERALOGIA
established in 1930

An International Journal of
MINERALOGY, CRYSTALLOGRAPHY, GEOCHEMISTRY, ORE DEPOSITS, PETROLOGY, VOLCANOLOGY
and applied topics on *Environment*, *Archaeometry* and *Cultural Heritage*

Synthesis and crystal-chemistry of amphiboles along the join richterite - ferrorichterite: a combined spectroscopic (FTIR, Mössbauer), X-ray and microchemical study

Giancarlo Della Ventura[1*], Gunther Redhammer[2], Gianluca Iezzi[3] and Jean-Louis Robert[4]

[1]Dipartimento di Scienze, Università Roma Tre, I-00146 Roma
[2]Department of Materials Science & Physics, University of Salzburg, 5020 Austria
[3]Dipartimento di Ingegneria & Geologia, Università G. d'Annunzio, 66100 Chieti
[4]IMPMC, Université Pierre et Marie Curie, 75252 Paris Cedex 05 France
*Corresponding author: *giancarlo.dellaventura@uniroma3.it*

Five amphiboles were synthesized by hydrothermal techniques at 500-600 °C, 1 kbar $P_{(H2O)}$ and internally-buffered fO_2 conditions along the nominal join richterite [$^{A}Na^{B}(NaCa)^{C}Mg_5{}^{T}Si_8O_{22}{}^{W}(OH)_2$] – ferrorichterite [$^{A}Na^{B}(NaCa)^{C}Fe^{2+}{}_5{}^{T}Si_8O_{22}{}^{W}(OH)_2$], hence ^{C}Mg is ideally substituted with $^{C}Fe^{2+}$. The resulting run powders were studied by a combination of EMPA and FESEM (field emission scanning electron microscopy), XRD and FTIR and ^{57}Fe Mössbauer spectroscopy. Due to crystal-size limitations, only the Fe-end member could be analysed by EMP, while two additional samples could be analysed by FESEM-EDS. Rietveld refinement of X-ray diffraction patterns show that, albeit a linear trend is evident in the amphibole cell-parameters, there is a significant decrease in the amphibole yield along the join, counterbalanced by an increase in clinopyroxene (cpx), up to 27 wt.%, for the Fe-end member.

^{57}Fe Mössbauer spectra, could be fitted on the basis of known spectral parameters of similar amphiboles in the literature (e.g., Iezzi et al., 2004; Della Ventura et al., 2005), and corrected for the spectral contribution of cpx. The results show that Fe^{3+} is completely ordered at M(2), while Fe^{2+} is disordered over all available C-sites; no ferrous iron is resolved at M(4). The OH-stretching FTIR spectra show complex patterns for intermediate compositions with up to eight bands; these can be assigned to the various configurations involving Mg/Fe^{2+} at *M*(1,3), locally associated with both full and empty A-sites (Burns and Strens, 1966; Della Ventura et al., 1997; Iezzi et al., 2005).

Details in the crystal chemistry for all amphiboles in the series were obtained on the basis of the spectroscopic methods, and the resulting data were in reasonable agreement with those derived by WDS-EDS analyses for the Fe-richer samples. For increasing Fe in the system, the amphibole composition deviates toward sodic compositions following the exchange vector $^{C}(Fe^{2+})^{B}Ca^{C}Fe^{3+}{}_{-1}{}^{B}Na_{-1}$ whereby a progressive decrease of ^{B}Ca is coupled to an increase of Na

at M(4) plus Fe^{3+} at M(2). This structural rearrangement suggests a possible instability of end-member ferro-richterite for stereochemical reasons.

Interestingly, along the studied series, there is a general increase in the amphibole crystal size and a clear evolution of the crystal morphologies, from extremely acicular at the Mg-end member composition, to prismatic and stubby for the Fe-richer compositions.

References

Burns, R.G. and Strens, R.G.J. (1966) - Infrared study of the hydroxyl bonds in clinoamphiboles. *Science*, 153, 890-892.

Della Ventura, G., Robert, J.-L., Raudsepp, M., Hawthorne, F.C., Welch, M. (1997) - Site occupancies in synthetic monoclinic amphiboles: Rietveld structure-refinement and infrared spectroscopy of (nickel, magnesium, cobalt)-richterite. *American Mineralogist*, 82, 291-301.

Della Ventura, G., Iezzi, G., Redhammer, G.J., Hawthorne, F.C., Scaillet, B., Novembre, D. (2005) - Synthesis and crystal-chemistry of alkali amphiboles in the system Na2O-MgO-FeO-Fe_2O_3-SiO_2-H_2O as a function of f_{O2}. *American Mineralogist*, 90, 1375-1383.

Iezzi, G., Cámara, F., Della Ventura, G., Oberti, R., Pedrazzi, G. e Robert, J.-L. (2004) - Synthesis, crystal structure and crystal-chemistry of ferri-clinoholmquistite, $\square Li_2Mg_3Fe3+_2Si_8O_{22}(OH)_2$. *Physics and Chemistry of Minerals*, 31, 375-385.

Iezzi, G., Della Ventura, G., Hawthorne, F.C., Pedrazzi, G., Robert, J.-L., Novembre, D. (2005) - The (Mg,Fe2+) substitution in ferri-clinoholmquistite, $\square Li_2$ $(Mg,Fe2+)_3$ $Fe3+_2$ Si_8 O_{22} $(OH)_2$. *European Journal of Mineralogy*, 17, 733-740.

Periodico di Mineralogia, ECMS 2015, 59-60

PERIODICO di MINERALOGIA
established in 1930

An International Journal of
MINERALOGY, CRYSTALLOGRAPHY, GEOCHEMISTRY,
ORE DEPOSITS, PETROLOGY, VOLCANOLOGY
and applied topics on *Environment*, *Archaeometry* and *Cultural Heritage*

Physico-chemical properties of quartz from industrial manufacturing and its cytotoxic effects on alveolar macrophages: the case of green sand mould casting for iron production

Francesco Di Benedetto[1,*], Elena Gazzano[2,3], Maura Tomatis[3,4], Francesco Turci[3,4], Luca Pardi[5], Simona Bronco[5], Gabriele Fornaciai[6], Massimo Innocenti[6], Giordano Montegrossi[7], Maurizio Muniz-Miranda[6], Alfonso Zoleo[8], Fabio Capacci[9], Bice Fubini[3,4], Dario Ghigo[2,3] and Maurizio Romanelli[1]

[1] Department of Earth Sciences, Università di Firenze, Firenze (Italy)
[2] Department of Oncology, Università degli studi di Torino, Torino (Italy)
[3] "G. Scansetti" Interdepartmental Center for Studies on Asbestos and other Toxic Particulates, Università degli studi di Torino, Torino (Italy)
[4] Department of Chemistry, Università degli studi di Torino, Torino (Italy)
[5] Istituto per i Processi Chimico-Fisici (CNR-IPCF), Pisa (Italy)
[6] Department of Chemistry, Università di Firenze, Sesto Fiorentino (Italy)
[7] Istituto di Geoscienze e Georisorse (CNR-IGG), Florence (Italy)
[8] Department of Chemical Sciences, Università di Padova, Padova (Italy)
[9] Health Agency of Florence, Firenze, Italy
* Corresponding author: *francesco.dibenedetto@unifi.it*

The knowledge of the relationships between quartz surface reactivity and the mineralogical and physico-chemical context experienced by the materials undergoing an industrial process is a key information to get a deeper understanding of the specific features of the production itself and may help to clarify the variability of health hazard associated to inhalation of crystalline silica dusts.

In this study, industrial samples coming from the production of the cast iron are considered. A quartz rich sand before use to form the mould and the material recovered after the dismantling of the mould were sampled. Samples were investigated by XRD and SEM/EDS microanalysis, to check the mineralogical speciation and the sand morphology, by ATR and micro-Raman spectroscopies, to gain details about the nature of the phase associated to the sand dur-

ing the processing, and by cw- and pulsed EPR spectroscopies, to investigate the presence and the speciation of the radicals associated to quartz microcrystals. EPR, associated to the spin trapping technique, was also used to evaluate the potential of samples to generate particle-derived free radicals in cell-free tests. Finally, cytotoxic effects of the dust recovered after mould demolition were evaluated on murine alveolar macrophages (MH-S cell line).

Sand before its use in the casting process reveals the unique presence of hAl radicals, conventionally found in many quartz-bearing raw materials. Conversely, powder material recovered from the dismantled mould exhibits a single paramagnetic species, attributed to a carbonaceous radical, interacting with neighbouring protons and related to the presence of a carbon coating. Remarkably, under the adopted experimental conditions, the intensity of the original signal attributed to the hAl radicals appears as depleted below the detection limit in the processed powders. Sand recovered after mould dismantling contains a slightly larger amount of respirable particles than the raw sand, is able to catalyze carboxyl radical generation, but shows lower surface reactivity in hydroxyl radical generation with respect to the raw material and does not elicit cytotoxic response in alveolar macrophages.

Physico-chemical modifications, occurring during cast iron production, lead, thus, to a quartz-rich dust largely contaminated by a poor reactive amorphous carbon, which probably hide some of the reactive surface sites responsible for hydroxyl radical generation and cell-particle interaction. The change in radical speciation also occurs involving a complete annihilation of the inorganic radicals present in the original sand.

Periodico di Mineralogia, ECMS 2015, 61-62

PERIODICO di MINERALOGIA
established in 1930

An International Journal of
MINERALOGY, CRYSTALLOGRAPHY, GEOCHEMISTRY, ORE DEPOSITS, PETROLOGY, VOLCANOLOGY
and applied topics on *Environment*, *Archaeometry* and *Cultural Heritage*

Raman study of $MgAl_2O_4$–$FeAl_2O_4$ and $MgAl_2O_4$–$MgFe_2O_4$ spinel solid solutions

Veronica D'Ippolito[1,*], Giovanni B. Andreozzi[1], Pier Paolo Lottici[2] and Danilo Bersani[2]

[1] Sapienza University of Rome, Department of Earth Sciences, Piazzale Aldo Moro 5, Rome, Italy
[2] University of Parma, Department of Physics and Earth Sciences, Parco Area delle Scienze 7/a, Parma, Italy
* Corresponding author: *veronica.dippolito@uniroma1.it*

Spinels oxides are minerals or synthetic materials which are nowadays attracting considerable interests because of their physical and chemical properties.

Ten synthetic spinels belonging to the $MgAl_2O_4$–$FeAl_2O_4$ solid-solution and four synthetic spinels belonging to the $MgAl_2O_4$–$MgFe_2O_4$ solid-solution have been studied by Raman spectroscopy to verify the effects of the Fe^{2+} and Fe^{3+} cations on the vibrational spectra. The Raman modes are affected by the substitution of Mg by Fe^{2+} into the tetrahedrally coordinated sites in the first series, $MgAl_2O_4$–$FeAl_2O_4$, and by the Fe^{3+} substitutions for Al into the octahedrally coordinated sites in the second series, $MgAl_2O_4$–$MgFe_2O_4$.

The spinels have been synthetized by flux growth method and analysed chemically by electron microprobe and structurally by single-crystal X-ray diffraction. Raman spectra were collected with a Jobin Yvon LabRam micro-spectrometer using two different laser excitation wavelengths. A blue 473.1 nm solid-state laser was used for the samples with high Fe^{2+} content, whereas the other samples were recorded with a red 632.8 nm He-Ne laser.

While the substitution $Fe^{2+} \rightarrow Mg$ proceeds along the $MgAl_2O_4$–$FeAl_2O_4$ series, no change in the wavenumber of the E_g, $F_{2g}(3)$, and A_{1g} modes is observed up to Fe^{2+} ~20%. After this value, all Raman-active modes show a shift toward lower wavenumbers in agreement with the heavier cation mass of Fe^{2+} (Fig. 1a). The slow and non-linear decrease in the wavenumber observed for these modes is also due to cation disorder and to the concomitant incorporation of low amounts of Fe^{3+} in the spinel structure. The presence of Fe^{2+} and Fe^{3+} in the octahedron strongly influences the vibrational spectra because of the heavier cation mass of Fe than that of Al. As a matter of fact, the $F_{2g}(3)$ mode exhibits a two-mode behaviour: the intensity of the peak at 670 cm^{-1} (typical of Fe-poor spinels) decreases almost linearly, whereas that of the peak at ~610 cm^{-1} grows with increasing Fe^{2+} content.

Along the $MgAl_2O_4$–$MgFe_2O_4$ series, the Raman spectra are considerably different, suggesting that trivalent cation strongly affect vibrational dynamics (Fig. 1b). A general decrease

toward lower wavenumber is observed for all the Raman modes. Besides the substitution $Fe^{3+} \rightarrow Al$, the Raman spectra are affected by cation disorder, because the magnesioferrite end-member ($MgFe_2O_4$) has an almost fully inverse structure, with divalent cation occurring in the octahedron and trivalent cations distributing almost equally between the tetrahedron and the octahedron. While increasing the Fe^{3+} content, the intensity of the ~720 cm^{-1} peak, the one assigned to the trivalent cation occurring at the tetrahedron in the $MgAl_2O_4$ end-member, increases, whereas that of the 765 cm^{-1} peak, the one assigned to divalent cation occurring at the tetrahedron, decreases.

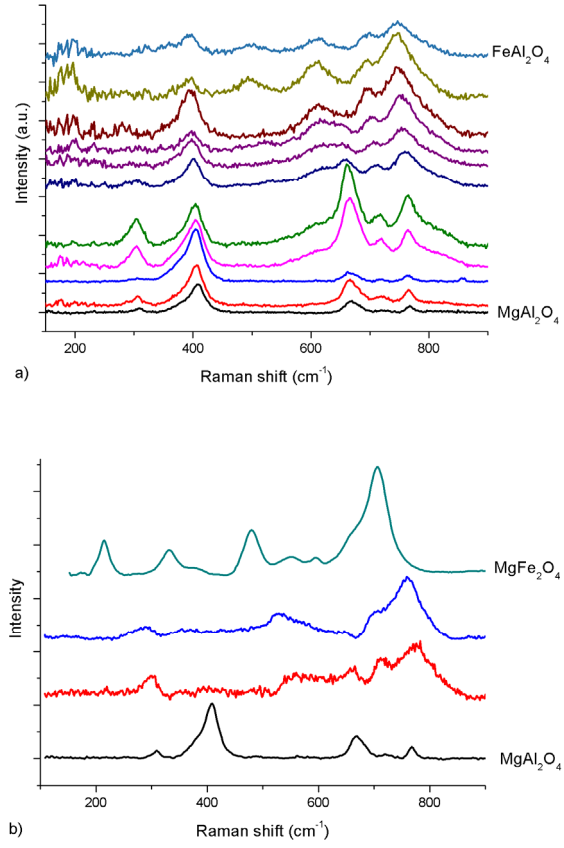

Fig. 1 - The evolution with composition of the Raman spectra measured on synthetic spinels belonging to (a) the $MgAl_2O_4$–$FeAl_2O_4$ series and (b) the $MgAl_2O_4$–$MgFe_2O_4$ series.

Periodico di Mineralogia, ECMS 2015, 63-64

PERIODICO di MINERALOGIA
established in 1930

An International Journal of
MINERALOGY, CRYSTALLOGRAPHY, GEOCHEMISTRY, ORE DEPOSITS, PETROLOGY, VOLCANOLOGY
and applied topics on *Environment*, *Archaeometry* and *Cultural Heritage*

Hydrogen bonding in mineral-related $M_{2-x}M_{12}(OH)_6(HXO_4)_2(H_{2x/3}XO_4)_6$ compounds: synergy of X-ray diffraction and infrared spectroscopy

Tamara Đorđević* and Eugen Libowitzky

Institut für Mineralogie und Kristallographie, Geozentrum, Universität Wien,
Althanstr. 14, A-1090 Vienna, Austria
* Corresponding author: *tamara.djordjevic@univie.ac.at*

Single-crystal X-ray diffraction and infrared (IR) micro-spectroscopy have been used to study hydrogen bonding in polar, mineral-related $M1_{2-x}M2_{12}(OH)_6(H_{2x/3}X1O_4)_6(HX2O_4)_2$ compounds ($M = Mg^{2+}$, Ni^{2+}, Co^{2+}; $X = V^{5+}$, As^{5+}). Single crystals of $Ni(1)_{1.14}Ni(2)_{12}(OH)_6(H_{0.285}As(1)O_4)_6(HAs(2)O_4)_2$ (**1**), $Co(1)_{1.74}Co(2)_{12}(OH)_6(H_{0.085}As(1)O_4)_6(HAs(2)O_4)_2$ (**2**), $Mg(1)_{1.19}Mg(2)_{12}(OH)_6(H_{0.27}As(1)O_4)_6(HAs(2)O_4)_2$ (**3**), $Mg1_{1.4}Mg2_{12}(OH)_6(H_{0.2}V1O_4)_3(HV2O_4)$ (**4**) were obtained using hydrothermal synthesis.

The crystal structures of **1** – **4** ($P6_3mc$, $Z = 1$) consist of two parts: the first part is made up of a partly occupied chain of face-sharing $M1O_6$-octahedra, and the second one is based on a 3D octahedral framework having the topology of the zeolite cancrinite (Figure 1). The main part of a 3D framework is the double [001] chain consisting of $M2O_6$-octahedra, which share edges and, within the (001). The *M*2-based double chains are interconnected through O atoms in a 3D framework, where two types of [001] channels are formed. The first larger channel is filled with the *M*1-based octahedral chain and the second with $HX2O_4$-tetrahedra. The *M*1 sites contain a significant number of vacancies. The distance along [001] between adjacent *M*1 sites ($c/2$ = 2.513, 2.561, 2,546 and 2.538 Å for **1**–**4**, respectively) is too short to allow full occupancy of the *M*1 site, which also shows a very large displacement parameter along [001] (U_{33} = 4.0(2), 6.4(3), 3.7(5), 4.4(6) $Å^2$, for **1**–**4**, respectively). This suggests a local displacement of the *M*1 cation from its average position, probably to an adjacent empty *M*1 site. The *M*2 site is fully occupied. The partial substitution of $X1O_4$ with $HX1O_4$ is necessary to achieve charge neutrality. In all investigated structures a fully occupied OH^- is linked to the double chains (O4–H4···O5 = 3.123(6), 3.227(12), 3.302 (5), 3.223(5) Å, for **1**–**4**, respectively). The position of the H atom belonging to the $HX2O_4$-group could be identified (O6–H6···O4 = 3.164(4), 3.215(8), 3.236(4), 3.210(4) Å, for **1**–**4**, respectively).

The H atom responsible for the partial protonation of the $X1O_4$-tetrahedra occupies these sites only at the *M*1 vacancies. Some of the proton sites within the crystal structure of these compounds represent a very small proportion of total proton content (0.285, 0.085, 0.27 and 0.2 H pfu for **1**–**4**, respectively) and therefore are difficult to detect using X-ray diffraction. Using single-crystal micro- IR spectroscopy we obtained distinct signals from the protons (Figure 2). The wavenumber region between 4000 and 3300 cm^{-1} contains bands assigned to the protons attached to the $M2_2O_7(OH)_2$ dimers of face-sharing $M2O_4(OH)_2$ octahedra, and the protons bonded to the apical O atom of the $X2O_4$ group that lies in the trigonal channel at approximate same wavenumbers in IR spectra of all compounds under discussion. From the IR bands found in the wavenumber region below 3300 cm^{-1} O3–H3···H2 distances between 2.5 and 2.65 Å are expected (Libowitzky, 1999). These distances are incompatible with those obtained from the X-ray diffraction study, in which distances between O atoms that can accept a H3 proton are all longer than 2.8 Å (O3···O2 =2.847(3), 2.894(6), 2.859(7), 2.918(3) Å, for **1**–**4**, respectively). This confirms that H3 atoms are associated with octahedral vacancies where the structure is locally distorted.

Using the combination of these two techniques we propose the following proton distribution: the H3 protons are concentrated in the vicinity of structural defects likely to be *M* octahedral vacancies, where they form $HX1O_4$ tetrahedra. These protons are strongly hydrogen bonded (2.6-2.7 Å). The corresponding O–H···O angles are expected to approach 180°, and so these protons would vibrate along the unshared edges of the vacant octahedron.

Financial support of the Austrian Science Foundation (FWF) (Grant V203-N19) to T.Đ. is gratefully acknowledged.

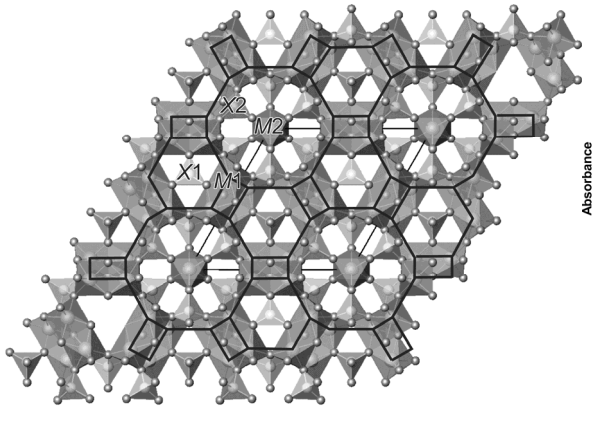

Figure 1

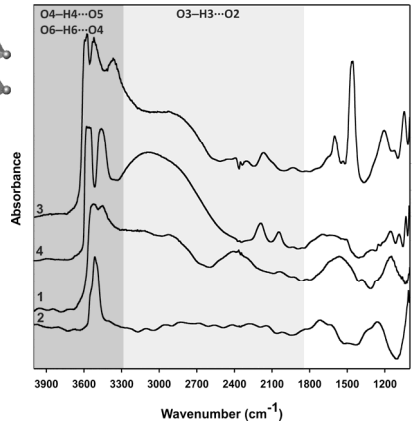

Figure 2

References

Libowitzky E. (1999) - Correlation of O–H stretching frequencies and O–H···O hydrogen bond lengths in minerals. *Montashefte für Chemie*, 130, 1047-1059.

Periodico di Mineralogia, ECMS 2015, 65-66

PERIODICO di MINERALOGIA
established in 1930

An International Journal of
MINERALOGY, CRYSTALLOGRAPHY, GEOCHEMISTRY,
ORE DEPOSITS, PETROLOGY, VOLCANOLOGY
and applied topics on *Environment*, *Archaeometry* and *Cultural Heritage*

Turquoise zircon: new diffraction and optical data – an overview of V^{4+} crystal chemistry and optical spectroscopy in minerals

Michele Dondi[1,*], Matteo Ardit[2] and Giuseppe Cruciani[2]

[1] CNR-ISTEC, Institute of Science and Technology for Ceramics, via Granarolo 64, Faenza, Italy
[2] University of Ferrara, Department of Physics and Earth Sciences, via Saragat 1, Ferrara, Italy
* Corresponding author: *michele.dondi@istec.cnr.it*

Vanadium-doped zircon exhibits a deep turquoise color that drew attention to this ceramic pigment since its discovery in 1946.

Questions about vanadium valence state and its location in the zircon structure (Fig. 1) gave rise to many diffraction and spectroscopy studies. An overall convergence emerges from this literature about the occurrence of tetravalent vanadium. In contrast, the accommodation of V^{4+} at the Si tetrahedral site or at the Zr cubic site was for a long time disputed, until convincing diffraction and spectroscopic data (Siggel and Jansen 1990; Niesert et al. 2002) pointed to V^{4+} hosted at a peculiar four-fold coordinated interstitial site of the zircon structure.

Data from the literature on the optical spectroscopy and crystal chemistry of V^{4+} in zircon (low to intermediate V contents) and isostructural phases (hafnon, coffinite and thorium germanate) were gathered and integrated new experimental results performed on four industrial pigments (representing high V concentrations). In addition, the optical and crystal chemical features of tetravalent vanadium occurring in minerals and synthetic analogues (cavansite, minasgraite, forsterite, apophyllite, goslarite) was overviewed. The zircon pigments were characterized by X-Ray Fluorescence spectrometry (XRF), X-Ray Powder Diffraction (XRPD) and Diffuse Reflectance Spectroscopy (DRS) to get chemical composition, unit-cell and structural parameters (e.g. metal-oxygen bond lengths, polyhedral volumes, and distortion parameters), energy of the main optical bands and crystal field strength (10*Dq*).

The V^{4+} incorporation into the zircon structure is testified by a progressive increase of the unit-cell volume with the V concentration. XRF analysis indicates a deficiency in Si suggesting a Si - V balanced substitution. Such a substitution is supposed to occur (1) at the Si tetrahedral site 4*b* (point symmetry -4*m*2 or D_{2d}) through a Si^{4+} by V^{4+} substitution or (2) at the interstitial site 16*g* (point symmetry 2 or C_2) where the V^{4+} can be hosted, and the lattice electroneutrality is maintained by the formation of a Si vacancy. The optical spectra of V-doped zircon exhibit

three main bands in the 4000 - 22000 cm^{-1} range, which can be attributed to electronic transitions of V^{4+} in tetrahedral coordination. The spectral features are different from those of minerals containing the $(VO_2)^{2-}$ vanadyl ion (cavansite, minasgraite) where V^{4+} is in a five-fold, square planar coordination. The crystal field strength of tetravalent vanadium in zircon and isostructural phases scales with the mean <V-O> distances at the interstitial tetrahedron, as obtained by diffraction (in zircon on average 1.894 Å).

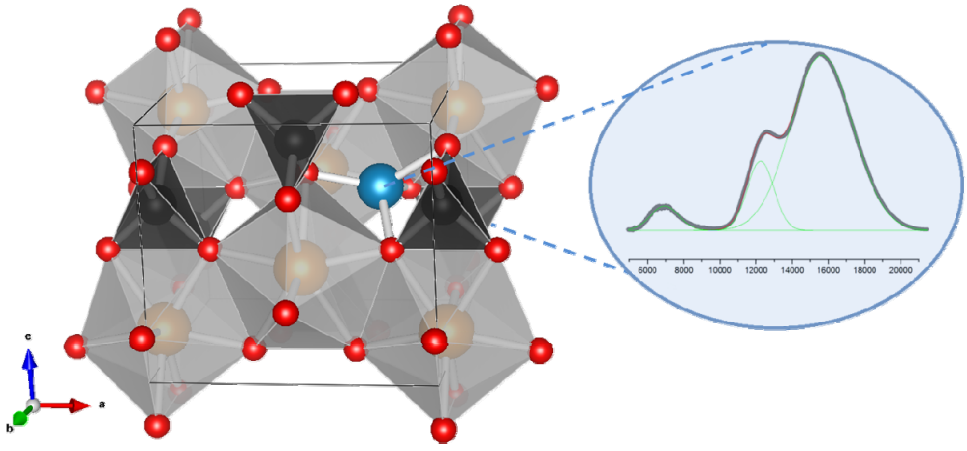

Figure 1. Polyhedral representation of the tetragonal structure of the zircon, space group $I4_1/amd$. Isolated SiO_4 tetrahedra share corners and edges with ZrO_8 dodecahedra. These latter are arranged in chains parallel to the *ab* plane through edge-sharing. These chains are cross linked by sharing corners with SiO_4 tetrahedra. In this representation the position of the V^{4+} ion is depicted at the interstitial site 16*g* (blue sphere within an interstitial void of between two structural chains), and its spectral features.

This observation needs caution, since 10*Dq* is challenging to be calculated, because of the three-fold splitting of the $^2T_2$ band due to the low point symmetry of the interstitial site. The optical spectra of vanadium-doped zircon appear to depend in a complex way on the amount of V^{4+} actually incorporated, local environment at the interstitial site, Zr/Si ratio in zircon, and particle size distribution.

References

Niesert A., Hanrath M., Siggel A., Jansen M. and Langer K. (2002) - Theoretical study of the polarized electronic absorption spectra of vanadium-doped zircon. *Journal of Solid State Chemistry*, 169, 6-12.

Siggel A. and Jansen M. (1990) - Röntgenographische Untersuchungen zur Bestimmung der Einbauposition von Seltenen Erden (Pr, Tb) und Vanadium in Zirkonpigmenten. *Zeitschrift für anorganische und allgemeine Chemie*, 583, 67-77.

Periodico di Mineralogia, ECMS 2015, 67-68

PERIODICO di MINERALOGIA
established in 1930

An International Journal of
MINERALOGY, CRYSTALLOGRAPHY, GEOCHEMISTRY,
ORE DEPOSITS, PETROLOGY, VOLCANOLOGY
and applied topics on *Environment*, *Archaeometry* and *Cultural Heritage*

Raman investigation of new and potentially new minerals of nabimusaite supergroup

Mateusz Dulski[1,2,*], Roman Wrzalik[2,3], Irina Galuskina[4] and Evgeny Galuskin[4]

[1]Institute of Material Sciences, University of Silesia, 75 Pułku Piechoty 1a, 41-500 Chorzow, Poland
[2]Silesian Center for Education and Interdisciplinary Research, 75 Pułku Piechoty 1a, 41-500 Chorzow, Poland
[3]A.Chelkowski Institute of Physics, University of Silesia, Uniwersytecka 4, 40-007 Katowice, Poland
[4]Department of Geochemistry, Mineralogy and Petrography, Faculty of Earth Sciences, University of Silesia, Bedzińska 60, 41-200 Sosnowiec, Poland
* Corresponding author: *mdulski@us.edu.pl*

In pyrometamorphic rocks of the Hatrurim Complex (Israel, Palestinian Autonomy) new minerals: nabimusaite, $KCa_{12}(SiO_4)_4(SO_4)_2O_2F$; zadovite, $BaCa_6[(SiO_4)(PO_4)](PO_4)_2F$, and aradite $BaCa_6[(SiO_4)(VO_4)](VO_4)_2F$ (Galuskin et al., 2015a, b), were recently described. These minerals belong to the one family (nabimusaite supergroup) with modular structure of antiperovskite type where octahedra are anion-centered and tetrahedra are cation-centered. Zadovite-type structure (1:1) is described by general crystal chemical formula, $AB_6(TO_4)_2(TO_4)_2W$, whereas nabimusaite-type structure (3:1) is characterized by $AB_{12}(TO_4)_4(TO_4)_2W_3$, where A = Ba, K, Sr...; B = Ca, Na...; T = Si, P, V^{5+}, S^{6+}, Al...; W = O^{2-}, F^-. Antiperovskite single $\{[WB_6](TO_4)_2\}$ and triple $\{[W_3B_{12}](TO_4)_4\}^{3+}$ layers intercalate with single $A(TO_4)_2$ layers in minerals of the zadovite and nabimusaite groups, respectively (Gfeller et al., 2013; Galuskin et al. 2015a, b). A few next potentially new mineral were detected in pyrometamorphic rocks in the zadovite group: $BaCa_6(SiO_4)_2(SO_4)_2O$ and $BaCa_6[(SiO_4)_{1.5}(SO_4)_{0.5}]$ $[(V,P)^{5+}O_4)]_2F$; and in the nabimusaite group: $BaCa_{12}(SiO_4)_4(PO_4)_2F_2O$, $BaCa_{12}(SiO_4)_4(SO_4)_2O_3$, $BaCa_{12}(SiO_4)_4[(PO_4)_{1.5}(CO_3)_{0.5}]F_{1.5}O_{1.5}$. New and potential new minerals of the nabimusaite supergroup might be well distinguished on the base of Raman spectra by typical vibration of the (TO_4) tetrahedral group: $(PO_4)^{3-}$, $(VO_4)^{3-}$, $(SiO_4)^{4-}$ and $(SO_4)^{2-}$. Moreover, structural layer arrangements allows for the possibility of distinguish the symmetric (ν_1) and antisymmetric (ν_3) stretching vibrations of (TO_4) associated with bands above 800 cm^{-1}. The vibrations of bending character (ν_2, ν_4) are ascribed to bands in the 300-700 cm^{-1} range while below 300 cm^{-1} one observes stretching vibrations of Ca-O and molecular group rotation modes, especially of $R(TO_4)$ and $T(TO_4)$ (Fig. 1). Interestingly, in minerals of zadovite series the splitting of $\nu_1(SiO_4)^{4-}$ band is not observed while the band splitting is appearing on nabimusaite Raman spectra indicating Si incorporation at two different tetrahedral positions. Similar interpretation can be done for other elements occupying the tetrahedral position within the modular structure. Hence, Raman spectroscopy was applied to follow structural changes as well as the varying mineral chemical

composition within nabimusaite group. These differences are reflected by changing of band intensity e.g. Raman band at ca. 1000 cm^{-1} is a result of sulfur, due to deconvolution: two bands at ca. 835 cm^{-1} and ca. 860 cm^{-1} are an indicator of vanadium and silicon while band at ca. 960 cm^{-1} reflects the varying phosphorus content (Fig. 1).

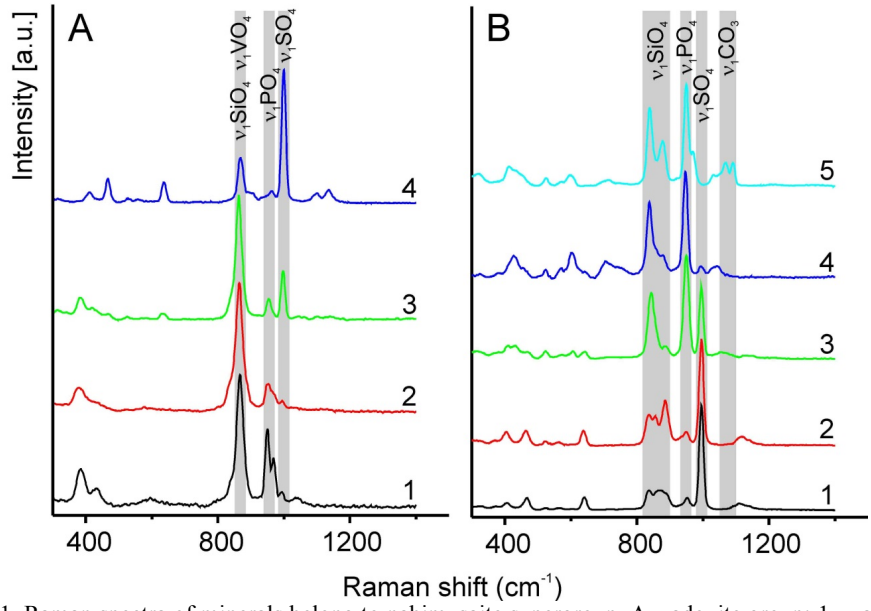

Fig. 1. Raman spectra of minerals belong to nabimusaite supergroup. A. zadovite group: 1 - zadovite, 2 – aradite, 3 - $BaCa_6[(SiO_4)_{1.5}(SO_4)_{0.5}]$ $[(V,P)^{5+}O_4)]_2F$, 4 - $BaCa_6(SiO_4)_2(SO_4)_2O$. B. nabimusaite group: 1 - nabimusaite, 2 - $BaCa_{12}(SiO_4)_4(SO_4)_2O_3$, 3 - $BaCa_{12}[(SiO_4)_{3.5}(PO_4)_{0.5}][(PO_4)_{1.8}(SO_4)_{0.2}]O_{1.7}F_{1.3}$, 4 - $BaCa_{12}(SiO_4)_4(PO_4)_2F_2O$, 5 - $BaCa_{12}(SiO_4)_4[(PO_4)_{1.5}(CO_3)_{0.5}]F_{1.5}$.

References

Galuskin E.V., Gfeller F., Armbruster T., Galuskina I.O., Vapnik Y., Murashko M., Włodyka R. and Dzierżanowski P. (2015) - New minerals with modular structure derived from hatrurite from the pyrometamorphic Hatrurim Complex, Part I: Nabimusaite, $KCa_{12}(SiO_4)_4(SO_4)_2O_2$ F, from larnite rocks of Jabel Harmun, Palestinian Autonomy, Israel. *Mineralogical Magazine, in press*.

Galuskin E.V., Gfeller F., Galuskina I.O., Pakhomova A., Armbruster T., Vapnik Y., Włodyka R., Dzierżanowski P., Murashko M. (2015) - New minerals with modular structure derived from hatrurite from the pyrometamorphic Hatrurim Complex, Part II: Zadovite, $BaCa6[(SiO_4)(PO_4)](PO_4)_2F$, and aradite, $BaCa_6[(SiO_4)(VO_4)](VO_4)_2F$, from paralavas of the Hatrurim Basin, Negev Desert, Israel. *Mineralogical Magazine, in press.*

Gfeller F., Galuskin E.V., Galuskina I.O., Armbruster T., Vapnik Ye., Włodyka R. and Dzierzanowski P. (2013) - Natural $BaCa_6[(SiO_4)(PO_4)](PO_4)_2F$ with a new modular structure type, *Goldschmidt2013, Conference Abstract*, DOI:10.1180/minmag.2013.077.5.7.

Periodico di Mineralogia, ECMS 2015, 69-70

PERIODICO di MINERALOGIA
established in 1930

An International Journal of
MINERALOGY, CRYSTALLOGRAPHY, GEOCHEMISTRY,
ORE DEPOSITS, PETROLOGY, VOLCANOLOGY
and applied topics on *Environment*, *Archaeometry* and *Cultural Heritage*

Bosiite, a new member of the tourmaline supergroup

Andreas Ertl[1,2,*], Ivan A. Baksheev[3] and Gerald Giester[2]

[1] Mineralogisch-Petrographische Abt., Naturhistorisches Museum, Burgring 7, 1010 Wien, Austria
[2] Institut für Mineralogie und Kristallographie, Universität Wien, Althanstrasse 14, 1090 Wien, Austria
[3] Geology Department, Lomonosov Moscow State University, Leninskie Gory, Moscow 119991, Russia
* Corresponding author*: andreas.ertl@a1.net*

Bosiite, $NaFe^{3+}{}_3(Al_4Mg_2)(Si_6O_{18})(BO_3)_3(OH)_3O$, is a new member of the tourmaline supergroup. It is named after Ferdinando Bosi, Ph.D. (Sapienza University of Rome, Italy) and it occurs as well-shaped prismatic crystals up to ~200 μm in length and up to ~50 μm in diameter in the Darasun mine, located in the Transbaikal region, Russia, which was the second mine in terms of gold reserves. This deposit is hosted in basic and intermediate igneous rocks. The most ancient rock is metamorphosed Early Paleozoic gabbro, which was intruded by Middle Palaeozoic and Middle Mesozoic granodiorite, diorite, granite, granosyenite, and syenite, and also by granitic rocks of the Amanansky complex of Early Jurassic age. Ores of this deposit are enriched in sulfides (up to 60%). Gangue minerals are quartz, tourmaline, calcite, and dolomite. Bosiite was found in a gold-bearing quartz vein. It is intimately associated with other tourmalines. The first tourmaline generation is bosiite, which is followed by a second generation of oxy-dravite (Bosi and Skogby, 2013), and a third generation, which is represented by dravite. Bosiite crystallized under hydrothermal conditions. The fluid inclusions in the associated quartz indicate that this tourmaline-type mineral precipitated from boiling fluids at low pressure. Boiling favored the increasing oxygen fugacity and resulted in the increase of Fe^{3+} in this tourmaline-type mineral (Baksheev et al., 2011). Further associated minerals are calcite, dolomite, pyrite, arsenopyrite, chalcopyrite, pyrrhotite, tetrahedrite, sphalerite, galena, and gold.

Ertl et al. (2002) showed that the bond-angle distortion ($\sigma_{oct}{}^2$) of the ZO_6 octahedron in a tourmaline is largely a function of the <*Y*-O> distance of that tourmaline, although the occupant of the *V* site also affects that distortion. The correlation coefficient of <*Y*-O> and $\sigma_{oct}{}^2$ of the ZO_6 octahedron is –0.99 for all investigated tourmalines whose *V* site is occupied by 3(OH) groups. Bosiite (with ${}^Z\sigma_{oct}{}^2 = 42.47$ and <*Y*-O> 2.054 Å) lies exactly on the *V* site = 3(OH) line. Hence, the *V* site of bosiite is completely occupied by $(OH)_3$. No H associated with the O(1) site (≡ *W* site) was found by refinement. Hence, this site is clearly dominated by oxygen, as indicated by the chemistry. The amounts of Al, Fe^{3+} and Mg over the *Y* and *Z* site were optimized

according to the mean atomic numbers and the bond valences. Chemical characterization based on electron microprobe analysis, single-crystal structure refinement and Mössbauer spectroscopy resulted in the empirical structural formula:

$^{X}(Na_{0.73}Ca_{0.23}\square_{0.04})$ $^{Y}(Fe^{3+}{}_{1.47}Mg_{0.80}Fe^{2+}{}_{0.59}Al_{0.13}Ti^{4+}{}_{0.01})$ $^{Z}(Al_{3.23}Fe^{3+}{}_{1.88}Mg_{0.89})$ $(Si_{5.92}Al_{0.08}O_{18})$ $(BO_3)_3$ $(OH)_3$ $^{W}[O_{0.85}(OH)_{0.15}]$

According to the IMA-CNMNC guidelines (Henry et al., 2011), the *X* site is dominated by Na, the *Y* site is the dominated by Fe^{3+}, the *Z* site is dominated by Al along with Mg (*valency-imposed double-site occupancy*), and the *W* site by O^{2-}. Accordingly, this tourmaline is a new species.

In addition, to accommodate the Mg-Al disorder over *Y* and *Z*, we used the procedure recommended by Henry et al. (2013), which leads to the formula:

$^{X}(Na_{0.73}Ca_{0.23}\square_{0.04})$ $^{Y}(Fe^{3+}{}_{2.40}Fe^{2+}{}_{0.59}Ti^{4+}{}_{0.01})$ $^{Z}(Al_{3.36}Mg_{1.69}Fe^{3+}{}_{0.95})$ $(Si_{5.92}Al_{0.08}O_{18})$ $(BO_3)_3$ $(OH)_3$ $^{W}[O_{0.85}(OH)_{0.15}]$

Bosiite is a Na-, Fe^{3+}- and Mg-bearing tourmaline, which is related to the other Na-rich, Fe^{3+}- and/or Mg-bearing tourmalines povondraite, fluor-buergerite, oxy-dravite (Bosi and Skogby, 2013) and dravite, respectively.

Acknowledegements

This work was supported by Austrian Science Fund (FWF) project no. P26903-N19 to AE.

References

Baksheev I.A., Prokof'ev V.Yu., Yapaskurt V.O., Vigasina M.F., Zorina L.D. and Solov'ev, V.N. (2011) - Ferric-iron-rich tourmaline from the Darasun gold deposit, Transbaikalia, Russia. *Canadian Mineralogist*, 49, 263-276.

Bosi F. and Skogby H. (2013) - Oxy-dravite, $Na(Al_2Mg)(Al_5Mg)(Si_6O_{18})(BO_3)_3(OH)_3O$, a new mineral species of the tourmaline supergroup. *American Mineralogist*, 98, 1442-1448.

Ertl A., Hughes J.M., Pertlik F., Foit F.F. Jr., Wright S.E., Brandstätter F. and Marler B. (2002) - Polyhedron distortions in tourmaline. *Canadian Mineralogist*, 40, 153-162.

Henry D.J., Novák M., Hawthorne F.C., Ertl A., Dutrow B., Uher P. and Pezzotta F. (2011) - Nomenclature of the tourmaline-supergroup minerals. *American Mineralogist*, 96, 895-913.

Henry D.J., Novák M., Hawthorne F.C., Ertl A., Dutrow B., Uher P. and Pezzotta F. (2013) - *Erratum*. Nomenclature of the tourmaline supergroup minerals. *American Mineralogist*, 98, 524.

Periodico di Mineralogia, ECMS 2015, 71-72

PERIODICO di MINERALOGIA
established in 1930

An International Journal of
MINERALOGY, CRYSTALLOGRAPHY, GEOCHEMISTRY,
ORE DEPOSITS, PETROLOGY, VOLCANOLOGY
and applied topics on *Environment*, *Archaeometry* and *Cultural Heritage*

Exploiting XPS for clarifying toxicity of mineral fibers

Marzia Fantauzzi[1*], Alessandro Pacella[2], Giovanni B. Andreozzi[2], Paolo Ballirano[2,3], Antonio Gianfagna[2] and Antonella Rossi[1]

[1] Università di Cagliari, Dipartimento di Scienze Chimiche e Geologiche, SS 554 – bivio per Sestu, I-09042 Monserrato (CA); Italy.
[2] Sapienza Università di Roma, Dipartimento di Scienze della Terra, Piazzale A. Moro 5, I-00185 Roma, Italy.
[3]Laboratorio Rettorale Fibre e Particolato Inorganico, Sapienza Università di Roma, Piazzale A. Moro 5, I-00185 Roma, Italy.
* Corresponding author: *fantauzzi@unica.it*

The chemistry of surface layers of nanometer thickness can dramatically change the reactivity of a material. X-ray photoelectron spectroscopy (XPS) combines a high surface sensitivity in the nm range with far greater spatial resolution and accuracy than ever before, allowing the understanding of the mechanisms of the chemical reactions occurring at the samples surface. These features together with the possibility of quantitative analysis of the outermost layers of the materials make XPS technique extremely versatile for the characterization of mineral fibers, which are responsible for serious health problems and respiratory diseases. In the present work the results obtained investigating by XPS fluoro-edenite (Fantauzzi et al., 2012), crocidolite (Pacella et al., 2014), tremolite (Pacella et al., 2015) and, recently, erionite (Ballirano et al., 2015) from different countries and after different surface treatments are summarized and discussed.

Iron in fibrous minerals is reputed to be important for its biological effects, since it may catalyze the Haber – Weiss reaction, generating the reactive oxygen species •OH. An analytical strategy was developed in order to be able to differentiate between Fe(II) and Fe(III), being the toxicity of the two cations different. In fluoro-edenite the iron chemical state was related to radical production and proposed to account for the toxicity of such fibers (Fantauzzi et al., 2012). Notably, fluoro-edenite has been declared highly dangerous for human health by the International Agency for Research on Cancer in 2014. The same XPS approach was also useful for the identification of iron chemical state following fiber incubation in solution. The surface composition of crocidolite (Pacella et al., 2014) and tremolite (Pacella et al., 2015) samples immersed in a buffered H_2O_2 solution (pH = 7.4) up to 168 h was monitored to shed a light on the dissolution dynamics that may occur in vivo.

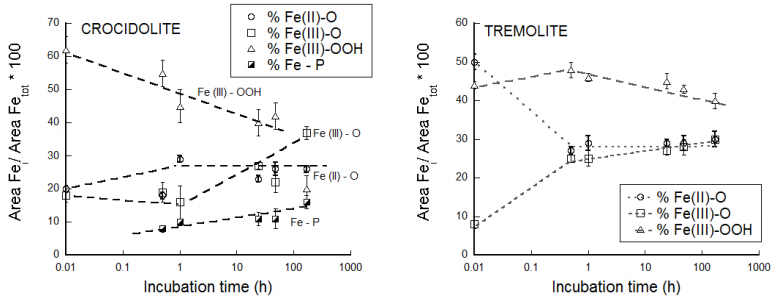

Figure 1: relative intensities of $Fe2p_{3/2}$ signal components for crocidolite and for tremolite in the range 0–168 h. Dashed lines are given as guides to the eye.

XPS provided evidence of iron enrichment at the crocidolite surfaces and, after one hour of exposure to the solution, an increase of Fe(II) content at the surface was found, indicating that the dissolution reaction was faster than the oxidation. Longer incubation time revealed that the Fe(II) content on the surface remained unchanged while Fe(III) bonded to the silicate structure increased (Fig. 1). Also an increase of Fe oxide-hydroxide content and the precipitation of Fe-phosphate were reported suggesting the formation of a coating upon time. In the case of tremolite it was found that Fe(III) content rapidly increases both in the silicate framework and in oxy-hydroxides, while Fe(II) content decreases upon incubation (Fig. 1). It can be thus concluded that for tremolite the oxidation reaction is faster than the dissolution one. Finally, XPS allowed the characterization of erionite surface in an investigation involving chemical, structural and surface modifications of samples of fibrous erionite after incubation in $FeCl_2$ solutions at different salt concentrations (Ballirano et al., 2015). XPS results demonstrated that the iron content increases with ferrous loading and that iron is present as Fe(II). Simultaneously, sodium depletion was observed, thus elucidating that Fe(II) is fixed by the fibers within the erionite structure through an ion-exchange process mainly involving Na.

References

Ballirano P., Pacella A., Cremisini C., Nardi E., Fantauzzi M., Atzei D., Rossi A. and Cametti G. (2015) - Fe (II) segregation at a specific crystallographic site of fibrous erionite: A first step toward the understanding of the mechanisms inducing its carcinogenicity. *Microporous and Mesoporous Materials*, 211, 49 – 63.

Fantauzzi M., Pacella A., Fournier J., Gianfagna A., Andreozzi G.B. and Rossi A. (2012) - Surface chemistry and surface reactivity of fibrous amphiboles that are not regulated as asbestos. *Analytical and Bioanalytical Chemistry*, 404, 821 – 833.

Pacella A., Fantauzzi M., Turci F., Cremisini C., Montereali M.R., Nardi E., Atzei D., Rossi A. and Andreozzi G.B. (2014) - Dissolution reaction and surface iron speciation of UICC crocidolite in buffered solution at pH 7.4: A combined ICP-OES, XPS and TEM investigation. *Geochimica et Cosmochimica Acta*, 127, 221 – 232.

Pacella A., Fantauzzi M., Turci F., Cremisini C., Montereali M.R., Nardi E., Atzei D., Rossi A. and Andreozzi G.B. (2015) - Surface alteration mechanism and topochemistry of iron in tremolite asbestos: A step toward understanding the potential hazard of amphibole asbestos. *Chemical Geology*, 405, 28 – 38.

Periodico di Mineralogia, ECMS 2015, 73-74

PERIODICO di MINERALOGIA
established in 1930

An International Journal of
MINERALOGY, CRYSTALLOGRAPHY, GEOCHEMISTRY,
ORE DEPOSITS, PETROLOGY, VOLCANOLOGY
and applied topics on *Environment*, *Archaeometry* and *Cultural Heritage*

Calculated ion-atom core-level shifts for use in estimating atomic and ionic radii of free atoms and ions

Giuseppe Fierro[1] and Giuliano Moretti[2,*]

[1]Consiglio Nazionale delle Ricerche (CNR) - Istituto per lo Studio dei Materiali Nanostrutturati (ISMN), c/o Dipartimento di Chimica, Sapienza Università di Roma, P.le A. Moro 5, 00185 Roma, Italy
[2]Dipartimento di Chimica, Sapienza Università di Roma, P.le A. Moro 5, 00185 Roma, Italy
* Corresponding author: *giuliano.moretti@uniroma1.it*

In X-ray photoelectron spectroscopy (XPS) core-level shifts of an atom in different chemical environments, including the atom-free ion chemical change, result from both initial- and final-state effects (Egelhoff, 1987). The initial state effect is a static shift in the orbital energies in the ground state of the atom before core ionization. It is directly related to the nature of the chemical bonds in which the atom is involved. The charge distribution of an atom in molecules or solids, or as a free ion, in fact, changes the potentials of core electrons, even though the spatial character of the core electron wave function remains strongly localized within the atom. Instead, the final state effects are related to the degree to which core and valence electrons and the environment of the atom can polarize in response to ionization.

Nowadays, state-of-the-art quantum chemical methods allow to calculate core-level shifts with high accuracy. However, it is still important to combine such computational approaches with simpler methods able to emphasize both the underlying physics and the chemical information which can be obtained by the core-level binding energy shifts.

In this contribution we propose a simple method to estimate atomic and ionic radii of free atoms and ions which can be interestingly compared to the same radii reported for the solid or molecular states.

We use non-relativistic, numerical Hartree-Fock data reported by Broughton and Bagus (1980). The core-level binding energy for most of the common atoms and ions in the periodic table (excluding the actinides and lanthanides) from self-consisted field calculations (ΔSFC) were reported for the cations of the groups 1-16 (metallic and semi-metallic elements), and for the anions of the groups 16-17.

The core electron binding energy for the free ion may be calculated using the equations reported in Moretti (2013):

$$E_b^{v}\,(\text{free ion}) = E_b^{V}(\text{free atom}) + k°Q° - kQ + (Q° - Q)\,R_1^{a} \qquad (1)$$

where: Q° and Q are the number of valence electrons in the free atom and in the free ion, respectively, expressed in units of number of electrons; k° and k are the coupling constants be-

tween the core electron and the valence electrons in the free atom and in the free ion respectively. The k° and k values (in eV) are given by 14.4/r° and 14.4/r, where r° and r are the atomic and the ionic radius (in Å), respectively; R_l^a is the average relaxation (or polarization) energy per valence electron, which takes into account a decrease or an increase of the valence charge of the core-ionized cations or anions. A change in the valence charge with respect to the free atom leads to variations of the intra-atomic relaxation energy of the photoexcited atom. These variations are included in the term k. Accordingly, k depends, for a given core electron, on the ground state valence charge q = Q° – Q (Moretti, 2013).

The theoretical data tabulated by Broughton and Bagus (1980) are used together with Eq. (1) to calculate the ion-atom core-level shifts, [E_b^v (free ion) – E_b^V(free atom)], and the average relaxation energies per valence electron, R_l^a. Then the parameter for the free atom k° and r° = 14.4/k°Q°, and finally the parameter for the free ions k and r = 14.4/kQ were calculated.

As a representative picture, the calculated radii for free atoms and free ions of the 3d transition series are reported in figure. Further work is in progress to obtain empirical relations between the atomic and ionic radii and the electronic polarizability of the free atoms and ions.

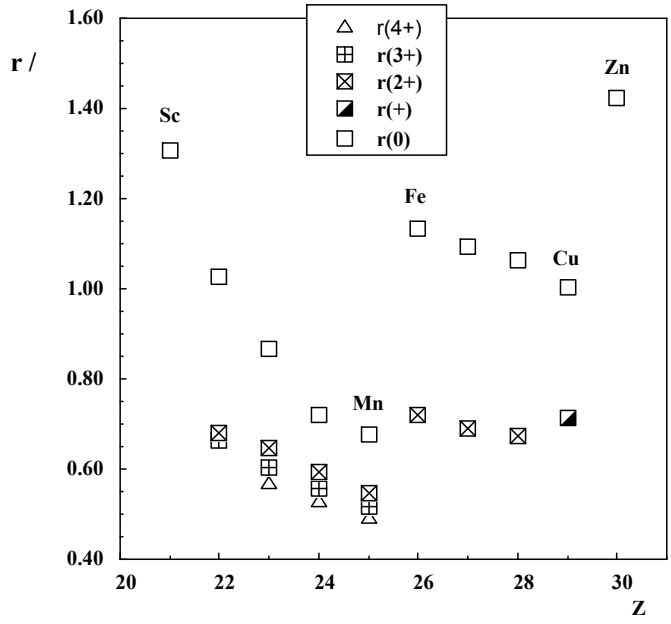

References

Egelhoff, W.F. Jr. (1987) - Core-level binding-energy shifts at surfaces and in solids. *Surface Sciences Reports*, 6, 253-415.

Broughton J.Q. and Bagus P.S. (1980) - ΔSFC calculations of free atom-ion shifts. *Journal of Electron Spectroscopy Related Phenomena*, 20, 127-148.

Moretti G. (2013) - The Wagner plot and the Auger parameter as tools to separate initial- and final-state contributions in X-ray photoemission spectroscopy. *Surface Sciences*, 618, 3-11.

Periodico di Mineralogia, ECMS 2015, 75-76

PERIODICO di MINERALOGIA
established in 1930

An International Journal of
MINERALOGY, CRYSTALLOGRAPHY, GEOCHEMISTRY, ORE DEPOSITS, PETROLOGY, VOLCANOLOGY
and applied topics on *Environment*, *Archaeometry* and *Cultural Heritage*

Combined Mössbauer and X-ray photoelectron spectroscopy approach for identification of metal substitution into nearly-amorphous secondary iron oxides emerging from advanced technologies of water treatment (iron nanoparticles/ferratesIV,V,VI)

Jan Filip[1,*], Jiří Tuček[1], Jan Kolařík[1], Martin Petr[1], Robert Prucek[1] and Radek Zbořil[1]

[1] Regional Centre of Advanced Technologies and Materials, Palacký University in Olomouc, Czech Republic
* Corresponding author: *jan.filip@upol.cz*

Some of the recently-invented innovative technologies of water treatment, being well applicable for organic/inorganic contaminants removal from polluted waters and soils, are based on utilization of inorganic nanocrystalline materials like zero-valent iron (nZVI) particles or iron(IV)/(V)/(VI) compounds (so-called ferrates). In such technologies, nZVI particles act as efficient reducing agent, while ferrates are used as strong oxidizing agents. In both cases, the commonly-formed reaction products (i.e., after nZVI oxidation or ferrate reduction at reasonable range of pH/redox conditions) are nanocrystalline, frequently nearly-amorphous iron(III) oxides/oxyhydroxides with naturally-occurring counterparts. The nanocrystalline phases either co-precipitate with targeted inorganic pollutants or they further act as highly-efficient nanosorbents. Based on experiments aimed at removal of various chlorinated solvents and (heavy) metals (namely Al, Cr, Co, Ni, Cu, Zn, Cd and As) under controlled laboratory conditions (see Figure 1) and detailed characterization of iron-based reaction products (i.e., employing combination of instrumental methods including X-ray powder diffraction, Mössbauer spectroscopy, X-ray photoelectron spectroscopy, transmission electron microscopy), we have defined the mechanisms and efficiencies of contaminants removal, as well as the way of metals substitution into secondary iron-oxide/oxyhydroxide-based solid phases. The identified secondary phases from oxidation processes are mainly represented by nanocrystalline maghemite, nearly-amorphous ferric oxyhydroxides or ferrous hydroxide (Prucek et al., 2013) depending on experimental conditions and used remediation technology. The results of laboratory experiments on model solutions (Prucek et al., 2015) were compared with attenuation of metals from real contaminated waters (i.e., in laboratory-scale experiments) and also with results from localities

treated by nZVI/ferrates in pilot scale. The removal of metals using of nZVI particles follows typically different pathways (Rodová et al., 2015), as well as the final reaction products are completely different from oxidation processes – they are represented mainly by green rust or magnetite (Filip et al., 2014).

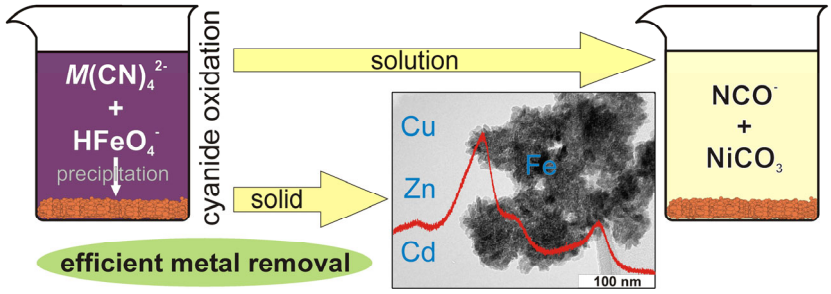

Figure 1: Schematic representation of metal removal (metal-cyanide oxidation by ferrateVI; Filip et al., 2011) by co-precipitation with nanocrystalline iron oxides.

The authors gratefully acknowledge the support by the Technology Agency of the Czech Republic "Competence Centres" (project No. TE01020218) and by Ministry of Education, Youth and Sports of the Czech Republic (project LO1305).

References

Filip J., Yngard R.A., Siskova K., Marusak Z., Ettler V., Zboril R. and Sharma V.K. (2011) - Mechanisms and Efficiency of the Simultaneous Removal of Metals and Cyanides by Using Ferrate(VI): Crucial Roles of Nanocrystalline Iron(III) Oxyhydroxides and Metal Carbonates. *Chemistry-A European Journal*, 17, 10097-10105.

Filip J., Karlický F., Marušák Z., Černík M., Otyepka M. and Zbořil R. (2014) - Anaerobic Reaction of Nanoscale Zerovalent Iron with Water: Mechanism and Kinetics. *Journal of Physical Chemistry C*, 118, 13817-13825.

Prucek R., Tuček J., Kolařík J., Filip J., Marušák Z., Sharma V.K. and Zbořil R. (2013) - Ferrate(VI)-Induced Arsenite and Arsenate Removal by In-Situ Structural Incorporation into Magnetic Iron(III) Oxide Nanoparticles. *Environmental Science & Technology*, 47, 3283-3292.

Prucek R., Tuček J., Kolařík J., Hušková I., Filip J., Varma R.S., Sharma V.K. and Zbořil R. (2015) - Ferrate(VI)-Prompted Removal of Metals in Aqueous Media: Mechanistic Delineation of Enhanced Efficiency via Metal Entrenchment in Magnetic Oxides. *Environmental Science & Technology*, 49, 2319-2327.

Rodová A., Filip J. and Černík M. (2015) - Arsenic immobilization by nanoscale zero-valent iron. *Ecological Chemistry and Engineering S*, 22, 45-59.

Periodico di Mineralogia, ECMS 2015, 77-78

PERIODICO di MINERALOGIA
established in 1930

An International Journal of
MINERALOGY, CRYSTALLOGRAPHY, GEOCHEMISTRY,
ORE DEPOSITS, PETROLOGY, VOLCANOLOGY
and applied topics on *Environment*, *Archaeometry* and *Cultural Heritage*

Cation Order-Disorder Behavior in Silicate Garnet Solid Solutions

Charles A. Geiger[1,*], Aaron C. Palke[2] and Jonathan F. Stebbins[3]

[1] Department of Materials Science and Physics, Salzburg University, Hellbrunnerstrasse 34, A-5020 Salzburg, Austria
[2] Gemological Institute of America, 5355 Armada Drive, Carlsbad, CA 92008, USA
[3] Department of Geological and Environmental Sciences, Stanford University, Stanford, CA 94305-2115, USA
* Corresponding author: *ca.geiger@sbg.ac.at*

Most rock-forming silicates are substitutional solid solutions and extensive research has been done to determine their cation order-disorder behavior. In the case of aluminosilicate garnet ($X_3Al_2Si_3O_{12}$ with X = Mg, Fe^{2+}, Mn^{2+} and Ca) both synthetic and natural solid-solution crystals have random long-range X-cation disorder in space group $Ia\bar{3}d$, as given by X-ray single-crystal diffraction measurements (Armbruster et al., 1992; Merli et al., 1995). Short-range order can occur in symmetry $Ia\bar{3}d$, and is not detectable by standard diffraction measurements. Indeed, the number of methods that can be used to address the question of short-range order in minerals is very limited, if nonexistent in a practical sense. Little is understood about the local structural state of garnet solid solutions.

NMR spectroscopy is an excellent experimental method to investigate the local state of atomic order-disorder in crystals and it has been used to study several non-transition-metal-bearing solid solutions (e.g., Bosenick et al., 1995; 1999). However, nearly all natural garnets contain paramagnetic cations and this causes substantial resonance broadening and loss of signal in MAS ^{29}Si and ^{27}Al NMR spectra. However, recent research on both synthetic and natural solid solution garnets shows that paramagnetically shifted resonances, greatly shifted in frequency from the main, but broadened, central resonances, can be measured (Stebbins and Kelsey, 2009; Palke and Stebbins, 2011; Palke et al., 2015a). Importantly, these resonances can be assigned to various local Fe^{2+}-cation configurations in eight-fold coordinated dodecahedra located around AlO_6 and SiO_4 groups. Silicate garnet appears to offer relatively simple NMR spectra that can be fully interpreted in a crystal chemical sense (cf. olivine). We present an analysis of the structural state of various garnet solid solutions and we focus on their local cation order-disorder behavior.

Published ^{29}Si MAS NMR spectra of a series of synthetic transition-metal-free pyrope-grossular garnets indicate that possible slight degrees of short range Mg-Ca order in intermediate compositions (Bosenick et al., 1995; 1999).

NMR ^{29}Si and ^{27}Al spectra recording paramagnetic resonances of relatively iron-poor natural and synthetic pyrope-almandine, grossular-almandine and grossular-andradite solid solutions do not appear to show any overt cation order, but zoning and compositional heterogeneity complicate the analysis (Palke et al., 2015a).

In a further investigation, a ternary garnet solid solution $Alm_{23}Prp_{30}Grs_{47}$ $[(Fe_{0.23}Mg_{0.30}Ca_{0.47})_3Al_2Si_3O_{12}]$ occurring in a mantle grospydite xenolith taken from the Roberts Victor kimberlite, South Africa, was chosen for detailed ^{27}Al and ^{29}Si MAS NMR study (Palke et al., 2015b). Its composition and, also importantly, the lack of measurable zoning or compositional heterogeneity, as well as the mode of occurrence, make this garnet a key sample for investigating the structural state of a ternary solid solution. The NMR spectra do not indicate any measureable short-range X-cation order.

References

Armbruster, T., Geiger, C.A. and Lager, G.A. (1992) - Single crystal X-ray refinement of almandine-pyrope garnets at 298 and 100 K. *American Mineralogist*, 77, 512-523.

Bosenick, A., Geiger, C.A., Schaller, T. and Sebald, A. (1995) - An ^{29}Si MAS NMR and IR spectroscopic investigation of synthetic pyrope-grossular garnet solid solutions. *American Mineralogist*, 80, 691-704.

Bosenick, A., Geiger, C.A. and Phillips, B. (1999) - Local Ca-Mg distribution of Mg-rich pyrope-grossular garnets synthesized at different temperatures revealed by ^{29}Si NMR MAS spectroscopy. *American Mineralogist*, 42, 1422-1433.

Merli, M., Callegari, A., Cannillo, E., Caucia, F., Leona, M., Oberti, R. and Ungaretti, L. (1995) - Crystal-chemical complexity in natural garnets: structural constraints on chemical variability. *European Journal of Mineralogy*, 7, 1239-1249.

Palke, A.C. and Stebbins, J.F. (2011) - Variable-temperature ^{27}Al and ^{29}Si NMR studies of synthetic forsterite and Fe-bearing Dora Maira pyrope garnet: Temperature dependence and mechanisms of paramagnetically shifted peaks. *American Mineralogist*, 96, 1090-1099.

Palke, A.C., Stebbins, J.F., Geiger, C.A., and Tippelt, G. (2015a) - Cation order-disorder in Fe-bearing pyrope and grossular garnets: An ^{27}Al and ^{29}Si MAS NMR and ^{57}Fe Mössbauer spectroscopy study. *American Mineralogist*, 100, 536-547.

Palke, A.C., Geiger, C.A., and Stebbins, J.F. (2015b) - An investigation of local X-cation order-disorder in garnet from a grospydite using paramagnetically shifted ^{27}Al and ^{29}Si MAS NMR resonances. *European Journal of Mineralogy* (in press).

Stebbins, J.F. and Kelsey, K.E. (2009) - Anomalous resonances in ^{29}Si and ^{27}Al NMR spectra of pyrope ($[Mg,Fe]_3Al_2Si_3O_{12}$) garnets: effects of paramagnetic cations. *Physical Chemistry and Chemical Physics*, 11, 6906-69.

Periodico di Mineralogia, ECMS 2015, 79-80

PERIODICO di MINERALOGIA
established in 1930

An International Journal of
MINERALOGY, CRYSTALLOGRAPHY, GEOCHEMISTRY,
ORE DEPOSITS, PETROLOGY, VOLCANOLOGY
and applied topics on *Environment*, *Archaeometry* and *Cultural Heritage*

Characterization of structure and growth of electrodeposited Cu-S ultra-thin films

Andrea Giaccherini[1,*], Serena Cinotti[1], Ferdinando Capolupo[1], Francesco Carlà[2], Giordano Montegrossi[3], Annalisa Guerri[1], Roberto Felici[2], Massimo Innocenti[1] and Francesco Di Benedetto[4]

[1] Chemistry Department, University of Firenze, Firenze, Italy
[2] ESRF, Grenoble, Cedex, France
[3] The Institute of Geosciences and Earth Resources, CNR, Firenze, Italy
[4] Department of Earth Sciences, University of Firenze, Firenze, Italy
* Corresponding author: *andrea.giaccherini@unifi.it*

Calchogenides such as CdSe and CdTe thin-films are well known semiconductors, used in manufacturing of last generation photovoltaic components. Toxicity and shortage of the involved elements must be considered in the advancement of technology. Hence scientific community is focusing attention on new compounds based on economic and low-environmental impact elements such as Cu, Sn, Fe and Zn. In particular, quaternary semiconducting materials based on the kesterite (Cu_2ZnSnS_4) mineral structure are the most promising candidates to overtake the current generation of light-absorbing materials for thin-film solar cells. Electrodeposition is known as a low-cost semiconductor growth technique for applications in electronic devices. Surface limited electrodeposition of atomic layers, can be performed exploiting by means of Electrochemical Atomic Layer Deposition (E-ALD) technique to obtain sulphides ultra-thin films. In-situ SXRD measurements were performed at ESRF (Grenoble) and focused to the investigation of the growth mechanism of Cu-S ultra-thin films on the 111 crystal plane of a silver single crystal, commonly used as a working electrode. The growth of the film was monitored by following the evolution of the Bragg peaks after each E-ALD step. Results point to the occurrence of a self-standing film with a definite crystal structure after 15 E-ALD cycles. After the Bragg reflections are observed for the first time, only minor changes of the structural arrangement are registered.

Breadth and profile analysis of the Bragg peaks lead to a qualitative interpretation of the growth mechanism, in the normal and in-plane directions, with respect to the Ag surface. Namely, the contribution of crystal strain and crystallite size were identified in the width of the Bragg reflections.

The preliminary interpretation of the experimental reciprocal lattice, coupled to the SEM investigation, suggests that the samples show a pseudo single crystal diffraction pattern. This

can be described by a new hexagonal unit cell. The crystal structure of this electro-deposited $Cu_{2-x}S$ could be related to that of chalcocite, in particular considering the layering of triangular Cu sites and octahedral Cu sites. The influence of the applied electric potential on the stability of the electro-deposited crystal structure has been monitored by means of SXRD measurements performed during the switch off of the potential. A structural change was, in fact, registered, and correlated to the occurrence of the stable phases under conventional laboratory conditions.

Periodico di Mineralogia, ECMS 2015, 81-82

PERIODICO di MINERALOGIA
established in 1930

An International Journal of
MINERALOGY, CRYSTALLOGRAPHY, GEOCHEMISTRY,
ORE DEPOSITS, PETROLOGY, VOLCANOLOGY
and applied topics on *Environment*, *Archaeometry* and *Cultural Heritage*

A spectroscopic investigation of pyrite nanoparticles for energy conversion and storage

Andrea Giaccherini[1], Ivan Colantoni[2], Francesco D'Acapito[3], Giordano Montegrossi[4,*], Maurizio Romanelli[1], Massimo Innocenti[1] and Francesco Di Benedetto[5]

[1]Chemistry Department, University of Firenze, Firenze, Italy
[2] Department of Physics, Sapienza University of Rome, Rome, Italy
[3] ESRF, Grenoble, Cedex, France
[4] The Institute of Geosciences and Earth Resources, CNR, Firenze, Italy
[5] Department of Earth Sciences, University of Firenze, Firenze, Italy
* Corresponding author: *montegrossi@igg.cnr.it*

Pyrite (FeS_2) nanoparticles were produced by one-pot solvothermal synthesis, carried out at room pressure and mild temperature (≈180 °C). With this approach the sulfide anion is co-generated during the synthesis. This method allows one to reduce the environmental impact, because the solvent, Fe and S are the only reactants involved in the process. A thorough characterization of the synthesis products was performed by SEM micromorphology, XRD, Diffuse Reflectance Spectroscopy (DRS) and XAS spectroscopy (both in the XANES and EXAFS regions).

Morphological analysis by SEM reveals the presence of aggregates of individual particles having an approximate dimension of few hundreds of nm. The lack of a definite crystal morphology is attributed to the absence of specific surfactants in the batch of reactants. Nevertheless, some particles exhibit euhedral morphology. The XRD and XANES patterns point to pyrite as the unique product of the synthesis. The Scherrer analysis of the profile parameters suggest that the individual particles observed by SEM inspection are clusters of smaller crystallites, having a mean size of ~25 nm. Moreover, both XRD and EXAFS measurements point to a small but significant increase of the lattice constant (+0.3%). This change is attributed to both the enhanced surface effects and to the increased presence of point defects due to the small size of the crystallites. The DRS spectra, elaborated through the use of the Tauc plot, confirm that the pyrite nanoparticles exhibit an optical behavior indistinguishable from that of the bulk pyrite.

The results of the present study suggest that the one-pot synthesis is an efficient and "green" method to produce pyrite nanoparticles, and it may represent a promising process for

the industrial scale up. Our synthesis product shows persistence at the nanoscale of the main properties of bulk FeS_2, and it can find useful applications both in solar energy conversion and storage (in the Li-ion batteries). Moreover, the presence of a defect structure near to the particle surface could be potentially applied to specific reactive processes (as e.g. in waste remediation).

Periodico di Mineralogia, ECMS 2015, 83-84

PERIODICO di MINERALOGIA
established in 1930

An International Journal of
MINERALOGY, CRYSTALLOGRAPHY, GEOCHEMISTRY, ORE DEPOSITS, PETROLOGY, VOLCANOLOGY
and applied topics on *Environment*, *Archaeometry* and *Cultural Heritage*

Structure of iron- and cobalt-doped ZnO as anode material for Li-ion batteries

Gabriele Giuli[1,*], Angela Trapananti[2] , Franziska Mueller[3], Dominic Bresser[3], Francesco D'Acapito[2] and Stefano Passerini[3]

[1] University of Camerino, School of Science and Technology, Geology Division, 62032 Camerino, Italy
[2] CNR-IOM-OGG, European Synchrotron Radiation Facility, 71 avenue des Martyrs, 38043 Grenoble, France
[3] Helmholtz Institute Ulm (HIU), Helmholtzstr. 11, 89081, Ulm, Germany
* Corresponding author: *gabriele.giuli@unicam.it*

Transition-metal-doped zinc oxide has gathered significant interest in the scientific community because of its potential for application in spintronics devices. This same material has been recently demonstrated to be also a very promising alternative anode material for Li-ion batteries (Bresser et al., 2013). Remarkably, the doping of ZnO nanoparticles by iron and cobalt substantially enhances the electrochemical performance of the un-doped oxide.

Herein, we report a complete structural study of the pristine anode material by X-ray diffraction (XRD) and X-ray absorption spectroscopy (XANES and EXAFS) to investigate the influence of the dopant on the crystalline wurtzite structure and to elucidate the major differences between Co- and Fe-doped ZnO nanoparticles regarding their oxidation state and structure around the dopant site (Giuli et al., 2015). Preliminary results from further studies performed on Fe-doped ZnO cycled anodes will be also presented.

ZnO nanoparticles having the general formula $Zn_{0.9}(TM)_{0.1}O$ (where TM = Fe or Co) were prepared through sucrose assisted wet chemical synthesis method (Bresser et al., 2013). Structural refinement of powder XRD data revealed the absence of reflections related to spurious oxide phases and showed small changes in the ZnO unit-cell parameters associated with doping. The full width at half maximum (FWHM) of the XRD reflections was found to increase in the order ZnO, $Zn_{0.9}Co_{0.1}O$, carbon coated $Zn_{0.9}Fe_{0.1}O/C$, and $Zn_{0.9}Fe_{0.1}O$ revealing that different dopants or synthesis conditions remarkably affect the average crystallites size.

XAS data were collected at the Italian BM08 beamline of the ESRF at the Fe, Co and Zn *K*-edges and showed that both Co and Fe substitute Zn in the host wurtzite structure. From the analysis of the XANES spectra, we found that Co is divalent, whereas Fe is trivalent in $Zn_{0.9}Fe_{0.1}O$, and 95% trivalent in $Zn_{0.9}Fe_{0.1}O/C$.

The Co-doped sample displays similar EXAFS features as that of pure ZnO (Figure 1). On the other hand, the EXAFS signals measured at the Fe *K*-edge of both $Zn_{0.9}Fe_{0.1}O$ and $Zn_{0.9}Fe_{0.1}O/C$ show oscillations strongly damped compared to those measured at Zn and Co *K*-edges in pure ZnO and $Co_{0.9}Fe_{0.1}O$. This was attributed to the occurrence of structural defects

(such as cationic vacancies and/or interstitial oxygen atoms) in the immediate environment of Fe^{3+} in tetrahedrally coordinated sites, in agreement with both the results on the crystallinity as obtained by XRD on the Fe oxidation state as derived from XANES. Indeed, the presence of defects is compatible with the aliovalent substitution of Fe^{3+} for Zn^{2+}.

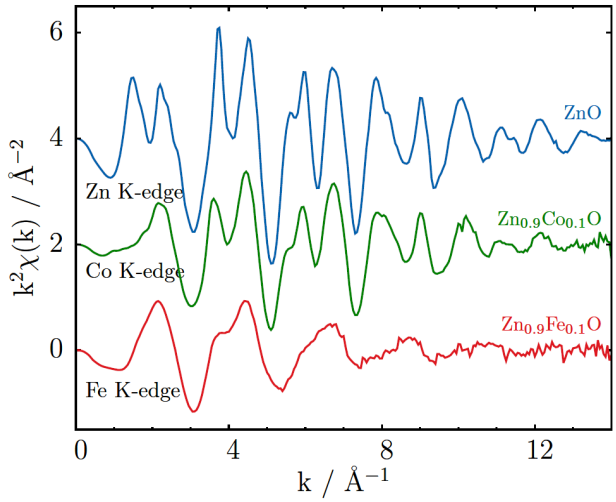

Figure 1. EXAFS signals collected at the K-edges of Zn (in pure ZnO), Co (in Zn0.9Co0.1O) and Fe (in Zn0.9Fe0.1O)

The influence of the dopant on the highly reversible conversion-alloying lithium storage mechanism of such materials in view of their application as lithium-ion battery anodes is still not completely understood. Therefore, the herein reported results may enable the further optimization and design of optimized and/or new active materials, enabling the realization of further enhanced energy and power densities.

References

Bresser D., Mueller F., Fiedler M., Krueger S., Kloepsch R., Baiter D., Winter M., Paillard E. and Passerini S. (2013) - Transition-Metal-Doped Zinc Oxide Nanoparticles as a New Lithium-Ion Anode Material. *Chemistry of Materials*, 25, 4977-4985.

Giuli G., Trapananti A., Mueller F., Bresser D., d'Acapito F., Passerini S. (2015) - Insights into the effect of iron and cobalt doping on the structure of nano-sized ZnO. *Inorganic Chemistry*, submitted.

Periodico di Mineralogia, ECMS 2015, 85-86

PERIODICO di MINERALOGIA
established in 1930

An International Journal of
MINERALOGY, CRYSTALLOGRAPHY, GEOCHEMISTRY, ORE DEPOSITS, PETROLOGY, VOLCANOLOGY
and applied topics on *Environment*, *Archaeometry* and *Cultural Heritage*

Determination of structure of highly carbonized organic matter using Raman spectroscopy in comparison with the HRTEM, SAXS and XRD data

Yevgeniy A. Golubev

Institute of Geology of Komi SC of RAS, 54 Pervomaiskaya st., Syktyvkar, Russia 167982
Corresponding author: *yevgenygolubev74@mail.ru*

Highly carbonized organic matter is widespread in the geological environment, especially in metamorphic rocks. The combination of HRTEM and Raman spectroscopy is an effective way to study the structure and transformation degree of organic matter (Beyssac et al., 2002). In fact, there are many difficulties in the analysis of the Raman spectroscopy results of partially ordered carbon structures. In particular, a formula to estimate the crystallites size by the Raman spectra was mostly empirically obtained by comparing the Raman spectroscopy and XRD data. However, intensity of XRD band is proportional to the sixth degree of crystallite size. On the contrary, the formation of the D band of the Raman spectrum depends on small crystallites. Therefore, a comparison of the XRD and Raman spectroscopy data is incorrect if the particle size has a too wide distribution. In this work we present results of structure study of natural X-ray amorphous carbon using Raman spectroscopy in comparison with the HRTEM, SAXS and XRD data.

We studied natural samples with highly carbonized organic matter with x-ray amorphous pattern from Karelia, Polar Ural, Novaya Zemlya islands and the Kyzylovskii fault zone (Eastern Kazakhstan). Carbon content is not less than 95% atomic percent. Samples were taken from deposits that differed in the genesis and in PT conditions, e.g., the temperature of heating varied from 300 to 600 ºC. The Raman spectra were recorded on a LabRam HR800 Raman spectrometer; He-Ne laser (λ = 632.8 nm); frequency range 0–4000 cm^{-1}. A FEI CM300UT FEG transmission electron microscope was used for the HRTEM investigation. The particle size distribution was evaluated using small angle X-ray scattering (SAXS).

The Raman spectra have a characteristic view for amorphous carbon materials. Two bands are observed at frequencies of 1330 and 1600 cm^{-1}. The relative intensity of the D and G bands (I_D/I_G) is considered as a measure of the uniformity of graphite with a regular structure. However, relative to a structure of the highly carbonized organic substances, this ratio indicates not so much about the degree of spatial regularity of the hexagonal structure as about the relation of the intensities of the stretching vibrations of single (sp^3) and double (sp^2) C-C bonds. Addi-

tionally, curved graphene layers influence the results of calculation of particle size by the Raman spectrum (Larouche and Stansfield, 2010). Comparison of Raman spectroscopy, XRD, SAXS and HRTEM data shows that the curvature substantially affects the calculation of average size of graphene layers. This is especially true when the distribution of particles by SAXS is lognormal. This has also influence on the parameters of the Raman bands (half-width, intensity). The structure of some natural carbons has features that complicate the interpretation of Raman spectra. An example is a natural carbon with fullerene-like structures, such as shungite of Karelia. For this sample the intensity of single (sp^3) and double (sp^2) C-C bonds depends not only on the ratio of graphite and disordered fragments of structures, but also on the degree of filling connections at the edges of graphene layers H, O, N, S often found as an impurity. This structural feature influences, for example, the local conductive properties of shungite (Golubev, 2013) and can be determined by analysis of relation of bands D and G.

This work was supported by grants RFBR 15-05-04369.

References

Beyssac O., Rouzaud J.N., Goffé B., Brunet F. and Chopin C. (2002) - Graphitization in a high-pressure, low-temperature metamorphicgradient: a Raman microspectroscopy and HRTEM study. *Contributions to Mineralogy and Petrology*, 143, 19-31.

Larouche, N. and Stansfield, B. L. (2010) - Classifying nanostructured carbons using graphitic indices derived from Raman spectra. *Carbon*, 48, 620-629.

Golubev E.A. (2013) - Electrophysical properties and structural features of shungite (natural nanostructured carbon). *Physics of the Solid State*, 55, 1078-1086.

Periodico di Mineralogia, ECMS 2015, 87-88

PERIODICO di MINERALOGIA
established in 1930

An International Journal of
MINERALOGY, CRYSTALLOGRAPHY, GEOCHEMISTRY,
ORE DEPOSITS, PETROLOGY, VOLCANOLOGY
and applied topics on *Environment*, *Archaeometry* and *Cultural Heritage*

Structural complexity and thermal expansion of Ba silicates

Liudmila A. Gorelova[1,2,*], Rimma S. Bubnova[1,2], Maria G. Krzhizhanovskaya[1], Stanislav K. Filatov[1] and Sergey V. Krivovichev[1]

[1] St Petersburg State University, Department of Crystallography, Russia, 199155, Saint-Petersburg, V.O., per. Dekabristov, d. 16
[2] Institute of the Silicate Chemistry of Acad. Russ. Sci., Russia, 199034, St. Petersburg, Makarov Emb. 2
*Corresponding author: *gorelova.ljudmila@gmail.com*

There are eight phases presently known in the $BaO–SiO_2$ system. In particular, there is the homologous series of barium silicates with the general formula $Ba_{M+1}[Si_{2M}O_{5M+1}]$ (M = 1, 3, 4, 5, ∞) (Liebau, 1985) and silicates with isolated tetrahedra. The thermal expansion of these materials was studied in details by Oelschlegel (1971, 1974) and Kerstan and Russel (2011), but the main coefficients of thermal expansion have not been calculated for the monoclinic phases.

This contribution reports on the synthesis, thermal behaviour and structural complexity of six Ba-silicates: Ba_2SiO_4 (with isolated tetrahedra), $BaSiO_3$ (chain silicate, M = 1) $Ba_2Si_3O_8$ (silicate with triple chains, M = 3), $Ba_5Si_8O_{13}$ (silicate with quadruple chains, M = 4) and $BaSi_2O_5$ (layered structures, M = ∞). These silicates have been obtained by solid-state reactions in the temperature range from 1300 to 1420 °C.

Thermal behaviour of the Ba silicates was studied by high-temperature X-ray powder diffraction in the temperature range 30–1100 °C and the temperature step of 40 °C. Tensors of the thermal expansion coefficients have been calculated using the program package TTT (Bubnova et al., 2013).

It was found that Ba_2SiO_4 has a weak anisotropy of the thermal expansion at room-temperature ($\alpha_{max}/\alpha_{min}$ = 2), and practically isotropic behaviour at 1100 ºC ($\alpha_{max}/\alpha_{min}$ = 1.2). All chain silicates have anisotropic expansion with their maximum thermal expansion directions oriented parallel to the chains of tetrahedra. Both layered silicates display the strongest anisotropic character of the thermal expansion with the maximum expansion within the layer and the minimum expansion in between the layers. In general, maximal thermal expansion correlates to the dimensionality of the anionic group. The silicates studied have similar volumetric thermal expansion coefficients, irrespective of the degree of polymerization of silicate anions (45 ± 5 $\times 10^{-6}$ °C^{-1}).

Structural complexity of Ba silicates was estimated using their Shannon information content per atom (I_G) and per unit cell ($I_{G,total}$) calculated according to the following formulae (Krivovichev, 2014):

$$I_G = -\sum_{i=1}^{k} pi \log 2\ pi \text{ (bits/atom)},$$
$$I_{G,\text{total}} = v \times I_G \text{ (bits/cell)},$$

where k is the number of different crystallographic orbits and p_i is the random choice probability for an atom from the ith crystallographic orbit, that is $p_i = m_i / v$, where m_i is a multiplicity of a crystallographic orbit relative to the reduced unit cell, and v is the number of atoms in the reduced unit cell. Complexity parameters have been calculated using the TOPOS software (Blatov et al., 2000).

It has been found that the information amount per cell ($I_{G\ total}$) increases along the $BaO–SiO_2$ line with the addition of SiO_2 from 70.606 bits/cell for silicate with isolated tetrahedra to 281.947 bits/cell for silicate with triple chains. Layered silicates demonstrate lower parameters of structural complexity; moreover, the monoclinic high-temperature modification $\alpha–BaSi_2O_5$ has higher complexity than the orthorhombic low-temperature phase $\beta–BaSi_2O_5$.

The XRD studies have been performed at the X-ray Diffraction Centre of St. Petersburg State University.

The main values of thermal expansion coefficients ($\times 10^6$ °C^{-1}) and structural complexity parameters for Ba-silicates

Compound	Ba_2SiO_4	$BaSiO_3$	$Ba_2Si_3O_8$	$Ba_5Si_8O_{21}$	$\alpha–BaSi_2O_5$	$\beta–BaSi_2O_5$
Sp.gr	*Pmcn*	$P2_12_12_1$	$P2_1/c$	$C2/c$	*Pcmn*	$C2/c$
α_{11}	19	21	18	16	12	24
α_{22}	13	12	18	19	21	10
α_{33}	14	17	5	6	8	11
μ (α_{33}^c)	–	–	27	33	25	–
α_V	46	50	41	41	41	45
$I_{G\ \text{total}}$, bits/cell	70.606	46.439	192.423	281.947	72.000	176.078

References

Blatov V.A., Shevchenko A.P. and Serezhkin V.N. (2000) – *TOPOS 3.2* – a new version of the program package for multipurpose crystal-chemical analysis. *Journal of Applied Crystallography*, 33, 1193.

Bubnova R.S., Firsova V.A. and Filatov S.K. (2013) – Software for determining the thermal expansion tensor and the graphic representation of its characteristic surface (Theta to Tensor-TTT). *Glass Physics and Chemistry*, 39, 347–350.

Kerstan M. and Russel C. (2011) – Barium silicates as high thermal expansion seals for solid oxide fuel cells studied by high-temperature X-ray diffraction (HT-XRD). *Journal of Power Sources*, 196, 7578–7584.

Krivovichev S.V. (2014) – Which inorganic structures are the most complex? *Angewandte Chemie International Edition*, 53, 654–661.

Liebau F. (1985) – Structural chemistry of silicates: *s*tructure, bonding and classification. *Springer-Verlag*, Berlin/Heidelberg.

Oelschlegel G. (1971) – Das binäre Teilsystem $BaO·2SiO_2–2BaO·3SiO_2$. *Glastechnische Berichte*, 44, 194–201.

Oelschlegel G. (1974) – Anisotrope Wärmedehung und Mischkristallbildung einiger Verbindungen des ternären Systems $BaO–Al_2O_3–SiO_2$. *Glastechnische Berichte*, 47, 24–41.

Periodico di Mineralogia, ECMS 2015, 89-90

PERIODICO di MINERALOGIA
established in 1930

An International Journal of
MINERALOGY, CRYSTALLOGRAPHY, GEOCHEMISTRY,
ORE DEPOSITS, PETROLOGY, VOLCANOLOGY
and applied topics on *Environment*, *Archaeometry* and *Cultural Heritage*

Structural refinement, crystal chemistry and optical spectra of Co-doped synthetic diopside

Claudia Gori[1,*], Mario Tribaudino[1], Luciana Mantovani[1], Henrik Skogby[2], Ulf Hålenius[2], Davide Delmonte[1,3], Francesco Mezzadri[3,4], Edmondo Gilioli[3] and Gianluca Calestani[3,4]

[1]Department of Physics and Earth Sciences "Macedonio Melloni", Parma, Italy
[2]Department of Mineralogy, Swedish Museum of Natural History, Stockholm, Sweden
[3]Institute of Materials for Electronics and Magnetism (IMEM-CNR), Parma, Italy
[4]Department of Chemistry, Parma, Italy
*corresponding author: *claudia.gori@studenti.unipr.it*

A new ceramic pink pigment, based on the Co-pyroxene ($CaCoSi_2O_6$) structure, has been recently synthesized (Mantovani et al., 2015). Co-pyroxene performs as a dye in most ceramic treatments, where the colour turns into blue. Here we present results of additional investigations on Co-pyroxene with varying substitutions of Mg for Co ($CaCo_xMg_{1-x}Si_2O_6$). The aim is to verify whether the same colouring performance can be obtained with lower Co content, and to provide a synthesis route for a material with higher melting point than pure $CaCoSi_2O_6$ pyroxene; it is hoped that the Mg-doped CaCo-pyroxene will be more stable in the aggressive environment typical of the ceramic industry. Moreover, substitution of less expensive Mg for Co will be beneficial from an economical point of view, and will also reduce environmental concerns related to Co toxicity.

Five samples with x = 0.20, 0.40, 0.50, 0.60 and 0.80 were synthesized by solid state annealing after cooling from melts of oxide mixtures. Here the only phase is always pyroxene, with single crystals sized up to 500 μm. All the runs produced a pink pigment with the same colour shades independent of the Co content. Syntheses were also performed by a flux growth method with the starting compositions x = 0.25, 0.50, 0.75, 1.00, producing larger crystals (~1 mm) suitable for polarised UV-VIS investigation. Powder diffraction showed that the only crystalline phase is pyroxene but the color here is pink-brownish probably due to a small amount of Co^{3+} in the structure.

The products were analysed by the combined application of X-ray diffraction analysis and optical absorption spectroscopy. Single crystals obtained by solid state annealing were investigated by single crystal X-ray diffraction, obtaining an agreement factor between 2.0 and 2.7%; Co is almost completely ordered at the M1 site with only a minor amount (< 0.04 a.p.f.u.) at the M2 site. Although the optical spectra of the pyroxenes produced by melt phase synthesis are poorly resolved, because of problems encountered with the orientation of the small monoclinic crystals, it is seen that all spectra are dominated by the strong absorption bands caused by Co^{2+}.

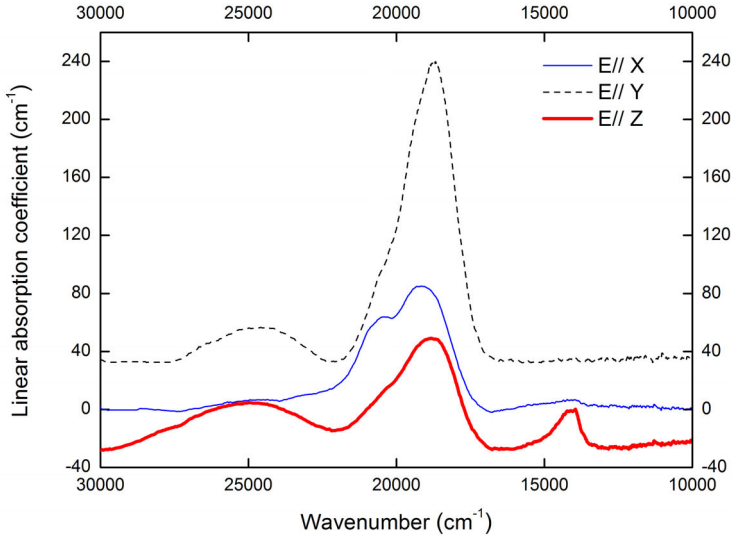

Figure 1. Polarized optical spectra of flux grown Co-pyroxene ($CaCoSi_2O_6$).

The flux grown samples could be oriented more precisely and spectra were measured along the optical indicatrix directions (Figure 1), and show a band shift from $CaCoSi_2O_6$ to $CaCo_{0.25}Mg_{0.75}Si_2O_6$. Although the samples obtained by the two different methods of synthesis show different colours in colorimetric analysis, the average peak positions of the spectra of the flux grown samples fit well with those obtained by the melting method. On this basis, and the good correlation between bands intensity and samples chemistry (combined Co and Mg occupancies in the M1 site) we assign the two main bands in the range 18700-20800 cm^{-1} to the split spin-allowed *d-d* transition $^4T_{1g}(^4F) \rightarrow {}^4T_{1g}(^4P)$ in Co^{2+} in an octahedral ligand field (Llusar et al., 2001).

References

Llusar M., Forés A., Badenes J. A., Calbo J., Tena M. A., and Monrós G. (2001) - Colour analysis of some cobalt-based blue pigments. *Journal of the European Ceramic Society*, 21(8), 1121-1130.

Mantovani L., Tribaudino M., Dondi M. and Zanelli C. (2015) - Synthesis and color performance of $CaCoSi_2O_6$ pyroxene, a new ceramic colorant. *Dyes and Pigments* (in press).

Periodico di Mineralogia, ECMS 2015, 91-92

PERIODICO di MINERALOGIA
established in 1930

An International Journal of
MINERALOGY, CRYSTALLOGRAPHY, GEOCHEMISTRY,
ORE DEPOSITS, PETROLOGY, VOLCANOLOGY
and applied topics on *Environment*, *Archaeometry* and *Cultural Heritage*

Iron meteorites and their weathering products: Mössbauer spectroscopy with a high velocity resolution of the iron-bearing minerals

Mikhail V. Goryunov, Grigory A. Yakovlev, Andrey V. Chukin, Victor I. Grokhovsky, Vladimir A. Semionkin and Michael I. Oshtrakh*

Institute of Physics and Technology, Ural Federal University, Ekaterinburg, 620002, Russian Federation
*Corresponding author: *oshtrakh@gmail.com*

Iron meteorites consist of Fe-Ni-Co alloy as a matrix with minor inclusions of iron-nickel phosphides, sulfides and some other mineral exsolutions. The main minerals of the matrix are kamacite α-Fe(Ni,Co), martensite α_2-Fe(Ni,Co), taenite γ-Fe(Ni,Co) and ordered tetrataenite γ-FeNi. Iron-nickel phosphides $(Fe,Ni)_3P$ are in the form of massive inclusions of schreibersite and microcrystals of rhabdite precipitated in kamacite matrix. Troilite FeS inclusions in kamacite matrix can contain small amount of daubréelite $FeCr_2S_4$. These minerals were formed in the space under extreme conditions, for instance, with cooling rates of 1–15° per million years in the γ–α transformation interval. Moreover, these minerals may be affected by meteorites or their parent bodies collisions and shock reheating. Therefore, these minerals have some structural features different from their terrestrial analogues. The terrestrial history of iron meteorites is related in part to their weathering processes. Meteoritic kamacite, martensite and taenite oxidation processes as a result of water, oxygen and other chemicals interactions with iron alloy can be also different from similar oxidation of terrestrial alloys. Therefore, investigation of meteoritic minerals and their weathering is of interest.

^{57}Fe Mössbauer spectroscopy is a powerful technique for studying iron-bearing minerals which allowed to carry out modal analysis of minerals in meteorites and to evaluate the ^{57}Fe hyperfine parameters. The latter information is very important for analysis of the iron local microenvironment in the iron-bearing minerals. Mössbauer spectroscopy with a high velocity resolution represents a further development of the technique with increased analytical possibilities, accuracy and precision (Oshtrakh and Semionkin, 2013), and was applied in this study.

Iron meteorites Aliskerovo IIIE-un, Sikhote-Alin IIAB, Anyujskij IIAB and Sterlitamak IIIAB were chosen for a comparative study using X-ray diffraction and Mössbauer spectroscopy. Mössbauer spectra revealed different number of spectral components for Sikhote-Alin IIAB and Anyujskij IIAB and for Aliskerovo IIIE-un and Sterlitamak IIIAB (Fig. 1). These components were related to kamacite and taenite with variations in Ni concentration within the phase.

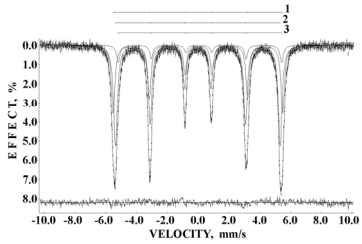

Figure 1a. Mössbauer spectrum of Anyujskij IIAB iron meteorite; 1–3 are components related to kamacite α-Fe(Ni,Co) regions with different Ni concentration. T = 295 K.

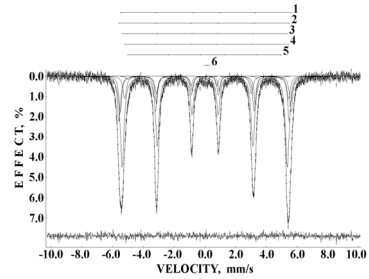

Figure 1b. Mössbauer spectrum of Sterlitamak IIIAB iron meteorite; components 1–4 are related to kamacite α-Fe(Ni,Co) regions (as in 1a), 5 is related to taenite γ-Fe(Ni,Co) in the magnetic state, 6 is related to taenite γ-Fe(Ni, Co) in the paramagnetic state. T = 295 K.

An analysis of iron meteorite weathering was carried out on the Dronino iron-ungrouped meteorite which terrestrial age is more than 1000 years. Surface oxidation products and concretions found in surrounding soil were studied using Mössbauer spectroscopy (Fig. 2). The results of the spectral fitting and interpretation demonstrated the presence of small particles of ferric hydrous oxide with different sizes in both samples indicating concretion formation by diffusion in soil products of Dronino metal oxidation.

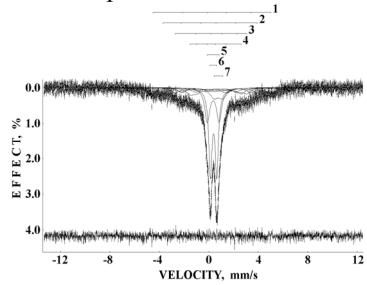

Figure 2a. Mössbauer spectrum of Dronino iron-ungrouped meteorite surface oxidation product; 1–4 are magnetic and 5–7 are paramagnetic components related to ferric hydrous oxide particles in superparamagnetic state. T = 295 K.

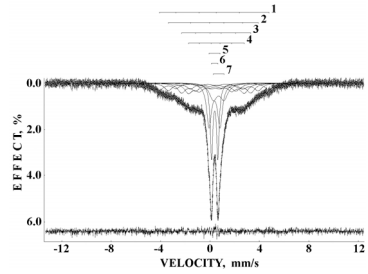

Figure 2b. Mössbauer spectrum of internal part of concretion in soil formed as a result of Dronino iron meteorite weathering; 1–4 are magnetic and 5–7 are paramagnetic components (as in 2a). T = 295 K.

The results obtained demonstrated new detailed information about iron-bearing minerals in iron meteorites and distinguish kamacite and taenite components with different hyperfine field. Iron meteorite weathering products in soil and similar minerals in concretions were detected.

This work was supported by the Ministry of Education and Science of Russian Federation.

References

Oshtrakh M.I. and Semionkin V.A. (2013) - Mössbauer spectroscopy with a high velocity resolution: Advances in biomedical, pharmaceutical, cosmochemical and nanotechnological research. *Spectrochimica Acta, A*, 100, 78–87.

Periodico di Mineralogia, ECMS 2015, 93-94

PERIODICO di MINERALOGIA
established in 1930

An International Journal of
MINERALOGY, CRYSTALLOGRAPHY, GEOCHEMISTRY,
ORE DEPOSITS, PETROLOGY, VOLCANOLOGY
and applied topics on *Environment*, *Archaeometry* and *Cultural Heritage*

Mixed uranyl sulfato-selenates: variable composition and crystal structures

Vladislav V. Gurzhiy[1,*], Olga S. Tyumentseva[1] and Sergey V. Krivovichev[1]

[1] Crystallography Dept., Institute Of Earth Sciences, St. Petersburg State University, 199034, University emb. 7/9, St. Petersburg, Russian Federation
* Corresponding author: *vladgeo17@mail.ru*

In the last decade, structural chemistry of uranium oxycompounds and oxysalts, in particular, attracted considerable attention due to both problems of storage and disposal of spent nuclear fuel and the possible design of novel functional materials based on uranium and transuranium elements. By applying a wide range of experimental techniques and synthesis conditions, and advanced analytical methods it was possible to identify new classes of actinide-containing compounds, in particular nanostructures based on uranium, neptunium and plutonium oxides, occurring as nanotubules and nanoclusters.

Uranium compounds containing oxoanions of the hexavalent ions are of special importance from the environmental and mineralogical points of view. Uranyl sulfates are one of the most widespread natural phases in secondary uranium mineralization. Uranyl selenates are not known yet as minerals but this family of compounds is most representative among the synthetic uranium compounds. It should be also taken into account that there are several isostructural compounds known for both the groups, which could be explained by a high isomorphism between Se^{6+} and S^{6+} cations. On this basis, studying the phase formation in mixed uranyl sulfato-selenate systems is very interesting from both the preparative chemistry and crystal chemistry viewpoints, and may explain the absence of uranyl selenates in Nature.

The model systems include uranyl nitrate hexahydrate and potassium hydroxide that have been dissolved in deionized distilled water with addition of sulfuric and selenic acids mixture taken in different ratio. Potassium uranyl selenate $K(H_5O_2)[(UO_2)_2(SeO_4)_3(H_2O)]$ (Gurzhiy et al. 2012, space group $P2_1/c$; a = 11.456(2), b = 10.231(1), c = 14.809(2) Å; β = 101.901(4)°, V = 1698.4(4) Å^3; Z = 4) has been recently obtained in the pure selenate system. Single-crystal XRD coupled with chemical and IR spectroscopy analyses reveal that mixed uranyl sulfato-selenate crystals grow in the same structural type when the Se/S ratio in the initial solution ranges from 50 to 100%. If the amount of Se^{6+} ions in the solution falls below 50% and down to the pure sulfate system, crystals of another structural type are obtained. For instance, a novel uranyl-containing compound with ideal formula $K_{2.5}(H_3O)_{1.5}[(UO_2)_3(SO_4)_5(H_2O)_2](H_2SO_4)_{0.5}(H_2O)_4$ (space group

*Amm*2; a = 12.705(1), b = 18.221(1), c = 13.259(1) Å; V = 3069.5(2) Å^3; Z = 4). Its structure is based upon layered complexes, and formed as a result of the condensation of $[UO_2]^{2+}$, $[UO_2(H_2O)]^{2+}$ and $[SO_4]^{2-}$ coordination units. The topology of the layered complexes is unprecedented for the structural chemistry of uranium and inorganic oxysalts. In both cases, there is a linear correlation between the Se/S ratio in the initial solution and in the crystal structure of the crystallized compounds. Thus the co-existence of both phases in the same system is likely to be impossible (or at least very metastable).

This work was supported by St. Petersburg State University (grant 3.38.136.2014) and President of Russian Federation grant for young scientists (no. MK-1737.2014.5 to VVG). The XRD studies have been performed at the X-ray Diffraction Centre of St. Petersburg State University.

Periodico di Mineralogia, ECMS 2015, 95-96

PERIODICO di MINERALOGIA
established in 1930

An International Journal of
MINERALOGY, CRYSTALLOGRAPHY, GEOCHEMISTRY,
ORE DEPOSITS, PETROLOGY, VOLCANOLOGY
and applied topics on *Environment*, *Archaeometry* and *Cultural Heritage*

Incorporation of BO_3 groups in dry olivine

Ulf Hålenius[1,*], Henrik Skogby[1] and Ferdinando Bosi[2]

[1]Department of Geosciences, Swedish Museum of Natural History, Box 50007, SE-10405 Stockholm, Sweden
[2]Department of Earth Sciences, Sapienza Università di Roma, Piazzale Aldo Moro 5, I-00185 Roma, Italy
* Corresponding author: *ulf.halenius@nrm.se*

Light elements are important tracers for transfer processes in subduction zones. Although fluid-olivine partition data (e.g., Chaussidon and Libourel, 1993) suggest that boron is highly incompatible during partial melting in the mantle, Kent and Rossman (2002) demonstrated that olivine can accommodate significant amounts of boron within the mantle and suggested that olivine is an important reservoir for boron within lithospheric and upper asthenospheric mantle lithologies.

Boron isotope fractionation is strongly influenced by boron coordination. Consequently, any conclusions regarding mass transfer processes based on isotope studies require crystal chemical information. However, direct observations of the structural incorporation of boron in common mantle minerals are scarce. On the basis of chemical and infrared spectroscopic data on natural borian olivines, Sykes et al. (1994) suggested that the coupled substitution $B(F,OH)Si_{-1}O_{-1}$ operates in the olivine structure and that boron occurs in $^{[4]}BO_4$ groups. Ingrin et al. (2014) demonstrated by single crystal FTIR spectroscopy the incorporation of boron as planar molecular BO_3 groups at defect tetrahedrally coordinated sites in hydrogen-bearing synthetic and natural olivine crystals. However, detailed studies on non-hydrogen assisted B-incorporation in olivine minerals are still lacking.

In the present study, synthetic single crystals of forsterite were produced by flux-growth techniques using mixed borate and vanadate fluxes under boron- and scandium-saturated conditions in the temperature range 1200-800 °C. Relatively large (up to 0.5 mm) short prismatic forsterite crystals with Sc-contents up to 0.017 apfu were obtained. As charge balance was attained by the exchange reaction $Sc^{3+} + B^{3+} \rightarrow Mg^{2+} + Si^{4+}$, the B-content is estimated to be identical, i.e., up to 0.017 apfu, corresponding to approximately 0.45 wt% B_2O_3.

Polarised single crystal FTIR-spectra of our B-substituted forsterite crystals (Figure 1) show a set of strongly polarised absorption bands between 1100 and 1400 cm^{-1}, which are not observed in spectra of B-free forsterite reference crystals. These bands occur in the frequency range where asymmetric ν_3 vibration modes of BO_3 groups are active and at distinctly higher energies than modes related to BO_4 tetrahedra (Weir and Schroeder, 1964). Two bands polar-

ized in $E||z$ at 1144 and 1177 cm^{-1} and two bands observed in $E||x$ at 1206 and 1248 cm^{-1} are on the basis of their polarisation and relative intensities assigned to isotopically (^{11}B and ^{10}B) split ν_3 and ν'_3 modes of BO_3 groups that lie on the O3-O1-O3 face of a vacant SiO_4-polyhedron. This site for boron incorporation is comparable to the one proposed by Ingrin et al. (2014) in OH- and B-bearing forsterite and recently refined by us using single-crystal XRD data (work in progress). However the BO_3-related modes in spectra of our dry synthetic samples occur at lower energies, which suggest somewhat longer B-O bond distances. Four additional bands, strongly polarised in $E||x$, occur at 1258, 1288, 1317 and 1330 cm^{-1}. These band energies suggest shorter B-O bond distances. Hence, we assign these bands tentatively to isotopically split ν_3 and ν'_3 modes of BO_3 groups that lie on the O3-O2-O1 face of vacant SiO_4-polyhedra.

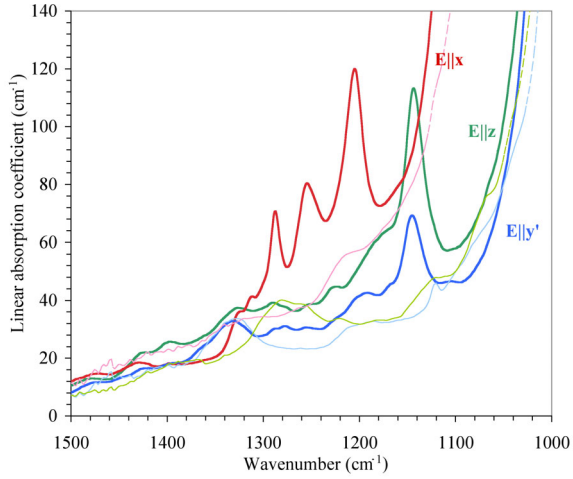

Figure 1. Polarized FTIR-spectra of B-bearing forsterite and B-free forsterite (thin lines).

The results of the present study demonstrate that appreciable amounts of boron can be incorporated in olivine minerals by means of exchange processes, which do not require any presence of hydrogen. In addition, it shows that BO_3 groups may occur as defects that are disordered over different faces of vacant SiO_4 polyhedra in the olivine structure.

References

Chaussidon, M. and Libourel, G. (1993) - Boron partitioning in the upper mantle: an experimental and ion probe study. *Geochimica et Cosmochimica Acta,* 57, 5053-5062.

Ingrin, J., Kovács, I., Deloule, E., Balan, E., Blanchard, M., Kohn, S.C. and Hermann, J. (2014) - Identification of hydrogen defects linked to boron substitution in synthetic forsterite and natural olivine. *American Mineralogist*, 99, 2138-2141.

Kent, A.J.R. and Rossman, G.R. (2002) - Hydrogen, lithium, and boron in mantle-derived olivine: The role of coupled substitutions. *American Mineralogist*, 87, 1432-1436.

Sykes, D., Rossman, G.R., Veblen, D.R. and Grew E.S. (1994) - Enhanced H and F incorporation in borian olivine. *American Mineralogist*, 79, 904-908.

Weir, C.E. and Schroeder, R.A. (1964) - Infrared spectra of the crystalline inorganic borates. *Journal of Research of the National Bureau of Standards*, 68A, 465-487.

Periodico di Mineralogia, ECMS 2015, 97-98

PERIODICO di MINERALOGIA
established in 1930

An International Journal of
MINERALOGY, CRYSTALLOGRAPHY, GEOCHEMISTRY,
ORE DEPOSITS, PETROLOGY, VOLCANOLOGY
and applied topics on *Environment*, *Archaeometry* and *Cultural Heritage*

Use of natural clays as sorbent materials for rare earth ions recovery from WEEE

Elena Maria Iannicelli-Zubiani[1], Cinzia Cristiani[1], Giovanni Dotelli[1], Paola Gallo Stampino[1], Renato Pelosato[1], Maria Lacalamita[2], Ernesto Mesto[2] and Emanuela Schingaro[2,*]

[1]Politecnico di Milano, Dipartimento di Chimica, Materiali e Ingegneria Chimica "Giulio Natta", Piazza Leonardo Da Vinci 32, 20133 Milano, Italy
[2]Università degli Studi di Bari "Aldo Moro", Dipartimento di Scienze della terra e Geoambientali, Via E. Orabona 4, 70125 Bari, Italy
* Corresponding author: *emanuela.schingaro@uniba.it*

Nowadays there is an increasing need for Rare Earth Elements (REEs) due to their usage in numerous high-technology applications such as: magnets, phosphors, metal alloys, catalysts, ceramics, glass and polishing. Each of these applications requires specific RE elements and they are not interchangeable (Iannicelli-Zubiani et al., 2013). Currently, each EU citizen produces about 17 kg of Waste Electrical and Electronic Equipment (WEEE) per year (EU, 2012). These wastes are rich in precious and strategic metals and, in many cases, have higher REEs contents than those of natural minerals. Different methods have been proposed for REEs recovery, but recently the use of Solid-Phase Extraction is obtaining more and more attention because of its advantages of high recovery, short extraction time, high enrichment factor, low cost and low consumption of organic solvents over liquid-liquid extraction. In particular, clays as solid-phase have outstanding advantages, such as low cost, high mechanical strength, good acid tolerance, convenient solid-liquid separation and excellent reusability. Furthermore, clay minerals show a natural adsorption behaviour towards REEs. For this reason, an investigation aimed at the recovery of valuable metals from WEEE was undertaken on two natural standard of smectite mineral clays, ***Ca-rich-STx and Na-rich-SWy*** (where "*STx*" and "*SWy*" stand for "State of Texas" and "State of Wyoming", respectively). Both REEs uptake and release tests were performed. Lanthanum was selected as representative of the REEs family. The solids were analysed by X-ray diffraction (XRD) and X-ray photoelectron spectroscopy (XPS), while optical emission spectroscopy (ICP-OES) analyses were performed on the liquid phase. The main results showed that: both clays are able to capture (efficiency around 50%) and release (efficiency around 70%) La ions, when the uptake and release processes are respectively performed at pH 5 and pH 1. The analysis of the basal d_{001} spacing, derived by the XRD patterns, and ICP-OES results suggest that La^{3+} uptake has occurred via a cation exchange mechanism, where La ions have displaced some interlayer Ca^{2+}, Mg^{2+} and Na^{+} ions to preserve the charge balance (Table 1).

Table 1 - Results of ICP-OES analysis of the liquid phase before and after uptake reaction.

	STx		SWy	
	Before Uptake	After Uptake	Before Uptake	After Uptake
Ca^{2+} (mmol/g_{clay})	0.54	0.29	0.49	0.40
Mg^{2+}(mmol/g_{clay})	0.08	0.03	0.14	0.07
Na^{+} (mmol/g_{clay})	-	-	0.50	0.09
La^{3+} (mmol/g_{clay})	-	0.25	-	0.23
Σ charge (mmol/g_{clay})	1.24	1.39	1.76	1.72

XPS analyses carried out on uncontacted and La^{3+} exchanged clay samples yielded similar indication. In both La-enriched clays only the signals of C, O, Mg, Si and Al are detected, whereas K and Na ions signals are missing suggesting their absence or occurrence below the detection limit. The La*3d* binding energy values are in agreement with those expected for $La(OH)_3$. In addition, as a consequence of screening effects in the final state (Schlapbach and Scherrer, 1982) the La$3d_{5/2,\ 3/2}$ peaks are split into two components. The magnitude of the splitting and the intensity ratio of each component are chemically diagnostic (Table 2).

Table 2 - Magnitude of the splitting of the La$3d_{5/2,\ 3/2}$ components.

Compound	Δ E La$3d_{5/2,\ 3/2}$ (eV)	Compound	Δ E La$3d_{5/2,\ 3/2}$ (eV)
La_2O_3	4.6	La-enriched STx	3.3
$La(OH)_3$	3.9	La-enriched SWy	3.4
La_2CO_3	3.5		

It is known that Lanthanum oxides may hydrolyse and/or react with CO_2 to form hydroxides or surface carbonate, which are characterized by a very close ΔE values, i.e. 3.9 eV and 3.5 eV for hydroxide and carbonate, respectively. On the other hand, the splitting of the La$3d_{5/2}$ component suggested that a part of La ions is embedded in the clay interlayer as hydrated form. This is also consistent with the occurrence of a minor H_2O component as derived by the deconvolution of the O1s signal. In conclusion, the XRD, ICP and XPS results, on both samples, indicate that La are allocated in the interlayer, both as carbonated and as hydrated species.

References

EU (2012) - Making raw materials available for Europe's future wellbeing proposal for a European innovation partnership on raw materials. European Commission.

Iannicelli-Zubiani, E.M., Cristiani, C., Dotelli, G., Stampino, P.G., Pelosato, R., Bengo, I., Masi, M. (2013) - Polymers modified clays for separating rare earths from WEEE. *Environmental Engineering and Management Journal*, **12**(4), 23-26.

Schlapbach, L. and Scherrer, H.R. (1982) - XPS core level and valence band spectra of LaH_3, *Solid State Communications,* **41**, 893-897.

Periodico di Mineralogia, ECMS 2015, 99-100

PERIODICO di MINERALOGIA
established in 1930

An International Journal of
MINERALOGY, CRYSTALLOGRAPHY, GEOCHEMISTRY, ORE DEPOSITS, PETROLOGY, VOLCANOLOGY
and applied topics on *Environment*, *Archaeometry* and *Cultural Heritage*

Diffusion of hydrogen in zircon

Jannick Ingrin [1,*], Peipei Zhang [1,2] and Qunke Xia [2]

[1] Unité Matériaux Et Transformations, CNRS UMR 8207, Université Lille1, Bâtiment C6, 59655 Villeneuve d'Ascq, France
[2] School of Earth and Space Sciences, University of Science and Technology of China, Hefei 230026, China
* Corresponding author: *jannick.ingrin@univ-lille1.fr*

The hydrogen mobility in gem quality zircon single crystals from Madagascar was investigated through H-D exchange experiments. Thin slices were annealed in a horizontal furnace flushed with a gas mixture of $Ar/D_{2(10\%)}$ under ambient pressure between 900 ˚C to 1150 ˚C (Fig. 1). FTIR analyses were performed on oriented slices before and after each annealing run. H diffusion along [100] and [010] follow the same diffusion law $D = D_0 \exp[-E/RT]$, with $\log D_0 = 2.24 \pm 1.57$ (in m^2/s) and $E = 374 \pm 39$ kJ/mol. H diffusion along [001] follows a slightly more rapid diffusion law, with $\log D_0 = 1.11 \pm 0.22$ (in m^2/s) and $E = 334 \pm 49$ kJ/mol. H diffusion in zircon has much higher activation energy and slower diffusivity than other NAMs below 1150 ˚C even iron-poor garnets which are known to be among the slower (Blanchard and Ingrin, 2004; Kurka et al., 2005).

During H-D exchange zircon incorporates also deuterium. This hydration reaction involves uranium reduction as it is shown from the exchange of U^{5+} and U^{4+} characteristic bands in the near infrared region during annealing (Fig. 1). It is the first time that the hydration reaction $U^{5+} + OH^- = U^{4+} + O^{2-} + 1/2H_2$ is experimentally reported. The kinetics of deuterium incorporation is slightly slower than hydrogen diffusion, suggesting that the reaction is limited by hydrogen mobility. Hydrogen isotopic memory of zircon is higher than other NAMs. Zircons will be moderately retentive of H signatures at mid-crustal metamorphic temperatures. At 500 ˚C, a zircon with a radius of 300 μm would retain its H isotopic signature over more than a million years. However, they are unlikely to retain this information for geologically significant times under high-grade metamorphism unless the grain size is large enough.

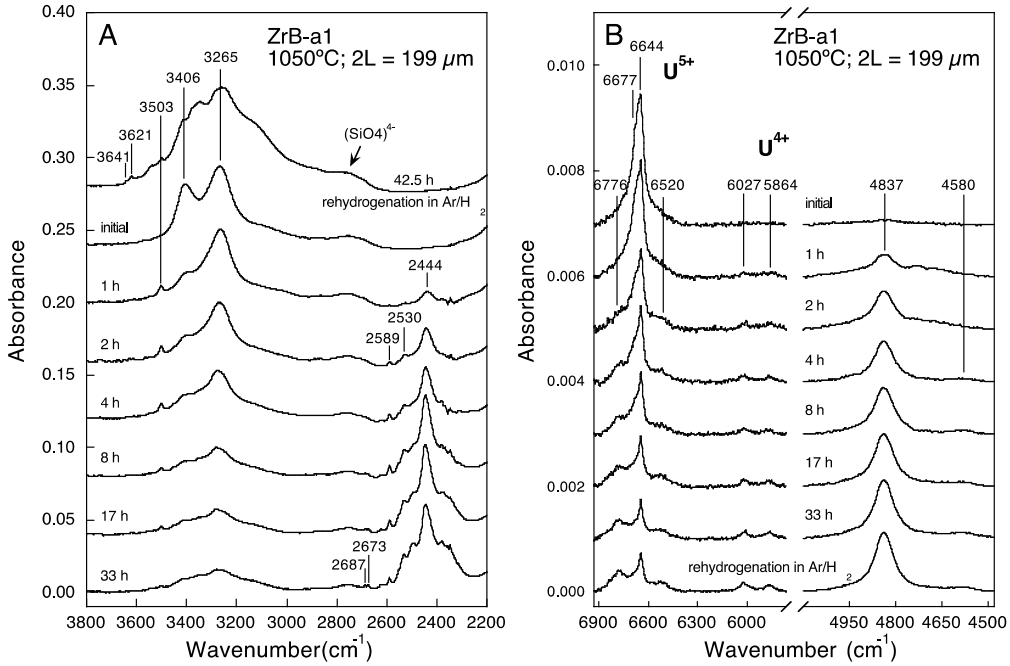

Figure 1. Representative unpolarized FTIR evolution of zircon with annealing. A. 3800-2200 cm^{-1} region showing the replacement of OH bands by OD bands during annealing under Ar/D_2 atmosphere. The uppermost spectrum shows the result after rehydrogenation in Ar/H_2 atmosphere for 42.5 h. The bands centered at 2750 cm^{-1} are related to three-phonon combination modes of internal SiO_4 stretching vibration in zircon. B. 6900-4500 cm^{-1} region showing stepwise reduction of U^{5+} to U^{4+} with time of heating under reducing condition. Band located at 6644 and 4837 cm^{-1} are the most characteristic absorption features of U^{5+} and U^{4+} respectively. Slice ZrB-a1, annealed at 1050 °C, with a thickness of 199 μm.

References

Blanchard M. and Ingrin J. (2004) Hydrogen diffusion in Dora Maira pyrope. *Physics and Chemistry of Minerals*, 31, 593-605.

Kurka A., Blanchard M. and Ingrin J. (2005) Kinetics of hydrogen extraction and deuteration in grossular. *Mineralogical Magazine*, 69, 359-371.

Periodico di Mineralogia, ECMS 2015, 101-102

PERIODICO di MINERALOGIA
established in 1930

An International Journal of
MINERALOGY, CRYSTALLOGRAPHY, GEOCHEMISTRY,
ORE DEPOSITS, PETROLOGY, VOLCANOLOGY
and applied topics on *Environment*, *Archaeometry* and *Cultural Heritage*

Bacterial, viral and protein substance influence on the formation of renal stones mineral phases

Alina R. Izatulina[1,*], Anton M. Nikolayev[1], Mariya A. Kuzmina[1], Olga V. Frank-Kamenetskaya[1] and Vladimir V. Malyshev[2]

[1] Crystallography Dept., Institute Of Earth Sciences, St. Petersburg State University, 199034, University emb. 7/9, St. Petersburg, Russian Federation
[2] S.M. Kirov Military Medical Academy, 194044, Acad. Lebedev str. 6, St. Petersburg, Russian Federation
* Corresponding author: *alina.izatulina@mail.ru*

The problem of mineral formation in the human body is one of the oldest known since ancient Egypt times. And even nowadays the interest on this issue is continuously growing, primarily due to the increasing number of people suffering from diseases associated with stone formation and accumulation in the human body organs. Significant progress in the study of stone formation processes in the human body occurs as the result of simulation experiments on crystallization of their analogues, especially in the presence of organic matter and, in particular, bacteria and viruses.

The present study is devoted to the study of crystalline phase formation in a physiological liquid (urine) prototype in the presence of the main pathogens which are present in the human urinary system during inflammatory processes: bacteria (Escherichia coli, Klebsiella, Pseudomonas aeruginosa, Staphylococcus ahrens) and viruses (hepatitis virus, coxsackie B, Rotavirus). Appropriate conditions to the physiological ones have been selected along with the nutrient media providing the growth of bacteria under experimental conditions.

Experimental results showed that the presence of bacteria, viruses and protein media plays a role in changing the pH of the solutions and significantly affects the phase composition of human renal stones. Pathogens and protein substance greatly accelerate the nucleation of calcium oxalate under the oxalate mineralization conditions, increasing the number of precipitating oxalates and stabilizing calcium oxalate dihydrate–weddellite. At phosphate mineralization conditions, pathogens and protein media significantly affect both the phase composition of the synthesized material and the position of the crystallization equilibria boundaries of the growing phases, which are shifted towards the more acidic (struvite, apatite) or the more alkaline (brushite) area.

Obtained results are considered as the scientific basis for the development of the novel renal stones formation prevention methods.

This work was supported by St. Petersburg State University (grant 3.38.243.2015). The XRD studies have been performed at the X-ray Diffraction Centre of St. Petersburg State University.

Periodico di Mineralogia, ECMS 2015, 103-104

PERIODICO di MINERALOGIA
established in 1930

An International Journal of
MINERALOGY, CRYSTALLOGRAPHY, GEOCHEMISTRY,
ORE DEPOSITS, PETROLOGY, VOLCANOLOGY
and applied topics on *Environment*, *Archaeometry* and *Cultural Heritage*

Diffusion of redox-variable elements in minerals: the example of Cr diffusion in pure forsterite and natural olivine

Michael C. Jollands, Hugh St C. O'Neill* and Andrew J. Berry

Research School of Earth Sciences, Australian National University, Canberra, ACT0200, Australia
* Corresponding author: *hugh.oneill@anu.edu.au*

How redox-variable elements diffuse through crystals raises many interesting questions about the fundamentals of the diffusion process. Here we present an experimental study of the diffusion of chromium in pure, synthetic forsterite and natural San Carlos olivine. Synthetic assemblages of magnesiochromite + protoenstatite + forsterite or magnesiochromite + periclase + forsterite, to buffer at high or low silica activity, respectively (e.g. Jollands et al, 2014), were coupled to oriented single crystals. These were then annealed to give Cr diffusion profiles in the olivines at 1400°C (in CO-CO_2 gas mixes to control the oxygen fugacity). ΣCr concentration profiles in the crystals were measured by LA-ICP-MS and EPMA, and Cr valence state and coordination environment were studied by XANES.

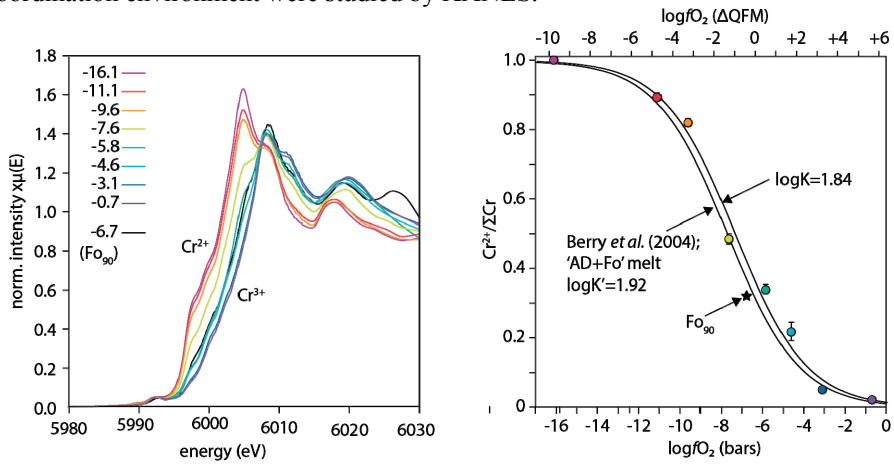

Figure 1: Left - XANES spectra from the crystal-buffer interface, as a function of fO_2. All spectra have been normalised in the near-EXAFS region (not shown). Right - $Cr^{2+}/\Sigma Cr$ as a function of fO_2; colours correspond to those on the left hand image, with best fit to a sigmoidal relationship that describes $Cr^{2+}/\Sigma Cr$ changing as a function of fO_2. Also shown is $Cr^{2+}/\Sigma Cr$ from a melt at 1400°C with forsterite on the liquidus (AD+Fo of Berry and O'Neill (2004)); i.e. no change in $Cr^{2+}/\Sigma Cr$ during olivine-melt partitioning.

Several independent methods have been used to verify that the crystal-powder interfaces represent equilibrium: the $Cr^{2+}/\Sigma Cr$ at the crystal rims and absolute concentrations of Cr^{2+} and Cr^{3+} as a function of fO_2 support this assumption (Figure 1). Cr^{3+} always substitutes onto the octahedrally coordinated site. At high silica activity Cr^{3+} uses M site vacancies ([vac]) for charge balance (i.e. $Cr^{3+}_{4/3}[vac]_{2/3}SiO_4$), whereas at low silica activity the mechanism is 'spinel-type', potentially charge balanced by Mg^{2+} on the tetrahedrally coordinated site ($Cr_2^{3+}MgO_4$). Cr^{2+} substitutes directly for Mg^{2+}, forming $Cr_2^{2+}SiO_4$ complexes.

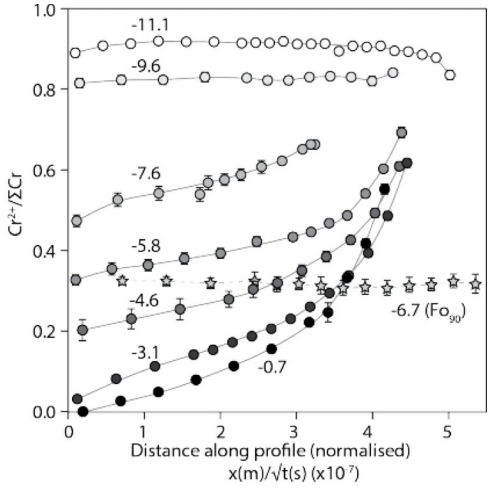

Figure 2: Changes in $Cr^{2+}/\Sigma Cr$ along diffusion profiles from all protoenstatite-buffered experiments in both forsterite (circles) and San Carlos olivine (stars). Numbers represent log fO_2 of each experiment.

Cr diffusion is faster than Fe-Mg diffusion (e.g. Chakraborty, 1997), highly anisotropic with $D_c>>D_b>D_a$ (Cr^{3+} diffusion is more anisotropic than Cr^{2+} diffusion), concentration dependent whenever Cr^{3+} is present, and strongly dependent on chemical activity – faster where silica activity is high. The geometry of Cr^{3+} profiles changes as a function of fO_2 from near 'error function' at high fO_2 to near linear at low fO_2, interpreted as a change in cation-vacancy binding energy.

The valence state of chromium ($Cr^{2+}/\Sigma Cr$) is not constant along diffusion profiles in pure forsterite; Cr is either oxidised or reduced during the diffusive process when buffered at low or high oxygen fugacity, respectively (Figure 2). Therefore, the external oxygen fugacity (fO_2) is not fully imposed on the crystal interior. Natural olivine shows no such change; electron transfer is allowed by iron redox and hence the Cr valence state ratio is always in equilibrium with the external fO_2.

Following characterisation of $Cr^{2+}/\Sigma Cr$ along the diffusion profiles, several crystals were hydroxylated in the piston cylinder at 850°C, 15 kbar in cold-sealed Ag capsules, with fO_2 controlled by Ni-NiO powder, silica activity controlled by forsterite + enstatite and water activity at unity. These were then characterised by FTIR-spectroscopy and again by XANES. Preliminary results of the effect of hydroxylation on the Cr valence state will be presented.

References

Berry, A.J., O'Neill, H.St.C (2004) - A XANES determination of the oxidation state of chromium in silicate glasses. *American Mineralogist,* 89, 790-798.

Chakraborty, S (1997) - Rates and mechanisms of Fe-Mg interdiffusion in olivine at 980-1300°C. *Journal of Geophysical Research – Solid Earth,* 102, 12317-12331

Jollands, M.C., O'Neill, H.St.C, Hermann, J. (2014) - The importance of defining chemical potentials, substitution mechanisms and solubility in trace element diffusion studies: the case of Zr and Hf in olivine. *Contribution to Mineralogy and Petrology,* 168, 1-19.

Periodico di Mineralogia, ECMS 2015, 105-106

PERIODICO di MINERALOGIA
established in 1930

An International Journal of
MINERALOGY, CRYSTALLOGRAPHY, GEOCHEMISTRY,
ORE DEPOSITS, PETROLOGY, VOLCANOLOGY
and applied topics on *Environment*, *Archaeometry* and *Cultural Heritage*

Shannon information and configurational entropy of crystalline solids

Sergey V. Krivovichev[1,*]

[1] Department of Crystallography, St. Petersburg State University, University Emb. 7/9, 199034 St. Petersburg Russia
* Corresponding author: *s.krivovichev@spbu.ru*

In the series of recent papers, we proposed to estimate the structural complexity of crystals in terms of the Shannon information amount per atom and per reduced unit cell (Krivovichev, 2013, 2014). The key equation is as following:

$$I_G = - \Sigma^k_{i=1} \Sigma p_i \log_2 p_i \quad (1),$$

where I_G is the Shannon information amount per atom, and p_i is defined as

$$p_i \equiv m_i / v \quad (2),$$

where m_i is the multiplicity of the ith crystallographic orbit relative to the reduced unit cell, v is the number of atoms in the reduced unit cell and k is the number of crystallographic orbits in the crystal structure.

The information per unit cell, $I_{G,total}$ can be calculated as

$$I_{G,total} = I_G \times v \quad (3).$$

It is generally assumed that information and entropy are closely related: the higher the information, the lower the entropy (Ben Naim 2008; Volkenstein 2009). The aim of this contribution is to clarify the relations between the structural information (that is, structural complexity) and thermodynamic entropy of crystalline solids.

According to the Boltzmann statistical mechanics, entropy S of a particular macrostate of a system is related to the number Ω of microstates, which realize the given macrostate as

$$S = k_B \ln \Omega \quad (4),$$

where k_B is the Boltzmann constant.

In the framework of the current thermodynamic theory (e.g., Fultz, 2014), thermodynamic entropy of crystals consists of contributions from the configurational, vibrational, and other entropies (e.g., magnetic (dis)order):

$$S = {}^{conf}S + {}^{vib}S + \ldots. \quad (5).$$

It is obvious that the structural complexity is directly related to the configurational entropy, which, in turn, influences the vibrational and other kinds of entropies.

Here we demonstrate that the configurational entropy (^{conf}S; without the contributions from the entropy of mixing in mixed crystals) and the Shannon information per atom (I_G) are related to each other via the equation:

$$^{conf}S = {}^{conf}S_{max} - N\,k_B\,I_G \ln 2 \quad (6),$$

where $^{conf}S_{max}$ is the maximum configurational entropy of the crystal in the case, when all atoms are symmetrically equivalent, i.e. when the crystal contains only one crystallographic orbit:

$$^{conf}S_{max} = k_B\,N \ln(N\text{-}1) \quad (7).$$

Here N is the number of atoms in a crystal. However, in order to get realistic values of ^{conf}S, N has to be specific for a particular crystalline substance and should be defined as the number of atoms that can exchange their positions in the crystal (N thus defines the 'mobility region' of the structure).

From the equation (6), we obtain

$$I_G = (^{conf}S_{max} - {}^{conf}S\,)/\,(N\,k_B\,I_G \ln 2) \quad (8),$$

which provides 'crystallographic' re-formulation of the Landauer principle that one bit of information at given temperature T is equivalent to the energy of at least $k_B T \ln 2$ (Toyabe et al. 2010).

This work was supported by the Russian Science Foundation through the grant 14-17-00071.

References

Ben Naim A. (2008) - A Farewell to Entropy. Statistical Thermodynamics based on Information. World Scientific Publishing, Singapore.

Fultz B. (2014) - Phase Transitions in Materials. Cambridge University Press, Cambridge.

Krivovichev S.V. (2013) - Structural complexity of minerals: information storage and processing in the mineral world. *Mineralogical Magazine*, 77, 275-326.

Krivovichev S.V. (2014) - Which inorganic structures are the most complex? *Angewandte Chemie International Edition*, 53, 654-661.

Toyabe S., Sagawa T., Ueda M., Muneyuki E. and Sano M. (2010) - Experimental demonstration of information-to-energy conversion and validation of the generalized Jarzynski equality. *Nature Physics*, 6, 988-992.

Volkenstein M.V. (2009) - Entropy and Information. Birkhäuser Verlag AG, Basel Boston Berlin.

Periodico di Mineralogia, ECMS 2015, 107-108

PERIODICO di MINERALOGIA
established in 1930

An International Journal of
MINERALOGY, CRYSTALLOGRAPHY, GEOCHEMISTRY, ORE DEPOSITS, PETROLOGY, VOLCANOLOGY
and applied topics on *Environment*, *Archaeometry* and *Cultural Heritage*

High pressure Raman spectroscopy on Ca-clinopyroxenes

Erica Lambruschi[1,*], Irene Aliatis[1], Luciana Mantovani[1], Mario Tribaudino[1], Danilo Bersani[1], Gunther Redhammer[2], Giacomo Diego Gatta[3] and Pier Paolo Lottici[1]

[1] Università di Parma, Dipartimento di Fisica e Scienze della Terra, Parco Area delle Scienze 7/A, 43124 Parma, Italy
[2] Universitaet Salzburg, Materialforschung und Physik, Hellbrunnerstr. 34, 5020 Salzburg, Austria
[3] Università degli Studi di Milano, Dipartimento di Scienze della Terra, Via Botticelli 23, 20133 Milano, Italy
* Corresponding author: *erica.lambruschi@difest.unipr.it*

Ca-rich clinopyroxenes are considered as major constituents of the Earth mantle. For this reason, they are the subject of several experiments aimed to describe their thermal and compressional behaviors in order to model the elastic properties of the mantle. However, little is known about the pressure-induced changes in the Raman spectra of Ca-rich clinopyroxenes. Ca-clinopyroxenes have monoclinic symmetry (space group *C*2/*c*). The general formula of pyroxenes is $M2M1T_2O_6$, where M2, M1, and T are cations hosted respectively in a distorted eight-fold-coordinated polyhedron (M2), in a regular octahedron (M1), and in a tetrahedron (T); the anion is invariably oxygen.

The samples of this study have formula $Ca^{2+}M1T_2O_6$, where M1 is populated by Mg^{2+} or Co^{2+}, and the T site by Ge^{4+} or Si^{4+}. They are all synthetic (Mantovani et al., 2015), except for Si diopside (Prencipe et al., 2000). An ETH-type diamond anvil cell (DAC) was used for the high-pressure experiments. The crystalline samples (100 x 60 x 50 μm) were placed in the gasket hole along with some ruby chips for pressure measurements by the ruby-fluorescence method (precision ±0.05 GPa). Methanol:ethanol = 4:1 mixture was used as hydrostatic pressure-transmitting medium (Angel et al., 2007). Room and high-pressure Raman spectra were collected in compression up to 7.6 GPa for silicates and to 8.27 GPa for germanates, respectively, using an Olympus BX40 microscope attached to a Jobin-Yvon Horiba LabRam confocal Raman spectrometer. The samples were excited with the 473.1 nm blue light of a doubled Nd:YAG laser. The spectra were collected in backscattering geometry in the spectral range 100-1000 cm^{-1}. Every measurement of the ruby fluorescence was calibrated using the emission lines of a spectroscopic zinc-vapour lamp. The positions of the fluorescence and Raman bands were obtained from a Gauss-Lorentzian deconvolution procedure with the LabSpec v. 5 software, with an uncertainty of about 1 cm^{-1}.

The high-pressure Raman experiments showed no phase transition within the *P*-ranges investigated, as all the peak positions vary linearly as a function of pressure. Our data confirm the previous experimental findings on Si-diopside (Chopelas et al., 2000). In all the investigated

samples, all the Raman peaks shift upon compression, but the major changes in wavenumber are attributed to the bending and stretching modes of the tetrahedral chains (*i.e.*, the building units of the pyroxene structure) (Figure 1). Upon compression, the kinking angle between tetrahedra decreases and the wavenumber of the bending mode increases (Lambruschi et al., 2015). Among the samples, Ge-pyroxenes show the higher *P*-induced peak-position shifts, being more compressible than corresponding silicates.

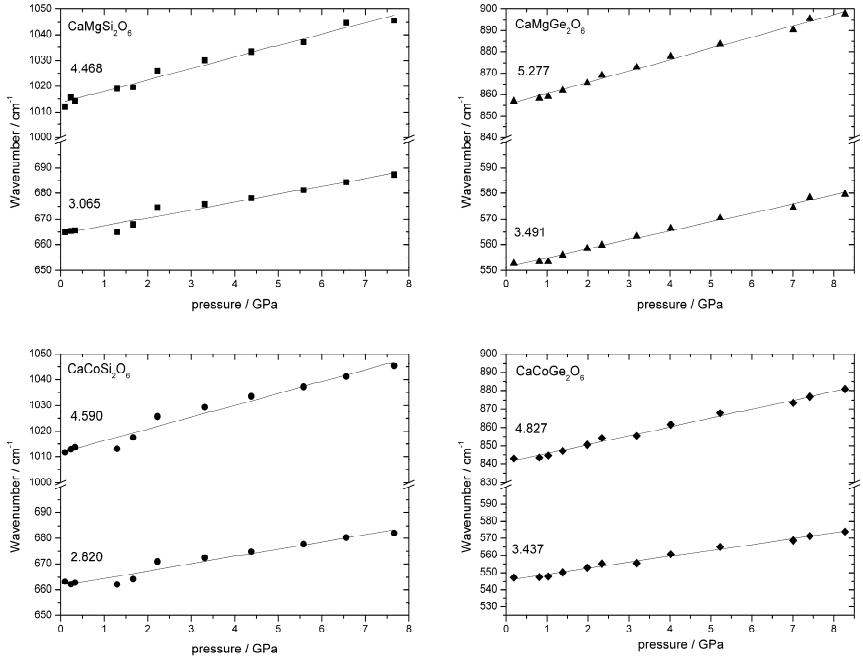

FIGURE 1: Raman shifts for selected bands vs. pressure for $CaMgSi_2O_6$, $CaMgGe_2O_6$, $CaCoSi_2O_6$, $CaCoGe_2O_6$. Lines are the fits through the data-points: their slopes $\Delta\nu/\Delta P$ are given.

References

Angel R. J., Bujak M., Gatta G.D., Jacobsen S.D. (2007) - Effective hydrostatic limits of pressure media for high-pressure crystallographic studies. *Journal of Applied Crystallographie*, 40, 26-32.

Chopelas A., Serghiou G. (2002) - Spectroscopic evidence for pressure-induced phase transitions in diopside. *Physics and Chemistry of Minerals*, 29, 403 – 408.

Lambruschi E., Aliatis I., Mantovani L., Tribaudino M., Bersani D., Redhammer G. J., Lottici P. P. (2015) - Raman spectroscopy of $CaM^{2+}Ge_2O_6$ (M^{2+}=Mg, Mn, Fe, Co, Ni, Zn) clinopyroxenes. *Journal of Raman Spectroscopy*, DOI 10.1002/jrs.4681.

Mantovani L., Tribaudino M., Aliatis I., Lambruschi E., Lottici P. P., Bersani D. Raman spectroscopy of $CaCoSi_2O_6$–$Co_2Si_2O_6$ clinopyroxenes (2015) - *Physics and Chemistry of Minerals*, 42, 179-189.

Prencipe M., Tribaudino M., Pavese A., Hoser A., Reehuis M. (2000) - A single-crystal neutron-diffraction investigation of diopside at 10 K. *Canadian Mineralogist*, 38, 183-189.

Periodico di Mineralogia, ECMS 2015, 109-110

PERIODICO di MINERALOGIA
established in 1930

An International Journal of
MINERALOGY, CRYSTALLOGRAPHY, GEOCHEMISTRY,
ORE DEPOSITS, PETROLOGY, VOLCANOLOGY
and applied topics on *Environment*, *Archaeometry* and *Cultural Heritage*

Crystal chemistry of amphiboles by Raman spectroscopy

Lisa Leissner[1], Jochen Schlüter[2], Ingo Horn[3] and Boriana Mihailova[1,*]

[1] University of Hamburg, Institute of Mineralogy, Grindelallee 48, D-20146 Hamburg Germany
[2] University of Hamburg, CeNak, Mineralogical Museum, Grindelallee 48, D-20146 Hamburg Germany
[3] Leibniz University Hannover, Institute of Mineralogy, Callinstr. 3, D-30167 Hannover, Germany
* Corresponding author: *boriana.mihailova@uni-hamburg.de*

Amphiboles ($AB_2C_5T_8O_{22}W_2$, C_5=$M1_2M2_2M3$, see Fig.1a) are rock-forming complex hydrous silicates of significant importance in geosciences as well as in environmental science and gemology. Often it is desirable to have a truly non-destructive, quick and easy-to-handle analytical method with μm-scale spatial resolution to identify amphibole groups and subgroups and to quantitatively determine the site occupancy. Raman spectroscopy has the great potential to be used for this purpose because (i) Raman-active phonon modes obey strict symmetry-related selection rules, i.e., the structure type can immediately be fingerprinted, (ii) the phonon wavenumbers depend on the masses and interatomic force constants of the atoms involved in the corresponding mode, i.e., Raman peak positions essential carry chemical information, which allows distinction between different species within the same mineral group, (iii) relative integrated peak intensities are indicative of the concentration of specific chemical species; (iv) Raman spectroscopy does not require any sample preparation and can be applied to mineral grains in crude rock samples and in glass-covered thin sections, in contrast to infrared spectroscopy.

In this contribution we provide guidelines how to use the Raman scattering arising from OH stretching modes for crystal-chemical quantitative analyses of amphiboles on the basis of thorough Raman spectroscopic and electron microprobe studies of 33 natural amphiboles covering the main amphibole subgroups as well as complementary laser-ablation inductively-coupled-plasma mass spectrometry on a few Li-containing amphiboles. Careful site-symmetry analysis revealed that only one Raman peak arising from O-H bond stretching is expected for amphiboles with no substitution disorder (Leissner et al., 2015). Thus the appearance of more Raman peaks in the range 3000-4000 cm^{-1} is due to diversity of chemical species and peak relative intensities and positions can be indeed used for site-occupancy analysis. Our results demonstrate that: (i) $^{C}(Mg, Fe)^{2+}$ at the M1M1M3 sites as well as $^{B}(Mg, Fe)^{2+}$ at the M4 site leads to two-mode behavior of the OH stretching mode (Fig. 1b) and the fractional intensities of split components can be used to quantify the concentration of chemical species at M1M1M3 as well as the overall $^{C}(Mg, Fe)^{2+}$ and to refine the occupancy of $^{B}(Mg, Fe)^{2+}$; (ii) the presence

of ^{B}(Li,Na,Ca) results in one-mode behavior of the OH-stretching Raman peaks; the total replacement of ^{B}Ca by ^{B}Na should reduce the peak positions by 6.5 cm^{-1}, whereas that of ^{B}Li by ~13 cm^{-1}; (iii) A-site occupancy leads to strong broadening as well as to a strong shift of the OH peaks toward higher wavenumbers (see Fig. 1c); ^{W}OH - ^{A}R^{+}- ^{W}F species and ^{W}OH - ^{A}R^{+} - ^{W}OH species in ^{T}Al-poor amphiboles can be discriminated by the magnitude of the M1M1M3-OH peak shift with respect to the peak position of ^{W}OH - ^{A}□ - ^{W}OH species; (iv) broad OH peaks may indicate high-content of ^{T}Al which can be verified by analyzing the width of the Raman peak near 670 cm^{-1} (Fig. 1d), generated by vibrations of bridging oxygen atoms in the double chains of TO_4 tetrahedra, which can also be considered as single chains of six-membered TO_4 rings (see Fig. 1a); (v) the occupancy of the ^{W}OH groups can be estimated using the intensity ratio η between the total Raman scattering generated by OH bond stretching and the Raman peak near 670 cm^{-1} generated by TO_4-ring vibrations; a small value of η (< 0.09) combined with the presence of strong Raman scattering near 750-780 cm^{-1} (caused by $^{C}TiO_6$) is indicative of oxo-amphiboles.

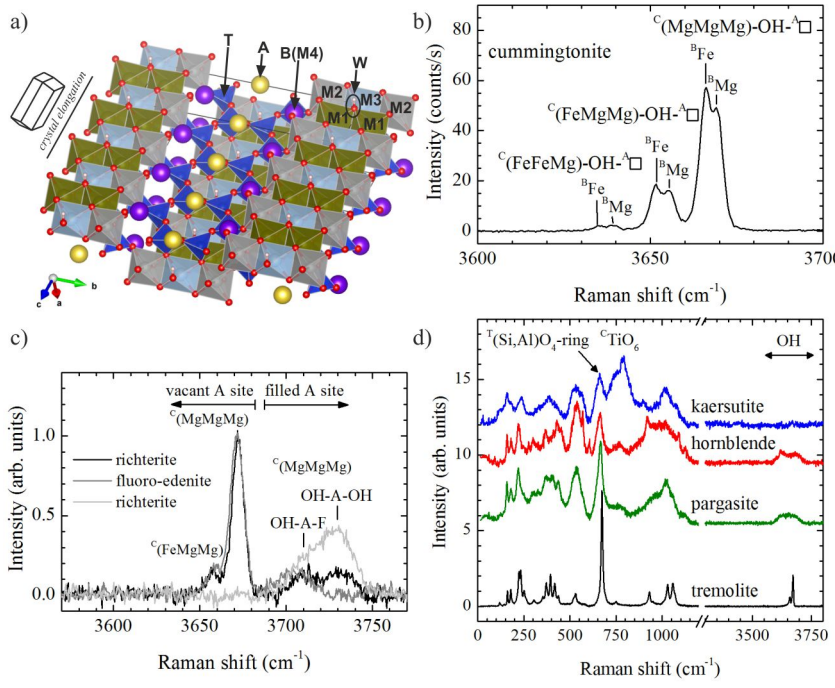

Fig.1. Structure of amphiboles (a); parallel polarized Raman spectra collected with the direction of crystal elongation perpendicular to the polarization of the incident light, demonstrating the effect of ^{C}(Mg,Fe)$^{2+}$ and ^{B}(Mg,Fe)$^{2+}$ (b), vacant/filled A site and ^{W}F (c), and ^{W}O as well as ^{T}Al and ^{C}Ti (d).

References

Leissner, L. Schlüter, J. Horn, I. and Mihailova, B. (2015) - Exploring the potential of Raman spectroscopy for crystallochemical analyses of complex hydrous silicates: I. Amphiboles; submitted.

Periodico di Mineralogia, ECMS 2015, 111-112

PERIODICO di MINERALOGIA
established in 1930

An International Journal of
MINERALOGY, CRYSTALLOGRAPHY, GEOCHEMISTRY,
ORE DEPOSITS, PETROLOGY, VOLCANOLOGY
and applied topics on *Environment*, *Archaeometry* and *Cultural Heritage*

EPR and XRD study of Co-bearing natural spinel from Vietnam

Davide Lenaz[1], Francesco Di Benedetto[2,*] and Boris Chauviré[3]

[1] Department of Mathematics and Geosciences, University of Trieste, Trieste, Italy
[2] Department of Earth Sciences, University of Florence, Firenze, Italy
[3] Laboratoire de Planétologie et Géodynamique de Nantes, France

* Corresponding author: *francesco.dibenedetto@unifi.it*

Blue spinel from Luc Yen district in north Vietnam are included in marble. These marbles (and the associated spinel) come from the intense metamorphism, linked to successive orogenies, of an ancient carbonate platform from the Paleo-Tethys Ocean. Previous chemical and spectroscopic analyses (Chauviré et al., 2015) indicated that the blue colour is due to cobalt (Co^{2+}), with some iron contribution. Chemistry by LA-ICP-MS shows that the most intense blue spinels have about 13000 ppm Fe, 2500 ppm Ni, 1200 ppm Co, 1100 ppm Cr, while Ga, V, Ti and Mn are in the range 200-400 ppm. Chauviré et al. (2015) demonstrated through UV-Vis spectra that the main absorption band between 500 and 670 nm, the dominant origin of color in these blue spinels, is composed of a series of bands at approximately 545, 550, 560, 580, 590, and 625 nm. Bands at 545, 550, 580, and 625 nm are due to cobalt (Co^{2+}) substituting for Mg^{2+} in tetrahedrally coordinated sites of the spinel structure while the remaining absorption bands are allocated to iron (Fe^{2+}) in tetrahedral sites of the spinel structure. Consequently, the spectra show transmission windows between 300 and 500 nm and between 700 and 900 nm that explains the blue colour. As expected, the spectra show that iron (Fe^{2+}) and cobalt (Co^{2+}) are the main chromophore elements. Chromium makes a significant contribution to the colour if the concentration is above 1000 ppm.

X-ray diffraction single-crystal analyses on several fragments show a unit-cell parameter of about 8.0864 Å and an oxygen positional parameter close to 0.2634.

Some fragments were analysed through Electron Paramagnetic Resonance (EPR) spectroscopy, at X band (~9.5 GHz) and room temperature. A complex spectrum was obtained, in which two distinct features can be identified: a sextet at g ~2.0, due to the hyperfine splitting, and ascribed to the Mn^{2+} ion. A second set of lines appear at g values in the range 1.6 and 2.0, whose variability as a function of the crystal orientation in the magnetic field point to an ion occurring in a medium-to-strong ligand field. Only Co^{2+} and Cr^{3+} can be proposed for the final attribution.

References

Chauviré B., Rondeau B., Fritsch E., Ressigeac P. and Devidal J.-L. (2015) - Blue spinel from the Luc Yen district of Vietnam. *Gems & Gemology*, 51, 2-17.

Periodico di Mineralogia, ECMS 2015, 113-114

PERIODICO di MINERALOGIA
established in 1930

An International Journal of
MINERALOGY, CRYSTALLOGRAPHY, GEOCHEMISTRY,
ORE DEPOSITS, PETROLOGY, VOLCANOLOGY
and applied topics on *Environment*, *Archaeometry* and *Cultural Heritage*

Raman spectroscopy and the inversion degree of natural Cr-bearing spinels

Davide Lenaz[1,*] and Vanni Lughi[2]

[1] Department of Mathematics and Geosciences, University of Trieste, Trieste, Italy
[2] Department of Engineering and Architecture, University of Trieste, Trieste, Italy

* Corresponding author: *lenaz@units.it*

The spinel structure is based on a nearly ideal cubic close-packed array of oxygen atoms with tetrahedral (T) and octahedral (M) cavities. In common 2-3 spinels, one eighth of the T sites and one half of the M sites are occupied by heterovalent cations A and B in the ratio AB_2O_4, where A = (Mg, Fe^{2+}, Zn, Mn^{2+}) and B = (Al, Fe^{3+}, Cr^{3+}). Commonly there exists octahedral-tetrahedral disorder of A and B cations depending on thermal history. Consequently, the crystal-chemistry of spinels is described by the general formula $^{IV}(A_{1-i}B_i)^{VI}(A_iB_{2-i})O_4$, where "i" refers to the inversion parameter. There are two ordered configurations stable at low temperature, one with i = 0 (normal spinel; e.g., $MgAl_2O_4$, $FeAl_2O_4$, $MgCr_2O_4$ and $FeCr_2O_4$) and one with i = 1 (inverse spinel; e.g., $MgFe_2O_4$ and $FeFe_2O_4$). With increasing temperature disorder takes place, i.e. A and B cations undergo increasing intersite exchange over the three cation sites per formula unit. Modifications of T-O and M-O bond distances to accommodate various chemical compositions and/or cation distribution determine variations in the oxygen positional parameter u and the cell edge a_0.

Cr-bearing spinels can be found in different geological environments, usually related to mafic and ultramafic rocks from great depth in the mantle as inclusions in diamonds (Lenaz et al., 2009; Nestola et al., 2014) to extra-terrestrial material (Lenaz et al., 2015). In nature, several cations can enter into the structure originating a solid solution with a general formula (Mg, Fe^{2+})(Al, $Cr)_2O_4$. Other cations such as Fe^{3+} or Ti can be present in low amounts - although in some cases the Fe^{3+} content can be very high. It's important to notice that almost all the major cations can move among the two sites apart from Cr that prefers the octahedral site. Given that, spinels with higher Cr content will show a limited possibility of inversion while those with high Mg and Al and low Cr could undergo different degrees of inversion.

In order to see the effects of order/disorder phenomena via Raman spectroscopy we analysed spinels already characterised by X-ray single crystal diffraction and electron microprobe, and many other spinels from the same suites characterised by electron microbe for a total of about 300 different natural Cr-bearing spinels with $0.03 < Cr < 1.68$ atoms per formula unit.

Preliminary data show that the relative intensities and shifts of the A_{1g} peak can be related to the Cr/(Cr+Al) ratio, being at about 690 cm^{-1} and 745 cm^{-1} for high and low Cr content, respectively. As far as the low Cr spinels are concerned, the Raman spectra of disordered spinels are characterised by a peak at about 162-166 cm^{-1} and a succession of smooth curves in the range 300-650 cm^{-1}. Ordered low Cr-spinels do not show the peak at 162-166 cm^{-1} but a peak at about 404 cm^{-1} and two others not well developed peaks/curves in the range 600-650 cm^{-1}.

References

Lenaz D., Logvinova A.M., Princivalle F. and Sobolev N.V. (2009) - Structural parameters of chromite included in diamonds and kimberlites from Siberia: a new tool for discriminating ultramafic source. *American Mineralogist*, 94, 1067-1070.

Lenaz D., Princivalle F. and Schmitz B. (2015) – First crystal-structure determination of chromites from an acapulcoite and ordinary chondrites. *Mineralogical Magazine*, in print.

Nestola F., Beriotto B., Andreozzi G.B., Bruschini E. and Bosi F. (2014) – Pressure-volume equation of state for chromite and magnesiochromite: A single crystal X-ray diffraction investigation. *American Mineralogist*, 99, 1248-1253.

Periodico di Mineralogia, ECMS 2015, 115-116

PERIODICO di MINERALOGIA
established in 1930

An International Journal of
MINERALOGY, CRYSTALLOGRAPHY, GEOCHEMISTRY,
ORE DEPOSITS, PETROLOGY, VOLCANOLOGY
and applied topics on *Environment*, *Archaeometry* and *Cultural Heritage*

Spectroscopic study of Chelyabinsk LL5 meteorite: structural peculiarities of iron-bearing minerals in different fragments

Alevtina A. Maksimova, Evgeniya A. Petrova, Andrey V. Chukin,
Aleksander S. Vokhmintsev, Victor I. Grokhovsky, Ilya A. Weinstein,
Vladimir A. Semionkin and Michael I. Oshtrakh*

Institute of Physics and Technology, Ural Federal University, Ekaterinburg, 620002, Russian Federation
* Corresponding author: *oshtrakh@gmail.com*

On February 15, 2013 a large fireball fall was seen in Chelyabinsk Region, Russian Federation. This fall was accompanied by several acts of parent body fragmentation and a powerful flash at the stopping point. A huge number of various meteorite fragments with weights ranging from several milligrams up to ~650 kg were found in the fall area. This meteorite was classified as ordinary chondrite LL5 group, S4 and W0, and named Chelyabinsk. Various fragments of the Chelyabinsk LL5 meteorite are different in color and petrography (Kohout et al., 2014). Therefore, we studied structural peculiarities of some fragments of Chelyabinsk LL5 meteorite using various physical techniques such as optical and scanning electron microscopy, X-ray diffraction, luminescence spectroscopy and ^{57}Fe Mössbauer spectroscopy with a high velocity resolution. Meteorite fragments chosen for investigation were with the same light lithology LL (No 1 and No 1a), with mixed light and dark lithology MLDL (No 2) and with black lithology BL (No 3). Fragments with black lithology are now considered as re-melted meteorite substance after shock reheating in the space.

Metallography showed that metal grains in the studied fragments consist of kamacite α-Fe(Ni,Co), taenite γ-Fe(Ni,Co) and plessite structure α-Fe(Ni,Co) + γ-Fe(Ni,Co). Troilite FeS grains were found as individual inclusions in silicate matrix, as assemblies with metal grains and as inclusions inside metal grains. Troilite shock-melted veins were observed in the BL fragment only. Chromite $FeCr_2O_4$ inclusions were observed in all studied fragments. Scanning electron microscopy with energy dispersive spectroscopy demonstrated some variations in Ni and Co content in both α- and γ-phases of the metal grains in different fragments. X-ray diffraction showed some similarities in the composition of studied fragments. However, evaluation of the unit cell parameters in the crystals of pyroxene $(Fe,Mg)SiO_3$ showed some small differences between fragments with LL and BL while those for the crystals of olivine $(Fe,Mg)_2SiO_4$ were the same. Cathodoluminescence spectra showed a more intensive peak at the 460 nm band for fragment with LL than that for fragment with BL (Fig. 1). Similar data were obtained for fragments with LL and BL using photoluminescence spectroscopy for the

peak at the 440 nm band. This result indicates that olivine in fragment with LL has larger part of forsterite Mg_2SiO_4 than that in fragment with BL (see Jones and Carey, 2006). Study of Chelyabinsk LL5 fragments with different lithology using Mössbauer spectroscopy with a high velocity resolution continues earlier started investigations (Oshtrakh et al., 2014; Maksimova et al., 2015). Representative Mössbauer spectrum of Chelyabinsk LL5 fragment No 2 is shown in Figure 2. It was possible to reveal Mössbauer spectral components related to ferromagnetic α-Fe(Ni,Co) and γ-Fe(Ni,Co) phases (1–3), troilite (4), the M1 and M2 sites in both olivine (5, 6) and pyroxene (7, 8), paramagnetic γ-Fe(Ni,Co) phase (9) and chromite (10). The modal analysis of the iron-bearing minerals demonstrated some differences in the relative content of these minerals in the studied fragments. These results demonstrated that fragments of Chelyabinsk LL5 meteorite with different lithology have small differences in both morphology and crystal structures. It was also shown that Mössbauer hyperfine parameters of corresponding iron-bearing minerals in different fragments were slightly different. This fact may be related to some variations in the ^{57}Fe nuclei local microenvironment in the M1 and M2 sites in olivine and pyroxene as well as to increase in troilite non-stoichiometry x ($Fe_{1-x}S$) in fragments with black lithology as a result of the iron lost after troilite re-melting.

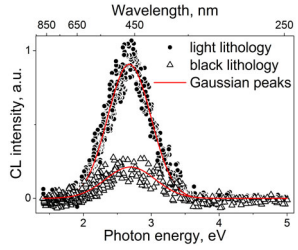

Figure 1. Cathodoluminescence spectra of Chelyabinsk LL5 fragments with light and black lithology.

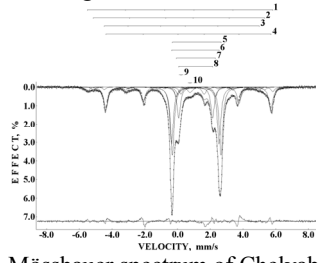

Figure 2. Mössbauer spectrum of Chelyabinsk LL5 fragment with mixed light and dark lithology at T=295 K.

This work was supported in part by the Russian Foundation for Basic Research, grant No 15-35-21164, and basic support from the Ministry of Education and Science of Russian Federation. A.A.M. is supported in part by the Ural Federal University development program for the young scientists' financial support and by the OPTEC, Inc. grant for young scientists.

References

Jones R.H. and Carey E.R. (2006) – Identification of relict forsterite grains in forsterite-rich chondrules from the Mokoia CV3 carbonaceous chondrite. *American Mineralogist*, 91, 1664–1674.

Kohout T. et al. (2014) – Mineralogy, reflectance spectra, and physical properties of the Chelyabinsk LL5 chondrite – insight into shock induced changes in asteroid regoliths. *Icarus*, 228, 78–85.

Maksimova A.A., Oshtrakh M.I., Petrova E.V., Grokhovsky V.I. and Semionkin V.A. (2015) – The ^{57}Fe hyperfine interactions in the iron bearing phases in different fragments of Chelyabinsk LL5 meteorite: a comparative study using Mössbauer spectroscopy with a high velocity resolution. *Hyperfine Interactions*, 230, 79–87.

Oshtrakh M.I., Petrova E.V., Grokhovsky V.I. and Semionkin V.A. (2014) – Characterization of a Chelyabinsk LL5 meteorite fragment using Mössbauer spectroscopy with a high velocity resolution. *Hyperfine Interactions*, 226, 559–564.

Periodico di Mineralogia, ECMS 2015, 117-118

PERIODICO di MINERALOGIA
established in 1930

An International Journal of
MINERALOGY, CRYSTALLOGRAPHY, GEOCHEMISTRY,
ORE DEPOSITS, PETROLOGY, VOLCANOLOGY
and applied topics on *Environment*, *Archaeometry* and *Cultural Heritage*

Potentiality of micro-Raman Spectroscopy for the identification of unclassified minerals preserved in old Museum collections

Paolo Mazzoleni[1], Germana Barone[1,*], Erica Aquilia[1], Danilo Bersani[2], Rosolino Cirrincione[1] and Simona Raneri[1]

[1]Department of Biological, Geological and Environmental Sciences, University of Catania, C.so Italia, 57 95129 Catania, Italy,
[2] Department of Physics and Earth Sciences, University of Parma, Parco Area delle Scienze, 7/A 43124 Parma, Italy,
*Corresponding author: *gbarone@unict.it*

Really interesting mineral collections are preserved in several Earth Science Research Institutions and exhibited in Museums. In view of the presence of rare minerals of a great scientific interest, these collections represent a really valuable heritage for users and collectors. However, in many cases, they include old specimens classified following outdated schemes. Furthermore, the frequent reshuffle of the exhibitions as well as of the documental archives has often caused a loose of classification and provenance information on minerals.

The Department of Biological, Geological and Environmental Sciences of the Catania University owns a rich collection consisting in thousands of minerals; the oldest collection is represented by minerals and rocks offered to the University by Giuseppe Gioieni in the 1781, at the same time of the institution of the "Gabinetto di Storia naturale" in Catania. Worth of note is that among the collection materials, several objects of high archeological and scientific interest belonging to the Princess of Biscari are also present.

This study is a part of a wide project finalized to the cataloguing and characterization of minerals scheduled to be exhibited in the Minerals and Rocks Museum set at the Department with the aim to enrich the existing collections; information on composition of these objects is in fact indispensable in view of a correct valorization and fruition of the Museum.

In this context, the use of micro-Raman spectroscopy represents a useful tool in the characterization of minerals; in fact, the method allows to perform non-destructive, fast and cheap analyses and obtain complete information on mineral composition, as demonstrated by its successfully use in several studies of precious and unique art objects, gems and museum materials (Adriaens, 2015; Azzi et al., 2014; Barone et al., 2014; Barone et al., 2015; Vandenabeele, 2004).

In the framework of this paper, micro-Raman measurements have been carried out by using a Jasco NRS-3100 apparatus, equipped with two laser excitation source at 532 and 785 nm, respectively. Overall, the preliminary micro-Raman results allow us to confirm previous identifications, as in the case of a pyromorphite sample (Figure 1a), identify numerous unclassified

minerals (*e.g.* crystals of cuproadamite; Figure 1b) and finally reclassify mistaken attributions, as for the sample shown in Figure 1c classified as barthite; the micro-Raman spectra collected on the mineral exhibits the typical bands of malachite.

On the basis of the analyses performed on minerals, a new classification can be therefore obtained, making the materials available for scientific, expositive and didactic purposes. Furthermore, taking in account the presence of really rare minerals among the materials preserved in the collections, this project may represent a contribution to the enlargement of the existing Raman databases, widely available also online.

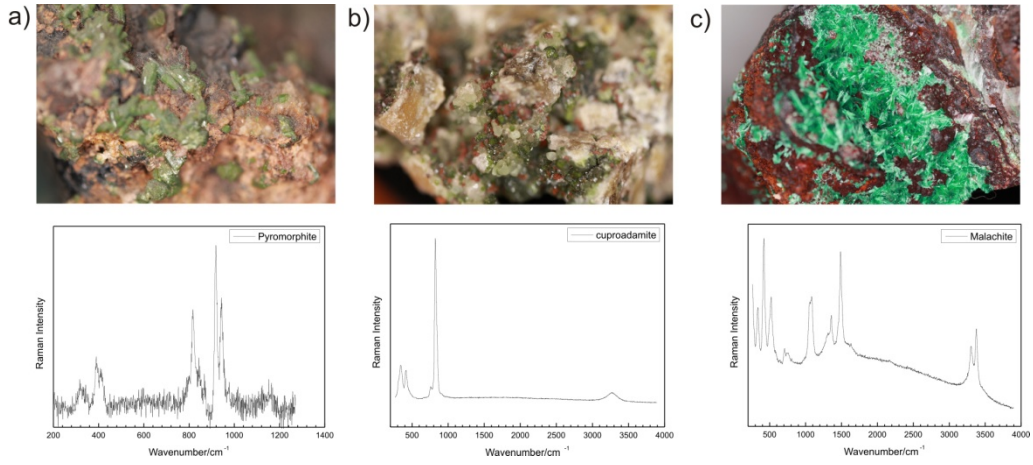

Fig. 1 Macrophotos and micro-Raman spectra collected by using a 532 nm excitation line on (a) phyromorphite (b) cuproadamite and (c) malachite samples, as examples of classified, unclassified and misclassified materials.

References

Adriaens A. (2005) - Non-destructive analysis and testing of museum objects: An overview of 5 years of research. *SpectrochimicaActa Part B: Atomic Spectroscopy*, 60, Pages 1503–1516.

Azzi G., Bersani D., Lottici P. P., Lambruschi E., Barone G., Mazzoleni P., Raneri S., Longobardo U. (2014) - Characterization of emeralds by micro-Ramanspectroscopy.*Journal of Raman-Spectroscopy*, 45, 1293–1300.

Barone G., Bersani D., Crupi V., Longo F., Longobardo U., Lottici P.P, Aliatis I., Majolino D., Mazzoleni P., Raneri S., Venuti V. (2014) - A portable versus micro-Raman equipment comparison for gemmological purposes: the case of sapphires and their imitations". *Journal of Raman Spectroscopy*, 45, 1309–1317.

G. Barone, D. Bersani, J. Jehlička, P. P. Lottici, P. Mazzoleni, S. Raneri, P. Vandenabeele, C. Di Giacomo, G. Larinà (2015) - Nondestructive investigation on the 17-18th centuries Sicilian jewelry collection at the Messina regional museum using mobile Raman equipment. *Journal of Raman Spectroscopy*. DOI: 10.1002/jrs.4649.

P. Vandenabeele (2004) - Raman spectroscopy in art and archaeology. *Journal of Raman Spectroscopy*, 35, 607–609.

Periodico di Mineralogia, ECMS 2015, 119-120

PERIODICO di MINERALOGIA
established in 1930

An International Journal of
MINERALOGY, CRYSTALLOGRAPHY, GEOCHEMISTRY,
ORE DEPOSITS, PETROLOGY, VOLCANOLOGY
and applied topics on *Environment*, *Archaeometry* and *Cultural Heritage*

A spectroscopic study of volcanic ashes from Mt. Etna, Catania (Italy)

Paolo Mazzoleni[1], Germana Barone[1], Francesco Di Benedetto[2,*], Marco Benvenuti[2], Pilar Costagliola[2], Giordano Montegrossi[3], Valentina Rimondi[2], Maurizio Romanelli[2], Fabrizio Bardelli[5] and Francesco d'Acapito[4]

[1] Università di Catania - Dipartimento di Scienze Biologiche, Geologiche e Ambientali
[2] Università di Firenze - Dipartimento di Scienze della Terra
[3] CNR – Istituto di Geoscienze e Georisorse
[4] CNR – Istituto Officina Materiali - OGG @ESRF (France)
[5] Università di Torino - Dipartimento di Scienze della Terra
* Corresponding author: *francesco.dibenedetto@unifi.it*

The surface of the volcanic ashes are widely modified during the explosive eruption by the interaction with the gas/areosol occurring in the plume. The mineralogical and compositional changes induced by this interaction have important consequences on the impact on the environment and human health.

The speciation of iron in relation to the mineralogical composition, to the particle granulometry, and to the interaction with water is largely unknown. In particular, the oxidation state and the formations of new phases due to the S, Cl, and F present in the plume are key points for the analysis of the consequences that these products may have on human health.

Several samples related to numerous explosive episodes occurred during 2013 were collected on volcanic tefra of the Mt. Etna and investigated using a multitechnique approach, which included conventional EPR, high field EPR, Electron Spin Echo, and XAS at the Fe K edge.

Being element selective, these techniques allowed to obtain a detailed information on the Fe valence state and coordination environment.

Samples revealed a complex mineralogical assemblage, mainly consisting of glass, but also hosting numerous crystalline phases, from the micrometer to the nanometer dimension. The pre-edge and the XANES regions of the XAS spectroscopy revealed the coexistence of Fe(II) and Fe(III) species in an almost constant ratio in the raw bulk samples, whereas significant changes were evidenced as a function of particle granulometry. Slight changes in the mean oxidation state of Fe were also detected when particles were let interact with water under labora-

tory conditions. Combined EPR and HFEPR revealed that Fe(III) occurs in at least two different phases, most of it being included in the volcanic glass, and the remaining hosted in a magnetic phase, probably an Fe oxide. HFEPR analyses suggested that a fraction of superparamagnetic Fe is hosted in crystallites with dimensions that do not allow a multidomain magnetic structure to be established. Finally, EXAFS structural refinements suggested that Fe mainly occurs in an inverse spinel structure, compatible with magnesioferrite or magnetite.

Periodico di Mineralogia, ECMS 2015, 121-122

PERIODICO di MINERALOGIA
established in 1930

An International Journal of
MINERALOGY, CRYSTALLOGRAPHY, GEOCHEMISTRY,
ORE DEPOSITS, PETROLOGY, VOLCANOLOGY
and applied topics on *Environment*, *Archaeometry* and *Cultural Heritage*

A combined micro-Raman spectroscopy and single-crystal X-ray diffraction approach: an example on natural and synthetic garnets

Niccolò Menegoni[1], Fabrizio Nestola[1,*], Matteo Alvaro[2,3] and Sula Milani[1]

[1]Università degli Studi di Padova, Dipartimento di Geoscienze, via Gradenigo 6, I-35131, Padova, Italy
[2]Università degli Studi di Pavia, Dipartimento di Scienze della Terra e dell'Ambiente, via Ferrata 1, I-27100, Pavia, Italy
[3]University of Glasgow, School of Geographical and Earth Sciences, G12 8QQ, Glasgow, UK
*Corresponding author: *Fabrizio.nestola@unipd.it*

Garnets are among the most abundant minerals found in diamonds as inclusions. Their study are crucial to understand the petrologic environment in which diamond crystallize and therefore they provide fundamental petrologic, geophysical and geodynamical information. However, very often they are investigated only by optical microscopy as this is of course a non-destructive technique and requests only a short time to analyse the sample. In general, it is thought that purple garnets are of peridotitic origin whereas orange garnets are of eclogitic origin. Even if this is absolutely true for most of the garnets investigated in diamond quite often the simple colour observed under an optical microscope can bring to erroneous identification: this could be due to a) a not sharp colour distinction between orange and purple and b) the presence of diamond faces not flat which do not allow to really distinguish the garnet colour.

A second crucial information that could be retrieved by studying garnets entrapped in diamonds is the depth of formation of the diamond-garnet pair. This kind of investigation is extremely complex and must follow a series of steps well described in Nestola (2015).

In this study we investigated a series of garnets, both entrapped in diamond and not entrapped in diamond, by a combined approach adopting micro-Raman spectroscopy (μ-Raman) and single-crystal X-ray diffraction (SCXRD) in order to get their chemical composition (thus their peridotitic *vs*. eclogitic origin) and pressure of formation.

Starting from the method of Bersani et al. (2009) which is based on the hypothesis that in a garnet solid solution the Raman frequencies depend linearly from the end-member frequencies weighted by their molar fraction, we used μ-Raman spectroscopy and SCXRD; the necessity to combine the two techniques is due to the possibility that garnets in diamonds are under a certain pressure and this could cause a clear Raman band shift, which cannot be included in the

Bersani et al. (2009) method. By SCXRD we can retrieve the number of electrons at each crystallographic site and provide, therefore, a constraint to the composition obtained by μ-Raman.

In general, our approach is based on a system of linear equations composed by the six wavenumber equations and two equations relative to the number of electrons at X and Y crystallographic garnet sites.

The method was tested on a suite of six natural kimberlite garnets and three synthetic garnets. Such garnets were first analysed by electron microprobe analysis in WDS mode (EMPA), SCXRD and μ-Raman in order to fully characterize their crystal chemistry and the relationship between chemistry and Raman spectra.

The EMPA analyses show that the six natural kimberlite garnets have a websteritic/peridotitic composition, the synthetic garnet has an eclogitic composition and the other two synthetic garnets were synthesized along the pyrope-almandine solid solution. SCXRD analyses are in good agreement with the EMPA results. The tests performed on natural and synthetic garnets not trapped in diamonds allowed us to confirm that our μ-Raman and SCXRD combined approach provide very satisfying results.

To provide an example we can consider one of the natural garnets analysed in our study, for which the EMPA results give the following formula:

$(Mg_{0.64}Fe_{0.21}Ca_{0.14}Na_{0.01})_3(Al_{0.94}Cr_{0.06})_2Si_3O_{12}$.

Using our combined approach, we obtained an extremely satisfying results being the calculated formula:

$(Mg_{0.65}Fe_{0.18}Ca_{0.17})_3(Al_{0.94}Cr_{0.06})_2Si_3O_{12}$.

Similar results are obtained on synthetic garnets.

The main differences between the calculated and observed formulae should be due to the knorringite end-member ($Mg_3Cr_2Si_3O_{12}$), which is not taken into account in the Bersani et al. (2009) protocol. Actually, in literature we could find only one micro-Raman spectrum but on a synthetic Si-rich knorrignite being $Mg_3(Cr_{1.58}Mg_{0.21}Si_{0.21})Si_3O_{12}$ (Bykova et al., 2014) and thus, we used such spectrum for our calculation.

Our results on natural and synthetic garnets are absolutely promising in order to evaluate the composition of garnets still trapped in their diamond hosts, which cannot be destroyed to analyse the inclusions.

References

Bersani D., Andò S., Vignola P., Moltifiori G., Marino I.G., Lottici P.P. and Diella V. (2009) - Micro-Raman spectroscopy as a routine tool for garnet analysis. *Spectrochimica Acta Part A: Molecular and Biomolecular Spectroscopy,* 73, 484-491.

Bykova E.A., Bobrov A.V., Sirotkina E.A., Bindi L., Ovsyannikov S.V., Dubrovinsky L.S. and Litvin Y.A. (2014) - X-ray single-crystal and Raman study of knorringite, $Mg_3(Cr_{1.58}Mg_{0.21}Si_{0.21})Si_3O_{12}$, synthesized at 16 GPa and 1600 °C. *Physics and Chemistry of Minerals*, 41, 267-272.

Nestola F. (2015) - The crucial role of crystallography in diamond research. *Rendiconti Lincei*, 26, 225-233.

Periodico di Mineralogia, ECMS 2015, 123-124

PERIODICO di MINERALOGIA
established in 1930

An International Journal of
MINERALOGY, CRYSTALLOGRAPHY, GEOCHEMISTRY,
ORE DEPOSITS, PETROLOGY, VOLCANOLOGY
and applied topics on *Environment*, *Archaeometry* and *Cultural Heritage*

Structural disorder in Narsarsukite from Murun (Russia)

Ernesto Mesto[1,*], Ekaterina Kaneva[2], Maria Lacalamita[1], Emanuela Schingaro[1], Fernando Scordari[2] and Nicolay Vlakykin[2]

[1] Università degli Studi di Bari "Aldo Moro", Dipartimento di Scienze della terra e Geoambientali, Via E. Orabona 4, 70125 Bari, Italy
[2] The A.E. Favorsky Institute of Geochemistry, Irkutsk, Russia.
* Corresponding author: *ernesto.mesto@uniba.it*

Narsarsukite, $[Na_2(Ti,Fe)Si_4(O,F)_{11}]$, is a rare titanosilicate mineral usually found in alkali pegmatitic rocks in Narsarsuk, Greenland. Titanosilicate minerals represent excellent materials for selective recovery of valuable ions from waste (Su and Balmer, 2000). They also exhibit exceptional catalytic activities and are selective for oxidation reactions (Clerici et al., 1997).

The microporous framework of narsarsukite is made up of tubular tetrahedral chains running parallel to the *c* direction and linked by corning-sharing Ti-octahedra. The cavities between the tetrahedral and octahedral chains contain Na^+ ions.

An EPMA, Micro-FTIR and SCXRD study of narsarsukite from Murun single crystals is here presented. Average chemical composition from EPMA was (wt%): SiO_2 62.4, Al_2O_3 0.16, Na_2O 16.2, MgO 0.08, K_2O 0.20, TiO_2 15.4, V_2O_3 0.24, Fe_2O_3 4.3, ZrO_2 0.2, BaO 0.08 and F 1.10. Total iron was assumed as Fe^{3+} on the basis of literature Mössbauer results (Wagner et al., 1991). The studied narsarsukite is an intermediate member of Ti-Fe narsarsukite series and its chemical content is close to narsarsukite-I from Lovozero massif, Russia (Kartashov, 1994).

The FTIR spectrum (Figure 1) was collected in the range 4000 to 400 cm^{-1} and evidences characteristic bands of the tetrahedral and octahedral vibrations at 1900-400 cm^{-1}. No relevant hydrogen absorption bands appear in the 3800-3400 cm^{-1} region pointing to an anhydrous composition. Similar features were found in Narsarsuk Zr-rich narsarsukite (sample n. 21739 in Wagner et al., 1991). However, in other Narsarsuk crystals the same authors described high-intensity infrared bands at 3550, 3478, 3416 and 3235 cm^{-1} that were assigned to stretching vibrations of water molecules located in the sodium cavities.

The structure refinements, carried out in the space group *I*4/*m*, show from difference Fourier maps, residual peaks of ≈6 and 1.4 $e^-/Å^3$. The former was interpreted as a splitting of the Ti site due to a $Ti^{4+} \rightarrow Fe^{3+}$ replacement and the latter as a positional disorder of Na site. The modeling of both kinds of disorder yielded a final *R*-index of ≈ 1.4 %. The Ti-octahedron is

strongly distorted compared to the Fe-octahedron. The ordered Na-polyhedron is seven-fold coordinated (<Na_{ord}-O> = 2.52 Å) whereas the disordered Na-ion is surrounded by 8 oxygen atoms (<Na_{dis}-O> = 2.72 Å).

In the narsarsukite structure there are five independent oxygen atoms: O1 and O2 are shared between Ti-octahedra, O4 is shared between Ti-octahedra and Si-tetrahedra, while O3 and O5 link Si-tetrahedra. As a consequence of the mentioned structural disorder the following arrangements in the structure are possible: a) octahedral chain consisting of only Ti octahedra; b) octahedral chain consisting of only Fe octahedra; c) Fe octahedra located between adjacent Ti octahedra; d) Fe octahedra adjacent and linked through the O2 oxygen; e) Fe octahedra adjacent and linked through O1 oxygen. Bond valence analyses for each of the listed cases indicate that the O1 and O2 sites can be occupied by F^-, $(OH)^-$ or O^{2-}. Taking the EPMA and SCXRD results into account, it can be hypothesized that the disordering of Na promotes $O^{2-} \rightarrow OH^-$ substitution, while the splitting of the Ti site, related to the amount of Ti^{4+} and Fe^{3+} in the structure, can affect the replacement of F^- for O^{2-} at the bridging O1 and O2 sites.

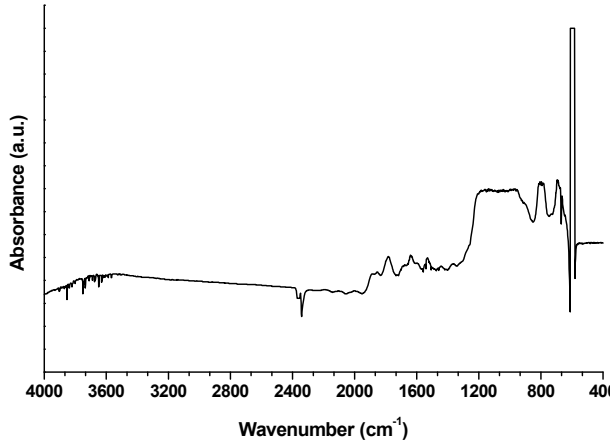

Figure. FTIR spectra of the studied narsarsukite in the range 4000-400 cm^{-1}.

References

Clerici M.G., Bellussi G. and Romano U. (1997) - Synthesis of propylene oxide from propylene and hydrogen peroxide catalyzed by titanium silicalite. *Journal of Catalysis.*, 129, 159-167.

Su Y. and Balmer M.L. (2000) - Raman Spectroscopic Studies of Silicotitanates. *Journal of Physical Chemistry B*, 104, 8160-8169.

Wagner C., Parodi G.C., Semet M., Robert J.-L., Berrahma M. and Velde D. (1991) - Crystal chemistry of narsarsukite. *European Journal of Mineralogy*, 3, 575-585.

Kartashov P.M. (1994) - Narsarsukite from fenitized rocks of Lovozero massif. *Proceedings of the Russian Mineralogy Society*, 4, 58-66.

Periodico di Mineralogia, ECMS 2015, 125-126

PERIODICO di MINERALOGIA
established in 1930

An International Journal of
MINERALOGY, CRYSTALLOGRAPHY, GEOCHEMISTRY,
ORE DEPOSITS, PETROLOGY, VOLCANOLOGY
and applied topics on *Environment*, *Archaeometry* and *Cultural Heritage*

Electronic high-spin to low-spin transition in siderite at high pressure and temperature

Jan Müller[1,*], Monika Koch-Müller[1] and Sandro Jahn[2]

[1]GFZ, German Research Centre for Geosciences, Telegrafenberg, 14473 Potsdam, Germany
[2]University of Cologne, Institute of Geology and Mineralogy, Greinstraße 4-6, 50939 Cologne, Germany
* Corresponding author: *jmueller@gfz-potsdam.de*

Carbonates are the most abundant carbon-bearing minerals on Earth. Through subduction processes carbonates can be transported into the Earth up to depths of the lower mantle. Magnesite-siderite solid solutions are the main carbon carriers in the deep Earth and therefore, understanding their stability may help understanding the long term carbon cycle.

Iron bearing minerals may undergo pressure induced electronic and structural phase transitions from a high-spin (HS) to a low-spin (LS) state. In case of the magnesite-siderite solid solutions series the high-pressure behavior is controversially discussed. Several recent experimental studies report on the pressure-induced spin-pairing transition of the d-orbital electrons of Fe^{2+} from high spin (HS) to low spin (LS) and the transition pressure reported for the Fe-endmember at ambient temperature range from 40 to 45 GPa (Lavina et al., 2010; Spivak et al., 2014; Lobanov et al., 2015). Liu et al. (2014) present a P-T phase diagram for magnesiosiderite ($Mg_{0.35}Fe_{0.65}CO_3$) showing a strong increase of the transition pressure with temperature. For the endmember siderite, however, the behavior with pressure and temperature is still unknown.
With the spin transition a large collapse of the unit cell volume is reported (Lavina et al., 2010). Therefore, vibrational spectroscopy in combination with diamond-anvil cell experiments is especially suited to map such phase diagrams.

Here we present in-situ Raman and infrared spectroscopic data of siderite up to ca. 60 GPa taken in internally heated diamond anvil cells. Our first results indicate the spin transition to start even at pressure below 40 GPa and indicate a steeper Clausius Clapeyron slope than reported for the magnesiosiderite by Liu et al. (2014).

References

Lavina B., Dera P. Downs R.T., Yang W., Sinogeikin Y.M., Shen G. and Schiferl D. (2010) - Structure of siderite $FeCO_3$ to 56 GPa and hysteresis of its spin-pairing transition, *Physical Review B*, 82, 064110.

Liu J., Lin J.-F., Mao Z. and Prakapenka V. (2014) - Thermal equation of state and spin transition of magnesiosiderite at high pressure and temperature, *American Mineralogist*, 99, 84-93.

Lobanov S.S., Goncharov A.F. and Litasov K.D. (2015) - Optical properties of siderite ($FeCO_3$) across the spin transition: Crossover to iron-rich carbonates in the lower mantle, *American Mineralogist,* 100, 1059-1064.

Spivak A., Solopova N., Cerantola V., Bykova E., Zakharchenko E., Dubrovinsky L. and Litvin Y. (2014) - Raman study of $MgCO_3$–$FeCO_3$ carbonate solid solution at high pressures up to 55 GPa, *Physics and Chemistry of Minerals*, 41, 633-638.

Periodico di Mineralogia, ECMS 2015, 127-128

PERIODICO di MINERALOGIA
established in 1930

An International Journal of
MINERALOGY, CRYSTALLOGRAPHY, GEOCHEMISTRY,
ORE DEPOSITS, PETROLOGY, VOLCANOLOGY
and applied topics on *Environment*, *Archaeometry* and *Cultural Heritage*

Photoluminescence spectroscopy: a tool for revealing stress caused by self-irradiation damage

Lutz Nasdala[1,*] and Christoph Lenz[1]

[1] Universität Wien, Institut für Mineralogie und Kristallographie, Althanstr. 14, 1090 Wien, Austria
* Corresponding author: *lutz.nasdala@univie.ac.at*

Radiative electronic transitions of rare-earth element (REE) related defect centers are most sensitive to changes of the short-range order. This is in particular the case for the quantitative estimation of structural damage caused by the corpuscular self-irradiation of actinide-bearing accessory minerals by means of laser-induced photoluminescence (PL; Nasdala et al., 2013; Lenz and Nasdala, 2015). Here we present first results of a PL study that has addressed stress-distribution patterns within heterogeneously radiation-damaged minerals.

The self-irradiation of actinide-bearing minerals results, among other changes, in significant volume expansion. Variable self-irradiation due to zoned incorporation of U and Th causes different degrees of volume expansion among neighboring growth zones. Once the critical stress is exceeded, the sample yields by fracturing (Chakoumakos et al., 1987). For instance, more radiation-damaged inner regions or cores of crystals are typically surrounded by patterns of radial cracks (Lee and Tromp, 1995). Such cracks or fractures are of crucial importance for potential alteration processes, as they are perfect fast diffusion pathways for migrating fluids.

As an example, we present in Fig. 1 PL analyses of a mildly radiation-damaged growth zone inside a heterogeneous, unaltered zircon crystal. The zone under discussion (which is internally fairly homogeneous) is bracketed by two growth zones that are strongly radiation-damaged and hence volume-expanded. This results in notable dilative stress in the less radiation-damaged zone under discussion. The tension is for instance recognized from lowered Raman-shift values and up-shifted PL emissions (Fig. 1b). Near fractures (which are typically oriented perpendicular to zone boundaries), the stress and hence the up-shift of PL lines is released (rad circles in Fig. 1b). This is visualized clearly in a hyperspectral PL map (Fig. 1c). Our study underlines again that the PL mapping technique has great analytical potential in study radiation-damaged accessory minerals non-destructively on a micrometer scale.

Acknowledgement: This research was funded by the Austrian Science Fund (FWF) through grant P244481–N19.

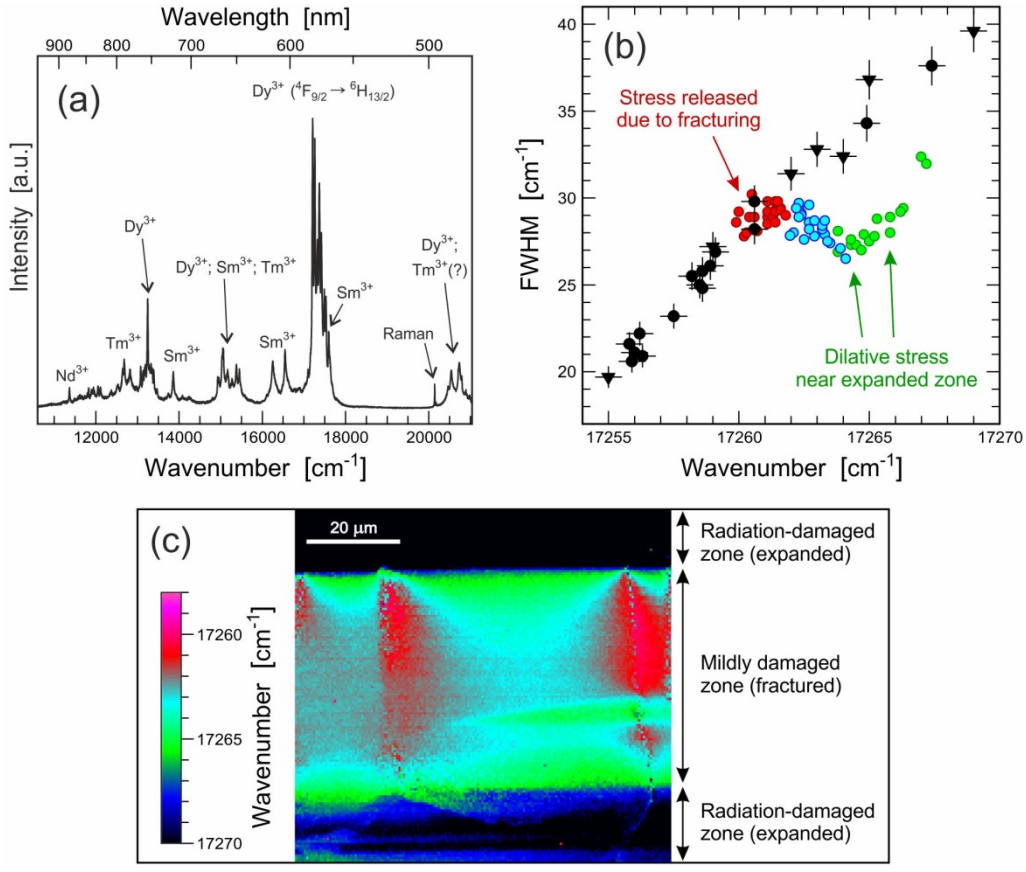

Fig. 1. PL study of a zoned zircon from Plešovice, Czech Republic. (a) PL spectrum (473 nm excitation) obtained within a mildly radiation-damaged growth zone. (b) Plot of FWHM against position of the Dy^{3+} emission line near 17,260 cm^{-1}. Black, data for variably radiation-damaged, unstressed zircon (from Lenz and Nasdala, 2015). (c) Hyperspectral PL map, visualizing stress release near fractures (red).

References

Chakoumakos B.C., Murakami T., Lumpkin G.R. and Ewing R.C. (1987) – Alpha-decay–induced fracturing in zircon: the transition from the crystalline to the metamict state. *Science*, 236, 1556–1559.

Lee J.K.W. and Tromp J. (1995) – Self-induced fracture generation in zircon. *Journal of Geophysical Research: Solid Earth*, 100, 17753–17770.

Lenz C. and Nasdala L. (2015) – A photoluminescence study of REE^{3+} emissions in radiation-damaged zircon. *American Mineralogist*, 100, 1123–1133.

Nasdala L., Grambole D. and Ruschel K. (2013) – Review of effects of radiation damage on the luminescence emission of minerals, and the example of He-irradiated $CePO_4$. *Mineralogy and Petrology*, 107, 441–454.

Periodico di Mineralogia, ECMS 2015, 129-130

PERIODICO di MINERALOGIA
established in 1930

An International Journal of
MINERALOGY, CRYSTALLOGRAPHY, GEOCHEMISTRY,
ORE DEPOSITS, PETROLOGY, VOLCANOLOGY
and applied topics on *Environment*, *Archaeometry* and *Cultural Heritage*

Clinopyroxenes from Pico Volcano (Azores Island, Portugal): crystal chemistry and water content

Sabrina Nazzareni[1,*], Valerio Barbarossa[2], Henrik Skogby[3] and Vittorio Zanon[4]

[1] University of Perugia Department of Physics and Geology, P.zza Università 1 I-06100 Perugia Italy
[2] Radboud University Nijmegen, Department of Environmental Science, Heyendaalseweg 135, 6524 AJ, Nijmegen, The Netherlands
[3] Swedish Museum of Natural History, Department of Geosciences, SE-10405 Stockholm, Sweden
[4] Centro de Vulcanologia e Avaliação de Riscos Geológicos, Universidade dos Açores, Rua Mãe de Deus, 9501-801 Ponta Delgada, Portugal
* Corresponding author: *sabrina.nazzareni@unipg.it*

The Pico volcanic island is located in the central Azores archipelago (Portugal). The morphology of the island is characterised by a perfect conical stratovolcano and an elongated ridge constituted by cinder cones aligned along NW-SE trending faults, which are associated to fissural eruptions. The island was built by three main volcanic complexes: the Montanha Volcanic Complex, to which Pico Mountain, the central volcano, belongs; the Sào Roque-Piedade Volcanic Complex, a fissure volcano, and the Topo-Lajes Volcanic Complex (Nunes et al., 1999).

Clinopyroxenes from the Montanha central cone were studied by polarized FTIR spectroscopy, Mössbauer spectroscopy, single crystal X-ray diffraction and electron probe micro analysis on the same crystals. In the Montanha eruptive material a particularly high content of clinopyroxene is present. During crystal growth, this early forming phase can incorporate H^+ that may be used to calculate the magmatic water content and contribute to the knowledge of evolution processes during magma crystallisation and ascent. The clinopyroxene samples are millimetre-sized euhedral phenocrysts from a cumulitic lava flows and centimetre-sized euhedral crystals from the Pic16 mugearite lava flow erupted during the 1718 AD eruption.

The studied clinopyroxenes are diopside (Wo45-46 En45-48 Fs06-09), and show very weak or absent OH^- vibrational bands in the IR spectra (except in Pic16), corresponding to H_2O contents ranging from 0 to 91 ppm H_2O. These low contents indicate H^+ loss during ascent to surface or post eruptive re-equilibration, which may occur via the redox reaction $Fe^{2+} + OH^- = Fe^{3+} + O^{2-} + ½H_2$. In order to restore H^+ that was possibly lost, we performed thermal annealing

experiments under H_2 gas flux at 700°C and 800°C. All the samples increased their hydrogen content and reached saturation after 65-83 hours, depending on crystal thickness. The new range of water thus obtained is 93-170 ppm for samples from the cumulitic lava and 120-182 ppm for Pic16. Mössbauer analysis gave a Fe^{3+}/Fe_{tot} ratio for untreated clinopyroxenes between 18.8-25.8%, after the thermal annealing the ratio remains constant or slightly decrease. Using the H-saturation values and the partition coefficients of Wade et al. (2008) we calculated 0.75-1.21 H_2O wt% in melt, which is slightly lower than the range measured in melt inclusions in olivines from the Pico fissural eruptions (Metrich et al., 2014).

The Pico primary magmas were produced at 3 GPa and 1352-1362°C, by a very low melting degree of a mantle source with 350 to 630 ppm of H_2O, then melts ascended up to 18 km, where olivine and clinopyroxene crystallised and accumulated in a storage areas (Zanon and Frezzotti, 2013). The crystal chemistry of clinopyroxenes suggests that they crystallized at 18 km depth and that the H^+ loss occurred during the ascent or a late stage of eruption.

References

Metrich N., Zanon V., Creon L., Hildenbrand A., Moreira M. and Marquez F.O. (2014) - Is the "Azores Hotspot" a wetspot? Insight from the geochemistry of fluid and melt inclusions in olivine of Pico Basalts. *Journal of Petrology*, 55, 377-393.

Nunes J. C., Camacho A., França Z., Montesinos F.G., Alves M., Vieira R., Velez E. and Ortiz E., (2006) - Gravity anomalies and crustal signature of volcano-tectonic structures of Pico Island (Azores). *Journal of Volcanology and Geothermal Research*, 156, 55–7.

Wade J.A., Plank T., Hauri E.H., Kelley K.A., Roggensack K. and Zimmer M. (2008) - Prediction of magmatic water contents via measurement of H_2O in clinopyroxene phenocrysts. *Geology*, 36, 799-802.

Zanon V. and Frezzotti M.L. (2013) - Magma storage and ascent conditions beneath Pico and Faial islands (Azores archipelago): A study on fluid inclusions. *G Cubed*, 14 (9), 3494-3514.

Periodico di Mineralogia, ECMS 2015, 131-132

PERIODICO di MINERALOGIA
established in 1930

An International Journal of
MINERALOGY, CRYSTALLOGRAPHY, GEOCHEMISTRY,
ORE DEPOSITS, PETROLOGY, VOLCANOLOGY
and applied topics on *Environment*, *Archaeometry* and *Cultural Heritage*

Combining structure refinement and spectroscopies: hints and warnings for more efficient tools to decipher the mechanisms of deprotonation in amphiboles

Roberta Oberti[1,*], Giancarlo Della Ventura[2] and M. Darby Dyar[3]

[1]CNR-Istituto di Geoscienze e Georisorse, UOS di Pavia, I-27100 Pavia
[2]Dipartimento di Scienze, Università Roma Tre, I-00146 Roma.
[3]Department of Astronomy, Mount Holyoke College, South Hadley, MA 01075, U.S.A.
*Corresponding author: *oberti@crystal.unipv.it*

Notwithstanding our present detailed knowledge of amphibole crystal-chemistry, HT behaviour in amphiboles is still a difficult issue to be addressed. Indeed, thermal annealing generally induces three simultaneous processes: thermal expansion, cation disordering, and deprotonation; hence, understanding the details of the different crystal-chemical mechanisms is not straightforward. The relations and the relative importance of the three processes, as well as their onset temperatures, vary as a function of composition; hence, a systematic work has been undertaken and is still in progress. First, the simplest compositions were studied, where both cation disordering and deprotonation processes are excluded. Then, the study was extended to more complex compositions, which are however of major relevance to petrology. In order to build the most accurate model as possible, different techniques were applied, and all were optimized in order to take into account the peculiarities of both the experimental setting and the mineral matrix. Indeed, it soon turned out that each of the techniques applied would have profited of a careful inter-calibration.

On the structural (crystallographic) side, *in operando* measurement of unit-cell parameters was combined with single-crystal structure refinement done at temperature values chosen to monitor the crucial step of the irreversible deprotonation/oxidation process. The same approach was applied on cooling, in order to investigate the behavior of the deprotonated phase. The available crystal-chemical knowledge was used to model changes in site-scattering, site and chain geometry, as well as in atomic displacement parameters. To make a very long story short, we concluded that oxidation proceeds by $^{M(4)}Fe^{2+}$ migration (when available) to the $M(1,3)$ sites and by its preferential oxidation at the $M(1)$ site. However, the structural response varies significantly as a function of composition.

On the spectroscopic side, extensive HT single-crystal FTIR analysis was applied to the most interesting compositions. Methodological details will be discussed by Della Ventura

(2015) and Susta et al. (2015), however, we anticipate here that compatible and reliable data must be based on FTIR spectra collected on quenched samples after each step of thermal annealing. FTIR data allowed an independent measure of the kinetics and of the completion of the deprotonation process, which vary as a function of the total Fe^{2+} content but also of the bulk composition.

Measuring the correct value of the $Fe^{3+}/\Sigma Fe$ is a further crucial issue for these studies. XANES data are severely affected by mineral anisotropy and the intensity of the pre-edge signal is very sensitive to polyhedral distortion and coordination. Dyar et al. (2016) studied a series of well-characterized (by EMPA, SREF, H_2O analysis and Mössbauer spectroscopy) amphibole single-crystals with variable Fe contents, including those partially or totally deprotonated *via* controlled thermal-annealing. These authors obtained a tremendous improve in the results when applying multivariate approaches (such as partial least-squares models with variable or constant numbers of components and especially *l*east *a*bsolute *s*hrinkage and *s*election *o*perator - *lasso* - regression) to XANES data collected in the *entire* XANES region with the beam polarized along the major optical directions (**X**, **Y**, and **Z**). This procedure could/should be extended to XANES analysis of other minerals. Hopefully, it will also help in the study of the role of Fe oxidation state in asbestiform minerals, many of which are amphibole species.

Hints for the use of Mössbauer data come from the work of Susta et al. (2015), who combined SREF, Mössbauer and FTIR data to follow iron oxidation in a sodic amphibole (riebeckite) at HT. Again, Mössbauer spectra are to be collected on samples quenched after heating experiments, in this case at different T and constant annealing time. The interpretation of the results is still underway; however, we can anticipate that our data suggests that the oxidation of $^{M(1)}Fe^{2+}$ can be detected some tenths of degrees before deprotonation is recorded in the FTIR spectra.

References

Della Ventura G. (2015) - FTIR spectroscopy at HT: applications and problems. *Periodico di Mineralogia*, ECMS 2015, 7-8.

Dyar M.D., Breves E.A., Gunter M.E., Lanzirotti A., Tucker J.M., Carey C.J., Peel S., Brown E.B., Oberti R., Lerotic M. and Delaney J.S. (2016) - Synchrotron Micro-XANES Analysis of Fe^{3+} in oriented amphiboles. *American Mineralogist,* submitted.

Susta U., Della Ventura G., Bellatreccia F., Hawthorne F.C. and Oberti R. (2015) - HT-FTIR spectroscopy of riebeckite. *Periodico di Mineralogia*, ECMS 2015, 167-168.

Periodico di Mineralogia, ECMS 2015, 133-134

PERIODICO di MINERALOGIA
established in 1930

An International Journal of
MINERALOGY, CRYSTALLOGRAPHY, GEOCHEMISTRY,
ORE DEPOSITS, PETROLOGY, VOLCANOLOGY
and applied topics on *Environment*, *Archaeometry* and *Cultural Heritage*

Crystal chemistry of Si-deficient B-bearing vesuvianite forming epitaxial intergrowths on wiluite

Taras L. Panikorovskii[1*], Sergey V. Krivovichev[1], Andrey A. Zolotarev[1], Vladimir V. Shilovskikh[2] and Eveny V. Galuskin[3]

[1]Department of crystallography, Institute of Earth Sciences, St. Petersburg State University, University Emb. 7/9, St.Petersburg, 199034, Russia
[2]Department of colloid chemistry Insitute of chemistry, St. Petersburg State University, Universitetskii pr. 26, Peterhof, St. Petersburg 198504, Russia
[3]Faculty of Earth Sciences, Department of Geochemistry, Mineralogy and Petrography, University of Silesia, Bedzinska 60, 41–200 Sosnowiec, Poland
* Corresponding author: *taras.panikorovsky@spbu.ru*

Vesuvianite $Ca_{19}(Al,Mg,Fe,Ti)_{13}(B,\square)_5(O,OH)_{10}O_{68}$ is a complex metasomatic mineral that may contain boron, which occupy two additional positions, T1 and T2 (Groat et al., 1998; Bellatrccia et al., 2005). In wiluite, the content of boron is greater than 2.5 apfu. Crystal structure of vesuvianite from the Wiluy river was solved by Warren and Model in 1931 in the space group *P*4/*nnc*.

In this contribution, we report on the occurrence of a hydrogarnet-type substitution in a B-rich secondary-formed autoepitaxial vesuvianite. The secondary-formed autoepitaxial Si-deficient B-bearing vesuvianite forms a yellow crust on the {101} faces of wiluite crystals. The crystal structure has been studied using single-crystal X-ray diffraction by means of an Excalibur Eos single-crystal difractometer (Mo*K*α X-radiation, 50 kV and 40 mA, frame width of 1° in ω, and 30 s in the range 2θ 6.12-64.56°). Empirical absorption correction was applied using CrysAlisPro program (CrysAlisPro, 2012). Structure refinement was carried out with the SHELXL-97 program.

The unit-cell parameters are as following: a = 15.5841(4), c = 11.7682(6) Å, V = 2858.0(2) Å^3). The structure was refined in the space group *P*4/*nnc* to R_1 = 0.044. Microprobe chemical analysis demonstrated that our sample contains only 16.8 apfu of Si if the formula is calculated on the basis of 19 Ca apfu. At the same time, single-crystal X-ray diffraction revealed increasing bond length <Si-O> up to 1.699(3) Å for the Z1 site, whereas the refined occupancy of the Z1 and Z2 sites are 0.70(1) and 0.899(6), respectively. The crystal chemical formula of the mineral can be written as $Ca_{\Sigma 19.00}(Al_{8.57}Mg_{3.03}Fe_{1.27}Mn_{0.08}Ti_{0.05})_{\Sigma 13.00}[SiO_4]_{8.8}[H_4O_4]_{1.20})_{\Sigma 10.00}$

$[Si_2O_7]_4(B_{1.00}\square_{4.00})_{\Sigma 5.00}(OH_{6.86}O_{2.94}Cl_{0.20})_{\Sigma 10.00}$), which corresponds to the hydrogarnet-type isomorphism with the substitution scheme $SiO_4^{4-} \leftrightarrow H_4O_4^{4-}$ (Galuskin et al., 2005, 2007).

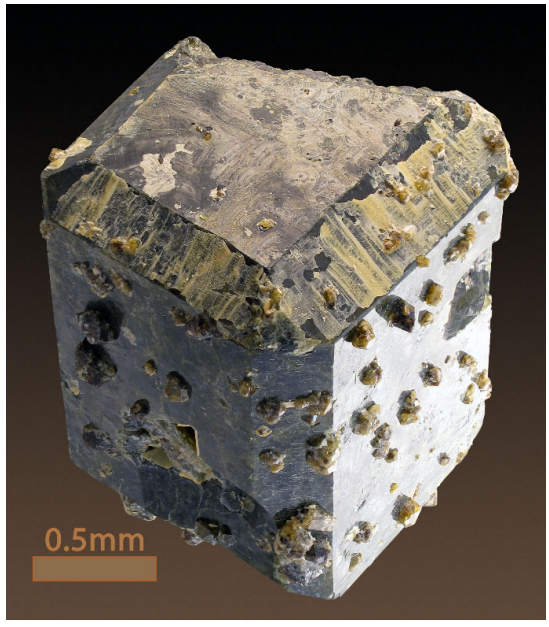

Figure 1. Yellow crust of autoepitaxial Si-deficient, B-bearing vesuvianite on the {101} faces of wiluite crystals.

This research was carried out using resources of the X-ray Diffraction Centre, Geo Environmental Centre "Geomodel" of St. Petersburg State University

References

Bellatreccia F., Camara F., Ottolini L., Della Ventura G., Cibin G. and Mottana A. (2005) - Wiluite from Ariccia, Latium, Italy: Occurrence and crystal structure. *Canadian Mineralogist*, 43, 1457-1468.

CrysAlisPro, Agilent Technologies, Version 1.171.36.20 release 27-06-2012.

Galuskin E.V. (2005) - Mineraly Grupy wezuwianu ze skal achtarandytowych (rzeka Wiluj, Jakucja). *Widawnictwo Uniwersytetu Slaskiego*, 1-193.

Galuskin E.V., Galuskina I.O., Stadnicka K., Armbruster T. and Kozanecki M. (2007) - The crystal structure of Si-deficient, OH-substituted, boron-bearing vesuvianite from the Wiluy River, Sakha - Yakutia Russia. *Canadian Mineralogist*, 45, 239-248.

Groat L.A., Hawthorne F.C., Ercit T.S. and Grice J.D. (1998) - Wiluite, $Ca_{19}(Al,Mg,Fe,Ti)_{13}(B,Al,\square)_5Si_{18}O_{68}(O,OH)_{10}$, a new mineral species isostructural with vesuvianite, from the Sakha Republic, Russian Federation. *Canadian Mineralogist*, 36, 1301-1304.

Warren B.E. and Modell D.I. (1931) - The structure of vesuvianite $Ca_{10}Al_4(Mg,Fe)_2Si_9O_{34}(OH)_4$. *Zeitschrift für Kristallographie*, 7-8, 422-432.

Periodico di Mineralogia, ECMS 2015, 135-136

PERIODICO di MINERALOGIA
established in 1930

An International Journal of
MINERALOGY, CRYSTALLOGRAPHY, GEOCHEMISTRY,
ORE DEPOSITS, PETROLOGY, VOLCANOLOGY
and applied topics on *Environment*, *Archaeometry* and *Cultural Heritage*

Precipitates around thermal springs in the catchment of the Rio Colca, Peru

Andrzej Paulo[1,*], Justyna Ciesielczuk[2], Adam Postawa[1], Wiesława Krawczyk[2], Tomasz Krzykawski[2], Krzysztof Gaidzik[2] and Jerzy Żaba[2]

[1] University of Science and Technology, Mickiewicza 30 30-059 Kraków Poland
[2] University of Silesia, Będzińska 60 41-200 Sosnowiec Poland
* Corresponding author: *andrzej.paulo@interia.pl*

The Rio Colca in Peru, also named Rio Majes and Rio Camana, is a major river in the Pacific catchment. About 50 thermal springs, many with associated crusts and efflorescences, occur in the basin of the Rio Colca and its tributary, the Rio Andamayo. Most of the surroundings of the hard-to-access canyon is rocky mountain desert rising to 1300-4800 m a.s.l. (Fig. 1).

Figure 1. Thermal springs in the Rio Colca catchment. Water types: sulphate (yellow diamonds), chloride

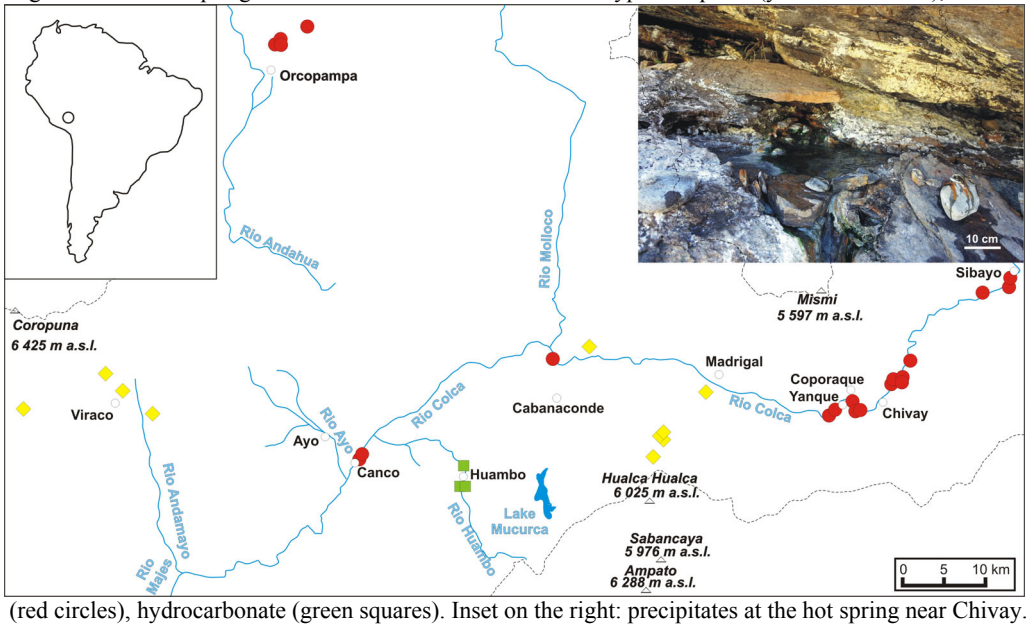

(red circles), hydrocarbonate (green squares). Inset on the right: precipitates at the hot spring near Chivay.

The composition of the precipitates is variable: 24 sulphate minerals, 3 carbonates, native sulphur, halite, hematite, goethite and amorphous silica were identified using XRD and SEM-

EDS. Hot springs flow from a variety of sedimentary Mesozoic formations and Cenozoic volcanic complexes. Their waters are generally of multi-ion type, but three subtypes may be distinguished: sulphate emanating H_2S, chloride which may emanate CO_2, and hydrocarbonate with no evident emanations. Proportions of the main cations Na, Ca and Mg differ and K rarely exceeds 10%. Other elements in significant amounts were not noted. Sulphate springs, located in fields of solfatara-altered volcanics near stratovolcanoes of Pliocene-Quaternary age usually have low TDS values of 0.5-1.5 g/l, and temperatures of 40-85°C. Chloride springs in tectonized siliciclastic rocks show TDS values of 1-5 g/l and temperatures of 40-68°C. The waters of karst-type hydrocarbonate springs (3rd magnitude) discharging from a large (10 km long and < 80 m thick) travertine body abounding in sinkholes have rather low TDS (~ 1.2 g/l), and temperatures of 17°C that exceed by several degrees the average daily temperature of the surrounding desert, suggesting recharge from hidden hot springs. The greatest diversity of precipitating minerals was found both around a geyser and around springs in the nearby solfatara field of the Hualca Hualca volcano and around the hottest springs discharging from fractured sandstone and pyrite-bearing blackshales near Chivay.

Precipitates on the northern slope of the Hualca Hualca volcano form thick crusts and ubiquitous efflorescences crystallizing on the fractured rocks, the soil surface and plants. Thermal waters of Ca-SO_4 type are characterized by TDS values ranging from 662-1266 mg/l. The following minerals were identified there: alunite $KAl_3[(SO_4)_2|(OH)_6]$, alunogene $Al_2(SO_4)_3 \cdot 17H_2O$, blödite $Na_2Mg(SO_4)_2 \cdot 4H_2O$, boussingaultite $(NH_4)_2Mg[SO_4]_2 \cdot 6H_2O$, copiapite $FeFe_4[(SO_4)_6|(OH)_2] \cdot 20H_2O$, coquimbite $Fe_2^{3+}[SO_4]_3 \cdot 9H_2O$, gypsum $CaSO_4 \cdot 2H_2O$, jarosite $KFe^{3+}{}_3(SO_4)_2(OH)_6$, mohrite $(NH_4)_2Fe[SO_4]_2 \cdot 6H_2O$, pickeringite $MgAl_2[SO_4]_4 \cdot 22H_2O$, rozenite $Fe[SO_4] \cdot 4H_2O$, thenardite Na_2SO_4, tschermigite $(NH_4)Al[SO_4]_2 \cdot 12H_2O$, voltaite $K_2Fe_5^{3+}[SO_4]_4 \cdot 18H_2O$ with Mg substitution and native sulphur. The wide variety of hydrated sulphate phases, and the quite low water mineralization, reflect the composition of evaporating soil waters as well as the limited pH-Eh stability fields typical for the most of the sulphates.

Sulphates, namely, alunogene, blödite, butlerite? $Fe(SO_4)(OH)_2 \cdot 2H_2O$, copiapite, coquimbite, gypsum, hexahydrite $MgSO_4 \cdot 6H_2O$, jarosite, magnesiocopiapite $MgFe(SO_4)_6(OH)_2 \cdot 20H_2O$, pertlikite $K_2(Fe^{2+},Mg)_2Mg_4Fe^{3+}{}_2Al(SO_4)_{12} \cdot 18H_2O$, pickeringite, picromerite $K_2Mg(SO_4)_2 \cdot 6H_2O$, rhomboclase $(H_5O_2)Fe^{3+}(SO_4)_2 \cdot 2H_2O$, sideronatrite $Na_2Fe(SO_4)_2(OH) \cdot 3H_2O$, tamarugite $NaAl(SO_4)_2 \cdot 6H_2O$, thenardite, halite and native sulphur occur around Na-Cl-HCO_3 springs near Chivay. Elevated TDS (3-5 g/l) favours sulphate precipitation here. One spring discharging in the Colca riverbed is surrounded not by sulphates but abundant goethite mud. Calcite crust due to evaporation covers the surrounding rocks.

Precipitates around thermal springs near Coporaque are composed of aragonite and calcite $CaCO_3$, halite and thenardite. Low TDS (1.3 g/l) and the Na-Cl water type limits precipitation. More mineral phases precipitate around Na-Cl-HCO_3 springs with higher TDS (3-4.5 g/l) near Sibayo. Apart from recurring aragonite, calcite, halite and thenardite, these precipitates also contain trona $Na_3H[CO_3]_2 \cdot 2H_2O$, burkeite $Na_6(CO_3)(SO_4)_2$, hematite, gypsum and blödite.

Precipitates around Na-Cl-SO_4 thermal springs with elevated TDS (3.6-3.8 g/l) in Canco include aragonite, calcite, eugstenite $Na_4Ca(SO_4)_3 \cdot 2H_2O$ and halite.

Finally, calcite-only precipitates around karst springs in Huambo village reflect evaporating nearly-saturated Ca-rich hydrocarbonate waters despite the relatively low TDS (1.2 g/l).

Periodico di Mineralogia, ECMS 2015, 137-138

PERIODICO di MINERALOGIA
established in 1930

An International Journal of
MINERALOGY, CRYSTALLOGRAPHY, GEOCHEMISTRY,
ORE DEPOSITS, PETROLOGY, VOLCANOLOGY
and applied topics on *Environment*, *Archaeometry* and *Cultural Heritage*

The influence of the Fe_2O_3 content on luminescence spectra of Cr^{3+}-containing sapphires

Diep T. M. Phan[1,*], Tobias Häger[1] and Wolfgang Hofmeister[1]

[1] Johannes Gutenberg University Mainz, Institute of Geosciences,
* Corresponding author: *thphan@students.uni-mainz.de*

In this paper, we present the influence of Fe_2O_3 content on the luminescence spectra of Cr^{3+}-containing sapphire. The laser-induced photoluminescence was excited by a frequency-doubled Nd-YAG laser (532.21 nm) of a LabRam con-focal micro-Raman-system HR-800 from Horiba Jobin Yvon coupled to an Olympus-BX41 microscope. The Fe_2O_3 content was determined by Electron Probe Micro Analysis (EPMA). Most of all the samples have a basaltic origin which is often characterized by high Fe_2O_3 content. The advantage of this study is a wide variety of samples collected from many mining regions and their Fe_2O_3 content range from below detection limit (0.01 wt% Fe_2O_3 by EPMA) to approximately 2 wt% Fe_2O_3.

Figure 1 show the shift of R_1 (around 694.2 nm) and R_2 (around 692.8 nm) of the luminescence with the Fe_2O_3 content. The maximum peak position of the R-lines is shifted towards smaller wavelength if the Fe_2O_3 content of the samples increases. This result has not ever been given in any reports. This relationship is described by two equations:

$$y(R_2) = 692.86 - 0.049x \quad (1)$$

$$y(R_1) = 694.29 - 0.047x \quad (2)$$

where x is Fe_2O_3 content in wt%, y is R line peak position (in nm). The scattering of the luminescence data points can be explained by the spectral resolution of 0.01 nm, the inhomogeneity of the samples and the difference between the measured EPMA and the luminescence area.

These two equations can be used to estimate the Fe_2O_3 content in the sample with a quite good regression R^2, respectively 0.754 for R_2 and 0.748 for R_1. This can be performed quickly since luminescence spectra are sensitive even with low chromium content.

This correlation can be explained as follows. If the octahedral oxygen coordination of α-Al_2O_3 is exposed to a high pressure, it gets locally compressed. According to the equations (3) and (4) (Schawlaw, 1961; Kaplyanskii and Przhevuskii, 1962; Ostertag, 1991), the R-lines shift towards longer wavelength.

$$R_1 \text{ line: } \Delta\nu(R_1) = 7.590P - 1.5S \quad (3)$$

$$R_2 \text{ line: } \Delta\nu(R_2) = 7.615P - 0.6S \quad (4)$$

In these two equations, $\Delta\nu(R_1)$ and $\Delta\nu(R_2)$ are the respective shifts of the R_1 and R_2 lines (in nm) and P and S are the hydrostatic and non-hydrostatic components of the stress or pressure (in GPa), respectively. If the stress is purely hydrostatic (S=0), the R_1 and R_2 lines shift equally with the applied hydrostatic stress P.

Contrary to this compression, the octahedral gets expanded when the Fe_2O_3 content in the sample increases due to the large ionic radius of Fe^{3+}. Consequently, when the Fe_2O_3 content in the sample increases, the R-lines are shifted towards smaller wavelength.

This contribution can be applied to estimate the Fe_2O_3 content in sapphire or in corundum in general by two equations in (1) and (2) and distinguish sapphire from different mining regions. Besides, the influence of Fe_2O_3 to the peak positions have to be considered, if the stress in sapphire or the remnant pressure around inclusion (Wanthanachaisaeng et al., 2006; Noguchi et al., 2013) in sapphire will be determined.

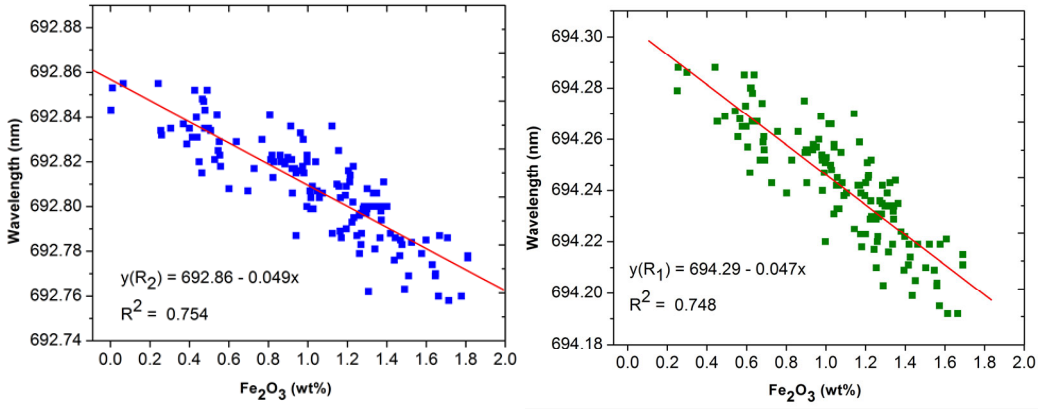

FIGURE 1:

The shifts of theR_2 (692.84 nm) and R_1 (64.28 m) lines corresponding to the Fe_2O_3 content (in wt%).

References

Kaplyanskii A.A. and Przhevuskii A.K. (1962) - The Piezospectroscopic Effect in Ruby Crystals. *Soviet Physics Doklady,* 7, 37.

Noguchi N., Abduriyim A., Shimizu I., Kamegata N., Odakea S. and Kagi H. (2013) - Imaging of internal stress around a mineral inclusion in a sapphire crystal: application of micro-Raman and photoluminescence spectroscopy. *Journal of Raman spectroscopy,* 44, 147-154.

Ostertag C.P., Robins L.H. and Cook L.P. (1991) - Cathodoluminescence measurement of strained alumina single crystals. *Journal of the European Ceramic Society,* 7, 109-116.

Schawlow A.L. (1961) - In *Advances in Quantum Electronics*, ed. J. R. Singer, Columbia University Press, New York, 50-62.

Wanthanachaisaeng B., Häger T., Hofmeister W. and Nasdala L. (2006) - Raman- und fluoreszenzspektroskopische Eigenschaften von Zirkon-Einschlüssen in chrom-haltigen Korunden aus Ilakaka und deren Veränderung durch Hitzebehandlung. *Zeitschrift der Deutschen Gemmologischen Gesellschaft,* 55, 123-136.

Periodico di Mineralogia, ECMS 2015, 139-140

PERIODICO di MINERALOGIA
established in 1930

An International Journal of
MINERALOGY, CRYSTALLOGRAPHY, GEOCHEMISTRY,
ORE DEPOSITS, PETROLOGY, VOLCANOLOGY
and applied topics on *Environment*, *Archaeometry* and *Cultural Heritage*

Expanding knowledge on crystal chemistry of uranyl sulfate minerals

Jakub Plášil[1,*]

[1] Institute of Physics, ASCR, v.v.i., Na Slovance 2, 182 21 Praha 8, Czech Republic
* Corresponding author: *plasil@fzu.cz*

Uranyl sulfate minerals are typical and abundant products formed during hydration–oxidation weathering of primary uranium minerals, such as uraninite, under the low pH conditions, resulting from the decomposition of associated sulfide minerals. Understanding of the crystal structures of these minerals help us to improve our ideas about mineral stabilities and their constraints. A great help in the understanding of these complex mineral structures and the stereochemical behavior of the weakly bonded constituents and their important role in these structures, provides us a so called "bond-valence approach" (Hawthorne and Schindler, 2008), standing on the fundamental of the bond-valence theory (Hawthorne, 2012).

In solid-state uranium(VI) forms two triple axial bonds to oxygen atoms, resulting in an uranyl ion, $(UO_2)^{2+}$, which is, in turn, usually coordinated in the equatorial plane (with respect to the axial bonds) by four, five or six ligands (O^{2-}, OH^- or H_2O), leading to square, pentagonal, or hexagonal bipyramidal coordination, respectively. The geometrical characteristics for these coordinations have been reviewed in detail by Burns et al. (1997) and Burns (2005). The strong directional anisotropy of the bond distribution observed in these coordinations favors formation of the lower-dimensional structures of U-oxide bonds (prevalence of 2D layers, less also 1D chains). Uranyl sulfates adopt mostly sheet topologies, where U-coordination polyhedra polymerize *via* sharing their edges and corners and such larger units are then linked through the SO_4 tetrahedra, occupying triangles or squares of the corresponding topology. Cluster and chain topologies were considered as to be seldom and not preferable due to crystal-chemical reasons.

During last five years a substantial number (~20) of the new uranyl sulfates minerals has been discovered. Among them several contain already known structure topologies, as e.g., zippeite topology (Plášil et al. 2011a), or phosphuranylite topology (Kampf et al., 2015). However, majority of the new minerals contains particularly interesting structural units – clusters and chains. Uranyl sulfate clusters have been observed yet in case of the synthetic Na^+-uranyl sulfates hydrates; however, they differ in the way of linking of SO_4 groups and UO_7 polyhedra. In case of synthetic compounds there is a bidentate linkage (Burns, 2005), while in case of minerals a monodentate linkage has been observed so far (Plášil et al., 2014).

The occurrence of particular structures and topologies of uranyl sulfates is primarily driven by the variation of the U:S ratio within the structural units (*su*). Even more, it is not only the U and S ratio; however, also the concentrations of particular metal cations and H_2O. The molecular H_2O plays an important role in the structures of oxysalts as the bond-valence transporter or transformer (Hawthorne and Schindler, 2008), or as depolymerizing agent. Upon constraints represented by paragenetical relations, observed at localities, and with the knowledge of crystal structures, the following conclusions can be drawn: 1) Minerals without any additional metal cation, with a high U:S ratio and a high H_2O content, are the very first minerals formed from initial weathering of uraninite. E.g., mineral uranopilite, $[(UO_2)_6(SO_4)O_2(OH)_6(H_2O)_6](H_2O)_8$. 2) Minerals containing M^+, M^{2+} or M^{3+} cations with the U:S ratio equal to 2:1, i.e. minerals of the zippeite-group, form *a)* more distant from the source of U, *b)* usually in the presence of both sulfides and carbonates in the gangue, *c)* hydrolysis of early formed alteration products, as e.g., uranopilite, usually takes place during formation of the zippeite-group minerals. 3) Minerals with U:S ratios equal to 1:1 or lower, with the low H_2O content. They have chain *su*, structures contain large alkali or alkaline earths cations (as K, Na); evaporation, or precipitation from oversaturated solution takes place during their formation. 4) Minerals with high content of S compared to U, low H_2O content, and high alkali- and alkaline earths contents, adopt structures with cluster units. Evaporation from highly saturated S-rich solutions probably also takes place there.

To conclude generally, the increasing molecular H_2O content within the *su* causes depolymerization from 2D→1D units; while increasing SO_4 content causes lowering of dimensionality from chains to cluster units. The novel topologies, which were not observed for minerals in past, document that the dimensionality and a topology in particular are driven by conditions and the composition of fluids from which these minerals crystallized.

References

Burns P.C. (2005) - U^{6+} minerals and inorganic compounds: insights into an expanded structural hierarchy of crystal structures. *Canadian Mineralogist*, 43, 1839-1894.

Burns P.C., Ewing R.C. and Hawthorne F.C. (1997) - The crystal chemistry of hexavalent uranium: polyhedron geometries, bond-valence parameters, and polymerization of polyhedra. *Canadian Mineralogist*, 35, 1551-1570.

Hawthorne F.C. (2012) - A bond-topological approach to theoretical mineralogy: crystal structure, chemical composition and chemical reactions. *Physics and Chemistry of Minerals*, 39, 841-874.

Hawthorne F.C. and Schindler M. (2008) – Understanding the weakly bonded constituents in oxysalt minerals. *Zeitschrift für Kristallographie*, 223, 41-68.

Kampf A.R., Plášil J., Kasatkin A.V. and Marty J. (2014) - Belakovskiite, $Na_7(UO_2)(SO_4)_4(SO_3OH)(H_2O)_3$, a new uranyl sulfate mineral from the Blue Lizard mine, San Juan County, Utah, USA. *Mineralogical Magazine*, 78, 639-649.

Plášil J., Dušek M., Novák M., Čejka J., Císařová I. and Škoda R. (2011a) - Sejkoraite-(Y), a new member of the zippeite group containing trivalent cations from Jáchymov (St. Joachimsthal), Czech Republic: description and crystal structure refinement. *American Mineralogist*, 96, 983-991.

Plášil J., Kampf A.R., Kasatkin A.V. and Marty J. (2014) - Bluelizardite, $Na_7(UO_2)(SO_4)_4Cl(H_2O)$, a new uranyl sulfate mineral from the Blue Lizard mine, San Juan County, Utah, USA. *Journal of Geosciences*, 59, 145-158.

Periodico di Mineralogia, ECMS 2015, 141-142

PERIODICO di MINERALOGIA
established in 1930

An International Journal of
MINERALOGY, CRYSTALLOGRAPHY, GEOCHEMISTRY,
ORE DEPOSITS, PETROLOGY, VOLCANOLOGY
and applied topics on *Environment*, *Archaeometry* and *Cultural Heritage*

^{23}Na nuclear magnetic resonance (NMR) spectroscopic study of loparite-(Ce)

Elena A. Popova[1,2,*], Boštjan Zalar[3] , Sergey G. Lushnikov[1] and Sergey V. Krivovichev[2]

[1] Ioffe Physical Technical Institute RAS, 194021 Saint Petersburg, Russia
[2] Saint Petersburg State University, Department of Crystallography, Saint Petersburg, Russia
[3] J. Stefan Institute, Jamova 39, 1000 Ljubljana, Slovenia
* Corresponding author: *elena.popova566@gmail.com*

Loparite-(Ce) – (Ce,Ca,Na,M)(Ti,Nb)O_3 (where M = Sr,REE,Th ..), a natural mineral of the perovskite group – is a subject of interest in geosciences as well as in condensed matter physics. It is well-known that, in the lower mantle, perovskite-type compounds dominate over other minerals. In view of non-trivial dependence of the lattice dynamics on both chemical composition and charge disordering, present in synthetic complex perovskites with A or B disorder, the coexistent A and B site disorder in loparite is thought to also result in an intricate physical behavior. Dielectric measurements and Raman spectroscopic experiments (Popova et al., 2014, 2015) have revealed a number of anomalies in the low-temperature lattice dynamics of loparite-(Ce). Analysis of the experimental data indicated that a ferroelectric phase transition occurs in the vicinity of 157 K, which was observed for the first time in natural perovskites. Thus, loparite-(Ce) is an interesting object to study the effect of chemical disorder upon phase transitions and lattice dynamics.

This report presents results of the ^{23}Na NMR study of single crystals of loparite from the Khibiny alkaline massif, Kola Peninsula (Marchenko peak) in the low-temperature range. To check the degree of local structural disorder, we have performed the ^{23}Na ($I = 3/2$) quadrupole-perturbed nuclear magnetic resonance study in the temperature range from 80 to 300 K at the Larmor frequency of 100.525 MHz ($B_0 = 9$ T). In a disordered perovskite system, the ^{23}Na spectrum is expected to consist of a broadened central (-1/2 → 1/2) transition line, superimposed on the broad, featureless satellite (-3/2 → -1/2, 1/2 → 3/2) background. The inhomogeneous broadening of both components originates from the broken cubic symmetry, resulting in the nonzero value of electric field gradient at the Na site, as demonstrated recently for $Na_{0.5}Bi_{0.5}TiO_3$ (Aleksandrova et al. 2006). The ^{23}Na spectra of loparite (Fig. 1) are consistent with the above scenario. However, in contrast to $Na_{0.5}Bi_{0.5}O_3$, angular dependence of the central transition line shape is barely detectable on rotating the single crystal sample about the 110-axis perpendicular to B_0. This demonstrates that sodium nuclei in loparite experience an effectively spherical (isotropic) environment as far as the disorder of the electric field gradient

(EFG) is concerned. This reveals that, in the case of loparite, we deal with an even stronger disorder than in synthetic perovskites, where the effective EFG environment is typically cubic.

The analysis of the temperature dependence of the ^{23}Na spin-lattice (T_1) magnetization relaxation profiles reveals the existence of two relaxation mechanisms, with their respective characteristic times exhibiting non-monotonous behavior at temperatures matching the temperatures of the anomalies detected in the dielectric and Raman spectroscopy.

The investigation was partly supported by Russian Science Foundation No. 14-12-00257.

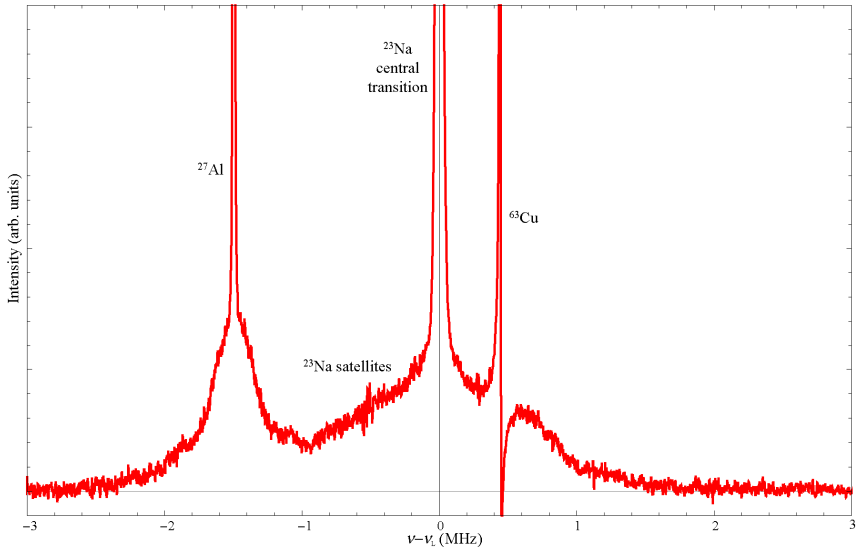

Fig. 1: ^{23}Na spectrum of loparite at T = 170 K, acquired via point-by-point frequency scan in the range from 97.525 MHz to 103.525 Mhz with a frequency step of 100 kHz.

References

Aleksandrova I.P., Ivanov Yu.N., Sukhovskiĭ A.A. and Vakhrushev S.B. (2006) - ^{23}Na NMR in the Relaxor Ferroelectric $Na_{1/2}Bi_{1/2}TiO_3$. *Physics of the Solid State*, 48, 1120-1123.

Popova E.A., Zalessky V.G., Yakovenchuk V.N., Krivovichev S.V. and Lushnikov S.G. (2014) - Loparite-(Ce), a natural ferroelectric with the perovskite-type structure. *Applied Physics Letters*, 105, 8, 082905.

Popova E.A., Yakovenchuk V.N., Lushnikov S.G. and Krivovichev S.V. (2015) - Structural phase transitions in loparite-(Ce): evidences from Raman light scattering. *Journal of Raman Spectroscopy*. 46, 1, 161-166.

Periodico di Mineralogia, ECMS 2015, 143-144

PERIODICO di MINERALOGIA
established in 1930

An International Journal of
MINERALOGY, CRYSTALLOGRAPHY, GEOCHEMISTRY,
ORE DEPOSITS, PETROLOGY, VOLCANOLOGY
and applied topics on *Environment*, *Archaeometry* and *Cultural Heritage*

Spectroscopic and diffractometric study of dye molecules confined in zeolite L channels: towards an effective transport of electronic excitation energy

Simona Quartieri[1*], Lara Gigli[2], Rossella Arletti[2], Jenny G. Vitillo[3], Gianmario Martra[4], Gabriele Alberto[4], GloriaTabacchi[3], Ettore Fois[3] and Giovanna Vezzalini[5]

1 Dipartimento di Fisica e Scienze della Terra, Università degli Studi di Messina, Viale Ferdinando Stagno d'Alcontres 31, 98166-Messina S.Agata, Italy
2 Dipartimento di Scienze della Terra, Università degli Studi di Torino, Via Valperga Caluso 35, 10125-Torino, Italy
3 Dipartimento di Scienza ed Alta Tecnologia, Università degli Studi dell'Insubria, Via Lucini 3, 22100-Como, Italy
4 Dipartimento di Chimica, Università degli Studi di Torino, Via Pietro Giuria 7, 10125-Torino, Italy
5 Dipartimento di Scienze Chimiche e Geologiche, Università degli Studi di Modena e Reggio Emilia, Via Giuseppe Campi 103, 41125-Modena, Italy
*Corresponding author: *squartieri@unime.it*

Photo-harvesting is one of the most promising approach to efficiently use solar light in many applications, going from sensing in analytical chemistry, medical applications, nano-diagnostics, luminescent solar concentrators, or processing and storage of information (Calzaferri et al., 2011; Gust et al., 2001; Li et al., 2011). Mimicking the chlorophyll molecules in leaves, in artificial photonic antennae the absorption and transport of photons to the reaction centers (Forster Resonant Energy Transfer-FRET) is possible using suitable dye molecules. It is crucial to avoid the formation of dye aggregates, since these responsible for quenching effects that can lower harvester efficiency. In artificial systems, aggregation is prevented by introducing the dye molecules into crystalline 1-D pores nanoscaffolds, such us zeolite L (ZL). It has been shown (Calzaferri et al., 2008; Fois et al., 2013) that the optical properties of the dye-ZL systems depend on loading, shape and size of the dyes - which affects the molecular packing inside the channels - and on the extraframework content (e.g. cations, H_2O molecules) controlling the intermolecular and the dyes/framework interactions.

In this study, we compare the optical properties of two different systems: *i)* a one-dye/ZL composite in hydrated and dehydrated form (tb-DXP/ZL) and *ii)* a two–dyes antenna system in which fluorenone (FL, donor molecules) and thionine (Th, acceptor molecule) are organized in zeolite L porosities.

For the first system, the ATR-IR spectra showed that the shift of the bands related to the

dye in its hydrated form is significantly higher than that in the dehydrated one, a clear indication that the water molecules present in the channels strongly affect the molecular structure of the dye and its interactions with the hosting framework. This fact was also evidenced by the blue shift of the diffuse reflectance UV-Vis spectrum, resulting from water removal.

Very interesting are the results obtained for the two–dyes antenna system (FL/Th) where the ZL channels were completed filled with FL, reaching for the first time the maximum loading equal to 1.5 molecules per unit cell. The FL distribution in these conditions can be considered as a self-assembly of planar dye molecules into a non-covalent nano-ladder, where the co-present water molecules do not play any rule, contrary to what seen for the tb-BDX dye.

The continuous nanostructure of FL molecules does not exhibit significant electronic interactions. Indeed, both absorption (recorded in the diffuse reflectance mode) and photoemission electronic spectra do not show significant changes of the spectral profiles. Noticeably, the combination and steady state and time resolved photoluminescence data indicated that − at the maximum loading − ca. 90% of FL molecules are photoluminescent, with a significant increase in the average quantum yield with respect to FL molecules in solution.

We are currently investigating the occurrence of energy transfer (FRET) from the excited FL molecules forming the non-covalent nano-ladder in the ZL channels and the Th molecules in the ground state, deposited on the external surface of the ZL particles at different concentrations.

Concerning the optical properties of our composites, we demonstrate that the co-presence of water molecules − mediating the interactions between the tb-DXP dye and the framework − effectively influence the absorption properties of the composite. On the contrary, in the antenna system no evidence of Davydov splitting emerged from our study, indicating that one of the main competitors of the FRET mechanism is not operative notwithstanding the close packed arrangement of FL. We believe that this feature is of overwhelming relevance in view of the application of such a system as artificial antenna.

References

Calzaferri G. and Lutkouskaya K. (2008) - Mimicking the antenna system of green plants. *Photochemical & Photobiological Sciences*, 7, 879 – 910.

Calzaferri G., Méallet-Renault R., Brühwiler D., Pansu R., Dolamic I., Dienel T., Adler P., Li H., Kunzmann A. (2011) - D*esigning dye-nanochannel antenna hybrid* materials for light harvesting, transport and trapping. *ChemPhysChem*, 12, 580−594.

Fois E., Tabacchi G., Devaux A., Belser P., Brühwiler D., Calzaferri G. (2013) - Host-Guest Interactions and Orientation of Dyes in the One-Dimensional Channels of Zeolite L. *Langmuir*, 29, 9188−9198.

Gust D., Moore T. A., Moore A. L. (2001) - Mimicking photosynthetic solar energy transduction. *Accounts of Chemical Research*, 34, 40-48.

Li Z., Luppi G., Geiger A., Josel H.-P., De Cola L. (2011) - Bioconjugated fluorescent zeolite L nanocrystals as novel labels in protein microarray. *Small*, 7, 3193−3201.

Periodico di Mineralogia, ECMS 2015, 145-146

PERIODICO di MINERALOGIA
established in 1930

An International Journal of
MINERALOGY, CRYSTALLOGRAPHY, GEOCHEMISTRY, ORE DEPOSITS, PETROLOGY, VOLCANOLOGY
and applied topics on *Environment*, *Archaeometry* and *Cultural Heritage*

Crystal chemistry and optical spectroscopy of Co_3TeO_6 and $(Co,Zn)_3TeO_6$ solid solutions

Dominik Reichartzeder[1], Matthias Weil[2] and Manfred Wildner[1,*]

[1] Department of Mineralogy and Crystallography, University of Vienna, Althanstr. 14, A-1090 Vienna, Austria
[2] Institute for Chemical Technologies and Analytics, Division of Structural Chemistry, Vienna University of Technology, Getreidemarkt 9/164-SC, A-1060 Vienna, Austria
* Corresponding author: *manfred.wildner@univie.ac.at*

Single crystals along the $(Co,Zn)_3TeO_6$ solid solution series (including the previously described endmembers; Becker et al., 2006; Weil, 2006) were synthesized by chemical transport reactions and investigated from single crystal and powder X-ray diffraction data as well as by polarized optical absorption and diffuse reflectance spectroscopy.

Me_3TeO_6 solid solutions ($Me_3 = Co_xZn_{3-x}$, monoclinic, $C2/c$, $V_{Co/Zn}$ = 1359.3/1346.1 Å^3, Z = 12) crystallize in the cryolite-related β-Li_3VF_6 type, and are composed of two types of fairly regular TeO_6 octahedra and five types of moderately (*Me*2,5) to extremely strongly (*Me*1,3,4) distorted MeO_z polyhedra. According to the very similar ionic radii of Co^{2+} and Zn^{2+}, lattice parameters stay within narrow ranges, whereas MeO_z polyhedral shapes change in part dramatically, as shown in Figure 1a for the *Me*–O distances. *Me*2 and *Me*5 have clear tetrahedral [4]- and octahedral [6]-coordination, respectively; from Co to Zn their mean <*Me*–O> bonds change slightly but just opposite to expectations from Shannon's (albeit very similar respective) coordination-dependent ionic radii. For *Me*1 a classification of the coordination as [4+2] for Co and [4] or [4+3] for Zn is appropriate, for *Me*3 perhaps [4+2] for Co and [4] for Zn, and for *Me*4 a [5]-coordination in both cases. It should be mentioned that for sixfold coordination Co1 and Co3 exceed previously summarized maximum distortion data for Co^{2+} (Wildner, 1992), Co1 concerning angular and Co3 the bond length distortion. Figure 1b shows clear preferences of the cation distribution on the 'well-behaved' *Me*2 and *Me*5 sites: Co prefers the octahedral *Me*5 and Zn the tetrahedral *Me*2 site; besides, there is also a minor preference of Co on *Me*1.

Optical spectra of Me_3TeO_6 samples are shown in Figures. 2a and b. According to the Laporte selection rule, the extremely strong absorption of Co-rich mixed crystals should be dominated by the tetrahedral *Me*2 site with maxima around 4050 [$^4T_2(F) \equiv 10Dq$], 6000 and 7000 [$^4T_1(F)$], 16700 and 18450 [$^4T_1(P)$] cm^{-1}. With preferred depletion of *Me*2 at lower Co_x (the breakdown of absorption between $Co_{0.30}$ and $Co_{0.15}$ in Figure 2b may indicate complete

depletion), superposition of absorptions by strongly distorted [5]- and [6]-coordinated sites severely complicates the detailed assignment of band components to electronic levels of specific sites, and, as a consequence, also hampers attempts for meaningful semiempirical crystal field calculations.

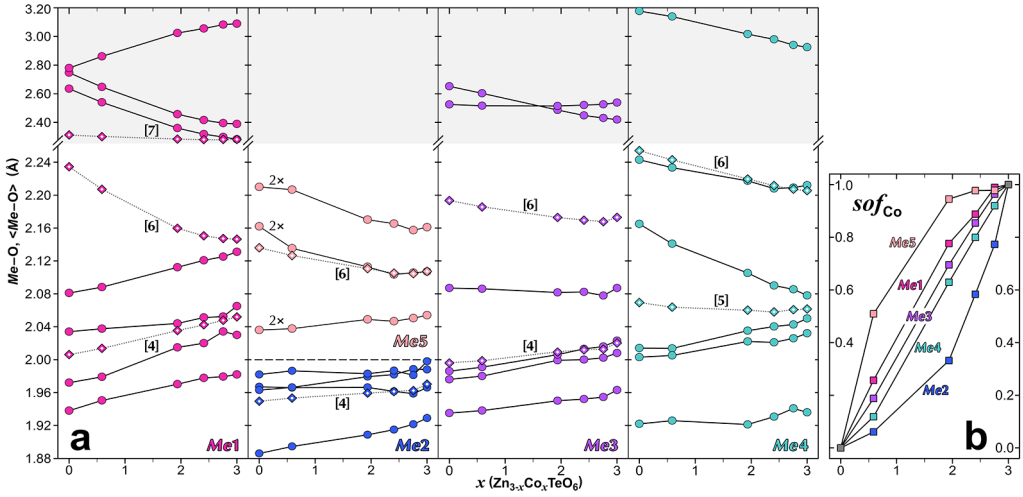

Fig. 1 – Crystal chemistry of $(Co,Zn)_3TeO_6$ solid solutions; (a) variation of *Me*–O distances; dotted lines/symbols denote mean values; note the compressed scale for long distances; (b) *Me* site occupancy factors.

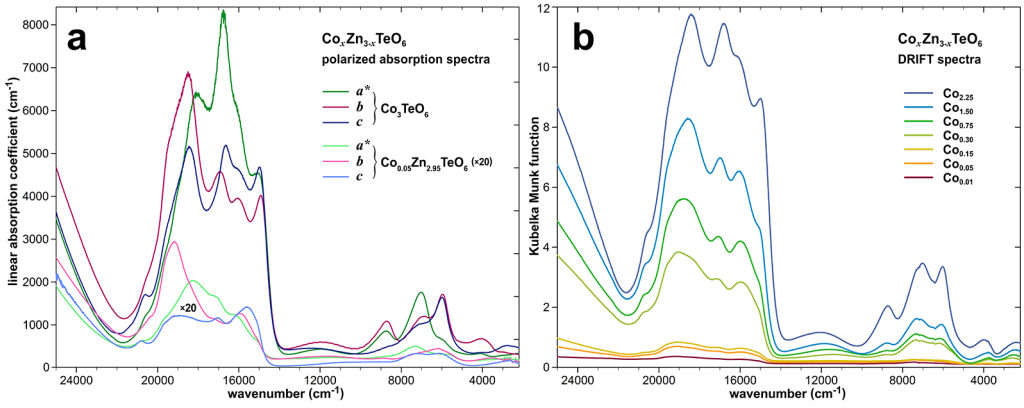

Fig. 2 – Optical spectra of $(Co,Zn)_3TeO_6$ solid solutions; (a) polarized absorption spectra of Co_3TeO_6 and $Co_{0.05}Zn_{2.95}TeO_6$ (enhanced by a factor of 20); (b) diffuse reflectance spectra for $Co_{0.01\text{-}2.25}$ solid solutions.

References

Becker R., Johnsson M., Berger H. (2006) – A new synthetic cobalt tellurate: Co_3TeO_6. *Acta Crystallographica*, C62, i67-i69.

Weil M. (2006) – Zn_3TeO_6. *Acta Crystallographica*, E62, i246-i247.

Wildner M. (1992) – On the geometry of $Co(II)O_6$ polyhedra in inorganic compounds. *Zeitschrift für Kristallographie*, 202, 51-70.

Periodico di Mineralogia, ECMS 2015, 147-148

PERIODICO di MINERALOGIA
established in 1930

An International Journal of
MINERALOGY, CRYSTALLOGRAPHY, GEOCHEMISTRY,
ORE DEPOSITS, PETROLOGY, VOLCANOLOGY
and applied topics on *Environment*, *Archaeometry* and *Cultural Heritage*

Analysis of luminescent calcite by laser-induced breakdown spectroscopy

Sari Romppanen[1,*], Saara Kaski[1] and Heikki Häkkänen[2]

[1] University of Jyväskylä, Department of Chemistry P.O.BOX 35 FI-40014 University of Jyväskylä
[2] University of Jyväskylä, Department of Biological and Environmental Science P.O.BOX 35 FI-40014 University of Jyväskylä
* Corresponding author: *sari.m.romppanen@jyu.fi*

When the luminescence of mineral samples is observed under ultraviolet light excitation, mainly it is an indication of presence of an activator element (*e.g.* manganese in the divalent state). Mn^{2+} ion can substitute Ca^{2+} ion in the structure of calcite ($CaCO_3$) and for example wide red luminescence band around 620 nm can be recognized (Gaft et al., 2005).

Laser-induced breakdown spectroscopy (LIBS) is a useful atomic emission spectroscopic method to analyze materials and their distributions on surfaces. In a LIBS technique, a high power laser pulse is focused on to a sample to create plasma. Emission from atoms and ions in plasma is collected via fiber optics and analyzed by using a spectrograph and a gated CCD-detector for time delayed detection. High resolution ($\lambda/\Delta\lambda = 7500$) emission spectra from 300–850 nm from a few laser pulses can be recorded in a fraction of a second allowing the very reliable qualitative identification of material. Previously, we have analyzed paper coatings, where LIBS has revealed the distribution of coating pigment (*e.g.* calcium carbonate) and fast fluorescence signal of the organic constituents, respectively (Häkkänen and Korppi-Tommola, 1993).

In our recent studies, high-resolution laser-induced breakdown spectroscopy (LIBS) has applied to an identification of possible activator elements in luminescent minerals. Elemental distributions of the mineral samples have been mapped with LIBS and compared with the corresponding luminescence determined with the time-resolved laser-induced fluorescence (LIF). For example manganese can be recognized in LIF spectra and analogous LIBS spectra (Figure 1). Also spatial Mn distribution is investigated and other possible activator elements from LIBS and LIF spectra are determined.

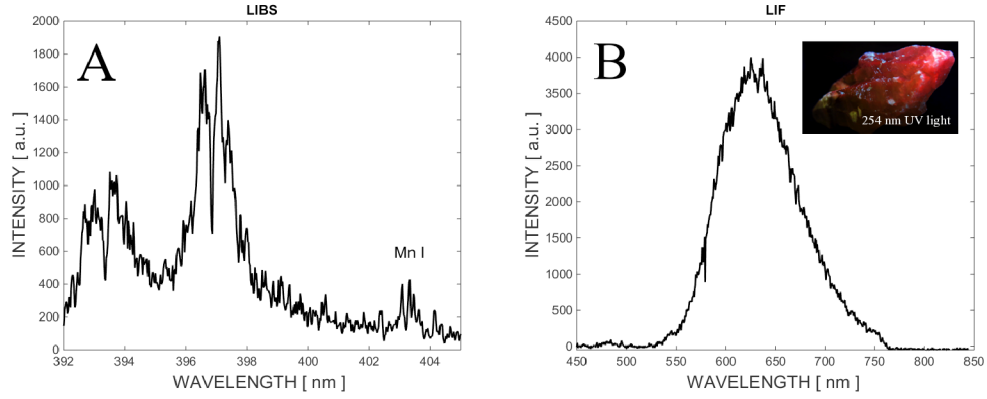

Figure 1. Manganese discovered in LIBS spectrum (A) and corresponding LIF spectrum from the calcite sample, which shows strong red luminescence under 254 nm UV-light (B).

References

Gaft M., Reisfeld R. and Panczer G. (2005) - Luminescence Spectroscopy of Minerals and Materials, Springer.

Häkkänen H.J. and Korppi-Tommola J.E.I. (1993) - Laser-Induced Fluorescence Imaging of Paper. *Applied Spectroscopy* 47, 2122-2125.

Periodico di Mineralogia, ECMS 2015, 149-150

PERIODICO di MINERALOGIA
established in 1930

An International Journal of
MINERALOGY, CRYSTALLOGRAPHY, GEOCHEMISTRY,
ORE DEPOSITS, PETROLOGY, VOLCANOLOGY
and applied topics on *Environment*, *Archaeometry* and *Cultural Heritage*

Ti-rich garnets: an EPMA, SIMS, Mössbauer, XRPD and SCXRD investigation

Emanuela Schingaro[1], Maria Lacalamita[1,*], Ernesto Mesto[1], Gennaro Ventruti[1], Giuseppe Pedrazzi[2], Luisa Ottolini[3] and Fernando Scordari[1]

[1]Università degli Studi di Bari "Aldo Moro", Dipartimento di Scienze della Terra e Geoambientali, via E. Orabona 4, I-70125, Bari, Italy
[2]Università di Parma, Dipartimento di Neuroscienze, via Volturno 39, I-43100, Parma, Italy
[3]CNR-Istituto di Geoscienze e Georisorse, Unità di Pavia, via A. Ferrata 1, I-27100 Pavia, Italy
*Corresponding author: *maria.lacalamita@uniba.it*

A suite of Ti-bearing garnets from magmatic, metamorphic and carbonatitic rocks was studied by Electron Probe Microanalysis (EPMA), X-ray Powder Diffraction (XRPD), Single Crystal X-ray Diffraction (SCXRD), Mössbauer spectroscopy and Secondary Ion Mass Spectrometry (SIMS) in order to fully define their crystal chemistry. The studied garnets show TiO_2 varying in the ranges 4.9(1) - 17.1(2) wt% and variable $Fe^{3+}/\Sigma Fe$ content. SIMS analyses allowed quantification of light elements yielding H_2O in the range 0.091(7)-0.46(4), F in the range 0.004(1) - 0.040(4) and Li_2O in the range 0.0038(2) - 0.014(2) wt%. Mössbauer analysis provided spectra with different complexity, which could be fitted to a number of components variable from one ($^{Y}Fe^{3+}$) to four ($^{Y}Fe^{2+}$, $^{Z}Fe^{2+}$, $^{Y}Fe^{3+}$, $^{Z}Fe^{3+}$). A good correlation was found between the $Fe^{3+}/\Sigma Fe$ resulting from the Mössbauer analysis and that derived from the Flank method (Höfer and Brey, 2007).

X-ray powder analysis revealed that the studied samples are a mixture of different garnet phases with very close cubic unit-cell parameters as recently found by other authors (Antao, 2013). Single crystal X-ray refinements using anisotropic displacement parameters were performed in the $Ia\bar{3}d$ space group and converged to R_1 in the range 1.63 - 2.06 % and wR_2 in the range 1.44 - 2.21 %. Unit cell parameters vary between 12.0641(1) and 12.1447(1) Å, reflecting different Ti contents and extent of substitutions at the tetrahedrally coordinated site.

The main substitution mechanisms affecting the studied garnets are: $^{Y}R^{4+} + {}^{Z}R^{3+} \leftrightarrow {}^{Z}Si + {}^{Y}R^{3+}$ (schorlomite substitution); $^{Y}R^{2+} + {}^{Z}R^{4+} \leftrightarrow 2\,{}^{Y}R^{3+}$ (morimotoite substitution); $^{Y}R^{3+} \leftrightarrow {}^{Y}Fe^{3+}$ (andradite substitution); in the above substitutions $^{Y}R^{2+} = Fe^{2+}, Mg^{2+}, Mn^{2+}$; $^{Z}R^{4+} = Ti$; $^{Y}R^{3+} = Fe^{3+}, Al^{3+}, Cr^{3+}$; $^{Z}R^{3+} = Fe^{3+}, Al^{3+}$. Minor substitutions, such as $2\,{}^{Y}Ti^{4+} + {}^{Z}Fe^{2+} \leftrightarrow 2\,{}^{Y}Fe^{3+} + {}^{Z}Si$,

$(SiO_4)^{4-} \leftrightarrow (O_4H_4)^{4-}$, $F^- \leftrightarrow OH^-$ and $^{Y}R^{4+} + {}^{X}R^{+} \leftrightarrow {}^{Y}R^{3+} + {}^{X}Ca^{2+}$, with $^{Y}R^{4+}$ = Ti, Zr; $^{Y}R^{3+} = Fe^{3+}$, Al, Cr^{3+}; $^{X}R^{+}$ = Na, Li also occur.

The garnet crystal chemistry and implications in terms of nomenclature and classification (Grew et al., 2013) are discussed.

References

Antao, S.M. (2013) - The mystery of birefringent garnet: is the symmetry lower than cubic? *Powder Diffraction*, 28, 281-287.

Grew E.S., Locock A.J., Mills S.J., Galuskina I.O., Galuskina E.V. and Hålenius U. (2013) - Nomenclature of the Garnet Supergroup. *American Mineralogist*, 98, 785-811.

Höfer H.E. and Brey G.P. (2007) - The iron oxidation state of garnet by electron microprobe: Its determination with the flank method combined with major-element analysis. *American Mineralogist*, 92, 873-885.

Periodico di Mineralogia, ECMS 2015, 151-152

PERIODICO di MINERALOGIA
established in 1930

An International Journal of
MINERALOGY, CRYSTALLOGRAPHY, GEOCHEMISTRY,
ORE DEPOSITS, PETROLOGY, VOLCANOLOGY
and applied topics on *Environment*, *Archaeometry* and *Cultural Heritage*

EPR study of quartz from the Peschanka porphyry Cu–Au–Mo deposit, Russia

Anastasiia D. Semina*, Lubov I. Marushchenko, Dmitry G. Koshchug, Ivan A. Baksheev and Sergey V. Vyatkin

Faculty of Geology, Moscow State University, Leninskiye Gory 1, Moscow, 119991, Russia
* Corresponding author: *nasemina@gmail.com*

Types of paramagnetic centers and trace elements concentration in 35 samples of the porphyry-stage quartz from the Peschanka deposit were studied by EPR and compared with the EPR data for quartz from other porphyry deposits, hydrothermal quartzites (advance argillic ateration), and greisens.

The giant alkali-related porphyry Cu–Au–Mo deposit Peschanka occurred in the Baimka trend located in the western Chukchi Peninsula, Russia and hosted in quarts porphyry monzodiorite of the Early Cretaceous Egdigkich pluton. Four types of altered rocks were identified at the deposit: potassic, propylite, phyllic and argillic. Potassic rock forming internal zone of metasomatic aureole is predominant. Propylite forming outer zone of hydrothermal alteration replaces intrusive, volcanic, and volcanic–sedimentary rocks. Phyllic alteration cuts potassic zone. The major ore minerals are bornite, chalcopyrite, pyrite (Chitalin et al., 2013).

$[AlO_4^-/h^+]^0$, $[TiO_4/Li^+]^0$, $[TiO_4/H^+]^0$, $[GeO_4^-/Li^+]^0$ paramagnetic centres in quartz from Peschanka, intermediate sulfidation (IS) prospect Pryamoy, Russia, from hydrothermal quartzite at the Semizbugu corundum, and Zhanet and Ush-Shoky Au epithermal deposits in Kazakhstan, and from greisen of the Severny granitic pluton, Russia, were detected and measured with EPR. Concentration of $[AlO_4^-/h^+]^0$-centres in the Peschanka quartz ranging from 29 to 185 ppm is close to that in the porphyry-stage quartz of the Malmyzh deposit, (32–115 ppm), IS epithermal quartz from the Pryamoy prospect (47-196), and quartz from hydrothermal quartzite (advance argillic alteration) of the Semizbugu, Ush-Shoky and Zhanet deposits (60–140). Concentration of $[AlO_4^-/h^+]^0$-centres (130-297 ppm) in greisen quartz from Severny is higher. Thus, greisen quartz is distinguished by the highest $[AlO_4^-/h^+]^0$-centre concentration.

Only $[TiO_4/Li^+]^0$ and $[TiO_4/H^+]^0$ centers were determined from the Peschanka quartz studied here. Concentration of $[TiO_4/Li^+]^0$ varies from 0.5 to 27 ppm (average 4 ppm); the $[TiO_4/H^+]^0$ content ranges from 0.3 to 6.3 ppm (average 2 ppm). Quartz from the Peschanka is characterized by uncommon high $[TiO_4/H^+]^0/[TiO_4/Li^+]^0$ value reaching 0.94. At the Malmyzh

deposit, the $[TiO_4/Li^+]^0$ and $[TiO_4/H^+]^0$ average concentrations are 3.9 and 1 ppm, respectively with the $[TiO_4/H^+]^0/[TiO_4/Li^+]^0$ value of 0.4. The average contents of $[TiO_4/H^+]^0$ and $[TiO_4/Li^+]^0$ centres in epithermal quartz from Pryamoy are 0.53 and 4.91 ppm, respectively; the $[TiO_4/H^+]^0/[TiO_4/Li^+]^0$ mean value of 0.1 is substantially lower than that in porphyry quartz. The $[TiO_4/M^+]^0$ centres were detected only in one sample of hydrothermal quartzite from Semizbugu; the $[TiO_4/H^+]^0/[TiO_4/Li^+]^0$ value is 0.1. The average $[TiO_4/H^+]^0$ and $[TiO_4/Li^+]^0$ contents in the Severny greisen quartz are 0.31 and 3.21 ppm, respectively; the $[TiO_4/H^+]^0/[TiO_4/Li^+]^0$ average value of 0.1 is substantially lower than that in porphyry quartz. Thus, the high $[TiO_4/H^+]^0/[TiO_4/Li^+]^0$ value (> 0.2) is typical of quartz from porphyry deposits

The $[GeO_4/H^+]^0$ center is caused by acidic mineral forming fluid (Balitsky et al., 1969). The similar fluid is responsible for the formation of the $[AlO_4^-/H^+]^0$ center. The $[TiO_4/H^+]^0$ centers are resulted from the loss under irradiation of electron and charge compensating by $[AlO_4^-/M^+]^0$-precursor and diffusion of both to Ti impurity.All studied quartz is formed from acidic fluids, but leading acid in the fluids is different: $HCl+H_2S$ in porphyry deposits (Migdisov et al., 2014), H_2SO_4 for hydrothermal quartzite (Rye et al., 1992), and HCl+HF for greisen (Korzhinsky, 1982). Taking into account that porphyry and greisen quartz have high concentration of $[TiO_4/H^+]^0$ center, we suspect that HCl provides incorporation of Ti into quartz. However, greisen solutions enriched in HF transport significant amount of Li that provides incorporation of elevated Al in quartz to form $[AlO_4^-/Li^+]^0$ center and $[TiO_4/Li^+]^0$. The high $[TiO_4/Li^+]^0$ content causes low $[TiO_4/H^+]^0$ $[TiO_4/Li^+]^0$ value in greisen quartz. H_2SO_4 fluids responsible for the formation of hydrothermal quartzite are not favorable to incorporation of Ti into quartz. Thus, the high $[TiO_4/H^+]^0/[TiO_4/Li^+]^0$ value is typical of quartz from porphyry deposits; high concentration of Ti in quartz indicates HCl-bearing mineral forming fluids.

This study has been supported by the Russian Foundation for Basic Research (project no. 14-05-31198).

References

Balitsky V.S. Samo'lovich M.I., Tsinoberg L.I. (1969) - Some features of the germanium substitution in crystals of quartz. *Geochemistry*, 4, 421–424.

Chitalin A.F., Usenko, V.V., Fomichev, E.V. (2013) - The Baimka ore zone – a cluster of large base and precious metal deposits in the western Chukotka AD, *Mineral Resources of Russia. Economics and Managment*, 6, 68–73.

Korzhinsky D.S. (1982) - The theory of metasomatic zoning. Moscow: Nauka, 104 pp.

Migdisov A. A., Bychkov A.Yu., Williams-Jones A.E., Van Hinsberg V.J. (2014) - A predictive model for the transport of copper by HCl-bearing water vapour in ore-forming magmatic-hydrothermal systems: Implications for copper porphyry ore formation, *Geochimica et Cosmochimica Acta*, 129, 33–53.

Rye R.O., Bethke P.M., Wasserman M.D. (1992) - The stable isotope geochemistry of acid sulfate alteration. *Economic Geology*, 87, 2, 225–262.

Periodico di Mineralogia, ECMS 2015, 153-154

PERIODICO di MINERALOGIA
established in 1930

An International Journal of
MINERALOGY, CRYSTALLOGRAPHY, GEOCHEMISTRY,
ORE DEPOSITS, PETROLOGY, VOLCANOLOGY
and applied topics on *Environment*, *Archaeometry* and *Cultural Heritage*

Chemical bonding and radiation stability of monazite-structure orthophosphates: *ab initio* and spectroscopy studies

Yuliya V. Shchapova[1,2,*], Nina S.Vinogradova[1], Sergey L. Votyakov[1] and Mikhail V.Ryzhkov[3]

[1]Institute of Geology and Geochemistry, Ural Branch, Russian Academy of Sciences, Ekaterinburg, Russia
[2]Ural Federal University, Institute of Physics and Technology, Ekaterinburg, Russia
[3]Institute of Solid State Chemistry, Ural Branch, Russian Academy of Sciences, Ekaterinburg, Russia
* Corresponding author: *shchapova@igg.uran.ru*

Phosphate minerals have high radiation stability as a result of structure recrystallization processes that take place during irradiation (Ewing et al., 2000). In particular, natural U, Th-bearing monazite (Ce,La,Nd)PO_4 remains crystalline in spite of high accumulated alpha-decay doses. For the monazite-structure orthophosphates, the critical amorphization temperatures are low and vary from 60°C ($LaPO_4$) to 210°C ($GdPO_4$) (Meldrum et al., 1997). A number of criteria has been proposed for the prediction of the radiation stability of the materials: ionicity, crystallization temperature, structural topology, bonding and structure (Ewing et al., 2000). However, the reasons for noticeable variations of critical amorphization temperatures and radiation stability within monazite-structure orthophosphates are still unclear.

In this work the electronic structure and chemical bonding in monoclinic monazite-structure orthophosphates $LnPO_4$ (Ln = Ce, Nd, and Sm) are studied by the *ab initio* discrete variation method within the extended cluster model (Ryzhkov et al., 2000) and by X-ray photoelectron spectroscopy. The relative radiation stability of these phases is discussed on the basis of electronic spectra, orbital overlap population (OOP) values, and effective atomic charges.

The valence band of orthophosphates is mainly formed by 2s, 2p states of O atoms with an admixture of P 3s, 3p orbitals, reflecting the covalent bonding effects of P and O atoms. Ln 5s, 5p, 4f, 6s, 6p orbitals are mixed to the oxygen states. The upper edge of the valence band is formed by O2p and Ln4f orbitals; the states of the lower edge of the conduction band are Ln5d and P3s, 3p orbitals. The density of states spectra of non-equivalent O1–O4 differ substantially from each other.

The spin splitting of Ln 4f states increases (0.55 eV for Ce, 2.81 eV for Nd, and 3.72 eV for Sm), the bandwidth of the Ln5d states increases (4.08 eV for Ce, 5.26 eV for Nd, and 6.27 eV for Sm), and the O2p–Ln5d energy band gap decreases (5.35 eV for Ce, 4.81 eV for Nd, and 4.72 eV for Sm) in the row $CePO_4 \rightarrow NdPO_4 \rightarrow SmPO_4$. Local magnetic moments of the Ln atoms increase from 0.98 μB for Ce to 3.47 μB for Sm, and 5.72 μB for Nd. The bandwidth of the (O1)2p states is 7.31 eV for CePO4, 7.68 eV for NdPO4, and 7.97 eV for SmPO4.

The OOP values are used as a measure of covalency of P-O and Ln-O bonds. For the P–O bonds, the overlap population of P3p–O2p orbitals gives the highest contribution to the P–O covalency; for the Ln–O bonds, the overlap population of Ln5d–O2p, Ln5d–O2s, and Ln6p–O2s are similar in value. The covalency of the P-O bonds decreases in the row $CePO_4$→ $NdPO_4$→$SmPO_4$, which is manifested in an increase in OOP values averaged over the four types of oxygen. On the other hand, the covalency of the Ln-O bonds decreases in this row. The effective atomic charges of P and Ln atoms slightly decrease in the row $CePO_4$→$NdPO_4$ →$SmPO_4$, which indicates a decrease in the ionic component of the bonds. *Ab initio* data obtained are in a good agreement with our experimental spectroscopic studies of synthetic orthophosphates $LnPO_4$ (Ln = Ce, La, Nd) and natural monazites by X-ray photoelectron spectroscopy.

The increase in the critical amorphization temperature (and related decrease in the radiation stability) for orthophosphates in the row $CePO_4$→$NdPO_4$→$SmPO_4$ (Meldrum et al., 1997) is interpreted on the base of our study as a result of an increase in covalency of the P–O bonds and a total decrease in the ionic component of the chemical bonding. The effect of covalency occurs exclusively due to the phosphorus-oxygen sublattice while the REE-oxygen sublattice becomes less covalently bonded. This result gives evidence of different roles of P and Ln sublattices in radiation stability of complex oxides. In particular, it appears to be incorrect to consider the PO_4 tetrahedra in phosphate minerals as invariable units because their electronic structure undergoes substantial changes and can result in changes in the properties.

The work is supported by RFBR, 14-05-00172.

References

Ewing R.C., Meldrum A., Wang L.M. and Wang S.X. (2000) - Radiation-induced amorphization. In: Transformation Processes in Minerals. Reviews in Mineralogy and Geochemistry, S.A.T. Redfern and M.A.Carpenter (eds), MSA, Washington (USA), 39, 319-361.

Meldrum A., Boatner L.A., Wang L.M. and Ewing R.C. (1997) - Displacive irradiation effects in the monazite- and zircon-structure orthophosphates. *Phys. Rev.*, B56, 13805-13814.

Ryzhkov M.V., Denisova T.A., Zubkov V.G. and Maksimova L.G. (2000) - Electronic structure and chemical bonding in $Pb_2Fe(CN)_6$. *Journal of Structural Chemistry*, 41, 1123–1131.

Periodico di Mineralogia, ECMS 2015, 155-156

PERIODICO di MINERALOGIA
established in 1930

An International Journal of
MINERALOGY, CRYSTALLOGRAPHY, GEOCHEMISTRY,
ORE DEPOSITS, PETROLOGY, VOLCANOLOGY
and applied topics on *Environment*, *Archaeometry* and *Cultural Heritage*

New tool for water calculation in Martian fluorapatite: a combined synchrotron FTIR, Raman spectroscopy, EMPA and TEM study

Ewa Słaby[1], Monika Koch-Müller[2,*], Richard Wirth[2], Hans-Jürgen Förster[2], Anja Schreiber[2], Ulrich Schade[3] and Dieter Rhede[2]

[1]Institute of Geological Sciences, Polish Academy of Sciences, Research Centre in Warsaw, Twarda 51/55, 00-818 Warsaw, Poland
[2]Deutsches GeoForschungsZentrum, GFZ, Telegrafenberg, 14473 Potsdam, Germany
[3]Helmholtz-Zentrum Berlin, Elektronenspeicherring BESSY II, Albert-Einstein-Str. 15, 12489 Berlin, Germany
* Corresponding author: *mkoch@gfz-potsdam.de*

Phosphates, like apatite, that occur in terrestrial and extraterrestrial basalts deserve special attention because they are an information source regarding melt chemistry, including the activities of the volatiles that are responsible for their formation (e.g., Rubin 1997; Boyce et al. 2014). Especially, hydrogen incorporation in apatite plays an important role. Its concentration is frequently estimated by combining electron-microprobe analyses of F and Cl with mineral stoichiometry. In apatite, Cl, F and OH are located along c-axis channels in the unit cell, which is assumed to be fully occupied and the volatiles should add up to 2 anions per formula unit (pfu; Hughes et al. 2014). Hydrogen concentrations can be also measured directly using secondary ion mass spectroscopy (SIMS). The advantage of this method is that it measures H, F and Cl in the material at the same time and the results can be evaluated by the mineral stoichiometry. However, with SIMS-measurements one cannot distinguish between intrinsic hydroxyl and OH introduced in response to pervasive terrestrial contaminations along microfractures (Boctor et al. 2003).

This study reports the volatile concentrations in fluorapatite from NWA 2975 shergottite obtained by electron microprobe and FTIR (Fourier Transform Infrared Spectroscopy) - and Raman-spectroscopy. We combined focused ion-beam sample preparation technique with polarized synchrotron-based FTIR- and Raman spectroscopy to identify structurally bound OH, F, Cl and CO_3 groups in fluorapatite from the NWA 2975 shergottite. In this study, the first FTIR spectra of the OH-stretching region from a Martian apatite are presented that show characteristic OH-bands of a F-rich , Cl- and OH- bearing apatite. Depending on the method of apatite formula recalculation, the FTIR-based quantification of the incorporated OH, expressed as wt % H_2O, is almost in good agreement with the OH concentration calculated according to

electron-microprobe analyses of F and Cl and mineral stoichiometry. However, microprobing apatite is afflicted with a great bunch of problems, thus any direct method of determining water should be given preference wherever possible (SIMS, FTIR). The TEM results indicated that the recognized volatile budget of fluorapatite is strongly related to its magmatic origin and was not altered during post-magmatic events.

Financial support under grant number NCN 2011/01/B/ST10/04541 to Ewa Słaby.

References

Boctor N.Z., Alexander C.M.O., Wang J., and Hauri E. (2003) - The sources of water in martian meteorites: Clues from hydrogen isotopes. *Geochimica et Cosmochimica Acta*, 67, 3971-3989.

Boyce J.W., Tomlinson S.M., McCubbin F.M., Greenwood J.P. and Treiman A.H. (2014) - The Lunar Apatite Paradox. *Science*, 344, 400-402.

Hughes J.M., Nekvasil H., Ustunisik G., Lindsley D.H., Coraor A.E., Vaughn J., Phillips B.L., McCubbin F.M. and Woerner W.R. (2014) - Solid solution in the fluorapatite-chlorapatite binary system: High-precision crystal structure refinements of synthetic F-Cl apatite. *American Mineralogist*, 99, 369-376.

Rubin A.E. (1997) - Mineralogy of meteorite groups. *Meteoritics & Planetary Science*, 32, 231-247.

Periodico di Mineralogia, ECMS 2015, 157-158

PERIODICO di MINERALOGIA
established in 1930

An International Journal of
MINERALOGY, CRYSTALLOGRAPHY, GEOCHEMISTRY, ORE DEPOSITS, PETROLOGY, VOLCANOLOGY
and applied topics on *Environment*, *Archaeometry* and *Cultural Heritage*

Reapproval of betalomonosovite as a valid mineral species: single-crystal X-ray diffraction, HRTEM, Raman and IR spectroscopy

Elena Sokolova[1,*], Frank C. Hawthorne[1], Yassir A. Abdu[1], Alessandro Genovese[2] and Fernando Cámara[3]

[1] Dep. Geological Sciences, University of Manitoba, Winnipeg, R3T2N2, Canada
[2] King Abdullah University of Science and Technology, Thuwal, Saudi Arabia
[3] Dipartimento di Scienze della Terra, Via Valperga Caluso, 35, 10125 Torino, Italy
* Corresponding author: *elena_sokolova@umanitoba.ca*

Gerasimovskiy and Kazakova (1962) described betalomonosovite, $Na_2Ti_2Si_2O_9 \cdot (Na,H)_3PO_4$, from the Lovozero alkaline massif, Kola Peninsula, Russia. The crystal structure of the mineral was studied five times, each time resulting in a different formula. However, agreement between the crystal structure and the chemical analysis has never been reached. The problems with the crystal structure of betalomonosovite arise from the poor quality of its crystals which is related to the extensive cation and anion disorder present in the structure (including H_2O). In 2013, betalomonosovite was discredited by CNMNC.

We refined the crystal structure of betalomonosovite, ideally $Na_6\square_4Ti_4(Si_2O_7)_2[PO_3(OH)][PO_2(OH)_2]O_2(OF)$, a 5.3331(7), b 14.172(2), c 14.509(2) Å, α 103.174(2), β 96.320(2), γ 90.278(2)°, V 1060.7(4) Å^3, from the Lovozero alkaline massif, Kola peninsula, Russia, in the space group $P\bar{1}$ to R = 6.64%. We determined chemical composition of betalomonosovite by electron-microprobe and did HRTEM, Raman and IR spectroscopy for betalomonosovite and lomonosovite, $Na_{10}Ti_4(Si_2O_7)_2(PO_4)_2O_4$.

Betalomonosovite, ideally $Na_6\square_4Ti_4(Si_2O_7)_2[PO_3(OH)][PO_2(OH)_2]O_2(OF)$, is a Group-IV TS-block mineral (Ti + Mg + Mn = 4 *apfu*) in accord with Sokolova (2006). The crystal structure of betalomonosovite is an alternation of TS and **I** blocks of the composition $Na_4Ti_4(Si_2O_7)_2O_2(OF)$ and $Na_2\square_4[PO_3(OH)][PO_2(OH)_2]$, respectively. The crystal structure of betalomonosovite is of the same topology as that of lomonosovite, $Na_{10}Ti_4(Si_2O_7)_2(PO_4)_2O_4$, with TS and **I** blocks of the composition $Na_4Ti_4(Si_2O_7)_2O_4$ and $Na_6(PO_4)_2$, respectively. Betalomonosovite is a Na-poor OH-bearing analogue of lomonosovite. The presence of OH groups in the **I** block and in the TS block is supported by IR spectroscopy and bond-valence calculations on anions. In the betalomonosovite structure, there is less Na in the in the **I** block

and in the TS block when compared to the lomonosovite structure [*cf*. **I** block: $Na_2\square_4[PO_3(OH)][PO_2(OH)_2]$ (betalomonosovite) and $Na_6(PO_4)_2$ (lomonosovite)]. There is extensive cation and anion disorder in the crystal structure of betalomonosovite: in the **I** block, two *Na* sites are fully occupied and four alkali-cation sites are < 50% occupied, and in the TS block, four *Na* sites have 65-78% occupancy.

HRTEM of lomonosovite shows the presence of pervasive microstructural intergrowths, accounting for the presence of signals from H_2O in the infrared spectrum of anhydrous lomonosovite. More extensive lamellae in betalomonosovite suggest a topotactic reaction from lomonosovite to betalomonosovite.

Based on our work, betalomonosovite, $Na_6\square_4Ti_4(Si_2O_7)_2[PO_3(OH)][PO_2(OH)_2]O_2(OF)$, has been reapproved by the Commission on new minerals, nomenclature and classification (CNMNC) (Nomenclature voting proposal 14-J, 2015).

References

Gerasimovskiy, V.I. and Kazakova, M.Ye. (1962) - Betalomonosovite. *Doklady Akademii Nauk SSSR, Earth Sciences* **142**, 118-121.

Sokolova, E. (2006) - From structure topology to chemical composition. I. Structural hierarchy and stereochemistry in titanium disilicate minerals. *Canadian Mineralogist* **44,** 1273-1330.

Periodico di Mineralogia, ECMS 2015, 159-160

PERIODICO di MINERALOGIA
established in 1930

An International Journal of
MINERALOGY, CRYSTALLOGRAPHY, GEOCHEMISTRY, ORE DEPOSITS, PETROLOGY, VOLCANOLOGY
and applied topics on *Environment*, *Archaeometry* and *Cultural Heritage*

Single-crystal elastic properties of thaumasite and ettringite: a combination of experiments and DFT computations

Sergio Speziale[1,*], Eva Scholtzová[2] and Daniel Tunega[3]

[1] GFZ German Research Centre for Geosciences, Telegrafenberg, 14473 Potsdam, Germany
[2] Institute of Inorganic Chemistry, Slovak Academy of Sciences, Dúbravská cesta 9, 845 36, Bratislava, Slovakia
[3] Institute for Soil Science, University of Natural Resources and Life Sciences, Peter-Jordan-Strasse 82, A-1190, Vienna, Austria
* Corresponding author: *speziale@gfz-potsdam.de*

Thaumasite [$Ca_3Si(OH)_6(SO_4)(CO_3)\cdot 12H_2O$, hexagonal] and ettringite [$Ca_6Al_2(OH)_{12}(SO_4)_3\cdot 26H_2O$, trigonal] are two members of the ettringite group. The minerals of the ettringite group are characterized by a structure based on columns of general formula $Ca_3[M(OH)_6(H2O)_m]$, where $M(OH)_6$ are octahedral units and $Ca_3(OH)_4(H_2O)x$ are trimers of edge-sharing Ca polyhedra. Ettringite and thaumasite form solid solution and occur mostly in contact metamorphic zones or as product of reaction between geothermal fluids and basalts or tuffs. In addition they are the natural structural analogues of two main sulfate solids formed in Portland cement both as primary phases during the first setting and as secondary alteration product due to sulfate attack reactions. Owing to the impact of secondary sulfate attack on the mechanical stability of concrete it is important developing quantitative models of secondary sulfates formation and growth in aging cement, which help understanding the complex of interplay between the intrinsic anisotropies of the secondary solids and the development of strongly directional microstructures and textures. Here we present the results of our studies of the single-crystal elastic anisotropy of thaumasite and ettringite by Brillouin spectroscopy and first principles computations. Our results give new insights in the relationship between structural and elastic properties of the minerals of the ettringite group and of their analogues formed in cement materials.
The experimentally based elastic moduli of both minerals are in excellent agreement with those determined from first principles with disagreement always between 5 and 10%.

Thaumasite is substantially stiffer and more rigid than ettringite. Its bulk modulus (incompressibility) and shear modulus (rigidity) are 41% and 52% larger than those of ettringite. However, both the longitudinal stiffness (C_{33}) and shear stiffness (C_{44}) of ettringite along the *c*-axis are only moderately lower than the corresponding ones of thaumasite with relative differences of 10% and 21% respectively. The main reason of the difference between the elastic

properties of the two minerals is the stiffness and rigidity within the *ab* plane, perpendicular to the *c*- axis. The longitudinal stiffness C_{11} and the shear stiffness C_{66} of ettringite are 40% and 49% softer than in thaumasite. Our results show that the difference between the two minerals is mostly due to the different connectivity between the stiff structural columns $Ca_3[M(OH)_6(H2O)_m]$ aligned along the *c*- crystallographic axis. The softness and low rigidity of ettringite in the *ab* plane, is due to the weak hydrogen bonds between water molecules and SO_4^{2-} ions compared with the stiffer ones between water molecules and CO_3^{2-} ions present in thaumasite. This is confirmed by density functional theory (DFT) calculations of the structural and vibrational properties of thaumasite, which contains both sulfate and carbonate groups in its structure (Scholtzová et al., 2014).

References

Scholtzová E., Kucková L., Kožíšek J., Páklová H. and Tunega D. (2014) – Experimental and computational study of thaumasite structure. *Cement and Concrete Research*, 59, 66-72.

Periodico di Mineralogia, ECMS 2015, 161-162

PERIODICO di MINERALOGIA
established in 1930

An International Journal of
MINERALOGY, CRYSTALLOGRAPHY, GEOCHEMISTRY, ORE DEPOSITS, PETROLOGY, VOLCANOLOGY
and applied topics on *Environment*, *Archaeometry* and *Cultural Heritage*

"Chlorellestadite" $Ca_5(SiO_4)_{1.5}(SO_4)_{1.5}Cl$, a potentially new mineral of the apatite supergroup from the Shadil Khokh volcano, Kel'sky Plateau, Southern Ossetia

Dorota Środek[1,*], Mateusz Dulski[2], Viktor M. Gazeev[3] and Irina O. Galuskina[1]

[1] University of Silesia Faculty of Earth Sciences, Będzińska 60, 41 – 200 Sosnowiec, Poland
[2] University of Silesia Institute of Material Sciences, 75 Pułku Piechoty 1A, 41 – 500 Chorzów, Poland
[3] Institute of Geology of Ore Deposits, Geochemistry, Mineralogy and Petrography (IGEM) RAS, Staromonetny 35, Moscow, Russia
* Corresponding author: *dsrodek@us.edu.pl*

Minerals of the ellestadite group consist of hexagonal and pseudo-hexagonal sulphato-silicates with the ratio $(SiO_4)^{4-}$:$(SO_4)^{2-}$ = 1:1 in the crystal chemical formula. At present, this group includes three members: hydroxylellestadite $Ca_5(SiO_4)_{1.5}(SO_4)_{1.5}OH$, fluorellestadite $Ca_5(SiO_4)_{1.5}(SO_4)_{1.5}F$ and mattheddleite $Pb_5(SiO_4)_{1.5}(SO_4)_{1.5}Cl$ (Pasero et al., 2010). Fluor- and hydroxylellestadite occurs in high-temperature skarns and pyromethamorphic rocks (McConnell, 1937; Pascal et al., 2001).

Samples containing high-temperature mineral associations were collected from altered xenolith on the north-west slope of the Shadil Khokh volcano which belongs to the Kel'sky volcanic area in the Greater Caucasus Mountain Range in Southern Ossetia. This area was formed as a result of the activity of 25 small volcanoes, which mostly consist of porphyritic and aphyric types of lavas, represented by plagiodacite, dacite, plagioriodacite and andesite. Ellestadite group minerals occur in altered limestone xenoliths within dacite lavas. This pyrometamorhpic rock is composed of spurrite, larnite, gehlenite, merwinite, bredigite, rondorfite and srebrodolskite (Gazeev et al., 2012).

In studied samples, minerals of ellestadite group are characterized by high Cl content and its average composition responds to the following crystal chemical formula – $(Ca_{4.98}Mg_{0.01}Sr_{0.01})_{\Sigma 5.0}[(SiO_4)_{1.54}(SO_4)_{1.43}(PO_4)_{0.02}(AlO_4)_{0.01}]_{\Sigma 3.0}[Cl_{0.39}F_{0.38}(OH)_{0.23}]_{\Sigma 1.0}$. Rarely, in ellestadites from paragenesis with chlor-bearing jasmundite ($Ca_{22}(SiO_4)_8O_4S_2$) and "albovite" ($Ca_3(SiO_4)Cl_2$), Cl is predominant at the channel positions, for example, $(Ca_5Na_{0.01}Mg_{0.01}Sr_{0.01})_{\Sigma 5.04}[(SiO_4)_{1.49}(SO_4)_{1.47}(AlO_4)_{0.01}]_{\Sigma 2.97}[Cl_{0.61}(OH)_{0.32}F_{0.12}]_{\Sigma 0.95}$.

The main bands of the Raman spectrum of ellestadites from Shadil Khokh are found at 274 (Ca–O vibrations), 460, 625 (SiO_4^{4-} and SO_4^{2-} bending vibrations), 855, 1007, 1085 and 1149 cm^{-1} (SiO_4^{4-} and SO_4^{2-} symmetric stretching vibrations).

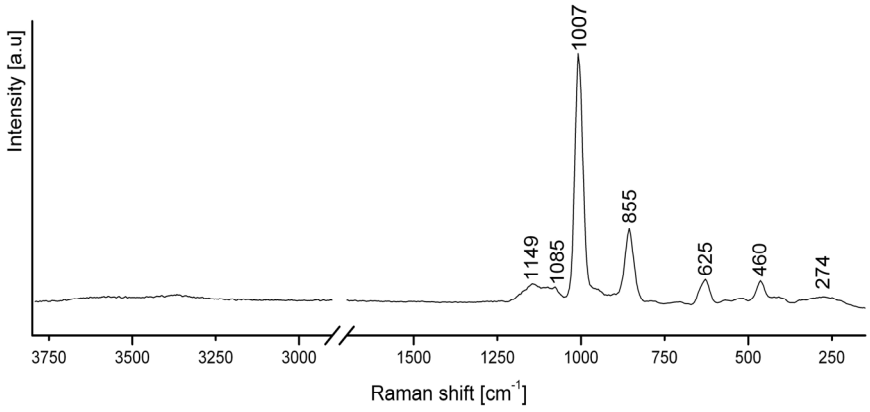

Fig.1. Raman specrum of ellestadite from Shadil – Khokh.

In the range 3300 – 3800 cm^{-1}, which corrresponds to vibrations of the hydroxyl groups, we observed very weak bands. This confirms that the OH content in the channel positions of the studied ellestadite is insignificant. These data allow to suggest a natural existence of Cl-dominant ellestadite with the end-member formula $Ca_5(SiO_4)_{1.5}(SO_4)_{1.5}Cl$.

Research was conducted with the support of funding of the project "DoktoRIS - scholarship for innovative Silesia".

References

Gazeev, V.M., Gurbanova, O.A., Zadov, A.E., Gurbanov, A.G., and Leksin, A.B. (2012) - Mineralogy of skarned carbonate xenoliths from Shadil-khokh volcano (Kelski Vulcan area of Great Caucasian Range). *Vestnik Vladikavkazskogo Nauchnogo Centra*, 2, 18-27 364 (in Russian).

McConnell D. (1937) - The substitution of SiO_4 and SO_4 groups for PO_4 groups in the apatite structure: ellestadite, the end-member. *American Mineralogist*, 22, 977-986.

Pascal M-L., Fonteilles M. and Verkaer J. (2001) - The melilite-bearing high temperature skarns of the Apuseni Mountains, Carpathians, Romania. *Canadian Mineralogist*, 39, 1405-1434.

Pasero M., Kampf A.R., Ferraris C., Pekov I.V., Rakovan J. and White T.J. (2010) - Nomenclature of the apatite supergroup minerals. *European Journal of Mineralogy*, 22, 163-179.

Periodico di Mineralogia, ECMS 2015, 163-164

PERIODICO di MINERALOGIA
established in 1930

An International Journal of
MINERALOGY, CRYSTALLOGRAPHY, GEOCHEMISTRY,
ORE DEPOSITS, PETROLOGY, VOLCANOLOGY
and applied topics on *Environment*, *Archaeometry* and *Cultural Heritage*

Ab initio modelling of vibrational spectra of minerals: studying Mercury's surface in remote sensing

Claudia Stangarone[1,*], Mauro Prencipe[2] and Mario Tribaudino[1]

[1] Physics and Earth Sciences, University of Parma
[2] Earth Sciences, University of Turin
* Corresponding author: *claudia.stangarone@studenti.unipr.it*

The accuracy of the CRYSTAL14 code (Dovesi et al., 2014), a quantum mechanical program for *ab initio* methods, enables the reliable modelling of vibrational spectra of crystalline structures. In this case of study, such program was used to perform a quantum mechanical simulation of the IR reflectance spectra, of ortho-enstatite, an orthopyroxene which is probably one of the major components of Mercury's surface (Sprague et al., 2007, 2009).

The simulation provided results in very good agreement with experimental data (Demichelis et al., 2012) with a maximum discrepancy in absolute average of 5.2 cm^{-1}.

Concerning the intensities of the IR signals, the reflection spectra have been simulated by computing the dielectric susceptibility tensors up to the third order, by means of the Coupled Perturbed Hartree-Fock or Kohn-Sham (CPHF/KS) method. With such a method it is also possible to compute the LO-TO splitting, and hence to simulate reflectance IR spectra, as it can be seen in Figure 1.

The aim of the work is to create a theoretical background to interpret HT-IR reflectance spectra that will be collected in remote sensing, by MERTIS, a spectrometer developed by Institute of Planetary Research at Deutschen Zentrums für Luft- und Raumfahrt (DLR), that will be on board of the next European Space Agency (ESA) spacecraft, BepiColombo, whose launch is scheduled for the beginning of 2017 (Hisinger and Helbert, 2010). The goal is to point out the most interesting spectral features for a geological mapping of Mercury and other rocky planetary bodies.

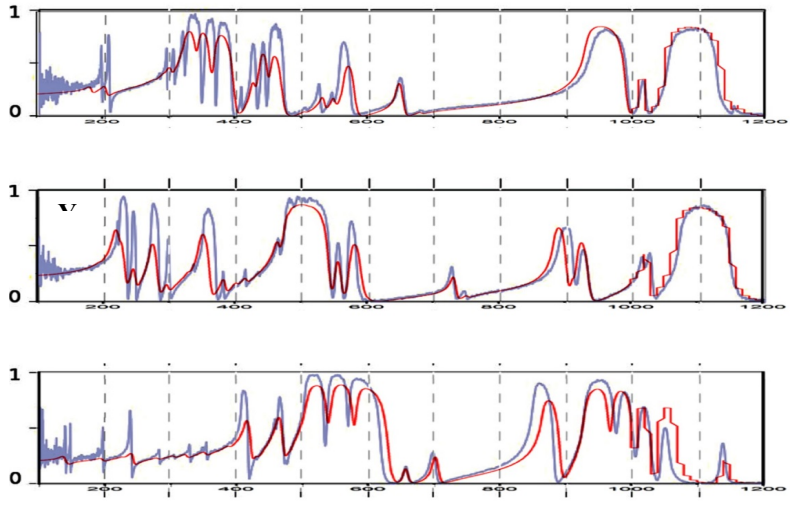

Figure 1. Reflection spectra of ortho-enstatite along the x, y and z axes: experimental spectra (blue line) are measured at 60 K (Demichelis et al. 2012), our calculated (red line) are overlaid.

References

Demichelis R., Suto H., Noel Y., Sogawa H., Naoi T., Koike C., Chihara H., Shimobayashi N., Ferrabone M. and Dovesi R. (2012) - The infrared spectrum of ortho-enstatite from reflectance experiments and first-principle simulations. *Monthly Notices of the Royal Astronomical Society,* 420, 147–154.

Dovesi R., Saunders V. R., Roetti C., Orlando R., Zicovich-Wilson C. M., Pascale F., Civalleri B., Doll K., Harrison N. M., Bush I. J., D'Arco P., Llunell M., Causà M. and Noël Y. (2014) - *CRYSTAL14 User's Manual*, University of Torino.

Hiesinger, H. and Helbert J. (2010) - The Mercury Radiometer and Thermal Infrared Spectrometer (MERTIS) for the BepiColombo mission. Comprehensive Science Investigations of Mercury: The scientific goals of the joint ESA/JAXA mission BepiColombo. *Planetary and Space Science*, 58, 144–165.

Sprague, A.L., Warell, J., Cremonese, G., Langevin, Y., Helbert, J., Wurz, P., Veselovsky, I., Orsini, S. and Milillo A. (2007) - Mercury's surface composition and character as measured by ground-based observations. *Space Science Review*, 132, 399–431.

Sprague, A.L., Donaldson Hanna, K.L., Kozlowski, R.W.H., Helbert, J., Maturilli, A., Warell, J.B. and Hora J.L. (2009) - Spectral emissivity measurements of Mercury's surface indicate Mg- and Ca-rich mineralogy, K-spar, Na-rich plagioclase, rutile, with possible perovskite, and garnet. *Planetary and Space Science*, 57, 364–383.

Periodico di Mineralogia, ECMS 2015, 165-166

PERIODICO di MINERALOGIA
established in 1930

An International Journal of
MINERALOGY, CRYSTALLOGRAPHY, GEOCHEMISTRY,
ORE DEPOSITS, PETROLOGY, VOLCANOLOGY
and applied topics on *Environment*, *Archaeometry* and *Cultural Heritage*

Valence state and symmetry mapping of Fe oxide exsolutions

Igor Stelluti[1] and Francesco d'Acapito[2,*]

[1] Dipartimento di Scienze della Terra, Sapienza Università di Roma, Piazzale Aldo Moro 5, I-00185 Roma, Italy
[2] CNR-IOM-OGG c/o European Sinchrotron Radiation Facility, Grenoble (F)
* Corresponding author:*dacapito@esrf.fr*

This contribution reports on an X-ray mapping study of Fe oxides exsolutions found in Etnean lavas through X-ray absorption spectroscopy (XAS). These lavas, belonging to the last phase of Ellittico volcanic activity, present particular mineralogical evidences and are characterized by a fissural emplacement (Stelluti et al., 2013, 2014). The study of Fe oxides exsolutions is an instrument of petrologic relevance, allowing comprehension of the evolutionary history of the volcanic products in study, especially if supported by geochemical studies. The oxides studied are likely to derivate from magnetite/titanium-magnetite after transformation and alteration processes, probably due to a slow cooling during magma arise as a typical process in the formation of "lavic dome" structures. The microanalysis of the oxides showed a variable composition, presenting different contents of Fe and Ti. From BSE-SEM analysis, the exsolutions showed to belong to the series ilmenite-hematite, and to have a size in the range of tens of nanometers.

The study presented here is based on X-ray mapping using different excitation energies around the Fe-*K* absorption edge in order to exploit the different levels of fluorescent yield (Fe-*K*α line) of various Fe compounds for the two dimensional mapping of thin sections (Sutton et al. 1995). This technique allows to obtain the surface distribution of the elements (Fe in this case) and a map of their oxidation state and local symmetry.

A rock thin section has been investigated, with focus on an area containing a crystal of clinopyroxene in contact with a Fe-Ti oxide (in order to get comparison). Results are represented in Figure 1: there is an evident contrast between the two mineral phases for iron content, oxidation state and local symmetry.

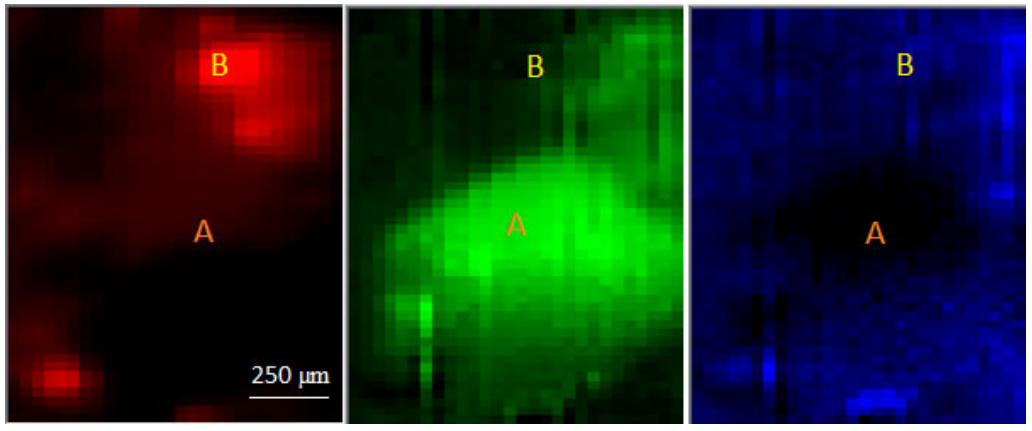

Figure 1. Rock thin section investigated: A = area occupied by clinopyroxene; B = area occupied by Fe-Ti oxide. Left picture: clinopyroxene showing lower abundance of iron and Fe-Ti oxide showing higher abundance of iron (in red); central picture: clinopyroxene showing the presence of divalent Fe and Fe-Ti oxide the presence of mainly trivalent Fe (in green); right picture: clinopyroxene showing evidence of Fe with octahedral coordination and Fe-Ti oxide showing evidence of Fe with distorted octahedral coordination (in blue).

References

Stelluti I., Mura F. and Gianfagna A. (2014) - FESEM-FIB-EDS investigation on fibrous and acicular volcanic orthopyroxenes from Etnean products, Italy. *A.1 Rendiconti Online della Società Geologica Italiana*, Supplement N.1 to Vol. 31, 376.

Stelluti I., Viti C. and Gianfagna A. (2013) - Mineralogical characterization and crystallization kinetics of fibrous and acicular volcanic orthopyroxenes from Mt. Etna, Sicily, Italy. *Mineralogical Magazine*, 77, 2261.

Sutton S.R., Bajt S., Delaney J., Schulze D. and Tokunaga T. (1995) - Synchrotron x-ray fluorescence microprobe: Quantification and mapping of mixed valence state samples using micro-XANES. *Review of Scientific Instrument*, 66, 1464.

Periodico di Mineralogia, ECMS 2015, 167-168

PERIODICO di MINERALOGIA
established in 1930

An International Journal of
MINERALOGY, CRYSTALLOGRAPHY, GEOCHEMISTRY,
ORE DEPOSITS, PETROLOGY, VOLCANOLOGY
and applied topics on *Environment*, *Archaeometry* and *Cultural Heritage*

HT-FTIR spectroscopy of riebeckite

Umberto Susta[1,*], Giancarlo Della Ventura[1], Fabio Bellatreccia[1], Frank C. Hawthorne[2], Massimo Boiocchi[3] and Roberta Oberti[4]

[1] Dipartimento di Scienze, Università Roma Tre, Roma, Italy
[2] Department of Geological Sciences, University of Manitoba, Winnipeg, Canada
[3] Centro Grandi Strumenti, Università degli Studi di Pavia, Italy
[4] CNR-Istituto di Geoscienze e Georisorse, Unità di Pavia, Italy.
*Corresponding author. *umberto.susta@uniroma3.it*

Changes in physical properties of Fe-amphiboles at increasing temperature (T) have been proven to be crucial in modeling the electrical conductivity of subducted rocks in convergent margins (Reynard et. al., 2011). Oxidation of Fe^{2+} to Fe^{3+} within the octahedrally coordinated sites, which in turn is aimed at achieving local electroneutrality during deprotonation occurring at high temperature (HT), is considered to be the reason for the observed increase in conductivity (e.g. Wang et al., 2012). Deprotonation mechanisms and their relationship with Fe oxidation within the amphibole structure are now being examined systematically combining single-crystal structure refinement with FTIR and Mössbauer spectroscopies. In particular, HT-FTIR spectroscopy has proved to yield *in operando* information concerning deprotonation and, in favorable conditions, oxidation processes of multi-valence octahedral constituents. The interpretation of FTIR data has been repeatedly tested by single-crystal structure refinement.

A riebeckite from Malawi was chosen for this study as a representative of the subgroup of the sodium amphiboles, which are common in high-pressure (HP) geological environments. Before studying its HT behavior, the sample was exhaustively characterized at room T (RT) by means of single-crystal XRD structure-refinement, EPMA, IR and Mössbauer spectroscopy. Its crystal-chemical composition turned out to be very close to that of the ideal end-member, i.e. $^{A}\square^{B}Na_2{}^{C}(Fe^{2+}{}_3Fe^{3+}{}_2)^{T}Si_8O_{22}{}^{W}(OH)_2$.

Interestingly, HT-IR data collected *in-situ* using short-term heating ramps on single-crystals showed a significant (apparent?) increase in the absorption coefficient with T, a feature already observed on potassic-ferro-richterite by Della Ventura et al. (2015). Spectra collected at RT during the ramp after fast quenching showed that the (OH) content does not change up to 550 °C and that hydrogen is rapidly lost in the 550-650 °C T interval.

Doubly-polished single crystals and powders were studied by HT-FTIR during long term isothermal annealing at several T values with the aim of studying the effects of H diffusion through the crystal on deprotonation kinetics. Notably, all experiments done on powders did

not show any apparent increase in the absorption coefficient at high T, suggesting that such a phenomenon is relevant to single crystals only.

Experiments done under isothermal conditions and different chemical/physical environments showed that the kinetics of deprotonation is strongly related to oxygen availability during the heating stage. In particular, deprotonation was found to be strongly inhibited both in single crystals heated under a N_2 flux and in powders embedded in a KBr pellet. Attempts to quantify and model the impact of the medium on hydrogen diffusion in riebeckite are still under way.

References

Della Ventura, G., Susta, U., Bellatreccia, F., Cavallo, A. and Oberti, R. (2015) - Synthetic potassic-ferro-richterite: HT behavior and deprotonation process by single-crystal FTIR spectroscopy and structure refinement (in preparation).

Reynard, B., Mibe, K. and Van de Moortèle, B. (2011) - Electrical conductivity of the serpentinised mantle and fluid flow in subduction zones. *Earth and Planetary Science Letters*, 307, 387-394.

Wang D., Guo Y. and Yu Y. (2012) - Electrical conductivity of amphibole-bearing rocks: influence of dehydration. *Contributions to Mineralogy and Petrology*, 164, 17-25.

Periodico di Mineralogia, ECMS 2015, 169-170

PERIODICO di MINERALOGIA
established in 1930

An International Journal of
MINERALOGY, CRYSTALLOGRAPHY, GEOCHEMISTRY,
ORE DEPOSITS, PETROLOGY, VOLCANOLOGY
and applied topics on *Environment*, *Archaeometry* and *Cultural Heritage*

The origin of colour of red beryl by LIBS analyses

Gioacchino Tempesta* and Giovanna Agrosì

Dipartimento di Scienze della Terra e Geoambientali (DiSTeGeo), University of Bari, Via E. Orabona 4, 70125 Bari, Italy
* Corresponding author: *gioacchino.tempesta@uniba.it*

Laser Induced Breakdown Spectroscopy (LIBS) represents a valuable technique to carry out qualitative and quantitative chemical analyses of all elements in one shot, including also the light ones (like Li and Be). LIBS does not require any sample preparation and allows to reveal all the atomic species even if in small amount (as trace elements).

Recently, this spectroscopic technique was used also in mineralogical field to study with a small damages oxides and silicates (De Giacomo et al., 2012; Rossi et al., 2014). Previous studies were performed also on natural beryl samples, to identify their different origin using the spectrum as fingerprint (Nancy et al., 2006), and on synthetic beryl samples distinguishing the different synthetic processes by quantitative chemical composition (Agrosì et al., 2014).

In this study, we use a new prototype of LIBS (Fig. 1a) coupled with a petrographic microscope to investigate the origin of colour of some samples of a rare variety of beryl, the red one, usually called "bixbite". The red colour of beryl was previously associated to different chromophores: in natural beryl samples from Utah the red colour was related to the Mn^{3+} content (Shigley and Foord, 1984) while in the synthetic homologous it was ascribed to Co^{2+} (Shigley et al., 2001).

In the 2003 one red beryl rich of Cs was discovered in Madagascar becoming a new mineral called Pezzottaite and its red orange colour was related to Fe^{3+} and Cr^{3+} contents (Laurs et al., 2003).

In this study all the elements of the red beryl has been identified (Fig. 1c) using a specific configuration of LIBS with a double pulse laser that intensify the signal (Si, Al, Be, Li, Mg, Mn, Na, Ti, Fe, K, Zn, etc.) (Fig. 1b). The use of the microscope allows to obtain a spot size of about 10÷40 μm depending from number of shots and the continuity of the crystal. Quantitative analyses have been performed by means of Standard Calibration-Free LIBS (CF-LIBS) method (Ciucci et al., 1999) and compared with those found in literature (Shigley and Foord, 1984; Aurisicchio et al, 1990; Shigley et al., 2001) verifying the goodness of the methodology.

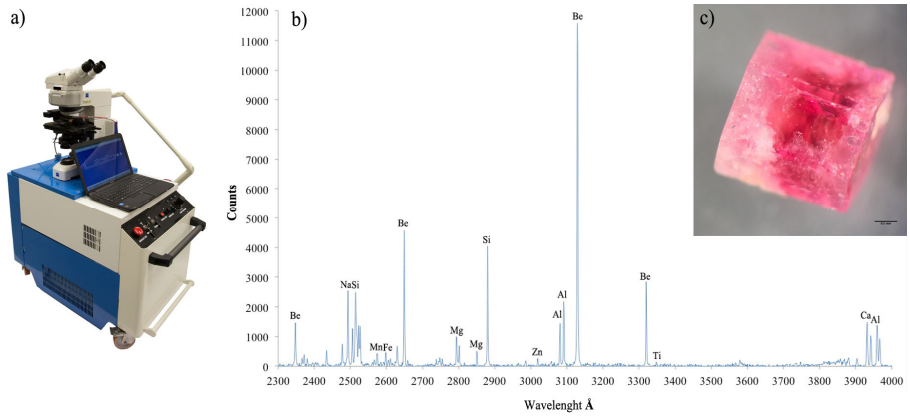

Fig. 1: a) Laser Induced Breakdown Spectroscopy (LIBS) Modì prototype coupled with a microscope; b) LIBS emission spectrum of red beryl analysed in the spectral range: 230-400 nm; c) specimen from Utah.

References

Agrosì G., Tempesta G., Scandale E., Legnaioli S., Lorenzetti G., Pagnotta S., Palleschi V., Mangone A., Lezzerini M. (2014) - Application of Laser Induced Breakdown Spectroscopy to the identification of emeralds from different synthetic processes, *Spectrochimica Acta Part B,* 102, 48–51.

Aurisicchio C., Fioravanti G., Grubessi O. (1990) - Genesis and growth of the red beryl from Utah (U.S.A.). *Atti Della Accademia Nazionale dei Lincei, Rendiconti Lincei, Scienze Fisiche e Naturali, 9th Series*, 1, 393–404.

Ciucci A., Palleschi V., Rastelli S., Salvetti A., Singh D.P., Tognoni E. (1999) - CF-LIPS: A new approach to LIPS spectra analysis, Laser Part. *Beams*, 17, 793.

De Giacomo A., Dell'Aglio M., Gaudiuso R., Santagata A., Senesi G.S., Rossi M., Ghiara M.R., Capitelli F., De Pascale O.A. (2012) - Laser Induced Breakdown Spectroscopy applica- tion based on Local Thermodynamic Equilibrium assumption for the elemental analysis of alexandrite gemstone and copper-based alloys. *Chemical Physics*, 398, 233–238.

Laurs B.M., Simmons W.B., Rossman G.R., Quinn E.P., McClure S.F., Peretti A., Armbruster T., Hawthorne F.C., Falster A.U., Günther D., Cooper M.A., Grobéty B. (2003) - Pezzottaite from Ambatovita, Madagascar: A new gem mineral. *Gems & Gemology*, 39, 284–301.

Rossi M., Dell'Aglio M., De Giacomo A., Gaudiuso R., Senesi G.S., De Pascale O., Capitelli F., Nestola F., Ghiara M.R. (2014) - Multi-methodological investigation of kunzite, hiddenite, alexandrite, elbaite and topaz, based on laser-induced breakdown spectroscopy and conventional analytical techniques for supporting mineralogical characterization. *Physics and Chemistry of Minerals.* 41, 127–140.

Shigley J.E., Foord E.E. (1984) - Gem-quality red beryl from the Wah Wah Mountains, Utah. *Gems & Gemology* 20, 208–221.

Shigley J.E., McClure S.F., Cole J.E., Koivula J.I., Lu T., Elen S., Demianets L.N. (2001) - Hydrothermal synthetic red beryl from the Institute of Crystallography, Moscow. *Gems & Gemology*, 37, 42–55.

Periodico di Mineralogia, ECMS 2015, 171-172

PERIODICO di MINERALOGIA
established in 1930

An International Journal of
MINERALOGY, CRYSTALLOGRAPHY, GEOCHEMISTRY,
ORE DEPOSITS, PETROLOGY, VOLCANOLOGY
and applied topics on *Environment*, *Archaeometry* and *Cultural Heritage*

Precious opals from the Raduzhnoe deposit (Russia): mineralogy, geochemistry

Vitaliia B. Tishkina*, Vera A. Pakhomova, Dimitry G. Fedoseev and Dimitry S. Ostapenko

Far East Geological Institute, Far Eastern Branch of Russian Academy of Sciences, 159,
prospect 100-letya Vladivostoka, Vladivostok, Russia 690022
* Corresponding author: *vtishkina@gmail.com*

The Raduzhnoe deposit of precious opals was found in the north of Primorsky Region (Far East of Russia) in 1986. Since 2008, the deposit has been exploited by a private company, supplying precious and common opal raw material of different colors to the foreign and domestic markets. The deposit is a part of the Alchan agate-opal-bearing area within the Western Sikhote-Alin volcanic zone. The area involves volcanic rocks of a basaltic andesite formation developed in the Upper Cretaceous and spatially associated with the agate-opal mineralization (Tishkina, 2015). Precious opals of the Raduzhnoe deposit occur in zones of strongly argillized, fractured and brecciated rocks, forming streaks in common opal, propylitized andesites and their tuffs.

The precious opals from the Raduzhnoe deposit are found in the following forms: as 5-30 mm-size nodules in dense illite-montmorillonite aggregates, as nests measuring 15×70×40 mm at the most, as zones of opalescence without distinguished boundaries in common opals. Common opals occur as thin streaks of transparent brightly colored differences of 15×10×5 mm average size, as veins and nests in the altered andesites, and as sinters of 25×50×15 mm average size often in association with chalcedony (Tishkina, 2004). The density of the opals varies from 1.85 to 2.07 g/cm^3; the hardness according to Mohs' scale is 4.5-5; water content is in the range of 2.5 - 5.8 wt% (calculated values), and the index of refraction in the range of 1.395 - 1.487. There are porous and fragile opals with low density and high refractive index which can be grouped into a special group.

Most of the precious opals of the Raduzhnoe deposit, regardless of change of their colors, are light, transparent, milky, and bluish-green. Besides, there are also transparent bright yellow and bright orange samples as well as almost opaque dark grey and dark brown ones. Only black and bluish opals were not found in the Raduzhnoe deposit. Some opal samples from the deposit exhibited blue luminescence (365 nm) of different intensity at low Fe content from 50 to 300 ppm, but two powdered samples (pink non-transparent and red-orange transparent

common opals) exhibited spotty luminescence at Fe content about 1500 ppm. The maximum content of U determined in test specimens is 8.92 ppm (in a specimen containing 3861 ppm of Fe); the average content is in the range between 0.03 - 0.97 ppm at varying Fe content (Tishkina, 2015). However, no sample showed green luminescence.

Based on the published data, Ba content can be used for recognizing opals from deposits of various types (Gaillou, 2008). Most of the analyzed samples with Ba content more than 100 ppm are normal opals, but some samples of precious opal had Ba content more than 130 ppm.

Chemical composition of opals from the Raduzhnoe deposit is similar to precious opals from the foreign deposits (Gaillou, 2008; Rondeau, 2010). Among uncommon elements, V (up to $8.5 \cdot 10^{-2}$ wt%), Rb (up to $2.24 \cdot 10^{-3}$ wt%), Sr (up to $4.09 \cdot 10^{-2}$ wt%), Zr (up to $9.73 \cdot 10^{-2}$ wt%), and Mg (up to 1.42 mass%) are observed.

The most common inclusions are mineral phases of cubic and octahedral shape of 1-100 μm size, which are uniformly distributed and whose content can reach 1-5 %. There is no doubt that the main diagnostic feature of the opals from the Raduzhnoe deposits is the presence of abundant inclusions of magnetite in forms of octahedron and cube. Magnetite inclusions are changed under the influence of metasomatic fluids.

The studies were supported by the Russian Basic Research Foundation, Grant 15-05-00809, 14-05-31032

References

Gaillou E., Delaunay A., Rondeau B., Bouhnik-le Coz M., Fritsh E., Cornen G. and Monnier C. (2008) - The geochemistry of opals as evidence of their origin. *Ore geology Reviews*, 34, 113-126.

Rondeau B., Fritsh E., Mazzero F., Gauthier J-P., Cenki-Tok B., Bekele E. and Gaillou E. (2010) - Play-of-color opal from Wegel Tena, Wollo Province, Ethiopia. *Gems and Gemology*, 46, 90-105.

Tishkina V., Zalishchak B., Pakhomova V. and Lapina M. (2004) - Opal from the Raduznoe deposit (Primorsky krai, Russia). *The Journal of The Gemmological Association of Hong Kong*, XXV, 79-82.

Tishkina V., Pakhomova V., Buravleva S. and Stepanov O. (2015) - Precious opal from Raduznoe deposit: mineralogy and origin. *Proceedings of the Russian Mineralogical Society*, Part 144 Issue 1, 100-114.

Periodico di Mineralogia, ECMS 2015, 173-174

PERIODICO di MINERALOGIA
established in 1930

An International Journal of
MINERALOGY, CRYSTALLOGRAPHY, GEOCHEMISTRY,
ORE DEPOSITS, PETROLOGY, VOLCANOLOGY
and applied topics on *Environment*, *Archaeometry* and *Cultural Heritage*

The temperature and oxygen fugacity dependence of hydroxyl incorporation in San Carlos olivine: an experimental and infrared study

Peter M.E. Tollan*, Hugh St C. O'Neill and Jörg Herman

Research School of Earth Sciences, The Australian National University
* Corresponding author: *peter.tollan@anu.edu.au*

The capacity for olivine to incorporate hydroxyl (OH^-) as a structural component is dictated by the availability of suitable point defect sites at which it can be stored. Therefore, a detailed understanding of how water storage capacity varies within Earth's upper mantle depends critically on our knowledge of how different thermodynamic parameters influence the stability of such point defects in olivine. Previous studies have come to contrasting conclusions regarding how oxygen fugacity, temperature and the presence of trace chemical components such as Al^{3+}, Cr^{3+}, Fe^{3+} and Ti^{4+} control point defect stability (Bai and Kolstedt 1993, Grant et al. 2007, Gaetani et al. 2014). Much of this discrepancy may be ascribed to variable degrees of equilibration between olivine and the imposed thermodynamic conditions of the experiments and/or application of 'bulk' analytical techniques to measure the hydroxyl, such as secondary ion mass spectrometry, which yields limited information on the nature of the different populations of point defects present. Here we present the results of a series of 'hydroxylation' experiments, whose premise is first to impose a point-defect population in natural olivine crystals at high temperatures at atmospheric pressure, before exploiting the rapid diffusion of hydrogen through olivine to decorate the imposed defect population with water at much lower temperatures and 15-25 kb pressure and pH_2O equal to total pressure. Fourier transform infrared spectroscopy is employed to identify the different types of OH^- substitution, and quantify the OH^- concentrations in each substitution mechanism.

Crystallographically-oriented cubes cut from a single San Carlos olivine crystal (Fo_{90}) were annealed at temperatures from 1000 to 1400 °C at atmospheric pressure, at oxygen fugacities (fO_2) from FMQ-3 to FMQ+2 and in the presence of enstatite or magnesiowüstite powders (high and low silica activity respectively). Annealed and un-annealed cubes were then hydroxylated together for 1-10 days under water-saturated conditions at 800-900 °C, 15-25 kb, with silica activity also buffered by enstatite or magnesiowüstite and fO_2 buffered by standard univariant equilibria (Ni-NiO, Re-ReO_2) or with graphite at the H_2O maximum.

Infrared spectra of hydroxylated olivines reveal the four defect sites characteristic of upper mantle olivine. The successful preservation of the pre-annealed defect structure is confirmed through spectral differences between equilibrium olivine crystallised from the buffer and the

hydroxylated cube, and through minimal differences in infrared peak positions and total absorbance of the olivine cubes when different silica activities and fO_2 are used in the hydroxylation stage. Variations in the temperature and oxygen fugacity of the pre-anneal stage impacts significantly the amount of water stored by olivine. Hydrous defects associated with Mg vacancies, Si vacancies and trivalent cations all increase in concentration with increasing oxygen fugacity within the limits FMQ-2 to +2, beyond which concentrations are constant. Concentrations of hydrous defects correlate positively with anneal temperature, such that for olivines equilibrated at conditions at or below 1100 ºC and oxygen fugacity equivalent to FMQ negligible hydroxyl is present. Varying pressure from 15 to 25 kb has no discernible effect on OH^- concentration, at least within this range. Future work will address the effects of elevated pressures at the annealing stage, and look at olivines of different compositions.

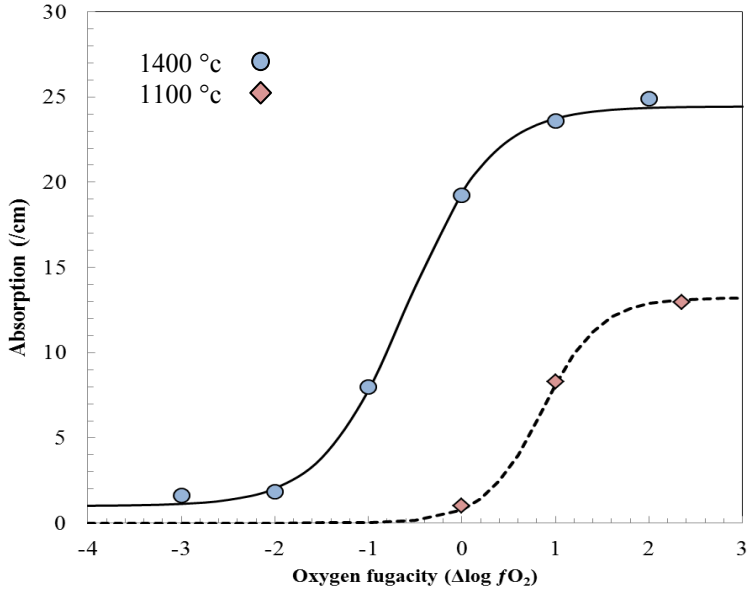

Absorbance associated with the trivalent cation point-defect, measured parallel to the c axis, for San Carlos olivine cubes annealed at 1400 ºC and 1100 ºC and various oxygen fugacity (fO_2) in the first stage, and hydroxylated at 800 °C, 15 kb and fO_2 equivalent to Ni-NiO

References

Bai Q., Kolstedt D.L., (1993) - Effects of Chemical Environment on the Solubility and Incorporation Mechanism for Hydrogen in Olivine. *Physics and Chemistry of Minerals*, 19, 460-471.

Gaetani G., O'Leary J.A., Koga K.T., Hauri E.H., Rose-Koga E.F., Monteleone B.D., (2014) - Hydration of mantle olivine under variable water and oxygen fugacity conditions. *Contributions to Mineralogy and Petrology*, 167, 965-979.

Grant K.J., Brooker R.A., Kohn S.C., Wood B.J., (2007) - The effect of oxygen fugacity on hydroxyl concentrations and speciation in olivine: Implications for water solubility in the upper mantle. *Earth and Planetary Science Letters,* 261, 217-229.

Periodico di Mineralogia, ECMS 2015, 175

PERIODICO di MINERALOGIA
established in 1930

An International Journal of
MINERALOGY, CRYSTALLOGRAPHY, GEOCHEMISTRY, ORE DEPOSITS, PETROLOGY, VOLCANOLOGY
and applied topics on *Environment*, *Archaeometry* and *Cultural Heritage*

2D mapping of Iron content, oxidation state and local structure by XANES: an application to natural volcanic glasses

Angela Trapananti[1], Gabriele Giuli[2,*], Maria Rita Cicconi[2], Eleonora Paris[2] and Francesco D'Acapito[1]

[1] CNR-IOM-OGG, European Synchrotron Radiation Facility, 71 avenue des Martyrs, 38043 Grenoble, France
[2] University of Camerino, School of Science and Technology, Geology Division, 62032 Camerino, Italy
*Corresponding author: *gabriele.giuli@unicam.it*

XANES imaging by collecting several X-ray fluorescence maps at various excitation energies across the absorption edge of a given element is a powerful tool for the characterization of heterogeneous samples such as rocks or cultural heritage artefacts. Examining the fluorescence yield at different energies can differentiate the oxidation state and/or the speciation at every pixel in the image. In fluorescence detection, even the chemical state of trace elements with concentration in the ppm range can be studied. We will report on XANES imaging experiments performed at the Italian beamline BM08 of the European Synchrotron Radiation Facility on thin sections of natural volcanic glasses from Pantelleria Island (Italy). By using a beam size of 200μm × 200μm we collected X-ray fluorescence maps at different energies across the Fe *K*-edge.

From the analysis of maps collected above the absorption edge and on selected features of the XANES such as the edge and pre-edge peak, we obtained qualitative information on the spatial distribution of iron in the sample as well as on variations of the Fe oxidation state and local symmetry within the sampled area. After the two-dimensional elemental and chemical mapping, full XANES spectra were collected in selected points in order to extract quantitative information on the Fe oxidation state and coordination from the pre-edge peak fitting (Giuli et al., 2011). Experiments with a probe size such as that currently available at BM08 beamline find applications for the characterization of cm-sized zones of samples for which the spatial resolution achieved with extreme micro-beams is not needed.

References

Giuli G., Paris E., Hess K.U., Dingwell D.B., Cicconi M.R., Eckhout S.G., Fehr K.T. and Valenti P. (2011) - XAS determination of the Fe local environment and oxidation state in phonolite glasses. *American Mineralogist*, 96, 631-636.

Periodico di Mineralogia, ECMS 2015, 177-178

PERIODICO di MINERALOGIA
established in 1930

An International Journal of
MINERALOGY, CRYSTALLOGRAPHY, GEOCHEMISTRY,
ORE DEPOSITS, PETROLOGY, VOLCANOLOGY
and applied topics on *Environment*, *Archaeometry* and *Cultural Heritage*

Structural complexity and polymorphism in borates

Olga S. Tyumentseva[1,*] and Sergey V. Krivovichev[1]

[1] St. Petersburg State University, Department of Crystallography, St. Petersburg, Russia
* Corresponding author: *o-tyumentseva@mail.ru*

Complexity is an important characteristic of crystal structures. Quantification of crystal-structure complexity using information theory (Krivovichev, 2012a, 2012b, 2013, 2014) allows both size- and symmetry-dependent properties of complex structures to be evaluated. The most obvious application of complexity measures (structural information content (I_G), total information content ($I_{G,total}$), information density (ρ_{inf})) is to compare the complexity of polymorphs of the same compound. The aim of this research is to obtain information-based complexity parameters of particular borate structures and their systematic investigation. The variation of the information along the path of phase transitions induced by changing pressure and temperature has been considered.

To date more than 1800 borates can be found in the ICSD (Inorganic Crystal Structure Database). The 108 borate structures with polymorphs were taken into account. Information based complexity parameters have been calculated for the borates extracted from the ICSD (Database 2012-1) using the TOPOS software (Blatov, 2000). Some examples of the investigated borate structures are provided in the Table below.

Table – The values of complexity parameters for the selected crystal structures of borates.

Compound	PI*	ICSD code	Space group	I_G, bits/atom	$I_{G,total}$, bits/u.c.	ρ_{inf}, bits/Å^3
B_2O_3	I, α	51575	$P3_121$	1.522	22.829	0.168
	II, β	34685	$Ccm2_1$	1.522	15.219	0.102
$Na_2B_4O_7$	α	2040	P-1	4.700	244.423	0.415
	HP	423429	$P3_221$	4.362	510.392	0.469
	γ	250194	P-1	5.285	412.261	0.522
$SrGaBO_4$	α	98932	$Pccn$	2.807	157.212	0.198
	β	51912	$P2_12_12$	3.807	213.212	0.261
$Ba_3Y(BO_3)_3$	α	99180	$P6_3cm$	3.740	359.020	0.265

Compound	PI*	ICSD code	Space group	I_G, bits/ atom	$I_{G,total}$, bits/u.c.	ρ_{inf}, bits/Å^3
	β	99537	*R*-3	2.577	82.451	0.059
CaB_2O_4	I	34641	*Pbcn*	1.950	54.606	0.177
	II	20097	*Pccn*	2.807	157.212	0.271
	III	23240	*Pna*2_1	4.392	368.955	0.449
	IV	23241	*Pa*3-	2.081	174.837	0.239
$Sr_2Cu(BO_3)_2$	α	202934	*P*2_1/*c*	2.550	56.107	0.208
	β	202935	*Pnma*	3.823	336.430	0.302
BiB_3O_6	α	48025	*C*2	2.522	25.219	0.113
	β	152400	*P*2_1/*n*	3.322	132.877	0.321
	γ	152401	*P*2_1/*n*	3.322	132.877	0.366
	δ	416822	*Pca*2_1	3.322	132.877	0.378
	ε	173746	*C*1	3.322	33.219	0.186
$Co_3B_7O_{13}I$	HT	201346	*F*4-3*c*	2.063	99.020	0.056
	LT	72828	*Pca*2_1	4.585	440.156	0.493
$KBe_2B_3O_7$	α	248202	*C*2/*c*	2.931	76.211	0.136
	β	248203	*Pmn*2_1	4.008	208.423	0.357
	γ	248204	*P*1211	5.285	412.261	0.478

PI* – polymorphic identification

The fact that complexity is a function of both information content and unit-cell volume makes it dependent upon temperature and pressure. Based on our observations the obviousness of the general trend of increasing structural complexity with the decreasing temperature and moderately increasing pressure can be assumed. However, under ultra-high pressures, the situation may be drastically different. The influence of high-temperature/high-pressure conditions on the formation of borates has not been studied completely. Overall, it can be concluded that more work is needed in order to investigate relations between temperature, pressure and structural complexity and their roles played in crystallization, stability and transformations of borates that can be performed on an example of other groups of inorganic compounds.

References

Blatov V.A., Shevchenko A.P., Serezhkin V.N. (2000) - TOPOS 3.2: a new version of the program package for multipurpose crystal-chemical analysis. *Journal of Applied Crystallography*, 33, 1193.

Krivovichev S.V. (2012a) - Topological complexity of crystal structures: quantitative approach. *Acta Crystallographica*, A68, 393-398.

Krivovichev S.V. (2012b) - Information-based measures of structural complexity: application to fluorite-related structures. *Structural Chemistry*, 23, 1045-1052.

Krivovichev S.V. (2013) - Structural complexity of minerals: information storage and processing in the mineral world. *Mineralogical Magazine*, 77, 275-326.

Krivovichev S.V. (2014) - Which inorganic structures are the most complex? Angewandte Chemie International Edition, 53, 654-661.

Periodico di Mineralogia, ECMS 2015, 179-180

PERIODICO di MINERALOGIA
established in 1930

An International Journal of
MINERALOGY, CRYSTALLOGRAPHY, GEOCHEMISTRY,
ORE DEPOSITS, PETROLOGY, VOLCANOLOGY
and applied topics on *Environment*, *Archaeometry* and *Cultural Heritage*

Deconvolution of instrumental broadening: A simple numerical approximation

Tamás Váczi

Department of Mineralogy, Eötvös Loránd University, Budapest, Hungary
Corresponding author: *vaczitamas@caesar.elte.hu*

This contribution presents a new, very simple yet precise numerical method to obtain the Lorentzian full width at half maximum (FWHM) from fitted Voigt or pseudo-Voigt FWHMs using a known instrument bandpass. The method is applicable for any dispersive optical spectrometer. The main advantages are good precision, unlimited applicability and the simplicity of the mathematical expression compared to previous solutions.

The deconvolution of instrumental influences in experimentally determined band profiles is an important aspect of quantitative or semi-quantitative Raman and photoluminescence (PL) spectroscopic analysis. Narrow-band spectroscopic signals that are of similar width as the instrument resolution (bandpass) are significantly broadened by light passing through optical slits (Fig. 1A). The pure instrumental contribution typically has a profile that is best approximated by a Gaussian function, whereas the Raman and PL spectroscopic signal is most often Lorentzian. The observable profile shape is the convolution of these two, which is described by the Voigt function.

The analytically correct Voigt deconvolution procedure is mathematically demanding, therefore it is typically not included in the software bundled with spectroscopic instruments. The widely available pseudo-Voigt function (a weighted linear combination of Gaussian and Lorentzian functions of the same FWHM) is a good approximation for the band shape and its convoluted width, but the formula is not suitable for an estimation of the FWHM of the pure contributions. Numerical methods approximating an analytical solution to Voigt deconvolution (Váczi 2014 and references therein) are very practical for individual bands in single spectra and for large datasets (e.g. maps created from fitted FWHMs) as well.

The new method employed an extended dataset of Gaussian, Lorentzian and associated Voigt FWHMs calculated analytically with eight-digit precision. In order to substitute the deconvolution procedure with a simple subtraction, the difference between the Voigt, or "experimental", FWHM (w_V) and the pure physical Lorentzian FWHM (w_L) was approximated, for which the knowledge of the Gaussian bandpass (w_G) was necessary. The calculated datasets allowed plotting values of ($w_V - w_L$) against w_V for several fixed w_G values, in which a normal-

ization by w_G (Fig. 1B) proved to benefit the fitting procedure greatly. The dose response function, also referred to as a four-parameter logistic (4PL) function, was empirically chosen to fit the $(w_V - w_L)/w_G$ vs. $w_V/w_G - 1$ curves. The formulation of the expressions allowed a simplification of the 4PL formula to the following form, using spectroscopic widths:

$$w_V - w_L = \frac{w_G}{1 + \left(\frac{w_V - w_G}{x_0} \right)^p},$$

which reduced the number of fitted parameters to two. With the refined parameters $x_0 = 1.11264$ and $p = 1.01091$, this function gave a very good approximation to the plotted data (Fig. 1B). For the sake of simplicity, these values were approximated by $x_0 \approx {}^{10}/_{9}$ and $p \approx 1$. The expression proposed for the correction of the instrumental broadening thus became

$$w_L \approx w_V - \frac{w_G}{1 + \left(\frac{w_V / w_G - 1}{10/9} \right)} = w_V - \frac{w_G^2}{0.9\, w_V + 0.1\, w_G}.$$

Compared to fitted values, the simplifications decrease the precision of the approximation. Still, the formula is still more than adequate for regular spectroscopic work: the difference between analytical and approximated $(w_V - w_L)$ never exceeds 0.5% of the bandpass (Váczi 2014). The simple formula is easily implemented in spreadsheet and plotting software, and can be used for the fast and precise batch deconvolution of large amounts of FWHM data (e.g. maps).

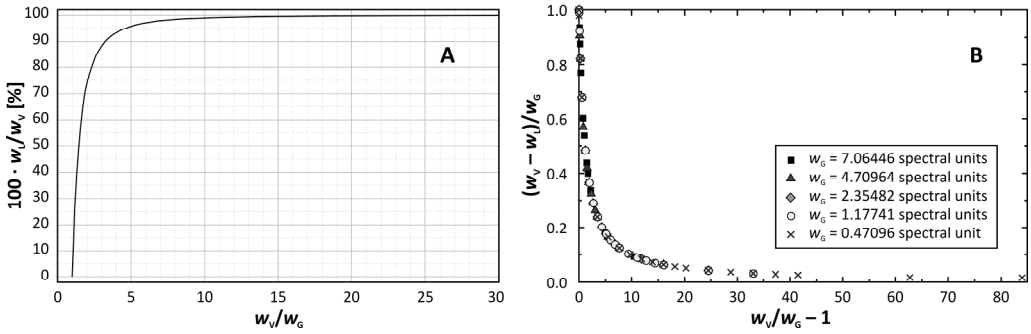

Figure 1. A: Percent Lorentzian contribution in the Voigt FWHM as a function of the bandpass-normalized Voigt FWHM. This chart may be used as a device-independent guide to assess the necessity of deconvolution. **B:** Bandpass-normalized Gaussian contribution in the Voigt FWHM as a function of the bandpass-normalized Voigt FWHM. (Modified from Váczi 2014.)

The financial support of the Research and Instrument Core Facility of the Faculty of Sciences, Eötvös Loránd University, is gratefully acknowledged.

Reference

Váczi T. (2014) – A new, simple approximation for the deconvolution of instrumental broadening in spectroscopic band profiles. *Applied Spectroscopy*, 68, 1274–1278.

Periodico di Mineralogia, ECMS 2015, 181-182

PERIODICO di MINERALOGIA
established in 1930

An International Journal of
MINERALOGY, CRYSTALLOGRAPHY, GEOCHEMISTRY,
ORE DEPOSITS, PETROLOGY, VOLCANOLOGY
and applied topics on *Environment*, *Archaeometry* and *Cultural Heritage*

Electron-beam irradiation of zircon: A discussion of spectroscopic phenomena

Tamás Váczi[1,*] and Lutz Nasdala[2]

[1] Department of Mineralogy, Eötvös Loránd University, Budapest, Hungary
[2] Institute of Mineralogy and Crystallography, University of Vienna, Austria
* Corresponding author: *vaczitamas@caesar.elte.hu*

A systematic, semi-quantitative investigation of the annealing (increase of structural order) in zircon induced by the electron-beam irradiation of zircon was performed previously (Váczi and Nasdala 2012). This study presents the main findings and discusses the properties of low-energy electron-matter interaction and the annealing process in zircon.

The electron microprobe, the most common tool to analyse the chemical composition of geological materials, uses a moderate-energy (typically 15-20 keV) electron beam to excite characteristic X-rays in the sample. The electron beam may cause changes in certain material properties, which are usually termed "beam damage". Electron beam-induced degradation includes a range of phenomena, such as element migration (diffusion), electrolysis, oxidation state changes, heating, reactions induced by electrons etc.

Four zircon samples spanning a wide range of natural self-irradiation levels (ca. 0.9–4.9×10^{18} alpha decay events per gram; Nasdala et al., 2004) were selected for analysis. A fully focused beam (20 kV) in a tungsten-cathode electron microprobe was used for electron irradiation. Beam current (10-200 nA) and irradiation time (10-500 s) were varied. The damage level of analysed points were determined from the fitted, deconvolved Lorentzian full width at half maximum (FWHM) values of the $\nu_3(SiO_4)$ Raman band of zircon (Fig. 1).

There has been no electron beam-induced damage (increase in FWHMs) observed. In any given sample, the observed decrease in FWHM apparently depends on the electron dose, heating effects are therefore excluded. At any given electron dose, the decrease in FWHM depends on the initial FWHM. The rate of the FWHM change flattens at higher doses (Fig. 1). The cross-section of an irradiated spot closely resembles the convolution of the confocal Raman information volume with the interaction volume of the electron beam in zircon (Fig. 2).

The decrease in the observed FWHMs is interpreted as the annealing of defects created by natural alpha decay. The electron beam induces defect reactions that annihilate phonon scattering centres, increasing phonon coherence lengths. The similar evolution of damage annealing across samples (Fig. 1) suggests that broadly similar processes occur in the different samples. The high initial rate of the FWHM change as well as the dependence of the FWHM change on

initial defect densities imply that higher defect concentrations permit more defect reactions. Significant damage remains after our annealing experiments, inferred from the lowest observed FWHM values. The remaining defects are characterised possibly by activation energies too high to be mobilised by the low-energy electrons, or there is a very large number of defects to be moved (amorphous clusters). It is not yet known whether complete annealing is possible with electron beam irradiation due to the limited electron dose range used in this study.

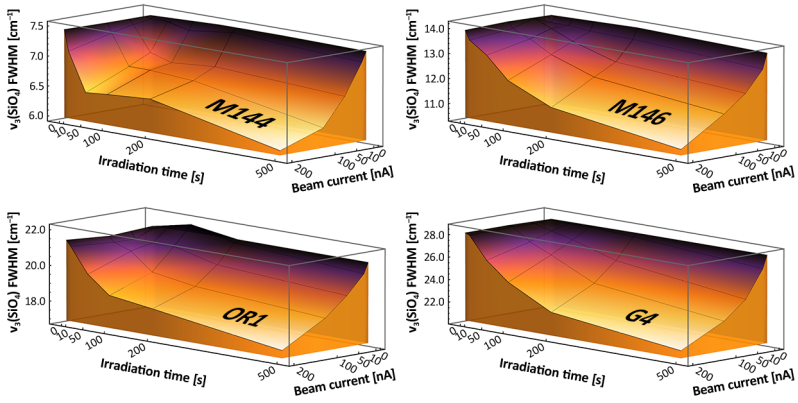

Fig. 1. Deconvolved Lorentzian FWHM of the $\nu_3(SiO_4)$ Raman band of zircon in untreated (back edges) and electron irradiated spots. Note the different *z* scales.

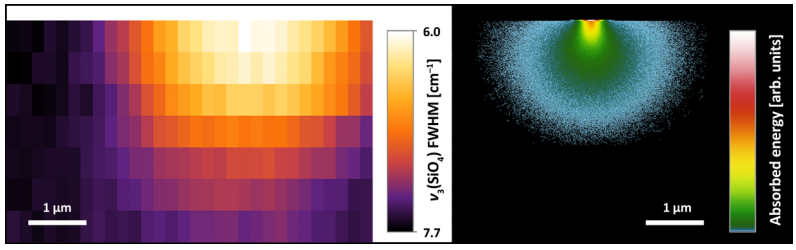

Fig. 2. Left: Raman depth section through an irradiated spot (M144, 200 nA, 500 s). Right: Monte Carlo simulation of absorbed energy from a 20 kV electron beam in zircon. The energy cut-off is at 50 eV.

References

Nasdala L., Reiners P.W., Garver J.I., Kennedy A.K., Stern R.A., Balan E. and Wirth R. (2004) – Incomplete retention of radiation damage in zircon from Sri Lanka. *American Mineralogist*, 89, 219–231.

Váczi T. and Nasdala L. (2012) – Semiquantitative evaluation of damage annealing caused by the electron beam irradiation of zircon. GEORAMAN 10 (Nancy, France) Book of Abstracts, 47–48.

Periodico di Mineralogia, ECMS 2015, 183-184

PERIODICO di MINERALOGIA
established in 1930

An International Journal of
MINERALOGY, CRYSTALLOGRAPHY, GEOCHEMISTRY,
ORE DEPOSITS, PETROLOGY, VOLCANOLOGY
and applied topics on *Environment*, *Archaeometry* and *Cultural Heritage*

The effect of Er:YAG dental laser treatment with low energy on the human tooth apatite studied by Raman and IR reflection micro-spectroscopy

Dimitar Vasilev[1], Galina Jegova[2], Maya Rashkova[2] and Rositsa Titorenkova[1*]

[1] Institute of Mineralogy and Crystallography, Bulgarian Academy of Sciences,
Acad. G. Bonchev Str. 107, Sofia, 1113, Bulgaria
[2] Faculty of Dental Medicine, Medical University Sofia, Georgi Sofiiski Str. 1, Sofia, 1431, Bulgaria
* Corresponding author: *rosititorenkova@dir.bg*

Biological apatite of human teeth enamel before and after dental Er-doped yttrium-aluminum-garnet pulse laser (λ = 2940 nm) treatment was studied by IR reflection and Raman micro-spectroscopy.

Cross-section tooth cuts were prepared by microtome. One side of the slices was subsequently polished by 3, 1 and 0.1 μm polishing suspensions. All samples were irradiated for 10 s along the direction perpendicular to the enamel–dentine junction. The applied energy of dental laser was 100 mJ, while the pulse frequency varied between 10 and 30 Hz. The pulse duration was 50 μs. Laser tip of 1 mm at a distance of 4-5 mm and maximum water-cooling of 39 ml/min were used. The total laser power was bellow ablation threshold. Results from sample treated with minimal energy of 1 W and minimal water cooling of 4 ml/min are also presented for comparison. The samples were examined by SEM to trace the possible changes in the surface layer as a result of dental laser treatment, and the change in chemical composition.

The IR reflectance spectra of untreated enamel reveal gradual change from the surface of the teeth to the enamel-dentine junction that consists in reducing the overall spectral intensity accomplished by a slight intensity ratios change of the characteristic peaks at 1050 and 1095 cm^{-1} (ν_3 PO_4). These spectral changes are due to a gradual increase of the carbonate content in apatite from the surface to dentine, which is also confirmed by the Raman spectra as a decrease of the peak at 1048 cm^{-1} (ν_3 PO_4) with increase of the peak at 1071 cm^{-1} (ν_1 B-type CO_3). The intensity of the Raman peak at 1073 cm^{-1} increase with B-type carbonate substitution which is consistent with the chemical spectral analyzes. Due to inhomogeneity of the enamel we consider the whole profile changes upon dental laser irradiation. The results reveal that the Er:YAG irradiation with energy 100 mJ and pulse frequency 10 Hz do not cause any visible morphological, structural and compositional changes when maximum water cooling was applied (Figure

1a and Figure 2a). However, lack of sufficient cooling at the same other laser and experimental parameters causes discloser of apatite rods (Figure 1b).

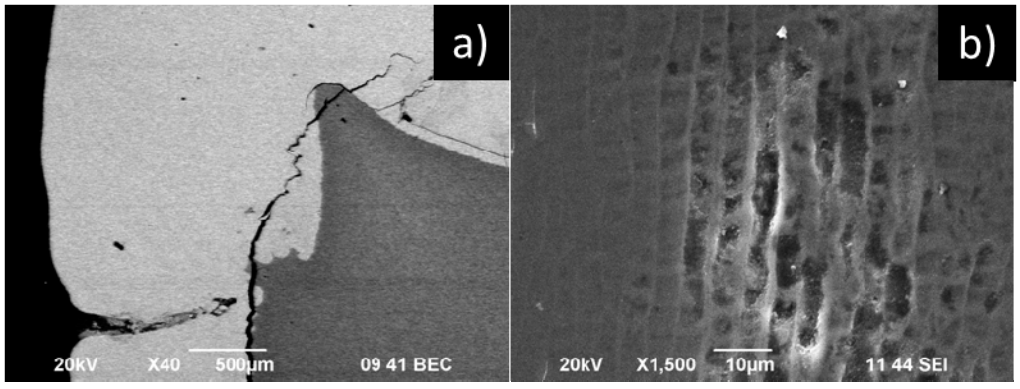

Figure 1. SEM images of Er-YAG treated sample with energy 100 mJ/10 Hz: a) with maximal water cooling of 39 ml/min and b) with minimal water cooling of 4 ml/min.

Using pulse frequency of 30 Hz also causes some superficial lesions and structural alterations stronger in the inner regions of the enamel. These changes are detected by the increase in the intensity of the peaks of the phosphate groups (ν_3 PO_4) collected from the internal areas of enamel as compared with the spectra of surface enamel (Figure 2b). Possible reasons will be discussed.

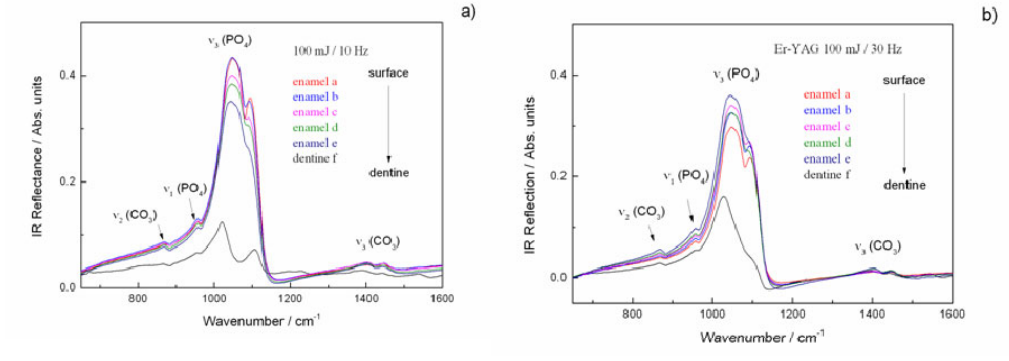

Figure 2. IR reflection spectra of Er:YAG laser irradiated enamel from the surface to the enamel-dentine junction: a) 100 mJ/10Hz and b) 100 mJ/30Hz.

Periodico di Mineralogia, ECMS 2015, 185-186

PERIODICO di MINERALOGIA
established in 1930

An International Journal of
MINERALOGY, CRYSTALLOGRAPHY, GEOCHEMISTRY,
ORE DEPOSITS, PETROLOGY, VOLCANOLOGY
and applied topics on *Environment*, *Archaeometry* and *Cultural Heritage*

Crystal structure of synthetic Ga, Fe-bearing tourmaline: SREF, EMPA and MS

Oleg S. Vereshchagin[1,*], Tatiana V. Setkova[2], Dina V. Deyneko[3], Konstantin V. Pokholok[3] and Ira V. Rozhdestvenskaya[1]

1 Department of Crystallography, Saint Petersburg State University, Universitetskaya nab. 7/9, Saint Petersburg, Russia
2 Institute of Experimental Mineralogy RAS, Institutskaya 4, Chernogolovka, Russia
3 Department of Chemistry, Lomonosov Moscow State University, Leninskie Gory 1–3, Moscow, Russia
*Corresponding author: *e-mail oleg-vereschagin@yandex.ru*

Tourmaline is a large supergroup of minerals having a complex composition of the general formula $XY_3Z_6(T_6O_{18})(BO_3)_3V_3W$ (Henry et al., 2011), where X = Ca, Na, K, □(vacancy); Y = Li, Mg, Fe, Al; Z = Mg, Al, Fe; T = Si, Al, B; V = OH, O; W = OH, F, O (typical space group $R3m$). Tourmaline is an indicator of the environmental conditions in its host (due to compositional sensitivity; Hinsberg et al., 2011). The tourmaline crystals possesses by valuable pyro and piezoelectric properties. Preparation of synthetic analogues of tourmaline makes it possible to study compositions, which do not occur in nature (simple compounds, high concentrations of cations; Setkova et al., 2011), and to detect crystal chemical patterns and structure-property correlations. Also synthesis of structural analogues of natural minerals in which Al and Si are substituted by Ga and Ge can reduce significantly the temperature and pressure of the process and improve functional properties. The present study is a part of our research on the crystal chemistry of tourmalines containing transitional metals (Rozhdestvenskaya et al., 2012; Vereshchagin et al., 2013).

Synthesis. Studies were performed under thermogradient conditions using chromium-nickel alloy autoclaves at temperature of 450-650° C and pressure of 100 MPa in boric-alkaline hydrothermal solutions. The duration of the runs was 14 days. Plates made from natural tourmaline crystals were used as seed crystals. Single crystals of quartz and corundum with addition of gallium oxide was used as charge material.

Electron microprobe analysis (EMPA). The chemical composition of the single crystal used for the structure refinement was analysed with a wavelength-dispersive EDX - AzTec Energy 35 using an automated Hitachi S-3400N electron microscope at the Geomode Center of Research park of Saint Petersburg State University (analyst V. Shilovskih).

Single-crystal structure refinement (SREF). X-ray data were collected using an X-ray single-crystal automatic diffractometer Agilent Technologies «Xcalibur» in the 6–76° 2θ range

applying MoK_α radiation at the Center for X-ray Diffraction Methods of Research park of Saint Petersburg State University. Intensities were corrected for the Lorentz and polarization factors. Crystal structure refinement was done in the space group *R*3*m* using reflections with $F > 4\sigma(F)$, the method of alternating least squares (taking into account the anisotropy of the displacement parameters of atoms) and analysis of differential Fourier maps using a CSD software package (Akselrud et al., 1989).

Mössbauer spectroscopy (MS). Mössbauer spectroscopy experiments were performed in transmission geometry using a constant acceleration Mössbauer spectrometer coupled with a 1024 multichannel analyzer. A ^{57}Co/Rh γ-ray source was used. The velocity scale was calibrated relative to α-Fe. All isomer shift values (δ) given hereafter are referred to α-Fe. Experiment was performed at 10 K and 300 K. The absorber consisted of ~1 mg mixture powdered of crystal and BN. Data collection time was 73 hours. Spectra treatment was performed using "UnivemMS" 20 and custom software.

Results. The Ga, Fe-rich tourmaline was grown on natural elbaite seed for the first time; the thickness of newly formed layer was up to 100 μm. In addition, Ga-rich tourmaline fine long prismatic crystals of spontaneous nucleation (10-100 μm in size) were observed on surface of the seed crystals and in the charge. According to MS iron cations are present in both the octahedrally coordinated sites (*Y* and *Z*) in the two valence states (Fe^{2+}, Fe^{3+}). The spectrum of the sample was fitted with four doublets with δ of 1.10, 1.09, 0.39 and 0.26 mm s^{-1} The crystal structure of synthetic Ga, Fe-rich tourmaline crystals of spontaneous nucleation with a gallium content of 24.50 wt. % GaO [a = 15.9999(4) Å, c = 7.2570(3) Å] has been refined to *R*-index of 3.2 %. It has been shown that Ga atoms are distributed not only over *Y*, but also over *Z* sites according to the empirical structural formula:

$(Na_{0.95}\square_{0.05})^{Y}(Ga_{1.37}Fe^{2+}_{0.66}Al_{0.45}Fe^{3+}_{0.26}Ni_{0.26})^{Z}(Ga_{1.87}Al_{3.29}Fe^{3+}_{0.45}Fe^{2+}_{0.39})(Si_{5.85}Al_{0.15}O_{18})(BO_3)_3{}^{V+W}[(OH)_{2.31}O_{1.69}]$.

This work was supported by the Russian Foundation for Basic Research (projects 14-05-31369 mol_a) and Saint Petersburg State University (grant 3.38.243.2015).

References

Akselrud L.G., Grin Yu.N., Zavalij P.Yu., Pecharsky V.K. and Fundamenskii, V.S. (1989) - CSD - Universal program package for single crystal and/or powder structure data treatment. 12th European crystallographic meeting: Abstract of papers, Moscow, 3, 155.

Henry D.J., Novák M., Hawthorne F.C., Ertl A., Dutrow B., Uher P. and Pezzotta F. (2011) - Nomenclature of the tourmaline-supergroup minerals. *American Mineralogist*, 96, 895-913.

Rozhdestvenskaya I.V., Setkova T.V., Vereshchagin O.S., Shtukenberg A.G. and Shapovalov Yu.B. (2012) - Refinement of the Crystal Structures of Synthetic Nickel- and Cobalt-Bearing Tourmalines. *Crystallography Reports*, 57(1), 57-63.

Setkova T., Shapovalov Yu. and Balitsky V. (2011) - Growth of tourmaline single crystals containing transition metal elements in hydrothermal solutions. *Journal of Crystal Growth,* 318, 904-907.

van Hinsberg V.J., Henry D.J. and Marschall H.R. (2011) - Tourmaline: An ideal indicator of its host environment: An introduction. *Canadian Mineralogist*, 49, 1-16.

Vereshchagin O.S, Rozhdestvenskaya I.V, Frank-Kamenetskaya O.V, Zolotarev A.A. and Mashkovtsev R.I. (2013) - Crystal chemistry of Cu-bearing tourmalines. *American Mineralogist*, 98, 1610-1616.

Periodico di Mineralogia, ECMS 2015, 187-188

PERIODICO di MINERALOGIA
established in 1930

An International Journal of
MINERALOGY, CRYSTALLOGRAPHY, GEOCHEMISTRY, ORE DEPOSITS, PETROLOGY, VOLCANOLOGY
and applied topics on *Environment*, *Archaeometry* and *Cultural Heritage*

Versatile high-sensitive appliance for analysis of spectrally resolved thermoluminescence in meteorites

Alexander S. Vokhmintsev and Ilya A. Weinstein*

Ural Federal University, NANOTECH Centre, Mira street 19, Ekaterinburg, Russia, 620002
* Corresponding author: *i.a.weinstein@urfu.ru*

Thermoluminescence (TL) spectroscopy is a well-proven experimental method for studying the spectral characteristics and kinetic mechanisms of radiation-stimulated processes in irradiated materials. In practice, various techniques, involving TL, are applied in archaeological and geological dating, commercial systems for dose monitoring and to solve specific problems of solid-state dosimetry of ionizing radiation. Besides, TL research provides powerful tools for characterizing thermal history, possible impact events, metamorphic processes and dominant type of silicates in extraterrestrial matter (Sears et al., 2013). One of the challenges in the study of spectral properties of meteorites is the low intensity of natural TL. In this case, as a rule, integral luminescent response is detected over a wide wavelength range. Such method is not always effective for meteorites characterized by simultaneous emissions in different bands (Biswas et al., 2011; Popova et al., 2013). Consequently, natural and laboratory TL spectral features cannot be analyzed at the required spectral resolution. Recently, we have developed a high-temperature accessory module for commercial fluorescence spectrometers and tested its performance in the room temperature (RT) – 773 K range (Vokhmintsev et al., 2014, 2015). In the present work we demonstrate the capabilities of our original high-temperature module by measuring spectrally resolved characteristic features of thermoluminescence in stony meteorites. Several fragments of Tsarev L5 and Chelyabinsk LL5 chondrites have been studied. The core of the meteorites was separated from the fusion crust and crushed into micropowder, which was treated in hydrochloric acid to remove metal particles. Luminescence measurements of the samples were carried out in phosphorescence regime using a LS55 Perkin Elmer spectrometer with our original heating accessory module (Vokhmintsev et al., 2014). The glow curves of the natural and laboratory TL were registered in the 440 ± 20 nm band within the range of RT – 873 K with $r = 2$ K/s. To excite laboratory TL response the samples were irradiated at UELR-10-15S linear accelerator with 10 MeV electrons. The radiation dose was 9.1 kGy. The TL spectra were measured in 300 – 700 nm range with scanning speed 800 nm/min and linear heating rate of $r = 0.5$ K/s.

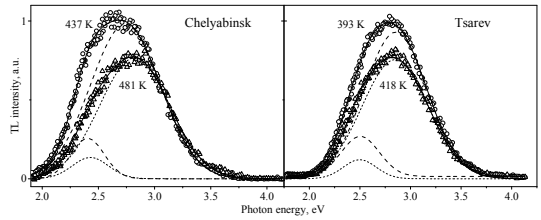

Figure 1. TL spectra for Chelyabinsk and Tsarev meteorites at different temperatures. Symbols – experiment; dash lines – Gaussians components for 437 and 393 K; short dash lines – Gaussians components for 481 and 418 K; solid lines – resulting approximation.

The TL spectra for the meteorites under investigation show (Figure 1) a wide band in the visible range, which is approximated by superposition of two Gaussians with maximum energies of 2.83 ± 0.05 and 2.45 ± 0.05 eV, half-widths of 0.73 ± 0.05 and 0.40 ± 0.05, respectively. For shown temperatures the 2.83 eV band dominates the TL emission with 4 - 6 times higher intensity than the 2.45 eV component. The natural TL response in Chelyabinsk LL5 chondrite is characterized by a peak in the 400 – 520 K range with a high-temperature shoulder at 520-750 K. These parameters are similar to the main TL peak in Dhajala meteorite (Biswas et al., 2011). The intensity varies by a factor of 2 –10 and the peak maximum shifts from 427 to 487 K for different samples. This can be due to inhomogeneous mineral phases or mineral compositions, or differences in irradiation doses in space (Sears et al., 2013). We found that the natural TL response of Tsarev L5 chondrite exhibits a low intensity peak with a maximum temperature T_{max} = 490 K and half-width ω_T = 60 K. In addition, we observed that, depending on the storage time, the laboratory TL maximum shifted to lower temperatures from 408 ± 5 to 394 ± 5 K and the half-width narrowed from 86 ± 5 to 62 ± 5 K. The observed TL faded 45% within 3 days of storage. This study demonstrated that thermoluminescence in Tsarev L5 and Chelyabinsk LL5 chondrites with dark-colored lithology (Weinstein et al., 2014) was characterized by similar spectral properties.

This work was supported in part by grant of the President of Russian Federation MK-5729.2015.2.

References

Biswas R.H., Morthekai P., Gartia R.K., Chawla S. and Singhwi A.K. (2011) - Thermoluminescence of the meteorite interior: A possible tool for the estimation of cosmic ray exposure ages. *Earth and Planetary Science Letters*, 304, 36–44.

Popova O.P. et al. (2013) - Chelyabinsk airburst, damage assessment, meteorite recovery, and characterization. *Science*, 342, 1069–1073.

Sears D.W.G., Ninagawa K. and Singhvi A.K. (2013) - Luminescence studies of extraterrestrial materials: Insights into their recent radiation and thermal histories and into their metamorphic history. *Chemie der Erde*, 73 (1), 1–37.

Vokhmintsev A.S., Minin M.G., Chaykin D.V. and Weinstein I.A. (2014) - A high-temperature accessory for measurements of the spectral characteristics of thermoluminescence. *Instruments and Experimental Techniques*, 57, 369–373.

Vokhmintsev A.S., Minin M.G., Henaish A.M.A. and Weinstein I.A. (2015) - Spectrally resolved thermoluminescence measurements in fluorescence spectrometer. *Measurement*, 66, 90–94.

Weinstein I.A., Vokhmintsev A.S., Ishchenko A.V. and Grochovsky V.I. (2014) - Luminescence characterization of different lithologies in Chelyabinsk LL5 chondrite. *Meteoritics & Planetary Science,* 49, A428.

Periodico di Mineralogia, ECMS 2015, 189-191

PERIODICO di MINERALOGIA
established in 1930

An International Journal of
MINERALOGY, CRYSTALLOGRAPHY, GEOCHEMISTRY,
ORE DEPOSITS, PETROLOGY, VOLCANOLOGY
and applied topics on *Environment*, *Archaeometry* and *Cultural Heritage*

Polarized IR and Raman spectra of the OH-dipole in zoisite

Franz A. Weis[1,2*], Peter Lazor[2] and Henrik Skogby[1]

[1]Naturhistoriska Riksmuseet, Department of Geosciences SE-114 18 Stockholm, Sweden
[2]Department of Earth Sciences, Uppsala University, SE-75236 Uppsala, Sweden
* Corresponding author: *franz.weis@nrm.se*

The crystal chemistry, structure and optical properties of the hydrous silicate mineral zoisite ($Ca_2Al_3Si_3O_{12}(OH)$) have by now been well established using a variety of analytical methods (e.g. Dollase, 1968; Linke, 1970; Langer and Raith, 1974; O'Leary et al., 2007). In particular, focus has also been put on the position and orientation of the OH-dipole within the mineral, which has been identified to be oriented approximately parallel to the c-axis forming a hydrogen bridge O(10)-H···O(4) (e.g. Linke, 1970; Langer and Raith, 1974; Langer and Lattard, 1980; Winkler et al., 1989). A common method to investigate hydroxyl groups within minerals is Fourier Transformed Infrared Spectroscopy (FTIR). Up to date, however, no polarized IR spectra to confirm the orientation of the OH-dipole in zoisite have been published. We present new polarized FTIR as well as Raman spectra on the dipole orientation in a gem quality crystal of zoisite whose crystallographic orientation has been determined using X-ray diffraction. For both, FTIR and Raman analysis, a strong vibrational OH-band at 3150 cm^{-1} (cf. Langer and Raith, 1974; Langer and Lattard, 1980; Winkler et al., 1989) is present in the c-axis direction. This OH-band attenuates or disappears entirely in the a- and b-axis directions of the crystal (Fig. 1a,b). Raman analysis revealed an additional OH-band at 3500 cm^{-1} which was present in all three directions. The high intensity of the band at 3150 cm^{-1} along the c-axis direction supports the orientation of the dipole parallel to that axis. The weak appearance of this OH-vibration in FTIR measurements along the a-axis direction, however, suggests a slight offset to the c-axis. This is expected (Dollase, 1968), since the hydrogen bridge O(10)-H···O(4) deviates by ~7.3° from the c-axis towards the a-axis (Fig. 2). Our results not only provide new insights into the OH-dipole orientation in zoisite but also extend the available spectroscopic data for this mineral.

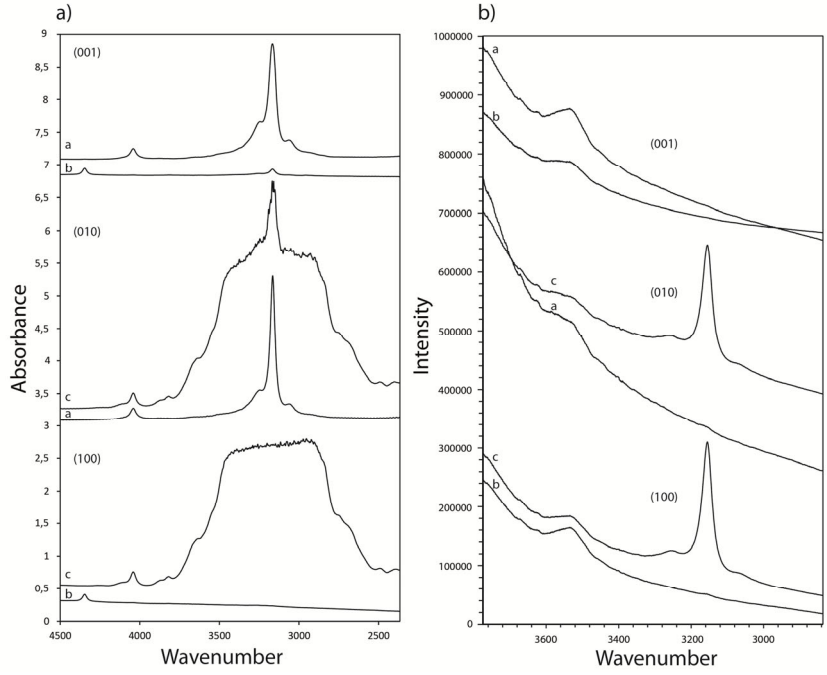

Figure 1 a) Polarized FTIR spectra along the a, b and c axis of our gem quality zoisite crystal. The main peak at 3150 cm^{-1} along the c-axis is strongly truncated due to excessive absorption, but indicates the orientation of the OH-dipole in this direction. A small deviation from c in the a direction is indicated by the same peak. b) Polarized Raman spectra showing the same peak behavior as for IR-measurements. An additional peak at 3550 cm^{-1} is observed. Thicknesses of crystal sections: (100) 165µm, (010) 165µm, (001) 145µm.

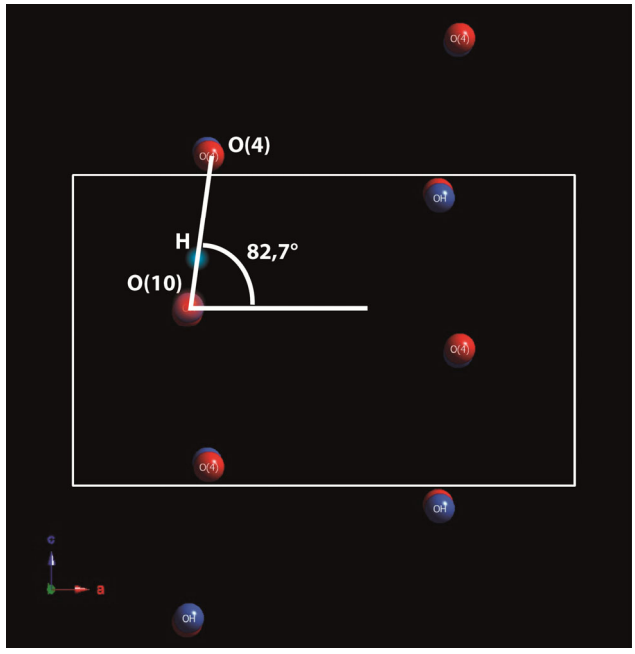

Figure 2. The dipole orientation and hydrogen bridge within the crystal structure of zoisite. A small deviation from the c-axis is expected which is reflected in the polarized spectra.

References

Dollase W.A. (1968) - Refinement and comparison of the structures of zoisite and clinozoisite. *American Mineralogist*, 53, 1882-1898.

Hurblut C.S. (1969) - Gem zoisite from Tanzania, *American Mineralogis*, 54, 702-709.

Langer K. and Raith, M. (1974) - Infrared spectra of A1-Fe(III)-epidotes and zoistes, $Ca_2(Al_{1-p}Fe^{3+}_p)Al_2O(OH)[Si_2O_7][SiO_4]$. *American Mineralogist*, 59, 1249-1258.

Langer K. and Lattard D. (1980) - Identification of a low energy OH valence vibration in zoisite. *American Mineralogist*, 65, 779-783.

Linke W. (1970) - Messungen des Ultrarot-Pleochroismus von Mineralen. X. Der Pleochroismus der OH^-Streckfrequenz in Zoisit. *Tschermaks Mineralogische und Petrographische Mitteilungen*, 14, 61-63.

O'Leary J. A., Rossman G. R. and Eiler J. M. (2007) - Hydrogen analysis in minerals by continuous-flow mass spectrometry. *American Mineralogist*, 92, 1990-1997.

Winkler B., Langer K. and Johannsen P.G. (1989) - The Influence of Pressure on the OH Valence Vibration of Zoisite - An Infrared Spectroscopic Study. *Physics and Chemistry of Minerals*, 16, 668-671.

Periodico di Mineralogia, ECMS 2015, 193-194

PERIODICO di MINERALOGIA
established in 1930

An International Journal of
MINERALOGY, CRYSTALLOGRAPHY, GEOCHEMISTRY,
ORE DEPOSITS, PETROLOGY, VOLCANOLOGY
and applied topics on *Environment*, *Archaeometry* and *Cultural Heritage*

Concentration self-quenching effect of Er^{3+} in mixed-framework barium rare-earth sorosilicates

Maria Wierzbicka-Wieczorek[1,*], Uwe Kolitsch[2,3], Christoph Lenz[3] and Gerald Giester[3]

[1] Friedrich-Schiller University Jena, Department of Mineralogy, Institute for Geosciences, Carl-Zeiss Promenade 10, Jena, Germany
[2] Natural History Museum, Department of Mineralogy and Petrography, Burgring 7, Vienna, Austria
[3] University of Vienna, Institute of Mineralogy and Crystallography, Geocentre, Althanstraße 14, Vienna, Austria
* Corresponding author: *maria.wierzbicka-wieczorek@uni-jena.de*

Mixed-framework sorosilicates containing trivalent lanthanide cations may possess not only zeolitic properties but also show strong photoluminescence (PL) (De Hair, 1980; Liu et al., 2008; Liu et al., 2013; Zhang et al., 2013; Xia et al., 2013). However, the concentration of the Ln^{3+} ion in the respective crystal structure has a significant effect on the intensity of the PL emission (concentration self-quenching). Here we present the PL properties of two flux-grown Er-doped Ba-Y-sorosilicates, $BaY_{1.3}Er_{0.7}(Si_3O_{10})$ and $BaY_3Er(Si_2O_7)(Si_3O_{10})$, and the flux-grown pure Er counterpart of the latter, $BaEr_4(Si_2O_7)(Si_3O_{10})$. Their crystal structures $P2_1/m$ are related to each other (Kolitsch et al., 2006; Wierzbicka-Wieczorek et al., 2013) and contain identical cationic crystallographic environments, namely, eight-fold coordinated Ba sites and octahedrally coordinated REE sites [one in $BaY_{1.3}Er_{0.7}(Si_3O_{10})$ and two in the mixed sorosilicates]. This allows a comparison of the intensity of the laser-induced PL emission spectra of these silicates with respect to the amount of Er^{3+} present.

Figure 1 shows characteristic emission bands of Er^{3+} in the green-yellow visible range (between 540 and 570 nm), which can be associated in all three sorosilicates with the $^4S_{3/2} \rightarrow {}^4I_{15/2}$ transition. In both doped silicates, $BaY_{1.3}Er_{0.7}(Si_3O_{10})$ and $BaY_3Er(Si_2O_7)(Si_3O_{10})$, the emission intensity is almost the same, with just a slightly higher intensity in the latter. The amount of Er^{3+} on the two Y sites is lower in $BaY_3Er(Si_2O_7)(Si_3O_{10})$ (Er:Y = 25:75) than in $BaY_{1.3}Er_{0.7}(Si_3O_{10})$ (Er:Y = 35:65). The strongly diminished intensity of the main $^4S_{3/2} \rightarrow {}^4I_{15/2}$ transition in $BaEr_4(Si_2O_7)(Si_3O_{10})$ is due to the full substitution by Er^{3+}, i.e. caused by pronounced concentration self-quenching.

The spectra were obtained from randomly oriented crystals at room temperature using Horiba Jobin Yvon LabRAM-HR 800 and HR Evolution spectrometers with 473 nm laser-

excitation. The single-crystal intensity datasets for the three sorosilicates were collected at room temperature using a Bruker APEXII single-crystal X-ray diffractometer and Mo-*K*α radiation.

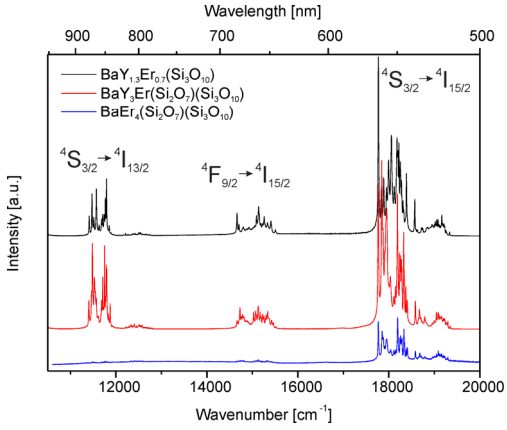

Figure 1. Comparison of the photoluminescence emission (λ_{ex} = 473 nm) spectra of Er^{3+} in doped $BaY_{1.3}Er_{0.7}(Si_3O_{10})$, $BaY_3Er(Si_2O_7)(Si_3O_{10})$, and the end-member $BaEr_4(Si_2O_7)(Si_3O_{10})$.

Acknowledgments

This work was financial supported by the German Research Foundation (DFG-WI 4132/1-1). C. L. gratefully acknowledges the Austrian Science Fund (FWF), grant number P24448-N19.

References

De Hair J.Th.W. (1980) - The luminescence spectra of Pr^{3+} presented in $BaY_4Si_5O_{17}$. *Journal of Solid State Chemistry*, 33, 33-36.

Kolitsch U., Wierzbicka M. and Tillmanns E. (2006) - $BaY_2Si_3O_{10}$, a new flux-grown trisilicate. *Acta Crystallographica*, C62, i97-i99.

Liu W.-R., Lin C.-C., Chiu Y.-C., Yeh Y.-T., Jang S.-M., Liu R.-S. and Cheng B.-M. (2009) - Versatile phosphors $BaY_2Si_3O_{10}$:RE (RE = Ce^{3+}, Tb^{3+}, Eu^{3+}) for light-emitting diodes. *Optical Express,* 17, 18103-18109.

Liu C., Xia Z., Lian Z., Zhoua J. and Yan Q. (2013) - Structure and luminescence properties of green-emitting $NaBaScSi_2O_7$:Eu^{2+}phosphors for near-UV-pumped light emitting diodes. *Journal of Materials Chemistry*, C1, 7139-7147.

Wierzbicka-Wieczorek M., Többens D. M., Kolitsch U. and Tillmanns E. (2013) - Simultaneous presence of $(Si_3O_{10})^{8-}$ and $(Si_2O_7)^{6-}$ groups in new synthetic mixed sorosilicates: $BaY_4(Si_2O_7)(Si_3O_{10})$ and isotypic compounds, studied by single-crystal X-ray diffraction, Raman spectroscopy and DFT calculations. *Journal of Solid State Chemistry*, 207, 94-104.

Xia Z., Liang Y., Yu D., Zhang M., Huang W., Tong M., Wu J. and Zhao J. (2014) - Photoluminescence properties and energy transfer in color tunable $BaY_2Si_3O_{10}$:Ce,Tb phosphors. *Optics and Laser Technology*, 56, 387-392.

Xia Z., Liang Y., Huang W., Yu D., Zhang M. and Tong M. (2013) - A novel charge transfer blue-emitting phosphor: $BaY_2Si_3O_{10}$. *Ceramics International*, 39, 7097-7100.

Zhang F., Wang Y. and Tao Y. (2013) - VUV spectroscopic properties of $Ba_2Gd_2Si_4O_{13}$:Re^{3+} (Re^{3+}= Ce^{3+}, Tb^{3+}, Dy^{3+}, Eu^{3+}, Sm^{3+}). *Materials Research Bulletin*, 48, 1952-1956.

Periodico di Mineralogia, ECMS 2015, 195-196

PERIODICO di MINERALOGIA
established in 1930

An International Journal of
MINERALOGY, CRYSTALLOGRAPHY, GEOCHEMISTRY,
ORE DEPOSITS, PETROLOGY, VOLCANOLOGY
and applied topics on *Environment*, *Archaeometry* and *Cultural Heritage*

Minerals of the bowieite – kashinite series from the Svetly Bor complex, Urals, Russia, and comparison with worldwide occurrences

Federica Zaccarini[1,*], Luca Bindi[2] , Evgeny Pushkarev[3], Giorgio Garuti[1] and Ronald J. Bakker[1]

[1] Department of Applied Geosciences and Geophysics, University of Leoben, Peter Tunner str. 5, A–8700 Leoben, Austria
[2] Dipartimento di Scienze della Terra, Università degli Studi di Firenze, via La Pira 4, I–50121 Firenze, Italy
[3] Institute of Geology and Geochemistry, Ural Division of Russian Academy of Sciences, Str. Pochtovy per. 7, 620151 Ekaterinburg, Russia
* Corresponding author: *federica.zaccarini@unileoben.ac.at*

The presence of a possible solid-solution series between bowieite (ideally Rh_2S_3) and kashinite (ideally Ir_2S_3), two rare platinum-group minerals (PGM), was postulated about 60 years ago on the basis of synthetic counterparts. Bowieite and kashinite were officially accepted as new minerals only in 1985.

After its official discovery in a Pt-Fe nugget from Goodnews Bay in Alaska, more than twenty occurrences of bowieite have been documented. In most of them, bowieite has been found as inclusion of Pt-Fe nuggets associated with placer deposits. Occasionally, bowieite has also been reported to occur in chromitite, in a Ni-rich laterite, in ultramafic rocks and in magnetite-bearing gabbros.

Kashinite was first described from the Niznhy Tagil Ural-Alaskan type complex, Urals, Russia. Then it was reported from several chromitites associated with ophiolites or Ural-Alaskan type complexes. More rarely, kashinite was found in placer deposits and from a sulfide poor ore. In spite of the significant number of reports of natural occurrences of bowieite and kashinite, few data are available about their chemical composition. So far, only the grains from the type localities and one grain form China have been studied by X-ray diffraction. Furthermore, members of the bowieite-kashinite series have been never investigated by Raman spectroscopy.

Here we present, for the first time, single-crystal X-ray diffraction and electron microprobe data and Raman spectra of selected grains in the bowieite-kashinite series from a dunite of the Svetly Bor Ural-Alaskan type complex, located in the central Urals, Russia. The studied mem-

bers of the bowieite-kashinite series occur associated with crystals of Pt-Fe that vary in size from 200 μm up to 1 mm. The host Pt-Fe alloys is chemically homogeneous with an isoferroplatinum-type composition. The bowieite-kashinite grains vary in size from 10 up to 100 μm (Figure 1) and under reflected light they are pinkish-grey in color and show a weak anisotropy. One grain of bowieite has been found associated with laurite (Figure 1A). One grain of kashinite is rimmed by an unnamed PGM (Figure 1B) that, according to the microprobe results, may correspond to $(Ir_{0.26}Rh_{0.13}Pt_{0.12}Ni_{0.18}Cu_{0.18}Fe_{0.11})_{\sum 0.98}S$. This unnamed PGM is grey in colour and darker compared to the associated kashinite, and it is slightly anisotropic. The analyzed kashinite from Svetly Bor dunite displays a limited compositional range, in terms of Ir/Rh ratio. On the contrary, bowieite shows a larger Rh and Ir compositional variation. Two fragments of bowieite and kashinite, about 100 μm in size, and corresponding to these chemical compositions $(Rh_{1.16}Ir_{0.82}Cu_{0.02})_{\sum 2.00}S_{3.00}$ and $(Ir_{1.06}Rh_{0.87}Cu_{0.04})_{\sum 1.97}S_{3.03}$, respectively, were extracted from the polished section. The single-crystal X-ray diffraction data confirm that the two selected minerals are orthorhombic. According to the obtained values, a = 8.46(1), b = 6.00(1), c = 6.14(1) Å for bowieite and a = 8.46(1), b = 5.99(1), c = 6.14(1) Å for kashinite, the two phases are not distinguishable. The same grains of bowieite and kashinite used for the diffraction study were also analyzed by Raman spectroscopy. All these PGM display very well-defined and characteristic peaks in the range of 250 to 400 cm^{-1}. Interestingly, the spectra of bowieite and kashinite are very similar, showing two narrow bands at about 287-308 cm^{-1} and 308-311 cm^{-1} and another relatively wider peak at about 374 cm^{-1} and 387 cm^{-1}, respectively.

As the cell parameters and the Raman spectra of bowieite and kashinite are very similar, the data presented in this contribution indicate that the ultimate methodology to distinguish these rare PGM is electron-microprobe analysis. According to the worldwide occurrences of bowieite-kashinite, with few exceptions, bowieite typically occurs as an inclusion in Pt-Fe alloy associated with Ural-Alaskan type complexes. Kashinite is a common inclusion in chromite crystals of ophiolitic and, to a lesser extent, Ural-Alaskan type chromitites. These observations suggest that both these PGM can be useful to define the nature of their source rocks where they occur solely in placer deposits.

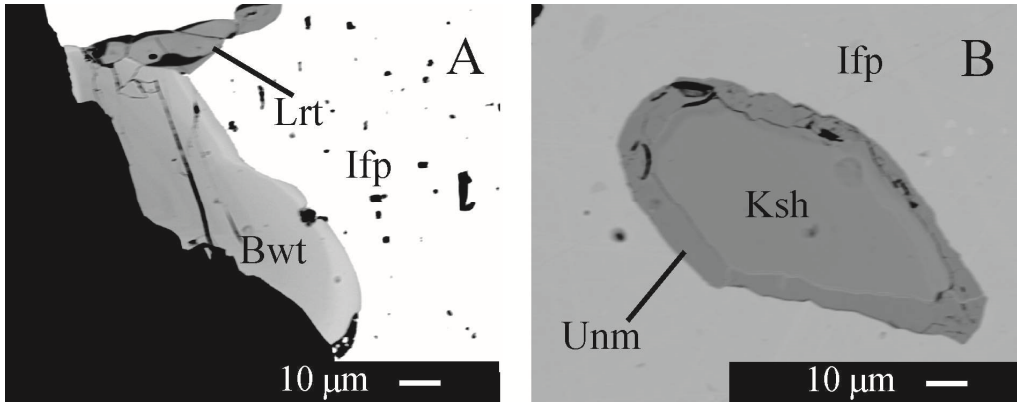

Figure 1. Back-scattered-electron (BSE) images showing morphology and mineral assemblages of the PGM included in isoferroplatinum of the Svetly Bor dunite. Abbreviation: Ifp = isoferroplatinum, Lrt = laurite, Bwt = bowieite, Ksh = kashinite, Unm = unnamed $(Ir_{0.26}Rh_{0.13}Pt_{0.12}Ni_{0.18}Cu_{0.18}Fe_{0.11})_{\sum 0.98}S$.

Periodico di Mineralogia, ECMS 2015, 197-198

PERIODICO di MINERALOGIA
established in 1930

An International Journal of
MINERALOGY, CRYSTALLOGRAPHY, GEOCHEMISTRY,
ORE DEPOSITS, PETROLOGY, VOLCANOLOGY
and applied topics on *Environment*, *Archaeometry* and *Cultural Heritage*

Effects of radiation damage on the Nd^{3+} luminescence of ekanite, $ThCa_2Si_8O_{20}$

Manuela Zeug[1,*], Katja Ruschel[1,2], Doris Blaimauer[1], Christian L. Lengauer[1] and Lutz Nasdala[1]

[1] Institut für Mineralogie und Kristallographie, Universität Wien, Althanstraße 14, 1090 Wien, Austria
[2] present address: Bundesamt für Strahlenschutz, Willy-Brandt-Straße 5, 38226 Salzgitter, Germany
* Corresponding author: *manuela.zeug@univie.ac.at*

Laser-induced photoluminescence (PL) spectroscopy is a most suitable tool for the quantitative detection of self-irradiation damage in U- and Th-bearing minerals (Nasdala et al., 2013; Lenz and Nasdala, 2015). Here we present results of an annealing study of metamict ekanite from gem gravels in the Ratnapura district, Sri Lankan Highland Complex (Zoysa, 2014).

Ekanite is a "radioactive gem". It is a Th-Ca-silicate (ThO_2 >25 wt%) that also incorporates significant amounts of uranium (i.e. up to several wt%). Ekanite was first recognised as new gem material in 1953, found near Eheliyagoda, Ratnapura district, Ceylon (now Sri Lanka). It was named after the discoverer F.L.D. Ekanayake (Anderson et al., 1961). Since then, the popularity of this rare mineral in the gem market has increased appreciably, and it is still commonly seen in the trade. Ekanite is typically found in the metamict state, i.e. it is amorphised (or at least heavily damaged, close to the amorphous state) due to the accumulation of high levels of damage caused by the radioactive decay of U and Th (Ewing, 1994).

We have investigated the structural reconstitution of ekanite upon thermal treatment by dry annealing in air. Here, the spectral characteristics of the laser-induced PL emission of Nd^{3+} ($^4F_{3/2} \rightarrow {}^4I_{9/2}$ electronic transition) was used to monitor changes of the short-range order (cf. Lenz et al., 2013). The PL spectra of natural ekanite show broad humps lacking any fine structure; the loss of any crystal-field splitting affecting the electronic transitions indicates amorphisation (Fig. 1). Notable changes of the PL are observed after annealing at 1000 °C (Fig. 1); they are assigned to thermally-induced random nucleation in the amorphous bulk. Our observations however indicate that a Ca-silicate phase different from ekanite is nucleated initially at 1000 °C. Ekanite is formed only at above 1100 °C; the degree of short-range order and crystallinity increases with T (indicated by decreasing widths of individual Stark lines; Fig. 1). The above interpretations based on PL results correlate well with Raman spectra and X-ray diffraction patterns obtained from the same samples. Due to the initially amorphous state and hence recovery based on nucleation, the run product is well-crystallised but polycrystalline ekanite.

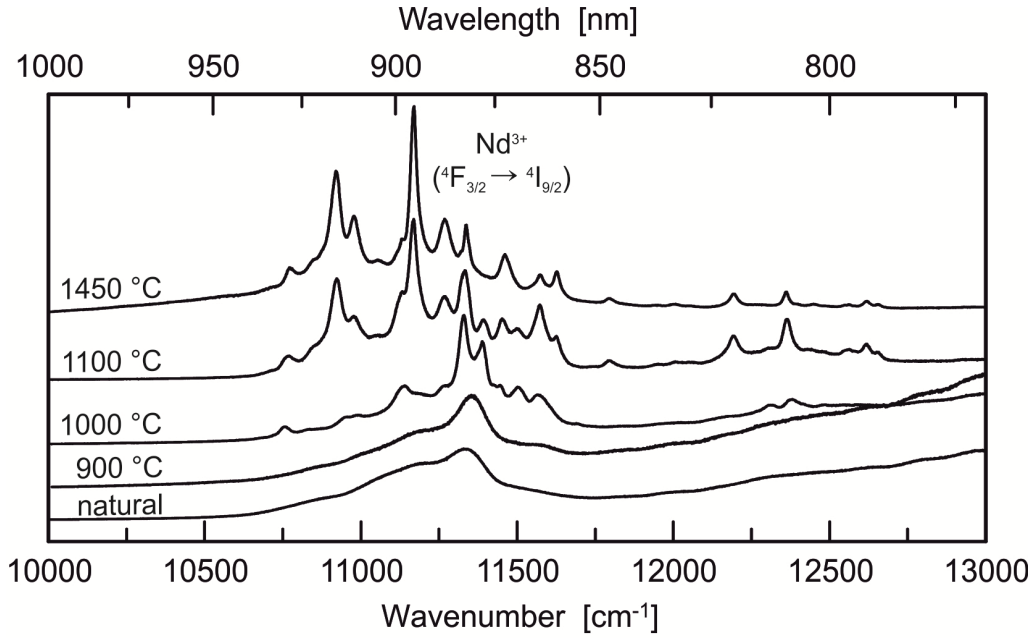

Figure 1. Structural reconstitution of initially metamict ekanite upon dry thermal annealing at different temperatures, monitored by changes of the PL (473 nm excitation) related to the $^4F_{3/2} \rightarrow {}^4I_{9/2}$ electronic transition of Nd^{3+}. The splitting into sublevels, indicating initial recrystallisation, starts at about 1000°C.

References

Anderson B.W., Claringbull G.F., Davis R.J. and Hill D.K. (1961) - Ekanite, a new metamict mineral from Ceylon. *Nature*, 190, 997.

Ewing R.C. (1994) - The metamict state: 1993 – the centennial. *Nuclear Instruments and Methods in Physics Research B*, 91, 22–29.

Lenz C. and Nasdala L. (2015) - A photoluminescence study of REE^{3+} emissions in radiation-damaged zircon. *American Mineralogist*, 100, 1123–1133.

Lenz C., Talla D., Ruschel K., Škoda R., Götze J. and Nasdala L. (2013) - Factors affecting the Nd^{3+} (REE^{3+}) luminescence in minerals. *Mineralogy and Petrology*, 107, 415–428.

Nasdala L., Grambole D. and Ruschel K. (2013) - Review of effects of radiation damage on the luminescence emission of minerals, and the example of He-irradiated $CePO_4$. *Mineralogy and Petrology*, 107, 441–454.

Zoysa G. (2014) - The geology and gem deposits of Sri Lanka. *InColor*, 27, 38–41.

Periodico di Mineralogia, ECMS 2015, 199-200

PERIODICO di MINERALOGIA
established in 1930

An International Journal of
MINERALOGY, CRYSTALLOGRAPHY, GEOCHEMISTRY,
ORE DEPOSITS, PETROLOGY, VOLCANOLOGY
and applied topics on *Environment*, *Archaeometry* and *Cultural Heritage*

High-temperature crystal chemistry of astrophyllite from Kola peninsula, Russia

Elena S. Zhitova[1,*], Maria G. Krzhizhanovskaya[1], Sergey V. Krivovichev[1], Frank C. Hawthorne[3], Victor N. Yakovenchuk[2] and Gregory U. Ivanyuk[2]

[1] St. Petersburg state University, Department of Crystallography, Russia, 199155, Saint-Petersburg, V.O., per. Dekabristov, d. 16
[2] Nanomaterials Research Center, Kola Science Center, the Russian Academy of Sciences, Russia, 184209, Apatity, Fersman Street 14
[3] University of Manitoba, Canada, MB R3T 2N2, Winnipeg
* Corresponding authors: *zhitova_es@mail.ru*

Astrophyllite is a characteristic accessory mineral in nepheline syenites of the Khibiny alkaline massif. Within the massif it was found at Marchenko Peak, Mts Eveslogchorr, Kukisvumcorr, Niorkpakhk, Yuksporr and Koashva. The mineral forms reddish-brown and golden-yellow individual lamellae, acicular crystals and small fibrous and lamellar aggregates (Yakovenchuk et al., 2005). From the crystal chemical point of view, astrophyllite is a layered titanosilicate, consisting of two types of layers: closest-packed octahedral $[MO_6]$ layer in between two heteropolyhedral layers $[TiSi_4O_{12})]^{4-}$, with K and Na cations are occupying interstitial sites. The two types of layers are in the 2:1 ratio and are stacked along [001] (Sokolova 2012; Piilonen et al., 2003).

The aim of this contribution is the high-temperature behavior of astrophyllite. High-temperature powder X-ray diffraction study revealed the presence of phase transition at 500 °C. The new phase exists from 500 to 775 °C and decomposes at the temperature above 775 °C. The transition is irreversible, and mineral grains become dark when heated above 500 °C. Differential scanning calorimetry did not detect any effects in the Ar-Ar atmosphere, but the exothermic effect was found at 584 °C in the Ar-O atmosphere.

The crystal structures of both initial and calcined astrophyllite were studied by means of single-crystal X-ray Bruker APEX II diffractometer, MoKα at the room temperature. The crystal structure of the initial sample was refined on the basis of 9883 reflections $|F_0| \geq 4\sigma_F$ to R_1 = 0.061. The space group is *P*-1, a = 5.3752(1), b = 11.8956(3), c = 11.6554(3) Å, α = 113.157(2), β = 94.530(2), γ = 103.112(2) º, V = 655.47(3) Å^3, Z = 1. The crystal structure of the high-temperature phase was refined on the basis of 2270 $|F_0| \geq 4\sigma_F$ to R_1 = 0.07. The space group is *P*-1, a = 5.3287(4), b = 11.790(1), c = 11.4332(9) Å, α = 112.530(8), β = 94.539(6), γ = 103.683(7) º, Z = 1, V = 633.01(9) Å^3.

Analysis of the Fe-O bond lengths in the calcined material indicated considerable bond-shortering within the octahedral formed by the Fe2, Fe3 and Fe4 sites (in the three of four octahedra), which allows to interpret the observed phase transition as resulting from the oxidation of Fe^{2+}. This hypothesis was confirmed by Mössbauer spectroscopic study which indicated 75.8 % of Fe^{2+} and 24.2 % of Fe^{3+} in the initial material; 24.5 of Fe^{2+} and 75.5 % of Fe^{3+} in the calcined material.

It is worth mentioning that the thermal expansion of the fresh and calcined astrophyllite phases is different. In the region from 25 to 500 °C the mineral experiences expansion along all three axes: *a*, *b* and *c*. In contrast, in the region from 525 to 775 °C the *a* and *c* parameters of astrophyllite decrease.

The research was supported by the Russian Foundation for Basic Research (grant 14-05-31229\15), SPbU internal grant № 3.37.222.2015 and the President of Russian Federation Grant for Young Candidates of Sciences (to AAZ, grant MK- 3296.2015.5).

The XRD studies have been performed at the X-ray Diffraction Centre of St. Petersburg State University.

References

Piilonen P.C., McDonald A.M., LaLonde A.E. (2003) - Insights into astrophyllite–group minerals. II. Crystal chemistry. *The Canadian Mineralogist,* 41, 27-54.

Sokolova E. (2012) - Further developments in the structure topology of the astrophyllite-group minerals. *Mineralogical Magazine*, 76, 863-882.

Yakovenchuk V., Ivanyuk G., Pakhomovsky Ya., Men'shikov Yu. (2005) - Khibiny. (ed): Wall F, Laplandia Minerals, Apatity, 172-182.

Periodico di Mineralogia, ECMS 2015, 201-202

PERIODICO di MINERALOGIA
established in 1930

An International Journal of
MINERALOGY, CRYSTALLOGRAPHY, GEOCHEMISTRY,
ORE DEPOSITS, PETROLOGY, VOLCANOLOGY
and applied topics on *Environment*, *Archaeometry* and *Cultural Heritage*

Low temperature single crystal X-ray diffraction study of quintinite-1*M* –, a natural layered double hydroxide (LDHs)

Elena S. Zhitova [1,*], Sergey V. Krivovichev [1], Taras L. Panikorovskiy[1], Victor N. Yakovenchuk [2] and Gregory U. Ivanyuk[2]

[1] St. Petersburg state University, Department of Crystallography, Russia, 199155, Saint-Petersburg, V.O., per. Dekabristov, d. 16
[2] Nanomaterials Research Center, Kola Science Center, the Russian Academy of Sciences, Russia, 184209, Apatity, Fersman Street 14
* Corresponding author: *zhitova_es@mail.ru*

Quintinite $[Mg_4Al_2(OH)_{12}](CO_3)(H_2O)_3$ is a natural representative of layered double hydroxides (LDHs). Recently the mineral was assigned to a separate quintinite group, which includes six minerals with M^{2+}:M^{3+} = 2:1 (Mills et al., 2012) and is a part of the hydrotalcite supergroup. Crystal structures of hydrotalcite-type minerals consist of positively charged metal-hydroxide layers and charge-balancing interlayer species. Due to their properties, synthetic analogues of hydrotalcite group minerals - (LDHs) found many important applications in pharmacology, as absorbents, CO_2-removers, flame redundant, catalysts, etc. (Wang, O'Hare, 2012).

The crystal structure of quintinite-1*M* from the Kovdor alkaline massif (Kola peninsula, Russia) has been described by us in detail in previous papers (Krivovichev et al., 2010; Krivovichev et al., 2012). The significant feature of the crystal structure of quintinite-1*M* is the M^{2+}-M^{3+} honeycomb-like ordering within the brucite-type octahedral layers. The stacking of the layers - is in accordance with the rhombohedral polytype $3R_1$ (Bookin and Drits, 1993). The species in the interlayer (carbonate groups and H_2O molecules) are strongly disordered, which can be seen clearly by the inspection of the residual electron-density maps. Although we assumed that the disorder has a positional and not dynamic character, this issue still needed clarification, which is the topic of present contribution.

The crystal of quintinite-1*M* was studied by means of Agilent Technologies «Xcalibur» single-crystal diffractometer (Mo-Kα, frame widths 1º, 80s count for each frame) at 80 °K and at room temperature.

The unit cell parameters of quintinite-1*M* at room temperature are: *C*2/*m*, *a* = 5.2746(3), *b* = 9.1328(4), *c* = 7.7790(5) Å, *β* = 103.069(6)°, d_{calc} = 7.58 Å. The unit cell parameters at 80 °K are: *C*2/*m*, *a* = 5.2642(2), *b* = 9.1180(4), *c* = 7.7432(4) Å, *β* = 103.075(5)°, d_{calc} = 7.54 Å. The crystal structures of quintinite-1*M* were refined to R_1 = 0.041/0.036 on the basis of 426/407

unique reflections $|F_0| \geq 4\sigma_F$ for data collected at room and low temperatures, respectively. The comparison of electron-density maps calculated at the interlayer level for the data obtained at room and low temperatures (Fig. 1) indicates no fundamental differences. In both cases electron-density maxima corresponding to O atoms in CO_3 groups form continuous toroidal regions instead of separate maxima, which is a clear confirmation of the positional disorder of carbonate groups.

Positional disorder of CO_3 might result in the appearance of additional bands in the IR and Raman spectra. For example, in hydrotalcite (CO_3-LDH), four bands are predicted in IR spectra from the planar triangular shape of CO_3 groups, they are normally observed at 1415, 1063, 879 and 680 cm^{-1}. Three more bands observed at 1490, 1388, 1362 cm^{-1} are attributed to the carbonate antisymmetric stretching region (Palmer et al., 2007).

The research was supported by the Russian Foundation for Basic Research (grant 14-05-31229\15), SPbU internal grant № 3.37.222.2015. The XRD studies have been performed at the X-ray Diffraction Centre of St. Petersburg State University.

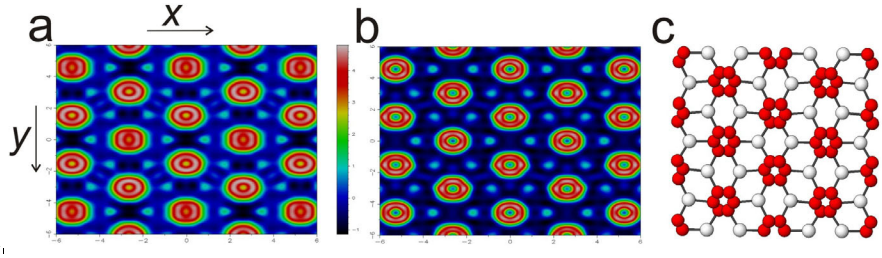

FIGURE 1

Electron density Fourier map of the interlayer in quintinite-1*M* at room temperature (a), 80 °K (b) and a model of the disordered interlayer arrangement of carbonate anions and water molecules (c).

References

Bookin A.S. and Drits V.A. (1993) - Polytype diversity of the hydrotalcite-like minerals. I. possible polytypes and their diffraction features. *Clays and Clay minerals,* 41, 5, 551-557.

Krivovichev, S.V., Yakovenchuk, V.N., Zhitova, E.S., Zolotarev, A.A., Pakhomovsky, Y.A., Ivanyuk, G.Yu. (2010) - Crystal chemistry of natural layered double hydroxides. 2. Quintinite-1*M*: First evidence of a monoclinic polytype in M^{2+}-M^{3+} layered double hydroxides. *Mineralogical Magazine*, 74, 5, 833-840.

Krivovichev S.V., Yakovenchuk V.N., Zhitova E.S. (2012) - Natural double layered hydroxides: structure, chemistry, and information storage capacity. *Minerals as Advanced Materials II*. (ed): S.V.Krivovichev. Springer-Verlag, Berlin Heidelberg, 87-91.

Mills S.J., Christy A.G., Génin J-M. R., Kameda T., Colombo F. (2012) - Nomenclature of the hydrotalcite supergroup: natural layered double hydroxides. *Mineralogical Magazine*, 76, 1289-1336.

Palmer S.J., Nguyen T., Frost R.L. (2007) - Synthesis and Raman spectroscopic characterisation of hydrotalcite with CO_3^{2-} and VO_3^- anions in the interlayer. *Journal of Raman Spectroscopy,* 38, 12, 1602–1608.

Wang Q., O'Hare D. (2012) - Recent Advances in the Synthesis and Application of Layered Double Hydroxide (LDH) Nanosheets. *Chemical Reviews,* 112 (7), 4124–4155.

Periodico di Mineralogia, ECMS 2015, 203-204

PERIODICO di MINERALOGIA
established in 1930

An International Journal of
MINERALOGY, CRYSTALLOGRAPHY, GEOCHEMISTRY, ORE DEPOSITS, PETROLOGY, VOLCANOLOGY
and applied topics on *Environment*, *Archaeometry* and *Cultural Heritage*

Ti-bearing dalyite from the charoite rocks (Murun massif, Russia): single-crystal structure refinement

Andrey A. Zolotarev[1], Nikolay V. Vladykin[2] and Sergey V. Krivovichev [1]

[1] Department of Crystallography, Institute of Earth Science, Saint-Petersburg State University, Russia
[2] Vinogradov Institute of Geochemistry of the Siberian Branch of the RAS, ISC, Russia
* Corresponding author: *aazolotarev@gmail.com*

Dalyite, $K_2ZrSi_6O_{15}$, is a rare accessory mineral that was first described in 1952 in peralkaline granites from the Ascension Island (Van Tassel, 1952) and later reported in other localities: peralkaline granites from Antarctica (Harris and Rickard, 1987); peralkaline quartz syenites from the Azores (Cann, 1967); potassic peralkaline syenites from Western Norway (Robins et al., 1983); lamproites (cancalites) from Sierra de Cabras, Cancarix, Spain (Linthout et al., 1988). For all known samples of dalyite, almost constant chemical composition was reported, which corresponds to the ideal formula $K_2ZrSi_6O_{15}$. For the sample from peralkaline granites of the Ascension Island, a partial substitution of K to Na was observed (Van Tassel, 1952). For other dalyite samples, a slight substitution of Zr by Ti (up to 8-9%) has been reported (Linthout et al., 1988). The crystal structure of the mineral was solved in 1965 on the material from the Ascension Island (Fleet, 1965). Here we present data of refinement of the crystal structure of the Ti-bearing dalyite from the rocks of the charoite complex of the Murun alkaline massif (Russia). The crystallographic data and refinement parameters are given in Table 1. The crystal structure of dalyite is based upon corrugated SiO_4 tetrahedra layers almost parallel to (010), which in turn are composed of distorted wollastonite-type chains, with their periodicity equal to three. The average Si-O distance is 1.615 Å. The silicate layers are linked by almost undistorted $(Zr,Ti)O_6$ octahedra with the average bond length of 2.040 Å. K^+ cations are in eightfold coordination with the average K-O distance of 2.993 Å. In the dalyite sample from the Murun massif, Zr is substituted by Ti by approximately 30%, as confirmed by the microprobe chemical analysis. Thus, the studied sample can be characterized as Ti-dalyite with the formula $K_2Zr_{0.70}Ti_{0.30}Si_6O_{15}$.

Acknowledgments. A. Zolotarev is grateful to President Federation Grant for Young Candidates of Sciences (MK-3296.2015.5).

TABLE. 1. Crystallographic data for Ti-dalyite

Diffractometer	Bruker Smart Apex II
Crystal system	Triclinic
Space group	*P-1*
a,(Å)	7.3306(9)
b,(Å)	7.6298(9)
c,(Å)	6.9167(8)
α,(°)	105.846(6)
β,(°)	112.328(5)
γ,(°)	99.368(6)
V (Å^3)	328.45(7)
Z	1
Radiation	MoKα (λ = 0.71073 Å).
Angle range (°)	5.818 to 69.994
Total reflections	12196
Unique reflections	2883 [R_{int} = 0.0282, R_{sigma} = 0.0239]
S	1.095
Final *R* indexes [I> =2σ(I)]	R_1 = 0.0231, wR_2 = 0.0550
Final *R* indexes [all data]	R_1 = 0.0269, wR_2 = 0.0569

$R_1 = \sum||Fo| - |Fc||/\sum|Fo|$; $wR_2 = \{\sum[w(Fo^2 - Fc^2)^2]/\sum[w(Fo^2)^2]\}^{1/2}$;
$w = 1/[\sigma^2(Fo^2)+(aP)^2 + bP]$, where $P = (Fo^2 + 2Fc^2)/3$; $S = \{\sum[w(Fo^2 - Fc^2)]/(n - p)\}^{1/2}$
where n is the number of reflections and p is the number of refinement parameters.

References

Cann, J.R. (1967) - A Second Occurrence of Dalyite and the Petrology of Some Ejected Syenite Blocks from São Miguel, Azores. *Mineralogical Magazine*, 36, 227-232.

Fleet S.G. (1965) - The crystal structure of dalyite. *Zeitschrift Fur Kristallographie*, 121, 349–368.

Harris C. and Rickard R.S. (1987) - Rare-earth-rich eudialyte and dalyite from a peralkaline granite dyke at Straums- vola, Dronning Maud Land, Antarctica. *Canadian Mineralogist*, 25, 755-762.

Linthout K., Nobel F.A. and Lustenhouwer W.J (1988) - First Occurrence of Dalyite in Extrusive Rock *Mineralogical Magazine*, 52, 705-708.

Robins B., Furnes H. and Ryan P. (1983) - A New Occurrence of Dalyite. *Mineralogical Magazine*, 47, 93-94.

Van Tassel R. and Hey M.H. (1952) Dalyite, a new potassium zirconium silicate, from Ascension Island, Atlantic. *Mineralogical Magazine*, 29, 850-857.

AUTHOR INDEX

PERIODICO di MINERALOGIA
established in 1930

An International Journal of
MINERALOGY, CRYSTALLOGRAPHY, GEOCHEMISTRY,
ORE DEPOSITS, PETROLOGY, VOLCANOLOGY
and applied topics on Environment, Archaeometry and Cultural Heritage

Instructions to authors

The Periodico di Mineralogia is a journal devoted to publishing original researches and review papers in mineralogy, crystallography, geochemistry, ore deposits, petrology, volcanology and applied topics on environment, archaeometry and cultural heritage.

Submission of a research article is understood to imply that both the whole and the parts of the manuscript are original and not being considered for publication elsewhere.

Papers must be written in English. No page limitations on the length of articles and number of tables and illustrations are required. Color print is free of cost.

Manuscripts must be prepared as a doc/docx file for the text and tiff/jpg for illustrations;
A pdf format must be submitted online utilizing the web site:
http://www.periodicodimineralogia.it

All pages must be numbered, and Times New Roman font, size 10, is required.

The parts of the manuscript should appear in the following order: 1. title; 2. full name(s) and surname(s) 3. address(es) of author(s); 4. abstract; 5. key words; 6. text; 7. list of references.

Please specify the e-mail address of a corresponding Author for correspondence.

Abstract, key words and text

All the contents must be typed in small letter.

The abstract must be concise, no more than 500 words long, without citations; it should include important data (e.g., thermodynamic data, temperature range, isotope range, etc.).

Key words (no more than six) must be typed in small letters and separated by a semicolon.

Appropriate headings are used to break the text into sections. First-order headings are centred and bold, second-order headings are left-justified and italics, third order headings are left-justified.

Don't use small capital and italics (except for flora and fauna) in the text, don't use footnotes.

Tables

For the tables, Author(s) should take into consideration the limitations set by the size (14 cm x 18.5 cm) of the Periodico di Mineralogia. Tables must be submitted as doc/docx/xls format in a separated file containing also captions and footnotes. Tables should be ready for 1:1 reproduction.

Illustrations

Illustrations (drawings and photographs) should respect the page format of the Periodico di Mineralogia (14 cm x 18.5 cm), and must have a 300 dpi resolution. The tiff, jpg and pdf format are accepted. Captions must be attached after the references, in the main text file. Lettering should also be as large as possible to allow for possible reduction without becoming illegible. Bar scales must be used.

References

All references quoted in the text, in the tables and figures or other parts of the paper, must be included in the list of references.

The reference list is arranged in alphabetical order following the surname of the first Author. In the case of multiple Authors they will be arranged following the further Authors; in the case of identical numbers of Authors, the different citations will be listed by year.

Typing the list of references please don't use any particular format (as small capitals); only the title of the journal must be in *italics*.

Styles of references are listed as follows:

McConnel J., McCammon C., Angel R. and Seifert F. (2000) - The nature of the incommensurate structure in akermanite, $Ca_2MgSi_2O_7$, and the character of its transformation from the normal structure. *Zeitschrift für Kristallographie*, 215, 669-677.

Larson A. and Von Dreele R. (1988) - General Structure Analysis System (GSAS). Los Alamos National Laboratory Report (LAUR 86-748), Los Alamos, NewMexico, 224 pp.

Shervais J. (1979a) - Ultramafic and mafic layers in the alpine-type lherzolite massif al Balmuccia (Italy). *Memorie della Società Geologica di Padova*, 33, 135-145.

Shervais J. (1979b) - Thermal emplacement model for the alpine lherzolite massif at Balmuccia (Italy). *Journal of Petrolo*gy, 20, 795-820.

Jambon A. (1996) - Melt growth. In: Crystal Growth in Earth Sciences. (eds): E. Scandale and A. Baronnet, EDISU, Torino (Italy), 98-128.

Citations

Citations should be placed in the appropriate position in the paper and cited as follow:
(London, 1999)
(London and Manning, 1995)
(Agrosì et al., 2006)
(Selway et al., 1999, 2002)

One page proof will be sent to the Author(s) to be checked only for typesetting/editing errors. Each corrisponding author will receive a personal pdf copy of his/her article. Reprints of the article may be purchased contacting ordini@nuovacultura.it.

For subscription, please contact: Edizioni Nuova Cultura, Piazzale Aldo Moro 5, I-00185 Roma, Italy
E-mail: *ordini@nuovacultura.it*

Annual subscription fee per volume (three issues)
Italy = € 100; Abroad = € 150

Student subscription rate has a discount of 30%.

For reprints, single articles and the entire collection please contact the Editor at *ordini@nuovacultura.it.*

Periodico di Mineralogia can be exchanged with other periodical journals.
Please contact the Scientific Editor of the journal.

For Advertising, please contact:
Edizioni Nuova Cultura, Piazzale Aldo Moro 5, I-00185 Roma, Italy
E-mail: *gennaroguerriero@nuovacultura.it*

Published three times a year. Property of Università degli Studi di Roma "La Sapienza"
Piazzale Aldo Moro 5, I-00185 Roma, Italy

[Int_978886812543_17x24col_LM04]

September, 2015 1-208

PERIODICO di MINERALOGIA

established in 1930

ECMS 2015 is sponsored by

SAPIENZA
UNIVERSITÀ DI ROMA